Wavelet-based Adaptive Multiresolution Tools Applied to Speech Recognition

Diploma Thesis

Andreas Simon

University of Kaiserslautern
Department of Mathematics

Wavelet-based Adaptive Multiresolution Tools Applied to Speech Recognition

Diploma Thesis

Andreas Simon

Supervisor:
HDoz. Dr. Volker Michel
michel@mathematik.uni-kl.de

Erwin-Schrödinger-Straße
67663 Kaiserslautern

University of Kaiserslautern
Department of Mathematics
Geomathematics Group
Kaiserslsautern, Germany

July 2006

Acknowledgments

Gratitude is expressed to Hdoz. Dr. Volker Michel for introducing the problem presented in this thesis as well as for being an inspiring and very patient supervisor.

With thanks it should also be mentioned that he put the author in contact with the company *CIBEK* and especially its manager Bernd Klein and that both gave the author full rein to research used and common techniques in the field of signal processing.

In addition, the author is much obliged to the former and current members of the Geomathematics Group in particular for offering their voices in order to set up a data set of spoken commands.

Thanks goes also to Oliver Schulte for discussing some technical problems.

Finally, Tanja Oberhofer, her and the author's family with their friendly encouragement and invaluable support are also gratefully acknowledged.

Contents

Notation

Sets

$\mathbb{K}$	a field, mostly $\mathbb{K}$ is considered as $\mathbb{K} = \mathbb{C}$ or $\mathbb{K} = \mathbb{R}$.
$\mathbb{C}$	Set of complex numbers
$\mathbb{R}$	Set of reals with optional restrictions: $\mathbb{R}_{\{\leqslant,\neq,\geqslant\}k} := \left\{x \in \mathbb{R} \,\middle|\, x \leqslant k \text{ or } x \neq k \text{ or } x \geqslant k, k \in \mathbb{R} \text{ arbitrary but fixed } \right\}$
$\mathbb{Z}$	Set of integers, $\{\ldots, -3, -2, -1, 0, 1, 2, 3, \ldots\}$
$\mathbb{N}$	Set of positive integers, i.e. $\mathbb{Z}_{>0} = \{1, 2, 3, \ldots\}$
$\operatorname{ran}(f)$	Range of a function f, i.e. $\operatorname{ran}(f) := \{y \mid f(x) = y\}$
$\operatorname{supp}(f)$	Support of a function f defined as the closure (w.r.t. the Euclidean norm $\lvert\cdot\rvert$) of a set not mapped to zero, i.e. $\operatorname{supp}(f) := \overline{\{x \mid f(x) \neq 0\}}$.

Spaces – see Section 3.1

C^k, $\mathrm{C}^k(\mathbb{R})$	both denote the space of $k \in \mathbb{N}$-times continuously differentiable functions
$\mathrm{C}^{k,\alpha}$	is the space of functions whose derivative up to order k is Hölder continuous with exponent α, $\alpha \in (0, 1)$. In particular, $f \in \mathrm{C}^{k,\alpha} \iff \lVert f\rVert_{\mathrm{C}^{k,\alpha}} := \sum_{i\leqslant k} \left\lVert f^{(i)}\right\rVert_{\mathrm{C}^{0,\alpha}} < \infty$ where $\lVert f\rVert_{\mathrm{C}^{0,\alpha}} := \sup_{x,y\in\mathbb{R}} \frac{\lvert f(x)-f(y)\rvert}{\lvert x-y\rvert^\alpha}$. A function is Hölder continuous with exponent α iff it is bounded w.r.t. the $\lVert\cdot\rVert_{\mathrm{C}^{0,\alpha}}$-norm.
C_0	is the set of continuous functions with $\lim_{\lvert x\rvert\to\infty} f(x) = 0$.
C_c	is the set of continuous functions with compact support.
L^p, ℓ^p	set of p-Lebesgue measurable functions and set of discrete signals with finite $\lVert\cdot\rVert_{\ell^p}$ norm, $p \in \mathbb{R}_{\geqslant 1}$.
$U \oplus V$	denotes a direct sum of two vector spaces U and V

Transforms

$\mathcal{F}$, $\mathcal{F}_g$, $\mathcal{W}$	The Fourier, windowed Fourier (with window function $g \in \mathrm{L}^2(\mathbb{R})$) and wavelet transform, respectively

INTERVALS

$[a, b]$	closed interval, i.e. $[a, b] = \{x \in \mathbb{R} \,\vert\, a \leqslant x \leqslant b\}$
$[a, b)$	right opened interval, i.e. $[a, b) = \{x \in \mathbb{R} \,\vert\, a \leqslant x < b\}$
(a, b)	opened interval, i.e. $(a, b) = \{x \in \mathbb{R} \,\vert\, a < x < b\}$
$(a, b]$	left opened interval, i.e. $(a, b] = \{x \in \mathbb{R} \,\vert\, a < x \leqslant b\}$
$[\![k, l]\!]$	'discrete' interval, i.e. $[\![k, l]\!] = \{k, k+1, \ldots, l-1, l \,\vert\, k, l \in \mathbb{Z}\}$

SYMBOLS

$\overline{z}$	complex conjugation of a complex number $z \in \mathbb{C}$, i.e. $\overline{a + ib} = a - ib$ for $z =: a + ib$
$\Re$, $\Im$	real and imaginary part of a complex number $z \in \mathbb{C}$, $2\Re(z) = z + \overline{z}$, $2\Im(z) = z - \overline{z}$
χ_I	characteristic function, $\chi_I(x) = 1$ iff $x \in I$ and $\chi_I(x) = 0$ otherwise.
$\delta_{j,k}$	is the so-called *Kronecker* delta and equals one if and only if $j = k$ and otherwise zero.
id	Identity operator or function; context dependent
$\forall$, $\exists$	quantors: *for all* and *there exists*
A^{T}	transpose of a matrix A
$f(a\cdot)$	denotes a function f in the dummy $\cdot$, i.e. $x \mapsto f(ax)$ with the constant a
$f^{(k)}$	stands for the k-th derivative of f w.r.t. its free variable, i.e. $f^{(k)} : x \mapsto \frac{\mathrm{d}^k}{\mathrm{d}x^k} f(x)$
$\hat{f}$	is an abbreviation for $\mathcal{F}(f)$.
$\langle f, g \rangle$	scalar product of f and g; if not otherwise stated $\langle \cdot, \cdot \rangle \equiv \langle \cdot, \cdot \rangle_{\mathrm{L}^2(\mathbb{R})}$
$\Vert f \Vert$	norm of a function f; again, if not otherwise stated it is considered to be the $\mathrm{L}^2(\mathbb{R})$-norm if the function f is defined over a continuum - in contrast to a sequence, $f = (f_j)_j \in \ell^2$. Then the corresponding norm is assumed to be the ℓ^2-norm.
$f = \mathcal{O}(g)$	*Landau symbol*: $\exists C : \lim_{x\to\infty} \frac{f(x)}{g(x)} \leqslant C$
iff	is an abbreviation for 'if and only if'
$:\Longleftrightarrow$	used to emphasise a definition
[ɪpɑːˈælfəbet]	is a so-called *IPA* notation for proper pronunciation of speech sounds, see Chapter 2

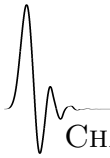

Chapter 1

Introduction

Most of the time human being's focus of attention is fixed on a particular thing capturing nearly all brain's conscious thoughts which chiefly ignores stationary stimuli caused by the environment. That focus is only attracted by sudden changes, so-called *transients*.

It may be the most important strategy pursued by the brain in concentrating on transients in order to extract crucial information from the vast amount of data bombarding human being's senses.

Music and speech have properties which highly vary in time. It is not only the amplitude which stresses important information by weighing it but also the variation of frequencies carrying the most content perceived by the ears.

It is therefore reasonable to restrict the attention to transforms which give rise to measurements of such spectral variations in time imitating the same processes which have has crystallised after millions of years of evolution.

The task at hand is first governed by a tricky and rather complicated field: linguistics. How shall one represent a speech or a small utterance in a readable way, i.e. readable for human beings or for a machine processing a sequence of these symbols and coefficients representing the meaning or additionally its 'intention' such as angriness, feeling of uncertainty or calmness?

Thus, what started as an effort to translate between languages evolved into an entire discipline devoted to understanding how to represent and process individual natural languages using computers.

For human beings, the well established *IPA* notation, see Chapter 2, can be considered as a more or less readable sequence of symbols with predetermined pronunciation with almost no freedom for variants.

That alphabet is of finite size (less than 200 symbols) and assumed to

'span' all possible words of every human language. Conversely, every possible speech sound, i.e. a sound pertinent to an utterance, can be written as a unique sequence of such symbols.

For mathematicians these properties are very well known and, generally speaking, are considered as sufficient and necessary for a set to form a basis of a particular space.

Therefore, it is a straightforward longing to find a function, which maps physical properties of speech sounds to *phones*, a realisation[1] of a corresponding IPA symbol.

This ansatz should then lead to a characterisation of any speech sound by means of a few physical properties associated to a phone.

As the goal of this thesis is to recognise only a small number of very different words, see Section 6.2, it may suffice to consider the course in time of high energetic spectral components, i.e. a path in the *phase plane* of high energies, in order to describe voiced segments. This approach is additionally motivated by the so-called formants, typical for voiced speech as presented in Chapter 2.

Henceforth, the author's aim will be to extract a sequence of $n \times 2$ matrices (first column: (mean) frequency, second column: pertinent energy), $n \in \mathbb{N}$, associated to an adapted partition of an arbitrary utterance which could then be used for further classification tasks.

Heisenberg's Uncertainty principle plays an important role in constructing and discussing any transform of a signal aiming a separation of information coming from both, time and frequency domain.

It is a well known fact that any signal (of compact support or of sufficient decay) can be characterised in these domains. Combining them into a *phase plane* reveals then a remarkably easy way of reading the properties of the considered signal.

Werner Heisenberg[2] was the first who also noted that higher accuracy in one space leads to a decrease of accuracy in the other and that the product of both 'uncertainties' is bounded from below by a constant - forever, see Section 3.6.

This means in particular that the information extracted from the phase plane is somehow contained in small boxes of widths corresponding to the uncertainties in frequency and time of fixed area but not necessarily of a

[1] For instance, reading aloud the IPA symbol [a] is a realisation of [a]. See also Chapter 2.

[2] His contributions to quantum physics were honored with the Nobel prize (in 1932) and a German postage stamp from the year 2001, cf. Figure 1.1, his 100th birthday anniversary, depicts his famous formula.

Fig. 1.1: German postage stamp with Heisenberg's uncertainty principle: product of impulse and space (time) uncertainty is proportional to Planck's constant h

fixed aspect ratio, see Section 3.6.
A fixed time - frequency analysis is a transform which always yields a fixed phase plane tiling regardless of the signal, in contrast to an adapted time - frequency analysis which is naturally of more potential in extracting relevant features of a signal since the phase-plane tiling is now dependent on the analysed signal.
Wavelets are adapted to local properties of functions to a larger extent than the Fourier basis. Their 'Heisenberg boxes', or more precisely, the aspect ratio changes with each level. This adaptation is done automatically in view of the existence of a 'second degree of freedom': the localisation in time - the time width decreases as the frequency uncertainty increases. The advantage of this 'multiresolution analysis' is that local properties of data can be seen immediately and thereby influence further analysis.
Unfortunately, the time resolution is much preferred over frequency resolution which is not justified by any physiological study on human hearing.
In contrast, a windowed Fourier transform is of much better frequency resolution and provides full control over the aspect ratio. However, the partitioning is always subjective and the aspect ratio of the 'Heisenberg boxes' is constant for each transform!
Wavelet packets and local trigonometric functions with an associated basis selection algorithm, cf. Chapter 5, resolve these problems for the wavelet and the windowed Fourier transform, resp., and provide an elegant and mathematically consistent realisation of this intuitive idea.
A special basis selection algorithm of only $\mathcal{O}(N)$ multiplications (and additions), if N is the number of samples of the analysed discrete signal, minimising a cost functional, finds a 'best adapted' partition (in time, if local trigonometric functions are used) such that a subsequent extraction of already mentioned $n \times 2$ matrices is then easily obtained.

Synopsis A detailed summary on basic and long (longer than twenty years) known facts is given in the next two chapters. Fundamentals of phonetics recapitulating a few properties of speech are considered in the first whereas the second chapter furnishes a foundation of some functional analysis principles used in the subsequent theory.

After a rigorous mathematical introduction to Gabor and wavelet frames in Chapter 4, their incapability for speech processing is discussed in Section 4.4.2.

Chapter 5 presents then a more sophisticated ansatz, since that approach permits more degrees of freedom, dealing with *local trigonometric* functions, folding operators and effective implementations with low computational complexity.

A mathematical model of the classification problem is formulated in Chapter 6 which gives a compelling need to study first a proper feature extraction. The ensuing algorithm which extracts a $n \times 2$ matrix, $n \in \mathbb{N}$, consisting of frequencies and energies associated to an adapted partitioning of a recorded utterance, sampled at 8 kHz, may be considered as such a feature extractor.

Reasoning arguments which motivates the usefulness of these features, dependence of cost functionals and typical phase plane plots concludes the chapter.

An outlook with possible improvements is given at the end of the thesis.

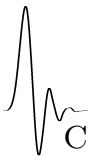

Chapter 2

Short Introduction to Phonetics

The goal of this thesis is of course a classification of distinct words spoken by human beings by means of mathematical transforms allowing an machine-readable algorithm which can then be processed by computers.

At the beginning, characteristics of speech are of major interest and will be studied shortly in the sequel. For further studies the reader may check [Hes05, ST95] and the references therein.

Phonetics is the study of sounds, especially voice sounds. It concerns the actual properties of speech sounds, called *phones* and their production, audition and perception.

Sound is a longitudinal wave. It is a time and space varying function of pressure resulting from an (averaged) oscillation of air particles (molecules and bigger pieces like dust) parallel to the direction of its propagation.

Each wave can be equivalently described by its superposition of frequencies which also may vary in time and space.

An everyday experience is that such a continuum, a speech, is segmented by the ear (and brain's capabilities) into small units which, for instance, can be written down as a sequence of letters or may be processed in other ways.

In the 1920's, some people longed for a similar but more accurate description of sound units used in speech. The advent of phonetics:

The goal here is to include pronunciation into the writing process such that, e.g., non-native speakers may imitate words of a foreign language properly.

This ansatz may be very prolific for tasks like classification and seems to be a natural starting point for further proceedings.

Following the general usage, classes of phonetic sounds, *phones*, will be indicated by a symbol enclosed in square brackets, e.g. [uə] as in the pronunciation of 'actual', [ai] as in 'lie', [ʌ] as in 'but' or [æ] as in 'cat'; by contrast a *phoneme* which will be denoted by a symbol enclosed within virgules (slashes), which is a minimal distinctive unit of a *language*, i.e. 'the smallest meaningful psychological unit of sound'.

There are over a hundred different phones recognised as distinctive by the *International Phonetic Association* (IPA) and transcribed in their International Phonetic Alphabet [IPA63]. These symbols will also be used in this thesis.

Example 2.0.1. (i) Consider the phones [t] and [f]. These are in German also phonemes, /t/,/f/ since the sounds [tiʃ] and [fiʃ] corresponds to different words, i.e. have different meaning (table and fish, resp.).

The same argumentation can be led for the *minimal pair* [sət] and [pət], which appear to differ only in their initial consonants [s] and [p]. Since these words are recognised as distinct by an Englishmen, i.e. they are meaningfully different in that language, /p/ and /s/ must be phonemes.

(ii) On the other hand, the different phones of 'l' in the words /wʊl/ (wool) and /laif/ (life) - in the first case it is a dark L and in the second a light L - are meaningless in English, which is already expressed by the corresponding phoneme notation, /l/.

This is not the case in Turkish. Dark 'L' and light 'L' are phonemes since they lead to meaningful differences, in particular, there are such minimal pairs, words which only differs in one phone and have different interpretation.

In Korean, for instance, the phones [r] and [l], which are of course two different sounds, i.e. have distinct physical entities as frequency for example, belong to the same phoneme!

(iii) Such a differentiation may be of some importance in classification tasks, too.

The German word *Notruf!* which stands synonymously for *emergency, call the doctor/police!* is of course different from a word which is perceived as [mo:tru:f]. However, since 'Motruf' does not make any sense, or generally speaking, if that word would not be part of a small dictionary, say consisting of five words, the classical phonemes /m/ and /n/could be identified with each other.

This could lead to a more robust (w.r.t noise) recognition and classification.

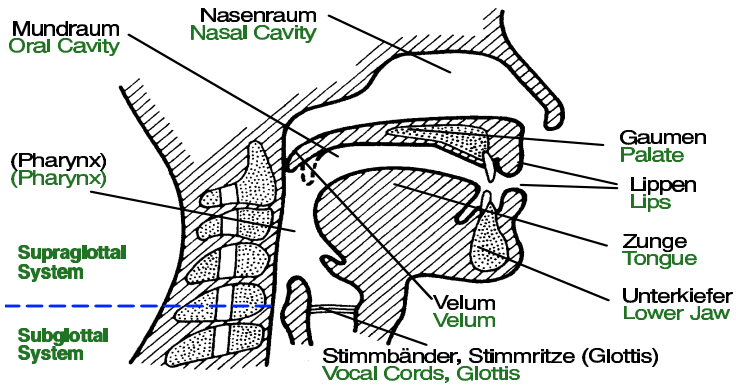

Fig. 2.1: Anatomic view of speech organs, cf. [Hes05].

(iv) That is also why the amount of phonemes varies from language to language. In English , the number of phonemes estimates typically range from 40 to 45 whereas Pirahã has only 10 and !Xóõ approximately 141, cf. `http://en.wikipedia.org/phoneme`.

'Phoneme' is an abstract mental construct. Thus, any *physical* property in the signal - like frequency - is referred to a *phone*.

In contrast, *phoneme* is the term to use if a sound is *interpreted* in the native speaker's mind. However, enough about phonemes for the time being.

2.1 Properties of (human) Speech

The intention of this section is to give a very short introduction as well as a foundation for different technical words typical in the phonetic community. For further reading, please check also other literature, e.g. [Hes05] which was naturally abridged here.

The subsequent section will also explain why the author believes that speech signals should be analysed in that way as it is done in Chapter 6. It is natural to study first the creation of speech-like signals in order to decide subsequently which characteristics of speech are necessary for the different classification tasks of concern.

In principle, any production of speech can be decomposed in two steps: *excitation* and *signal shaping*.

2.1.1 Sources of sound

Human beings are capable of quite different sounds. In speech however, there are primarily only three basic forms of excitation: *Voiced, Voiceless and Transient* excitation, namely.

Voiced excitation is a quasi-periodic, non-sinusoidal vocal cord vibration variable in its amplitude and frequency.

Pulmonary air flow passing the vocal cords in the larynx is periodically interrupted by the vibration of much the same cords.

The space between the vocal cords, called *glottis* is of much smaller cross-section compared to the cross-section below and above the larynx (cp. Figure 2.1). In fact, that spot is considered to be the narrowest of the entire speech organs (from lungs to radiation from the mouth) subdividing the tube into the subglottal (lungs, bronchi, trachea to larynx) and supraglottal system (pharynx, oral and nasal cavity) such that according to aerodynamics the velocity of flowing air stream is highest at that spot compared to anywhere else in the tube.

Assume that the vocal cords are flexed, hence, the glottis is closed (see Figure 2.2, (top), state (1-3)). If the difference in air pressure in the subglottal system and the atmospheric air pressure outside the speaker's body, for short: subglottal pressure, is sufficiently high in order to open the glottis, a stream of air coming from the lungs begins to flow at a relatively high speed, fast accelerating, through this small hole (cf. Figure 2.2, states (4-6)).

As soon as this begins, Bernoulli's force, – named after Daniel B. – acting on the vocal cords perpendicular to the air flow, grows gradually and embodies itself as an underinflation which necessitates the cords to move backwards to the starting position. In this short period of time the air stream gets faster and faster as the glottis became smaller which involves an increase of Bernoulli's force at a higher rate which again accelerates the closing of the glottis and so on. The whole closing process is therefore of a relatively short duration.

The air stream ceases abruptly to flow since the superposition of both, resetting force of the vocal cords and Bernoulli's force exceeds the opposed force resulting from subglottal overpressure, Figure 2.2, state (7).

Due to elasticity of the tissue, the cords keep moving. First, state (8), towards the centre, and then, like a bouncing ball, away, state (9), such that the glottis re-opens and due to little overpressure another air stream begins to flow.

Another cycle emerges (cf. also [vdB58]). The abrupt glotteral closing is also responsible for the presence of frequencies in the range of kHz. The averaged duration of one cycle is termed as *fundamental period* T_0 and the corresponding *fundamental frequency* F_0, or equivalently *pitch*, is then the reciprocal of T_0, i.e. $F_0 = T_0^{-1}$.

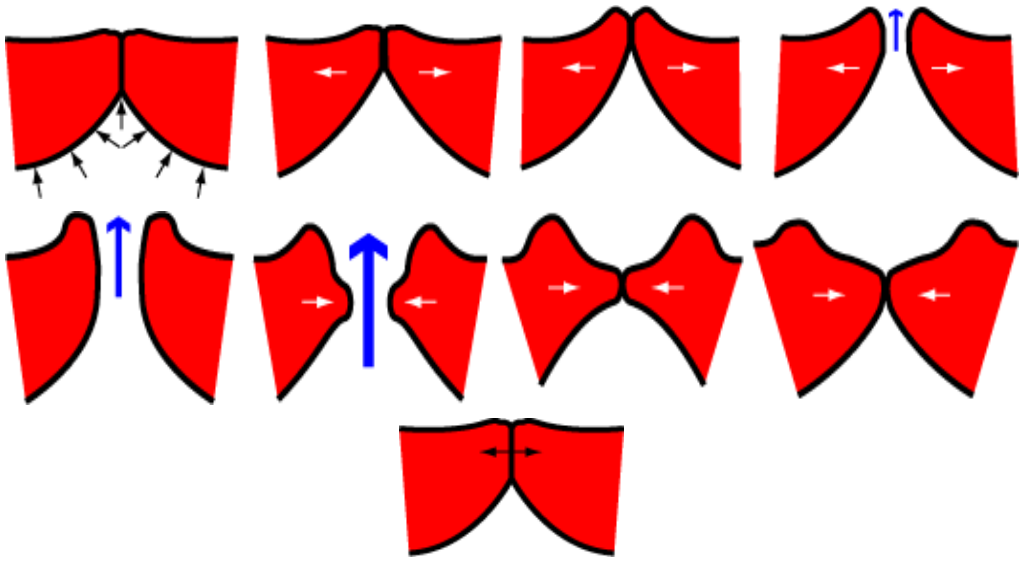

Fig. 2.2: One-cycle movement of Vocal cords. Corresponding arrows are, blue: air flow; black: acting force; white: direction of movement. Chronological order of occurrence: top, left to right, bottom, left to right.

Voiceless excitation occurs when the air stream (on ex-/inhalation - from or to the lungs) flows through an *open* glottis passing a constriction in the oral cavity or pharynx (see Figures 2.1 and 2.6) such that due to higher friction in this area turbulences appear with characteristic high frequency noise, coloured typically for the different places of origin.

Analogously to *voiced* excitation it is a stationary process and lasts as long as air streams. Both kind of excitations may occur in parallel (for instance, voiced fricatives like [ʒ] are produced by such an *mixed* excitation).

Transient excitation is naturally a non-stationary process. It is characterised by an occlusion phase, a pause where every acoustic signal is interrupted for a certain amount of time (20 - 100 ms). The sudden release of the congested air lasting only for 20 - 100 ms is perceived as a plosion noise. In European languages each plosion sound is an *explosion* sound (in contrast to some non-European languages with *click*-sounds resulting from implosions).

Again, voiced and transient excitation may coincide but there is always an occlusion phase which at most permits a slight vocal cord vibration, a so-called *voice bar*. Each subsequent sound is combined with the plosion.

This discussion yields already a first characterisation of sounds, cf. Figure 2.3. Quasi-periodic parts originating from voiced excitation, noise-like form of signal coming from turbulent flows typically for voiceless excitation

and a certain signature in time (voice(-less) excitation, occlusion phase, release burst, voice(-less) excitation) indicating a transient excitation can be easily recognised in such plots as in Figure 2.3.

Subplot (b), Figure 2.3, shows a quasi-periodic signal. Here, the fundamental frequency F_0 is nearly 110 Hz mainly resulting from glotteral vibrations. An average of 125 cycles per second is typical for an adult male, and approximately twice as fast (250 Hz) for an adult female, giving rise to the sensation of pitch.

2.1.2 Signal shaping

Of course there is much more about producing comprehensible speech than just these three kinds of excitation.

The position of the tongue and lips, respectively, which continuously vary in time, primarily contribute to sounds like [l],[p],[a] or [o].

Articulation stands for the process of all possible speech organ's positions, movements and their close succession in time. Everything in the vocal tract above the glottis - without the nasal cavity - is a speech organ (tongue, lips, teeth, palate,...).

A single position or movement of at least one speech organ is termed an *articulatory gesture* (cf. also Figure 2.6 for some illustrated articulatory gestures). Any speech sound generating a phone is uniquely determined by the corresponding excitation and one or more articulatory gestures. This is the so-called *shaping* of sound.

A first basic subdivision of speech sounds is made via two categories: *vowels* and *consonants*. The first class is characterised by

- purely voiced excitation *and*
- absence of any occlusion and substantial constriction in the vocal tract (above glottis) *and*
- radiation of sound mainly from the mouth.

In contrast, consonants

- are not purely voiced *or*
- there is a substantial constriction or occlusion in the vocal tract.

For the sake of simplicity, the geometry of the vocal tract is considered to form a tube of a constant cross-section, a length ℓ of approximately $\ell = 17$ cm, for men, as claimed in [Hes05], opened at one (mouth) and closed (glottis) at the other end.

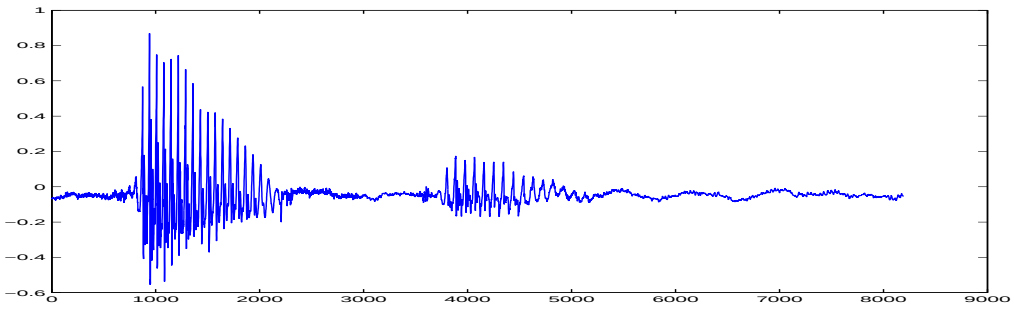

(a) enunciation of the German word ['fɛnstər]

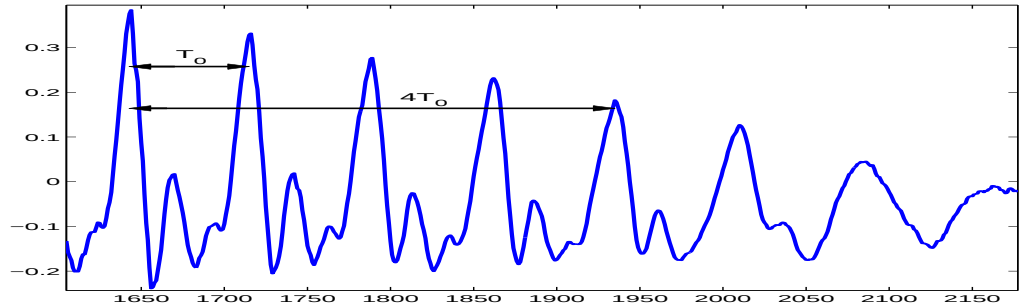

(b) voiced excitation; [ɛ]

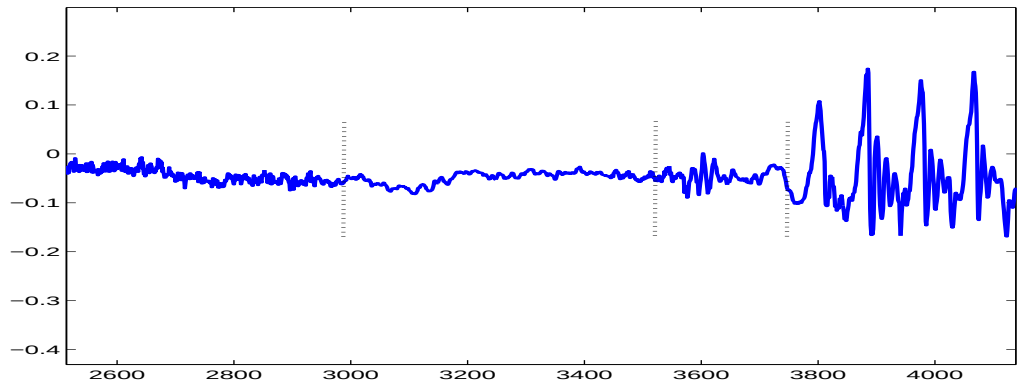

(c) voiceless, transient and voiced excitation: [s],[t],[ə]

Fig. 2.3: (a) Waveform of a 8kHz sampled signal of 1.02 seconds duration. This means in particular that every 150 μs the continuous function (here: pressure depending on time) is digitised with a constant bit rate such that in total, a sequence of 2^{13} discrete values is acquired. (b) This is a small part of the plot (a) corresponding to the phone [ɛ]. The fundamental period T_0 can be computed as $4T_0 = \frac{1935-1645}{8000} \approx 36$ms which is equivalent to a frequency of approximately 110 Hz. Subfigure (c) shows another extract from Plot (a). Dotted vertical lines illustrate the three different types of excitation. From left to first dotted boundary: voiceless excitation ([s]); occlusion phase is outlined by the timespan between first and second dotted line; followed by an explosion ([t] - between second and third dotted line) and concluding with a voiced excitation, [ə], between third dotted line and right boundary.

Furthermore, assume that the sound which is an acoustic signal, or more precisely a longitudinal wave, propagate with a constant velocity $c = 340$ m/s (meters per second). In fact, acoustic signals propagates as spherical waves. In that simplified case where the acoustic tube has impenetrable sides, i.e. infinite (acoustic) impedance[1], Z, defined as $Z = p/\nu$ – where p stands for pressure, force per unit area, and ν denotes the acoustic particle velocity – it suffices to restrict the direction of propagation to one dimension. Such waves are so-called *plane waves*.

Two boundary conditions for p and ν can be formed. At the open end, $p = 0$, and at the other, $\nu = 0$. This implies in particular that most frequencies will be attenuated. That frequencies of a signal which 'survive' are called *resonance frequencies* in physics. In this special setting it can be deduced that these are $f_k = \frac{(2k-1)c}{4\ell} = (2k-1)500$ Hz, for $k \in \mathbb{N}$, see Figure 2.4 for $k = 1, 2, 3$.

These overtones can be observed as peaks in a power spectrum, i.e. a representation of a signal rendered in frequency.

Such simplistic assumptions, especially that of a constant cross-section are in generally not fulfilled. Nevertheless, for the so-called *schwa*-sound, [ə], (read loud: 'schwa', then it is the sole voiced sound at the end), where the vocal tract behaves approximately as such a tube of constant cross-section, the first resonant frequency is near 500 Hz (cf. Figure 2.5, (b)).

The special about the human voice production is that it can 'colour' the radiated sound which is a result of modifying the geometry of the acoustic tube.

A simple reduction of the cross-section at some place yields by reflection and superposition different frequencies compared with f_k.

2.2 Formants

Formants are that frequency regions which contribute to a recognition of a voiced phone and will be denoted[2] by capital Fk, $k = 1, 2, \ldots$. They can be seen as relatively high energy parts of the signal – since otherwise it would be hard to perceive them as typical for that special vowel and so (by definition) they could not be a formant.

[1] Basically, a wave propagates unhindered and freely if the impedance is homogeneous, i.e. constant in space (and time). Whenever Z changes both, velocity and path (direction of propagation) changes. A change of impedance has then a *reflection* at that very spot as a consequence.

[2] The numbering is organised in an energy decreasing way, i.e. $F1$ is the most prominent formant perceived by the ears, $F2$ is the next crucial feature needed for association with a particular voiced utterance, etc.

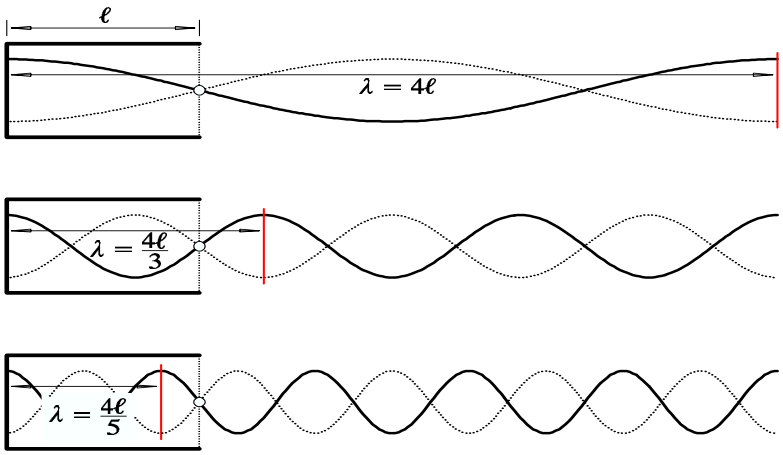

Fig. 2.4: Pressure p as a function of a space variable with boundary conditions $p(\ell) = 0$ and $p(0)$ maximal ($\Longleftrightarrow$ $\nu(0) = 0$). λ is the pertinent wavelength, i.e. $\lambda = \frac{c}{f}$. From top to bottom are the first three possible overtones with associated frequencies $f_{k=1,2,3}$, (after [Hes05]).

In order to simplify further considerations this term will be extended to all high energy parts above some threshold.

In practice, Fk varies in time – since the properties of the vocal tract may be changed by the position and movement of the speech organs – and in general vary widely from person to person (due to different geometry).

Furthermore, Fk cannot be considered as a multiple of another formant as it was the case for the overtones, f_k.

Voiced excitation is a relatively long-lasting phenomenon in speech. The spectral or frequency characteristics of a formant evolve as phones unfold and succeed one another. Formants which are relatively unchanging over time are found in the monophthong vowels[3], and the nasals[4].

More time-varying formants are found in the diphthong vowels[5] and the approximants[6], but in all cases the rate of change is relatively slow.

The inherent patterns in the first few formants, $k \leqslant n$, where n might be $n = 3, 4, 5$, are speaker independent and thus may be exploited for classification, at least for voiced parts and in particular for vowels.

The monophthong vowels have strong stable formants. In addition, these vowels can usually be easily distinguished by the frequency values of the first

[3] [iː] as in ‘b<u>ee</u>t’, [ɪ] as in ‘b<u>i</u>t’, [ə] as in ‘b<u>a</u>t’ [ʌ] as in ‘ab<u>o</u>ve’, [ɑ] as in ‘f<u>a</u>ther’, [u] as in ‘b<u>oo</u>t’, [ʊ] as in ‘b<u>oo</u>k’, ...

[4] [m] as in ‘<u>m</u>e’, [n] as in ‘<u>kn</u>ee’, [ŋ] as in ‘si<u>ng</u>’ or ‘su<u>ng</u>’

[5] [ei] as in ‘b<u>ay</u>’, [aɪ] as in ‘b<u>ey</u>’, [iʊ] as in ‘f<u>ew</u>’,...

[6] as in Figure 2.6, (a).

two or three formants.

For these reasons the monophthong vowels are often used to illustrate the concept of formants, cf. the so-called *formant chart*, Figure 2.5, where only $F1$ and $F2$ are plotted against each other, but it is important to remember that all voiced phones have formants, even if they are not as easy to recognise and classify as the monophthong vowel formants.

It is said (see e.g. [Hes05] and the references therein) that all higher formants, $k > n$ are speaker dependent features and rather contribute to a speaker identification.

The class of consonants consists of a huge mixture of voice-voiceless, voiceless-transient and pure voiceless, transient excitations in combination with a huge repertoire of articulatory gestures. Figure 2.6 illustrates some of them.

This class does not consist of purely voiced excited signals and it is therefore not as easy as for vowels to find features which are simply to describe and compute. Information about present frequencies alone does not suffice anymore!

Major tools for speech analysis used by people concerned with that field of study (phonology, phonetics,...) are *spectrograms* (also called *sonograms*) where the amplitude $|\mathcal{F}_g f|$ (in most cases coded by some color) of a windowed Fourier transformed signal f is plotted in the time-frequency plane. g denotes a window function and is mainly responsible for the time-frequency resolution and in particular which resolution is preferred over the other (see also Sections 3.6 and 4.1).

Despite its lack of adaptivity, see Section 4.4.2, the slow time development of formants can already be seen in such time frequency partitions, see Figure 2.7.

In general, the phonologist only distinguish between two kinds of spectrograms. The one uses a window spread of 3 - 8 ms (inverse of 333.33 - 125 Hz) and resolves therefore the individual cycle of the glottis vibration which is noticeable as a vertical structure in the plot, Figure 2.7, (a-b), Figure 2.8, (a) and left most subplots of Figures 2.10 and 2.11. Due to Heisenberg's uncertainty principle the frequency resolution is low.

Conversely, frequency resolution is preferred over time in case of bigger windows, typical in the range of 20 - 50 ms. In Figure 2.7, (c), the small 'burst' (resulting from the plosive[7] [t]) at the 0.3th second is not resolved which run counter to the resolution in frequency where even overtones are now visible.

[7]English has six bursts or explosive sounds produced by complete closure of the vocal tract followed by a rapid release of the closure - [p], [t], [k], [b], [d], [g].

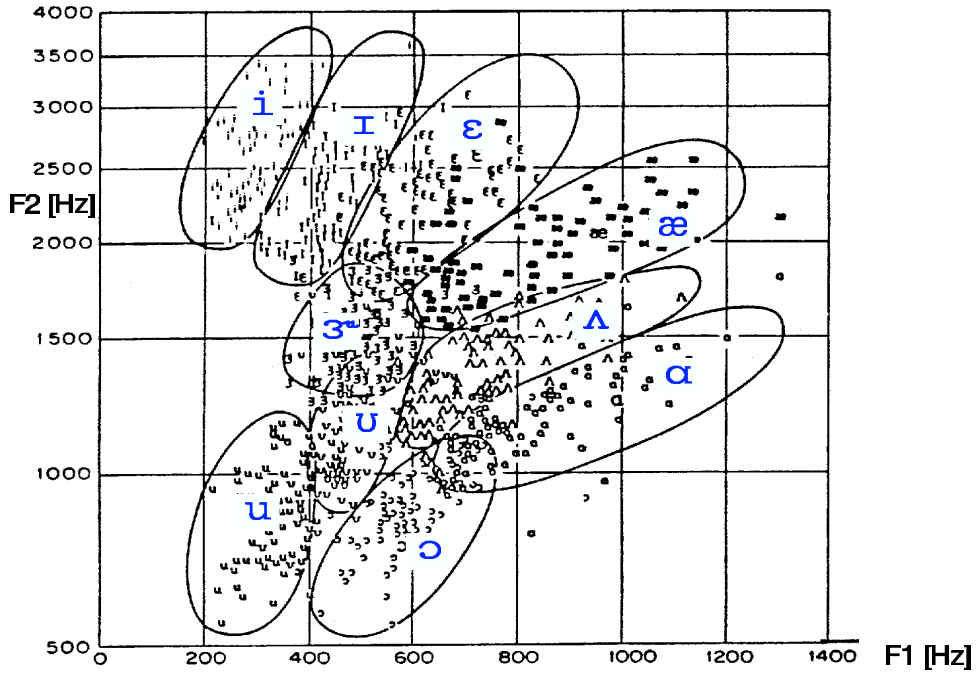

(a) General American English pronunciation - spoken by male, female and children; 76 speakers in total

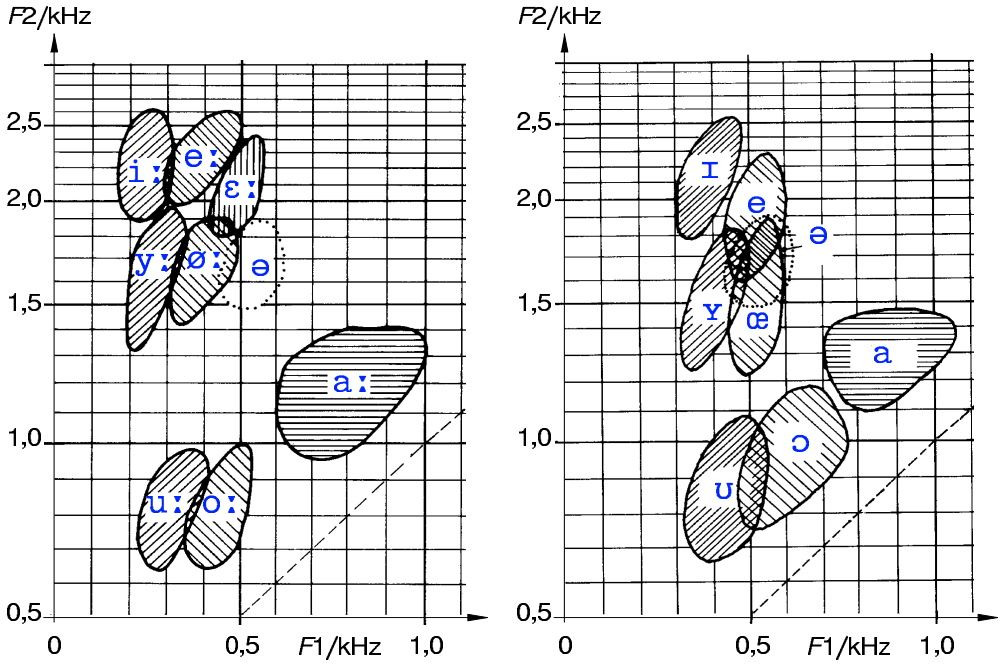

(b) German vowels - (left): long, (right) short vowels. Male and female speaker; 16 speakers in total

Fig. 2.5: Formant charts, [Hes05]. $F1$ vs. $F2$, (after [Hes05]). Note also in (b) the so-called *schwa*-sound, [ə], at $(F1, F2) = (0.5, 1.7)$ kHz, which is considered to be neutral, since the speech organs are in such a position where the simplistic assumptions of an acoustic tube are fulfilled (constant cross-section especially). Here, the theoretical derived frequency $F1 = 500$ Hz justifies in some sense the prior model.

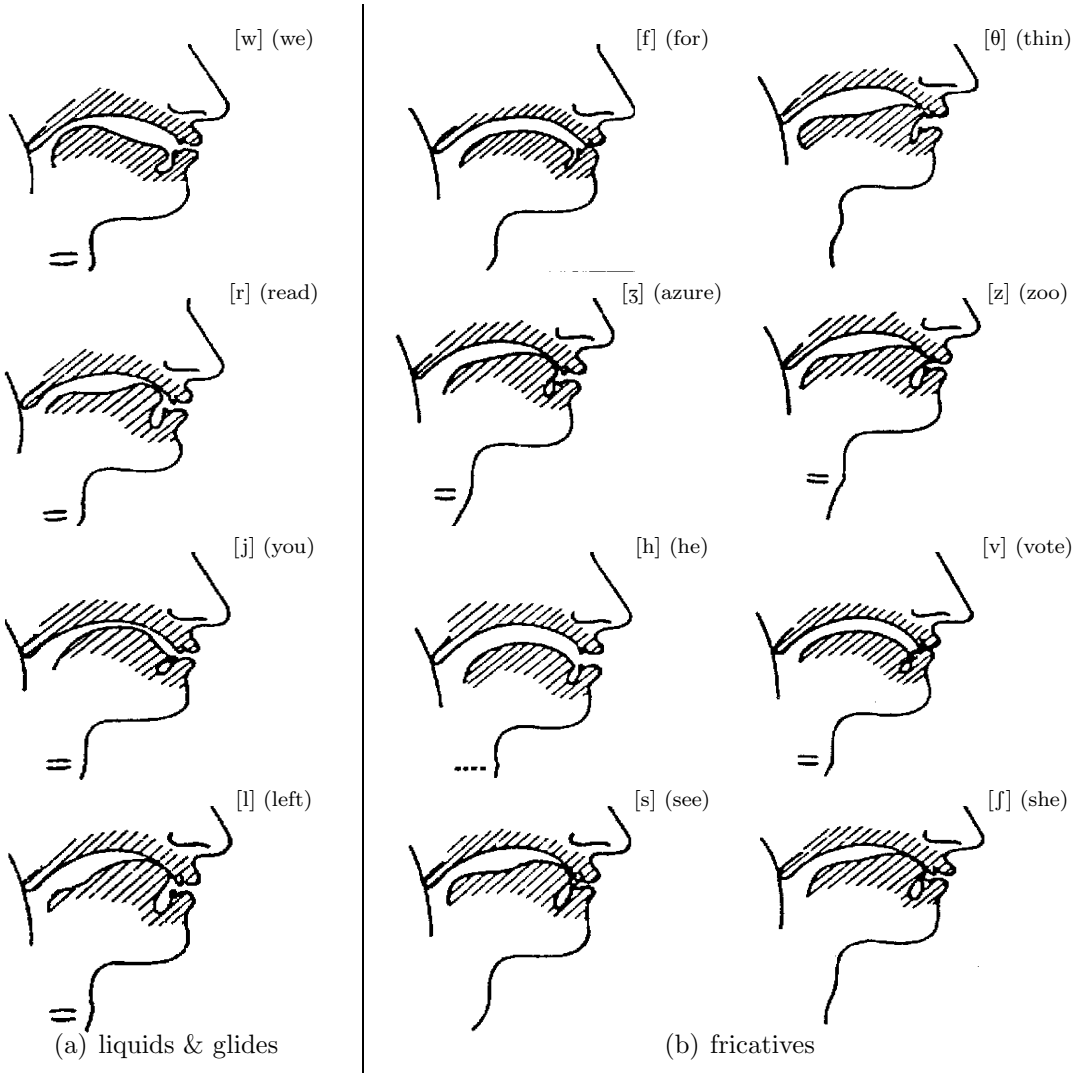

Fig. 2.6: Some articulatory gestures for liquids and fricatives (after [Hes05]).

The phase plots of the phrase [at:ha] also show the noise-like spectrum approximately between the 0.4th and 0.6th second. It is typical for fricatives (like [h] in 'hope') caused by turbulent flow of air in constricted areas.

Another example demonstrating the influence of the window support is shown in Figures 2.8 and 2.9. Here, the long vowels (each of approx. 1 s duration) [u:],[o:],[a:],[e:] and [i:] were pronounced by a male speaker and sampled at 16 kHz. One of the observations is that each vowel has distinctive formants. At least two of the formants per each vowel is noticeable as relatively high energetic stripes coloured from red over yellow to light blue, cf. Figure 2.8, (b). Moreover, the plot in Figure 2.8, (a), shows in addition to a frequency pattern a temporal one which can be deduced from the fact that the window support of g used by the windowed Fourier transform $\mathcal{F}_g$ is of such a small size that it even resolves the glotteral vibrations. The strongest temporal pattern is clearly that which corresponds to the first formant of [i:], red - yellow - red vertical stripes in the time interval ranging approximately from 3.7th to 5th second, Figure 2.8, (a). That precise formant has an estimated frequency of 300 Hz, seen from Figure 2.9, (c), and matches therefore the 'window-frequency' almost, $\frac{1}{3.1}$ ms^{-1} $\approx$ 322 Hz. The small discrepancy causes then a temporal aliasing, which is the observed temporal pattern!

Another conclusion which can be drawn from Figures 2.8 and 2.9 is that despite the long-lasting nature of the formants which hardly ever occurs in reality it is not nearly obvious which window support is optimal for formant extraction. Here, 'extraction' do not yet mean any algorithmic determination but a mere visual distinction made by the human eyes and brain. For instance, the second formant of the phones [e:] and [i:] is hard to detect and in the author's opinion is best perceived in Figure 2.8, (b) at $F2 \approx 1800$ Hz for [e:] and $F2 \approx 3$ kHz for [i:].

A concluding example, Figures 2.10 and 2.11, shows 8 kHz sampled realisations of the vowels [u], [o], [a], [e] and [i]. Here, 128 colours were used (Matlab's built-in functions '*colormap*' and '*jet*') and again the lowest 60% of all coefficients were thresholded and colored by the same 'colour': white, cf. Figure 2.11, (c).

As one can see, it is not intuitive how to choose the window size in order to obtain a good formant representation. A particular window size for one vowel might be optimal and for another quite the opposite.

Section 4.4.2 comes back to that difficulty and compares not only the influence of the window support of the windowed Fourier transform, see Figures 4.13, 4.14 and 4.16, but also the former with the discrete and continuous wavelet transform, cf. Figures 4.15 and 4.17.

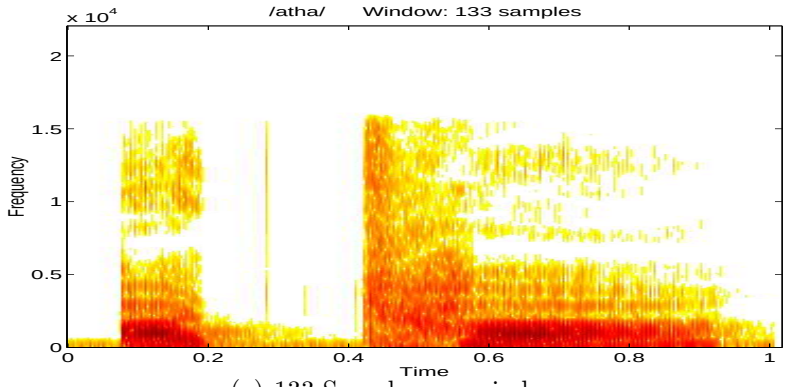

(a) 133 Samples per window

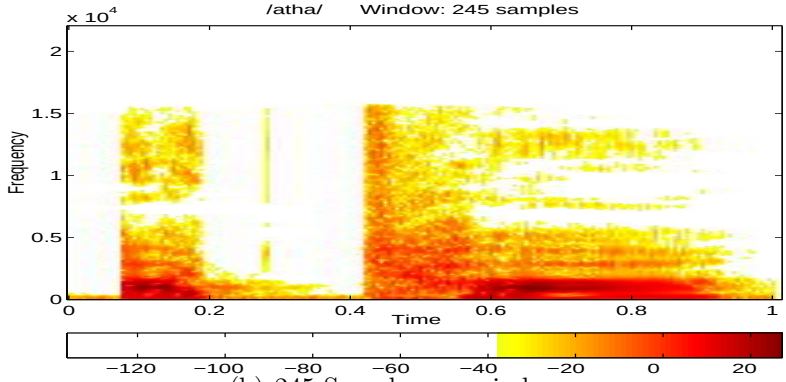

(b) 245 Samples per window

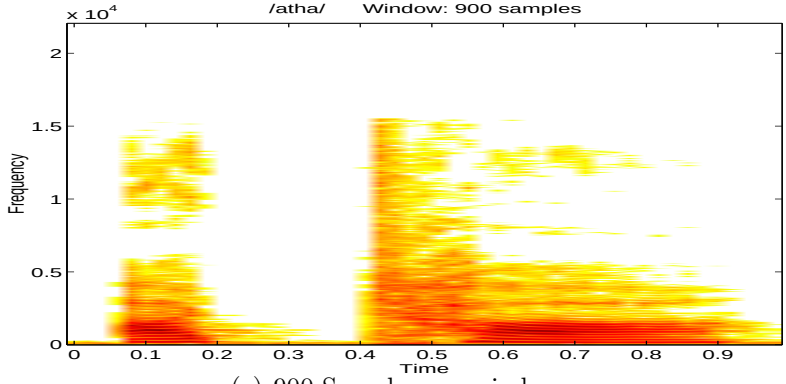

(c) 900 Samples per window

Fig. 2.7: Spectrogram of the phrase [at:ha] sampled with 44.1 kHz. The subplots (from top to bottom) correspond to different time spreads of the windowed function: 3, 5.6 and 20.4 ms. Note also the overtones in (c) visible as horizontal lines (dark red - red) whereas in (b) the formant structure is more evident. In (a) the window is too short in order to resolve frequencies. Such kind of plot was generated by Matlab's built-in function *specgram*. The color code is showed in the colour bar at the bottom of Subplot (b). For better illustration 60% of the lowest coefficients were thresholded (and are not resolved - white background !)

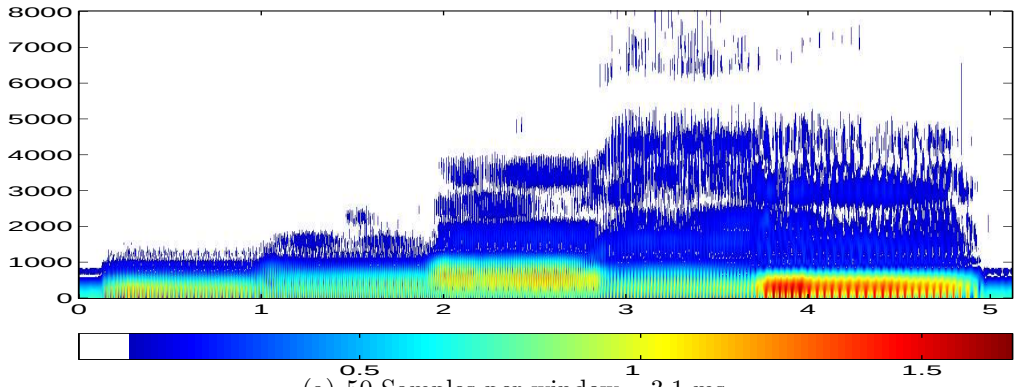

(a) 50 Samples per window – 3.1 ms

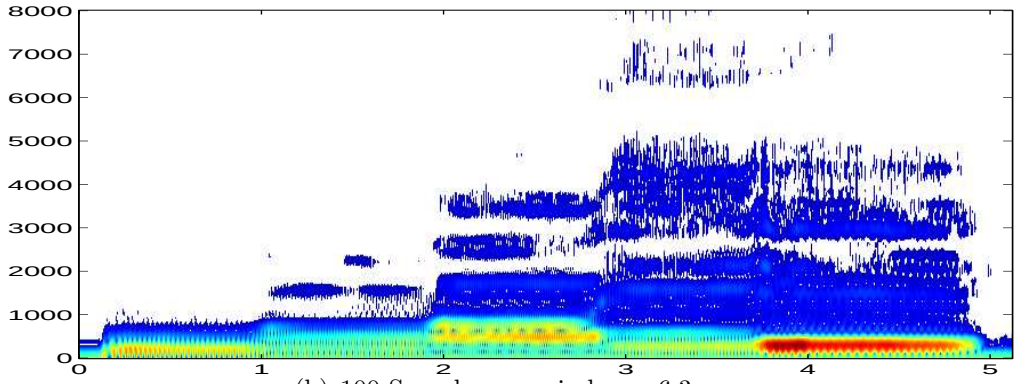

(b) 100 Samples per window – 6.3 ms

Fig. 2.8: see Figure 2.9

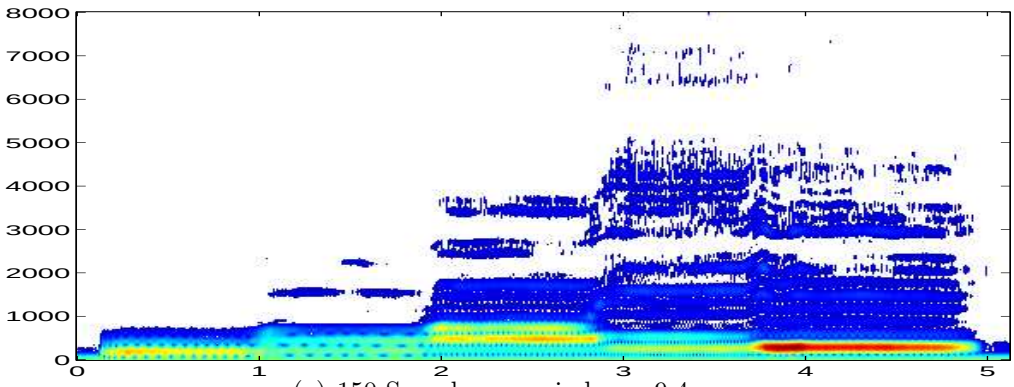

(a) 150 Samples per window – 9.4 ms

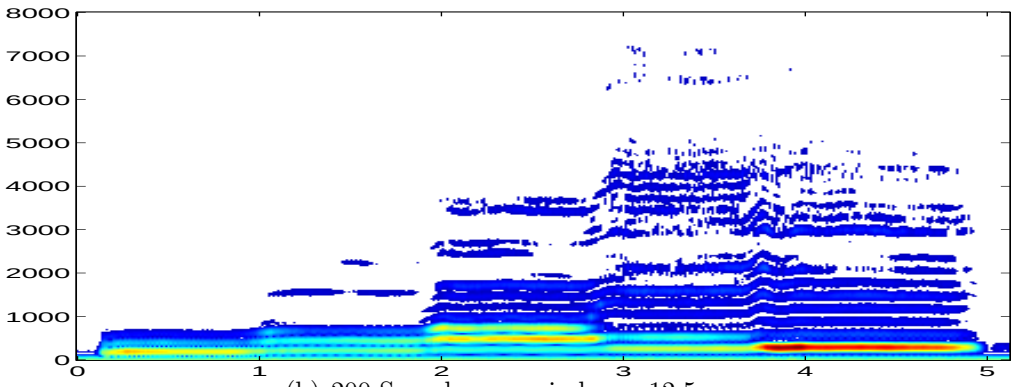

(b) 200 Samples per window – 12.5 ms

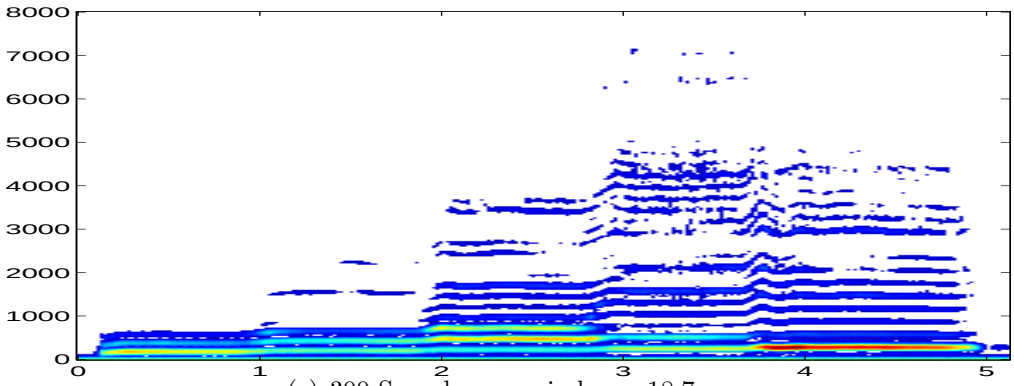

(c) 300 Samples per window – 18.7 ms

Fig. 2.9: Spectrogram of the phrase [uːoːaːeːiː]. 5% of the lowest coefficients were thresholded (and are not resolved - white background !).

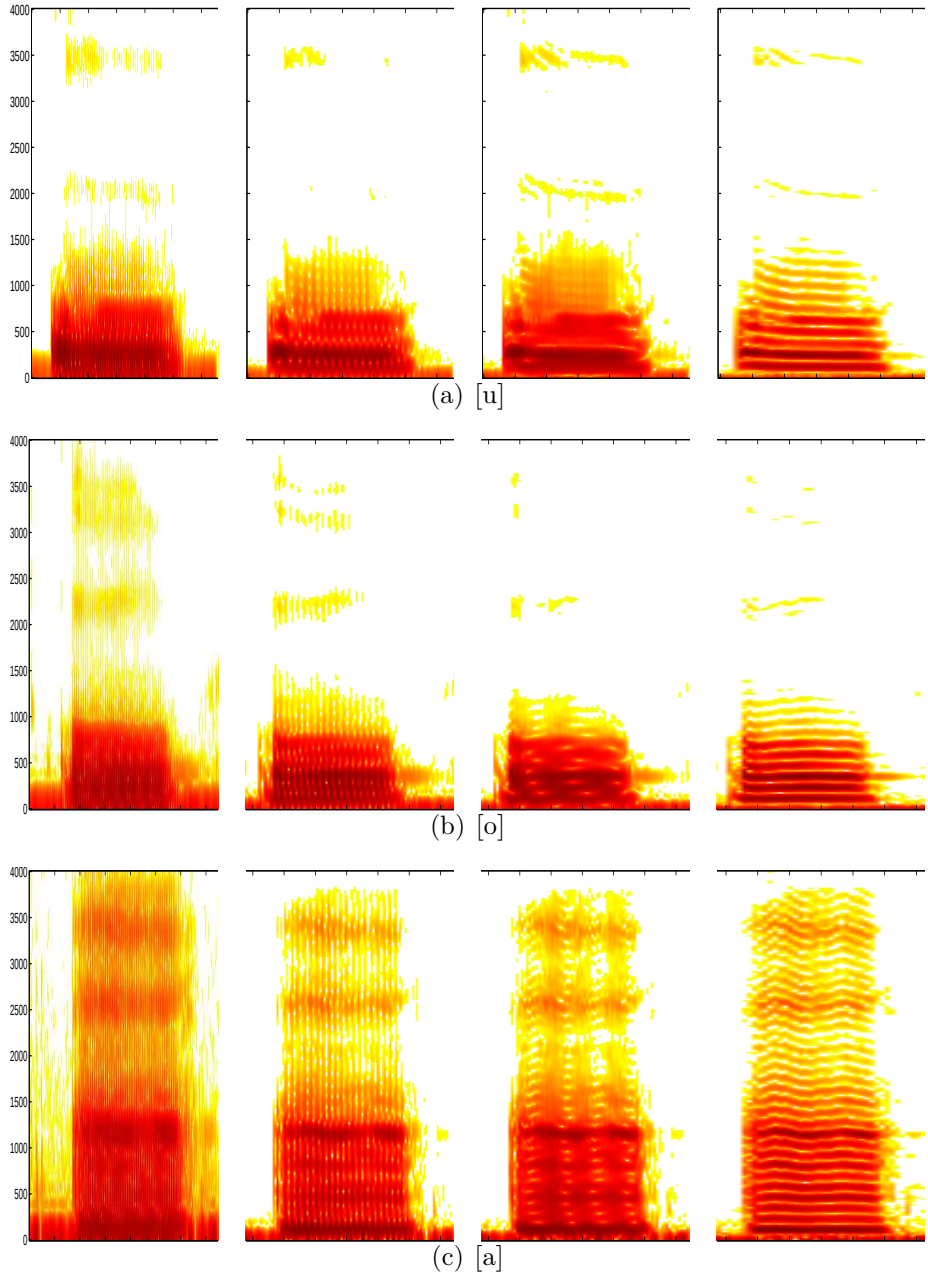

Fig. 2.10: In the second plot (from left) of (a), $F1$ and $F2$ can be restricted to the intervals $(F1, F2) \in (250, 450) \times (530, 700)$ which corresponds with Figure 2.5. Note that the last plot in (a) is not really of much use for formant extraction although the frequency resolution is much better than for the prior plots. The overtones do not allow to draw conclusions on which 'stripes' are pertinent to Fk. For the Subplot (c) the forth (from left) plot seems to be optimal for determining $F1 \in (500, 600)$ Hz and $F2 \in (1200, 1300)$ Hz. For more explanations see also Figure 2.11.

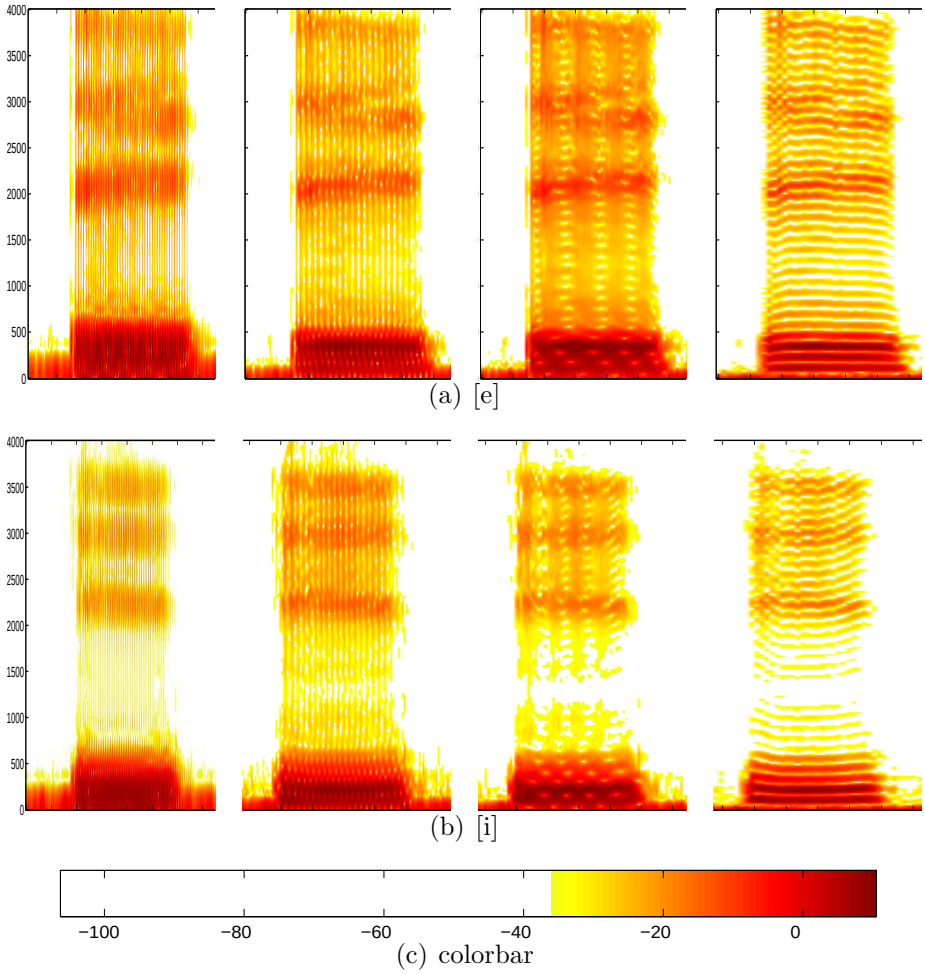

(a) [e]

(b) [i]

(c) colorbar

Fig. 2.11: from left to right: window sizes (in samples) are: 48, 96, 128, 256 corresponding to a window size of 6, 12, 16, 32 ms; the uncertainty in frequency can be estimated as the inverse, i.e. bigger than 166, 83, 62, 32 Hz; Subfigure (c) shows the corresponding colour bar. The frequency axis extends from 0 to 4 kHz.

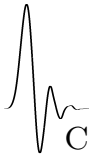

Chapter 3

Fundamentals

For the sake of completeness the following section will repeat the most basic definitions and theorems concerning the theory of Hilbert spaces. Elementary proofs which can be checked in appropriate literature dealing with functional analysis, e.g. [Wer95, Heu86], will be partly omitted.

3.1 Hilbert Spaces

Definition 3.1.1. Let $(\mathbb{X}, d)$ be a metric space.

(i) An arbitrary sequence $(x_n)_n \subset \mathbb{X}$ is called a *Cauchy sequence* $:\Longleftrightarrow$ $\forall \varepsilon > 0\ \exists\, N \in \mathbb{N}\ \forall\, n, m \geqslant N :\ d(x_n, x_m) < \varepsilon$.

(ii) $(\mathbb{X}, d)$ is called *complete* iff each Cauchy seq. $(x_n)_n$ is convergent *in* $\mathbb{X}$, i.e. $\exists\, \xi \in \mathbb{X} :\ d(x_n, \xi) \to 0$, as $n \to \infty$.

(iii) A normed and complete vector space $(\mathbb{X}, \|\cdot\|)$ is called a *Banach space*.

(iv) If additionally this norm $\|\cdot\| : \mathbb{X}^2 \to [0, \infty)$ is generated by a *positive semi-definite hermitian form* $\langle \cdot, \cdot \rangle : \mathbb{X}^2 \to \mathbb{K}$, i.e. $\|x\| := \sqrt{\langle x, x \rangle}$ then $(\mathbb{X}, \langle \cdot, \cdot \rangle)$ is called a *Hilbert space*.

(v) The corresponding mapping $\langle \cdot, \cdot \rangle$ is called *scalar* or *inner product*.

Example 3.1.2. (i) The space of k-times, $k \in \mathbb{N}$, continuously differentiable functions, i.e. $\big(\mathrm{C}^k(\mathbb{R}^n), \|\cdot\|_{\mathrm{C}^k}\big)$ and the space of Lebesgue k-integrable functions, $\big(\mathrm{L}^k(\mathbb{R}^n), \|\cdot\|_{\mathrm{L}^k}\big)$ are Banach spaces, where the

corresponding norms are:

$$\|f\|_{\mathrm{C}^k} := \sum_{i\leqslant k} \|f^i\|_{\mathrm{C}^0} < \infty,\ f^0 := f,\ \|f\|_{\mathrm{C}^0} := \sup_{x\in\mathbb{R}^n} |f(x)| < \infty,$$

$$\text{and} \quad \|f\|_{\mathrm{L}^k} = \left(\int_{\mathbb{R}^n} |f(x)|^k \,\mathrm{d}\mu(x)\right)^{1/k} < \infty, \quad \text{respectively.}$$

(ii) $(\mathrm{L}^2(\mathbb{R}^n), \langle\cdot,\cdot\rangle)$ is a Hilbert space, where the inner product is defined as $\langle f, g\rangle := \int_{\mathbb{R}^n} f(x)\overline{g(x)} \,\mathrm{d}\mu(x)$.

Remark 3.1.3. (i) Every integral is understood here and from now on always as a so-called Lebesgue integral:
Let $(M, \mathcal{M}, \mu)$ be a measurable space, i.e. M an arbitrary set with a σ-algebra $\mathcal{M}$ and a Lebesgue measure $\mu : \mathcal{M} \to [0, \infty]$. Furthermore, let $(\mathbb{Y}, d)$ be a metric space. Define the vector space of all step-functions as

$$\mathrm{T}(M, \mathbb{Y}) := \left\{ f :\ M \to \mathbb{Y} \,\middle|\, \begin{array}{l} \exists\, (a_k)_k \subset \mathbb{Y},\ k=1,\dots n, \\ \exists\, (M_k)_k \in \mathcal{M} : M = \dot{\bigcup}_{k\leqslant n} M_k \end{array} : f = \sum_{k\leqslant n} a_k \chi_{M_k} \right\}.$$

Then, defining the elementary integral for step functions $f \in \mathrm{T}(M, \mathbb{Y})$ as

$$\int_M f \,\mathrm{d}\mu := \sum_{k\leqslant n} a_k \mu(M_k),$$

it is possible to construct a semi-norm for $1 \leqslant p < \infty$ as

$$\|f\|_{\mathrm{semi},p} :\ \mathrm{T}(M, \mathbb{Y}) \to \mathbb{R}, \quad \|f\|_{\mathrm{semi},p} := \left(\int_M |f|^p \,\mathrm{d}\mu\right)^{1/p},$$

since $|f|^p \in \mathrm{T}(M, \mathbb{Y})$ holds for each $f \in \mathrm{T}(M, \mathbb{Y})$.

The completion – in the $\|\cdot\|_{\mathrm{semi},p}$-sense – of $\mathrm{T}(M, \mathbb{Y})$ is a complete vector space containing so-called *Lebesgue p-integrable* functions:

$$\mathscr{L}^p(M, \mathbb{Y}) := \left\{ f : M \to \mathbb{Y} \,\middle|\, \begin{array}{l} \exists\, (f_n)_n \subset \mathrm{T}(M,\mathbb{Y}) \text{ Cauchy sequence w.r.t. } \|\cdot\|_{\mathrm{semi},p}, \\ \exists\, N \subset M \text{ with } \mu(N)=0 \text{: } f \equiv \lim_n f_n \text{ on } M\setminus N \end{array} \right\}.$$

By identifying functions only on sets of non-zero measure the semi-norm property of $\|\cdot\|_{\mathrm{semi},p}$ extends to a norm $\|\cdot\|_p$, i.e.:

$$\mathrm{L}^p(M, \mathbb{Y}) := \mathscr{L}^p(M, \mathbb{Y})/\mathscr{N}^p = \left\{ f : M \to \mathbb{Y} \,\middle|\, f \text{ measurable},\ \|f\|_p < \infty \right\}$$

$$\text{where} \quad \mathscr{N}^p := \left\{ f \in \mathscr{L}^p(M, \mathbb{Y}) \,\middle|\, \|f\|_{\mathrm{semi},p} = 0 \right\} \quad \text{and}$$

$$\|f\|_p := \|f\|_{\mathrm{L}^p} := \|f + \mathscr{N}^p\|_p := \left(\lim_{n\to\infty} \int_M |f_n|^p \,\mathrm{d}\mu\right)^{1/p},\ (f_n)_n \subset \mathrm{T}(M, \mathbb{Y}).$$

By these constructions $(\mathrm{L}^p(M,\mathbb{Y}),\|\cdot\|_p)$ becomes a normed and complete vector space.

(ii) Analogously, the tuple $(\ell^p,|\cdot|_p)\,,\ 1\leqslant p<\infty$ with

$$\ell^p:=\Big\{x:=(x_n)_n\subset\mathbb{K}\,\Big|\,|x|_p:=\Big(\sum_{n\in\mathbb{Z}}|x_n|^p\Big)^{1/p}<\infty\Big\},$$

$$|x|_2:=\sqrt{\langle x,x\rangle},\quad \langle x,y\rangle:=\sum_{n\in\mathbb{Z}}x_n\overline{y_n}$$

is a Banach and for $p=2$ a Hilbert space.

(iii) Note that $\mathrm{L}^1\not\subseteq\mathrm{L}^2$ and $\mathrm{L}^1\not\supseteq\mathrm{L}^2$ which will be of some importance in defining the Fourier transform, for instance.

This is easily seen in the one-dimensional case for the functions:

$$f(x):=\begin{cases}1/\sqrt{x}, & x\in(0,1]\\ 0, & \text{else}\end{cases}\qquad g(x):=\begin{cases}1/x, & x\geqslant 1\\ 0, & \text{else}\end{cases}\quad.$$

Hence, $f\in\mathrm{L}^1(\mathbb{R})\setminus\mathrm{L}^2(\mathbb{R})$ and $g\in\mathrm{L}^2(\mathbb{R})\setminus\mathrm{L}^1(\mathbb{R})$.

Theorem 3.1.4. *Let $\mathbb{X}\neq\{0\}$ and $\mathbb{Y}$ be normed spaces.*

(i) A linear operator $T:\ \mathbb{X}\to\mathbb{Y}$ is continuous $\iff\ \exists\,C>0\,\forall\,x\in\mathbb{X}:$ $\|Tx\|_{\mathbb{Y}}\leqslant C\|x\|_{\mathbb{X}}$.

(ii) The space of all linear and bounded operators

$$\begin{aligned}\mathcal{L}(\mathbb{X},\mathbb{Y}):=&\Big\{T:\ \mathbb{X}\to\mathbb{Y}\,|\,T\text{ linear and continuous}\Big\}\\ =&\Big\{T:\ \mathbb{X}\to\mathbb{Y}\,|\,T\text{ linear and }\|T\|<\infty\Big\},\end{aligned}$$

with the operator norm defined as

$$\begin{aligned}\|T\|:=&\inf\Big\{C>0\,\Big|\,\|Tx\|_{\mathbb{Y}}\leqslant C\|x\|_{\mathbb{X}}\Big\}\\ =&\sup\Big\{\frac{\|Tx\|_{\mathbb{Y}}}{\|x\|_{\mathbb{X}}}\,\Big|\,x\in\mathbb{X},x\neq 0\Big\}=\sup_{\|x\|_{\mathbb{X}}\leqslant 1}\|Tx\|_{\mathbb{Y}},\end{aligned}$$

is a normed vector space and in case of $\mathbb{Y}$ being complete, it is even a Banach space.

(iii) $\forall\,T\in\mathcal{L}(\mathbb{X},\mathbb{Y}):\begin{cases}T\text{ is injective and }T^{-1}\in\mathcal{L}(\mathrm{ran}(T),\mathbb{X})\\ \iff\\ \exists\,c>0:\ c\|x\|_{\mathbb{X}}\leqslant\|Tx\|_{\mathbb{Y}}\quad\forall\,x\in\mathbb{X}\end{cases}$

(iv) A linear and bounded operator $T \in \mathcal{L}(\mathbb{X}, \mathbb{Y})$ *is called an* isomorphism $:\Longleftrightarrow T$ *is bijective and* $T^{-1} \in \mathcal{L}(\mathbb{Y}, \mathbb{X})$. *If* $\mathbb{X}$ *and* $\mathbb{Y}$ *are in particular complete, i.e. Banach spaces, then the inverse* T^{-1} *is automatically continuous due to the inverse mapping theorem, i.e.* $T^{-1} \in \mathcal{L}(\mathbb{Y}, \mathbb{X})$.

(v) A linear operator $T : X \to \mathbb{Y}$ *is called an* isometry $:\Longleftrightarrow \|Tx\|_{\mathbb{Y}} = \|x\|_{\mathbb{X}} \quad \forall\, x \in \mathbb{X}$.

(vi) A surjective isometric operator $T : \mathbb{X} \to \mathbb{Y}$ *is called* isometric isomorphism.

Note that an isometric operator T, *cf. point (v), implies* $T \in \mathcal{L}(\mathbb{X}, \mathbb{Y})$ *and* $T^{-1} \in \mathcal{L}(\mathrm{ran}(T), \mathbb{X})$*; and therefore, by additionally requiring surjectivity as in point (vi) the operator becomes an isomorphism.*

According to mathematical custom it is usual to reformulate complicated problems into a number of convenient and simple well understood objects which are easier to deal with. Analysing a signal $x \in \mathrm{L}^2(\mathbb{R})$ it is often useful to look at its not necessarily unique superposition (e.g. Eqs. (3.2b) or (3.8)) of such easy to handle atoms (i.e. the corresponding scalar products) where each of them partly describe the behaviour of x.

Basic properties like uniqueness, redundancy and numerical stability of such series will be described in the next three foregoing sections. Studies in frame theory may also be extended in [Chr06]

3.2 Bases

For the rest of this chapter consider $(\mathcal{H}, \langle\cdot,\cdot\rangle)$ as a separable Hilbert space and $\mathcal{I}$ as a countable index set if it is not explicitly stated otherwise.

Definition 3.2.1. (i) A series $(\sum_{i\in\mathcal{I}} x_j)_j$ is said to be *unconditionally converging* to $x \in \mathcal{H} :\Longleftrightarrow$ for each numbering $(i_n)_n$ of $\mathcal{I} : x = \sum_{n\geqslant 1} x_{i_n}$, i.e. reordering of summands does neither affect the convergence of the series nor the limit x.

(ii) Two families $(y_n)_n$, $(x_n)_n \subset \mathcal{H}$ are termed *biorthogonal* to each other $:\Longleftrightarrow \langle y_j, x_k\rangle = 0 \quad \forall\, j \neq k$.

(iii) A sequence $(x_n)_n \subset \mathcal{H}$ is an *orthogonal system* (abbr.: ogs) if it is biorthogonal to itself, i.e. $\langle x_j, x_k\rangle = 0 \quad \forall\, j \neq k$.

(iv) Iff an orthogonal system is additionally normalised, i.e. $\|x_j\|_{\mathcal{H}} = 1$, then $(x_n)_n$ is called an *orthonormal system* (abbr.: ons).

(v) A sequence $(x_j)_j \subset \mathcal{H}$ is said to be *complete* $:\Longleftrightarrow \forall\, x \in \mathcal{H}\ \exists\, (c_i)_i \subset \mathbb{K}$: $x = \sum_{i\in\mathcal{I}} c_i x_i$.

(vi) A complete ons is called an *orthonormal basis* (abbr.: onb).

Lemma 3.2.2 (Bessel inequality)**.** *For each orthonormal system* $(x_i)_{i\in\mathcal{I}} \subset \mathcal{H}$, $x \in \mathcal{H}$ *and* $\mathcal{J} \subset \mathcal{I}$*:*

$$\left\| x - \sum_{j\in\mathcal{J}} \langle x, x_j\rangle\, x_j \right\|^2 = \|x\|^2 - \sum_{j\in\mathcal{J}} |\, \langle x, x_j\rangle\, |^2, \tag{3.1a}$$

$$\|x\|^2 \geqslant \sum_{i\in\mathcal{I}} |\, \langle x, x_i\rangle\, |^2. \tag{3.1b}$$

Theorem 3.2.3. *Let* $(x_j)_j \subset \mathcal{H}$ *be an ons, then*

(i) $\exists\, (i_n)_n \subset \mathcal{I}$ *with* $\mathcal{H} \ni x = \sum_{n\geqslant n} c_{i_n} x_{i_n} \implies \mathcal{H} \ni x = \sum_{i\in\mathcal{I}} c_i x_i$ *i.e. unconditionally*

(ii) $\exists\, x \in \mathcal{H}$ *with* $\sum_{i\in\mathcal{I}} c_i x_i = x$, $c_i \in \mathbb{K} \implies (c_i)_{i\in\mathcal{I}}$ *is uniquely determined and given by* $c_i = \langle x, x_i\rangle$.

(iii) $\exists\, (c_i)_{i\in\mathcal{I}} \subset \mathbb{K}$ *with* $\sum_{i\in\mathcal{I}} |c_i|^2 < \infty \implies \sum_{i\in\mathcal{I}} c_i x_i \in \mathcal{H}$*, i.e. unconditionally*

Proof. All assertions follow by virtue of Bessel's equation (3.1a), linearity and continuity of the inner product. □

Corollary 3.2.4. *If* $(x_i)_{i\in\mathcal{I}} \subset \mathcal{H}$ *is an onb, then each of the following equivalent properties hold:*

$$\forall\, x \in \mathcal{H}\ \exists\, (c_i)_i \subset \mathbb{K} :\ x = \sum_{i\in\mathcal{I}} c_i x_i \tag{3.2a}$$

$$\forall\, x \in \mathcal{H} :\ x = \sum_{i\in\mathcal{I}} \langle x, x_i\rangle\, x_i \tag{3.2b}$$

$$\forall\, x \in \mathcal{H} :\ \|x\|_{\mathcal{H}}^2 = \sum_{i\in\mathcal{I}} |\, \langle x, x_i\rangle\, |^2 \tag{3.2c}$$

$$\forall\, x \in \mathcal{H} :\ \langle x, y\rangle = \sum_{i\in\mathcal{I}} \langle x, x_i\rangle\, \langle y, x_i\rangle \tag{3.2d}$$

Remark 3.2.5. Note that the equivalence of Eqs. ((3.2a) – (3.2d)) is already fulfilled by an arbitrary ons $(x_i)_i \subset \mathcal{H}$. If this system is even complete, i.e. is an onb then each of these claims is true.

In other words, if $(x_i)_i$ is an ons and $\overline{\operatorname{span}\{x_i | i \in \mathcal{I}\}}^{\|\cdot\|_{\mathcal{H}}} = \mathcal{H}$, then especially Eq. (3.2a) is true and thereupon Eqs. (3.2b) and (3.2c).

In this context, Eqs. (3.2c) and (3.2d) are called *Parseval identities*. In general, the Parseval identity can be understood as the invariance of inner products of two pre-Hilbert spaces $\mathcal{H}_{i=1,2}$ under an isometric operator, i.e. there exists a mapping $T:\ \mathcal{H}_1 \to \mathcal{H}_2:\quad \|Tx\|_{\mathcal{H}_2} = \|x\|_{\mathcal{H}_1} \Leftrightarrow \langle Tx, Ty\rangle_{\mathcal{H}_2} = \langle x, y\rangle_{\mathcal{H}_1}\ \forall\, x, y \in \mathcal{H}_1$.

Proof. (3.2a) $\Rightarrow$ (3.2b) $\Rightarrow$ (3.2c) is a direct implication of Theorem 3.2.3 and Eq. (3.2c) $\Rightarrow$ (3.2a) is again a consequence of Bessel's equality (3.1a).

It remains to show the equivalence of both Parseval identities, i.e.

$$\begin{aligned}&\text{Eq. (3.2c)} \Leftrightarrow \text{Eq. (3.2d) which itself is equivalent to}\\ &\|Tx\|_{\ell^2(\mathcal{I})} = \|x\|_{\mathcal{H}} \Leftrightarrow \langle Tx, Ty\rangle_{\ell^2(\mathcal{I})} = \langle x, y\rangle_{\mathcal{H}}\\ &\text{for some } T : \mathcal{H} \to \ell^2(\mathcal{I}), \quad x \mapsto (\langle x, x_i\rangle)_{i\in\mathcal{I}}.\end{aligned}$$

'$\Leftarrow$': Set $x = y$.
'$\Rightarrow$': Assume $\|Tx\|_{\ell^2(\mathcal{I})} = \|x\|_{\mathcal{H}}$, then $\forall\, \alpha \in \mathbb{K}$:

$$\begin{aligned}&\|x\|_{\mathcal{H}}^2 + 2\Re(\overline{\alpha}\,\langle x, y\rangle_{\mathcal{H}}) + |\alpha|^2\|y\|_{\mathcal{H}}^2\\ &\quad= \|x\|_{\mathcal{H}}^2 + |\alpha|^2\|y\|_{\mathcal{H}}^2 + \alpha\,\langle y, x\rangle_{\mathcal{H}} + \overline{\alpha}\,\langle x, y\rangle_{\mathcal{H}} = \|x + \alpha y\|_{\mathcal{H}}^2\\ &\quad= \|T(x + \alpha y)\|_{\ell^2}^2 = \langle Tx + \alpha Ty, Tx + \alpha Ty\rangle_{\ell^2}\\ &\quad= \|x\|_{\mathcal{H}}^2 + 2\Re(\overline{\alpha}\,\langle Tx, Ty\rangle_{\ell^2}) + |\alpha|^2\|y\|_{\mathcal{H}}^2\end{aligned}$$

The equality of both inner products arises from the fact that for $\alpha = 1$: $\Re(\langle x, y\rangle_{\mathcal{H}}) = \Re(\langle Tx, Ty\rangle_{\ell^2})$ and for $\alpha = \sqrt{-1}:\ \Im(\langle x, y\rangle_{\mathcal{H}}) = \Im(\langle Tx, Ty\rangle_{\ell^2})$. □

Example 3.2.6. (i) A well known orthonormal basis in $\mathrm{L}^2([a, b])$ is given by the trigonometric system

$$x_j(t) := \frac{e^{2\pi i j t/\ell}}{\sqrt{\ell}}, \quad \ell := b - a,\ i := \sqrt{-1},\ j \in \mathbb{Z}$$

Check ...

...orthonormality: $\forall\, j \neq k:\ j - k =: z \in \mathbb{Z}\backslash\{0\}$ and

$$\begin{aligned}\langle x_j, x_k\rangle &= \tfrac{1}{\ell}\int_a^b e^{2\pi i t(j-k)/\ell}\,\mathrm{d}t \overset{j\neq k}{=} \tfrac{\gamma}{2}\left(e^{\frac{2\pi i}{\ell}zb} - e^{\frac{2\pi i}{\ell}za}\right)\\ &= \tfrac{\gamma}{2}\left(e^{2\pi i z}e^{2\pi i z\frac{a}{\ell}} - e^{2\pi i z\frac{a}{\ell}}\right)\\ &= 0, \quad \gamma := \pi i z,\\ \|x_j\|_{\mathcal{H}} &= \tfrac{1}{\ell}\int_a^b e^0\,\mathrm{d}t = 1.\end{aligned}$$

The third equality is due to $\frac{b}{\ell} = 1 + \frac{a}{\ell}$.

... completeness: This is a straight implication of the Weierstraß approximation theorem known from analysis[1] and the fact that $\overline{\mathrm{C}_c^0(\mathbb{R}^n,\mathbb{R})}^{\|\cdot\|_{\mathrm{L}^p}} = \mathrm{L}^p(\mathbb{R}^n,\mathbb{R})$, where the prior Banach space contains all compactly supported continuous functions.

(ii) A second example which serves as an onb for $\mathrm{L}^2(\mathbb{R})$ was firstly described by Haar at the begining of the last century:

$$h(t) := \begin{cases} 1 & t \in [0,1/2) \\ -1 & t \in [1/2,1) \\ 0 & \text{else} \end{cases}, \quad h_{j,k}(t) := 2^{j/2} h(2^j t - k)$$

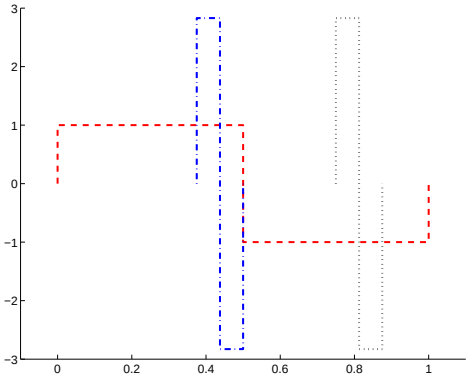

Fig. 3.1: $h_{0,0} = h$ is plotted as a dashed, $h_{3,3}$ as a dashed-dotted and $h_{3,6}$ as a dotted line

The orthonormality follows again directly by calculation and the substitution $\tau := 2^j t - k$:

$$\|h_{j,k}\|^2 = \int_{\mathbb{R}} 2^j |h(2^j t - k)|^2 \, \mathrm{d}t \overset{\tau := 2^j t - k}{=} \int_{\mathbb{R}} |h(\tau)|^2 \, \mathrm{d}\tau = 1$$

$$\langle h_{j,k}, h_{j,n} \rangle = \int_{\mathbb{R}} 2^j h(2^j t - k) h(2^j t - n) \, \mathrm{d}t = \int_{\mathbb{R}} h(\tau) h(\tau + k - n) \, \mathrm{d}\tau = 0,$$

since $\forall\, n \neq k : \overbrace{\mathrm{supp}(h)}^{=[0,1]} \cap \overbrace{\mathrm{supp}(h(\cdot + k - n))}^{=[n-k,n-k+1]}$ contains at most one point (for $n = k+1$) such that in total the intersection is of measure zero; on the other hand, $\forall\, n, k \in \mathbb{Z}$ and w.l.o.g. $j > m$:

$$\begin{aligned} \langle h_{j,k}, h_{m,n} \rangle &= \int_{\mathbb{R}} 2^{(j+m)/2} h(2^j t - k) h(2^m t - n) \, \mathrm{d}t \\ &= 2^{(m-j)/2} \int_{\mathbb{R}} h(\tau) h(\phi(\tau)) \, \mathrm{d}\tau = 2^{(m-j)/2} \int_{\mathbb{R}} h(\tau) c \, \mathrm{d}\tau = 0 \end{aligned}$$

[1] See [Heu02, pp. 112] for Weierstraßapproximation theorem for trigonometric polynomials.

with $\phi : [0,1) \to [\frac{k-n2^{j-m}}{2^{j-m}}, \frac{k-n2^{j-m}+1}{2^{j-m}}) =: I, \tau \mapsto \frac{\tau+k-n2^{j-m}}{2^{j-m}}$ and some $c \in \mathbb{R}$, since the image of ϕ, $\mathrm{ran}(\phi) = I$, is completely included in one of the disjoint intervals , i.e. $I \subset (-\infty, 0) \cup [0, 1/2) \cup [1/2, 1) \cup (1, \infty)$, and is constant on it, cf. Figure 3.1.

Completeness of $(h_{j,k})_{j,k\in\mathbb{Z}}$ is easily deduced from a wavelet approach, Section 4.2. Here, Corollary 4.3.10 implies completeness where the second and third item of that corollary are trivially fulfilled.

Summarising the properties of orthonormal systems (and bases, respectively) up to now it is clear (cf. Theorem 3.2.3, second item) that the values $\langle x, x_i\rangle$ determine uniquely an element $x \in \mathcal{H}$ and vice versa, considering an onb, each element $x \in \mathcal{H}$ is uniquely determined by its so-called *Fourier coefficients* $\langle x, x_i\rangle$.

Nevertheless, it is also well known that some of these 'decomposition properties'– similar to Eq. (3.2b) – can be achieved by larger sets $(x_i)_{i\in\mathcal{I}}$ which are neither orthonormal (as it is the case for Riesz bases) nor linearly independent (which is the general case for frames).

So, as a first generalisation of an onb a brief discussion about Riesz bases is given in the sequel. The presented theorems, Theorems 3.3.2, 3.3.3 and 3.3.4, will also be of much importance for Section 5.2.

3.3 Riesz Bases

Definition 3.3.1. (i) A sequence $(x_n)_{n\in\mathcal{I}} \subset \mathcal{H}$ is called a *Riesz basis in* $\mathcal{H} :\Longleftrightarrow (x_n)_n$ is complete in $\mathcal{H}$, $\exists\, A, B : 0 < A \leqslant B < \infty$ and for each finite $\mathcal{J} \subset \mathcal{I}$:

$$A \sum_{n\in\mathcal{J}} |a_n|^2 \leqslant \Big\| \sum_{n\in\mathcal{J}} a_n x_n \Big\|_{\mathcal{H}}^2 \leqslant B \sum_{n\in\mathcal{J}} |a_n|^2, \quad \forall a_n \in \mathbb{K}$$

The constants A and B are called *Riesz bounds*.

A Riesz basis can be seen as an image of an orthonormal basis in $\mathcal{H}$ under an isomorphism. This is shown in the next theorem.

Theorem 3.3.2. *The following assertions are equivalent:*

(i) $(x_n)_{n\in\mathcal{I}}$ *is a Riesz basis with bounds* A *and* B

(ii) For each orthonormal basis $(e_n)_n \subset \mathcal{H}$ *there exists an isomorphism* $T \in \mathcal{L}(\mathcal{H})$ *with* $A^{-1} \geqslant \|T^{-1}\|^2$, $\|T\|^2 \leqslant B$ *and* $Te_n = x_n$, $n \in \mathcal{I}$

So, a Riesz basis is indeed a basis since for all $x \in \mathcal{H}\, \exists!\, y \in \mathcal{H} :\ x = Ty$. For any onb $(e_i)_i$ in $\mathcal{H}$ there exists coefficients $(c_i)_i$ such that $y = \sum_i c_i e_i$ which implies by continuity of T: $x = Ty = \sum_i c_i Te_i = \sum_i c_i x_i$.

Proof. (i⇒ii) It will be showed:

- $\forall\, y \in \mathcal{H}\, \exists!\, a(y) \in \ell^2(\mathcal{I}) :\ y = \sum_{i\in\mathcal{I}} a_i(y) x_i$,
- $Ty := \sum_i \langle y, e_n\rangle\, x_i$ is bounded with
- the bounded inverse given by $T^{-1}y = \sum_i a_i(y) e_i$.

Since $(x_i)_i$ is complete for each element y of $\mathcal{H}$ there exists a sequence $(y_n)_{n\in\mathbb{N}} \subset \operatorname{span}\{x_i | i \in \mathcal{I}\}$, $y_n := \sum_{k\in\mathcal{J}_n} a_{k,n} x_k$ with $\|y - y_n\|_{\mathcal{H}} \xrightarrow{n\to\infty} 0$ where $\mathcal{J}_n \subset \mathcal{I}$ is an increasing index subset with n indices, i.e. $|\mathcal{J}_n| = n$.

Define $a_n := \left\{a_{n,k} \,|\, a_{n,k} := 0 \text{ for } k \notin \mathcal{J}_n\right\} \subset \ell^2(\mathcal{I})$. Then the 'Cauchy sequence property' of $(y_n)_n$ implies by the low Riesz bound that $(a_n)_n$ is a Cauchy sequence in $\ell^2(\mathcal{I})$, i.e. (w.l.o.g. $m \leqslant n$)

$$\sum_{k\in\mathcal{J}_n} |a_{m,k} - a_{n,k}|^2 \leqslant A^{-1} \left\| \sum_{k\in\mathcal{J}_n} a_{m,k}x_k - a_{n,k}x_k \right\|^2 = A^{-1} \|y_m - y_n\|^2 .$$

Completeness of $\ell^2(\mathcal{I})$ ensures then that $(a_n)_n$ converges in ℓ^2, say to $a(y) \in \ell^2(\mathcal{I})$, $\|a_n - a(y)\|_{\ell^2} \xrightarrow{n\to\infty} 0$.

Furthermore, it holds $y = \sum_{k\in\mathcal{I}} a_k(y) x_k$ since

$$\left\| y - \sum_{k\in\mathcal{I}} a_k(y) x_k \right\|_{\mathcal{H}} \leqslant \|y - y_n\|_{\mathcal{H}} + \left\| y_n - \underbrace{\sum_{k\in\mathcal{I}} a_k(y) k_k}_{=:z} \right\|_{\mathcal{H}} .$$

Due to the upper Riesz bound z is indeed in $\mathcal{H}$ since for any $(c_k)_k \in \ell^2$ the sequence $(z_n)_n$ with $z_n := \sum_{k\in\mathcal{J}_n} c_k x_x$ is a Cauchy sequence in $\mathcal{H}$ which also converges in $\mathcal{H}$ (otherwise $\mathcal{H}$ would be not complete).

Hence, the second sum in the triangle inequality can be estimated to

$$\|y_n - z\|_{\mathcal{H}}^2 \leqslant B \sum_{k\in\mathcal{J}} |a_{n,k} - a_k(y)|^2$$

which converges for $n \to \infty$ to zero.

Uniqueness of $a(y)$ follows from the lower Riesz bound. Suppose there exists $(b_k)_k \in \ell^2(\mathcal{I})$ such that $y = \sum_{k\in\mathcal{I}} b_k x_k$. Then, for w.l.o.g $n \leqslant m$ it

holds

$$\begin{aligned}\sum_{k\in\mathcal{J}_m} |a_k(y)-b_k|^2 &\leqslant A^{-1}\left\|\sum_{k\in\mathcal{J}_m} a_k(y)x_k - b_k x_k\right\|_{\mathcal{H}}^2 \\ &\leqslant A^{-1}\left\|\sum_{k\in\mathcal{J}_m} a_k(y)x_k - \sum_{k\in\mathcal{J}_n} b_k x_k\right\|_{\mathcal{H}}^2 \\ &\leqslant A^{-1}\sum_{k\in\mathcal{J}_m\setminus\mathcal{J}_n} \|a_k(y)x_k\|_{\mathcal{H}}^2 \xrightarrow[\Rightarrow m\to\infty]{n\to\infty} 0.\end{aligned}$$

By definition of T, $Ty = \sum_i \langle y, e_n\rangle\, x_i$, it follows $Te_n = x_n$ and $\|Ty\|^2 \leqslant B\sum |\langle y, e_n\rangle|^2 = B\|y\|$.

The operator $Sy := \sum_i a_i(y)e_i$ is well defined and is by lower Riesz inequality bounded, $\|Sy\|^2 \sum_i |a_i(y)|^2 \leqslant A^{-1}\|y\|^2$. Furthermore, $TSy = \sum_i a_i(y)Te_i = y \Rightarrow TS = \mathrm{id}$ and analogously $ST = \mathrm{id}$.

(ii⇒i) Since $T^{-1}y \in \mathcal{H}$ it follows that $T^{-1}y = \sum_i \langle T^{-1}y, e_n\rangle\, e_n$ and equivalently $y = TT^{-1}y = \sum_i \langle T^{-1}, e_n\rangle\, Te_n = \sum_i a_i(y)x_n$. From this relation, with $a_i(y) := \langle T^{-1}y, e_n\rangle$, the completeness of the system $(x_i)_i$ is an immediate consequence. Orthonormality of $(e_n)_n$ concludes the proof, i.e.

$$\begin{aligned}A\sum_{i\in\mathcal{J}_n}|a_i|^2 = A\Big\|\sum_{i\in\mathcal{J}_n} a_i e_i\Big\|^2 &= A\Big\|T^{-1}\sum_{i\in\mathcal{J}_n} a_i x_i\Big\|^2 \leqslant \Big\|\sum_{i\in\mathcal{J}_n} a_i x_i\Big\|^2 \\ &= \Big\|T\sum_{i\in\mathcal{J}_n} a_i e_i\Big\|^2 \leqslant B\Big\|\sum_{i\in\mathcal{J}_n} a_i e_i\Big\|^2 = B\sum_{i\in\mathcal{J}_n}|a_i|^2\end{aligned}$$

□

From the theorem above existence of a biorthogonal Riesz basis, a so-called dual basis can be deduced:

Theorem 3.3.3. *Let $(x_n)_n \subset \mathcal{H}$ be a Riesz basis with bounds A and B. Consider a fixed onb $(e_n)_n$ in $\mathcal{H}$ and an accompanying T as above. Then the following properties hold:*

$$\begin{aligned}\textit{Biorthogonality:}\quad & \exists!\,(\widetilde{x}_n)_n : \langle x_n, \widetilde{x}_m\rangle = \delta_{n,m} \\ \textit{Riesz basis:}\quad & \forall\, a_n \in \mathbb{K} : \frac{1}{B}\sum_{n\in\mathcal{J}}|a_n|^2 \leqslant \Big\|\sum_{n\in\mathcal{J}} a_n\widetilde{x}_n\Big\|_{\mathcal{H}}^2 \leqslant \frac{1}{A}\sum_{n\in\mathcal{J}}|a_n|^2 \\ \textit{Decom-/Superposition:}\quad & \forall y \in \mathcal{H} : \sum_{n\in\mathcal{I}}\langle y, \widetilde{x}_n\rangle\, x_n = y = \sum_{n\in\mathcal{I}}\langle y, x_n\rangle\,\widetilde{x}_n. \\ \textit{Adjoint of } T^{-1}:\quad & \widetilde{x}_n = (T^{-1})^* e_n\end{aligned}$$

In the end, an orthonormal basis is nothing else than a Riesz basis with surplus stipulations:

Theorem 3.3.4. *Let $(x_n)_n$ be a sequence in a separable Hilbert space $\mathcal{H}$. Then, (i) $\Longleftrightarrow$ (ii) $\Longleftrightarrow$ (iii), with*

(i) $(x_n)_n$ is an onb in $\mathcal{H}$

(ii) $(x_n)_n$ is a Riesz basis in $\mathcal{H}$ with $A = B = 1$

(iii) For each onb $(e_n)_n$ in $\mathcal{H}$ there exists an isomorphism T with $Te_n = x_n$ which is in addition unitary.

Proof. (i⇒ii)

Orthonormality implies $\| \sum_{i\in\mathcal{J}} a_i x_i\|^2 = \sum_{i,j\in\mathcal{J}} |a_i||a_j|| \langle x_i, x_j\rangle | = \sum_{i\in\mathcal{J}} |a_i|^2$ for arbitrary finite $\mathcal{J} \subset \mathcal{I}$, i.e.$A = B = 1$. $(x_n)_n$ is necessarily complete since $(x_n)_n$ is a basis.

(ii⇒iii)

By Theorem 3.3.2 there exists an isomorphism T with $Te_n = x_n$ and $\|T\|^2_{\mathcal{H}} \leqslant 1$, $\|T^{-1}\|^2_{\mathcal{H}} \leqslant 1$. Hence,

$$\|y\|_{\mathcal{H}} = \left\|T^{-1}Ty\right\|_{\mathcal{H}} \leqslant \|Ty\|_{\mathcal{H}} \leqslant \|y\|_{\mathcal{H}} \Rightarrow \|Ty\| = \|y\|$$

and analogously $\|T^*y\| = \|y\|$ such that by the Cauchy-Schwarz inequality

$$\Rightarrow \|y\|^2 = \langle Ty, Ty\rangle = \langle T^*Ty, y\rangle \overset{\text{C.S.}}{\leqslant} \|T^*Ty\|\,\|y\| = \|Ty\|\,\|y\| = \|y\|^2$$

which holds by the same calculation for $\|y\|^2 = \langle T^*y, T^*y\rangle \leqslant \|y\|^2$.

$$\Rightarrow T^*Ty = \mu_1 y \text{ and } TT^*y = \mu_2 y, \text{for some } \mu_{1,2} \in \mathbb{C}.$$

By $\|y\|^2 = \langle T^*Ty, y\rangle = \mu_1 \langle y, y\rangle = \mu_2 \langle y, y\rangle$ it follows that $\mu_1 = \mu_2 = 1$ which implies immediately $T^*T = TT^* = \mathrm{id}$.

(iii⇒i)

T is an isomorphism and by Theorem 3.3.2 $(x_n)_n$ is a Riesz basis, hence complete. The orthonormality follows by $\langle x_n, x_m\rangle = \langle Te_n, Te_m\rangle = \langle T^*Te_n, e_m\rangle = \langle e_n, e_m\rangle = \delta_{n,m}$. □

As for an orthonormal basis, a frame allows each element in the underlying Hilbert space to be written as an unconditionally convergent infinite linear combination of the frame elements; however, in contrast to the situation for a basis, the coefficients might not be unique.

Often it is impossible to construct an orthonormal basis having extra prescribed properties. It was observed early that some of the limitations can be removed by considering Riesz bases rather than orthonormal bases.

A frame is some kind of over-complete basis. The over-completeness of frames has already proved useful in the context of noise compression, and its use is currently investigated in several areas of signal processing.

3.4 Frames - Redundancy – Flexibility in the Representation

Definition 3.4.1. (i) An arbitrary system $(x_i)_{i\in\mathcal{I}} \subset \mathcal{H}$ is called a *frame in* $\mathcal{H}$ $:\Longleftrightarrow \exists\, A > 0,\ B < \infty\ \forall\, x \in \mathcal{H}$:

$$A\|x\|^2 \leqslant \sum_{i\in\mathcal{I}} |\, \langle x, x_i\rangle\, |^2 \leqslant B\|x\|^2 \tag{3.3}$$

A and B are the so-called *frame bounds*.

(ii) If $A = B$ then $(x_i)_{i\in\mathcal{I}}$ is called a *tight frame*.

(iii) *Normalised frames* are tight frames with $A = 1$.

Let $(x_i)_{i\in\mathcal{I}}$ be a frame in $\mathcal{H}$ then defining a kind of decomposition operator $T:\ \mathcal{H} \to \ell^2(\mathcal{I}),\ x \mapsto (\langle x, x_i\rangle)_{i\in\mathcal{I}}$ it is clear that

$$A^{1/2} \leqslant \|T\| \leqslant B^{1/2} \tag{3.4}$$

and due to Theorem 3.1.4 it follows that T is linear, bounded and injective and in particular possesses a continuous inverse on $\mathrm{ran}(T)$. Definition 3.4.1 allows therefore a stable decomposition into $(\langle x, x_i\rangle)_i$ and a stable reconstruction of the original $x \in \mathcal{H}$ from the values $\langle x, x_i\rangle\,,\ i \in \mathcal{I}$.

In order to understand this approach it is crucial to emphasise some differences and similarities between basis systems and frames.

Theorem 3.4.2. *Let* $dim(\mathcal{H}) = \tilde{n} < \infty$. *Then* $(x_i)_{i\leqslant n}$ *is a frame in* $\mathcal{H}$, $n \geqslant \tilde{n}$, $\Longleftrightarrow$ $\mathrm{span}\{(x_i)_i\} = \mathcal{H}$, *i.e.* $(x_i)_i$ *is a generating system of* $\mathcal{H}$.

Proof. Since $\dim(\mathcal{H}) < \infty$, the space $V :=\mathrm{span}\{x_i |\, i = 1, \ldots, n\}$ is closed in $\mathcal{H} \Rightarrow \exists\, W \subset \mathcal{H}:\ \mathcal{H} = V \oplus W.\ \forall\, x \in W:\ \langle x, x_i\rangle = 0\, \forall\, i \leqslant n \Rightarrow A\|x\|^2 \leqslant \sum |\, \langle x, x_i\rangle\, |^2 = 0 \Rightarrow x = 0 \Rightarrow W = 0$ and hence $V = \mathcal{H}$.

Vice versa, let $(x_i)_i$ be a generating system of $\mathcal{H}$.

$t:\ \mathcal{H} \to \mathbb{K}^n,\ x \mapsto \langle x, x_i\rangle_i$ is a linear mapping and therefore continuous (as $\mathcal{H}$ is of finite dimension) $\Rightarrow \exists\, B < \infty:\ \sum |\, \langle x, x_i\rangle\, |^2 \leqslant B\|x\|^2\, \forall x \in \mathcal{H}$.

t is injective since $tx = 0 \Rightarrow \langle x, x_i\rangle = 0\, \forall, i \leqslant n \Rightarrow x \in (\mathrm{span}\{x_i\})^{\perp}$. As $(x_i)_i$ is supposed to span all of $\mathcal{H}$ it follows that $x = 0 \Rightarrow t$ is inj. $\Rightarrow t^{-1}$ is cont. $\Rightarrow \exists\, A > 0$ with $A\|x\|^2 \leqslant \sum |\, \langle x, x_i\rangle\, |^2\, \forall\, x \in \mathcal{H}$ □

In particular, the elements of arbitrary frames are in general linearly dependent as it is clear from the next example:

Example 3.4.3. Consider the system of n-th complex roots $x_{j=0,\dots,n-1} := e^{2\pi ij/n}$, $x_j^n = 1$ where each element can be visualised as an arrow from the origin to the boundary of the unit circle in the complex plane $\mathbb{C}\widetilde{=}\mathbb{R}^2$ - cf. Figure 3.2.

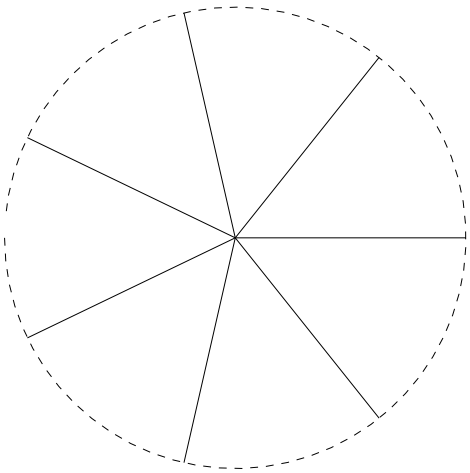

Fig. 3.2: Dashed line corresponds to the unit circle in $\mathbb{C}$ where $x_{j=0,\dots,6}$ are plotted as solid lines

Due to $1 - e^{4\pi ij/n} \neq 0 \,\forall\, n \geqslant 3$ it follows that

$$\sum_j \Re\left(e^{4\pi ij/n}\right) = \Re\left(\sum_j e^{4\pi ij/n}\right) = \Re\frac{1-e^{4\pi in/n}}{1-e^{4\pi i/n}} = 0,$$

which holds analogously for the imaginary part, and by

$$\sum_{j=0}^{n-1} |\,\langle x, x_j\rangle\,|^2 = \frac{n}{2}\overbrace{(a^2+b^2)}^{=\|x\|^2} + \frac{a^2+b^2}{2}\overbrace{\sum_j \cos(4\pi j/n)}^{=0} + ab\overbrace{\sum_j \sin(4\pi j/n)}^{=0},$$

where $x \in \mathbb{C}$, $a := \Re(x),\ b := \Im(x)$, it concludes in

$$\sum_{j=0}^{n-1} |\,\langle x, x_j\rangle\,|^2 = \frac{n}{2}\|x\|^2.$$

Although $\dim(\mathbb{R}^2) = 2$ the system $(x_j)_{j\leqslant n}$ constitutes a tight frame for each $n \geqslant 3$.

Strictly speaking, only two members of the frame $(x_j)_{j\leqslant n}$, $n \geqslant 3$ would be necessary to recover x from $\langle x, x_i\rangle_{i=1,2}$. The 'surplus information' coming from the outstanding frame vectors is sometimes useful for numerical stability. Given a particular frame it is possible to choose between these frame

vectors in order to obtain in some sense (i.e. w.r.t. some topology) the best generating system.

In this context it is usual to interpret the constant $\frac{n}{2}$ – and in general B/A – as a measure of redundancy.

Is it a mere suspicion which arises from this example that in case of a tight frame the frame bound says something about how far or close the frame itself fails to be a basis? The next theorem clarifies this context:

Theorem 3.4.4. *An arbitrary onb of a separable Hilbert space $\mathcal{H}$ is always a normalised frame in $\mathcal{H}$ and vice versa.*

Proof. '$\Rightarrow$': The Parseval equality, Eq. (3.2c), guarantees that $\forall\, x \in \mathcal{H}$: $\|x\|^2 = \sum_i |\langle x, x_i\rangle|^2$ which says that $(x_i)_i$ is in fact a normalised frame.

'$\Leftarrow$': It suffices to show the orthonormality: let $(x_i)_{i\in\mathcal{I}}$ be a norm. frame. Then $\forall\, x_i$:

$$1 = \|x_j\|^2 = \sum_i |\langle x_j, x_i\rangle|^2 = \underbrace{\|x_j\|^4}_{=1} + \sum_{j\neq i} |\langle x_j, x_i\rangle|^2 \Rightarrow \langle x_j, x_i\rangle = \delta_{i,j}$$

□

By the Riesz representation theorem there exists the adjoint operator of T, $T^* : \ell^2(\mathcal{I}) \to \mathcal{H}$ which can be interpreted as a synthesising operator and is represented via the frame $(x_i)_{i\in\mathcal{I}}$ as $\langle T^*c, x\rangle_{\mathcal{H}} = \langle c, Tx\rangle_{\ell^2} = \sum_j c_j\overline{\langle x, x_j\rangle} = \sum_j c_j \langle x_j, x\rangle$, i.e.

$$T^*c = \sum_{i\in\mathcal{I}} c_i x_i,\ c \in \ell^2(\mathcal{I}),$$

where the series converges in norm - see [Dau92, p. 101, note 4]. Due to the same theorem the adjoint operator is bounded by $A^{1/2} \leqslant \|T^*\| = \|T\| \leqslant B^{1/2}$. Hence, it is possible to define a hermitian operator by T^*T with some remarkable qualities:

Definition 3.4.5. The so-called *frame operator* $F : \mathcal{H} \to \mathcal{H}$ is defined as $F := T^*T$ with T prescribed by Eq. (3.4). The system $\widetilde{x}_i := F^{-1}x_i$ is called the *dual frame*.

Theorem 3.4.6. *For each arbitrary frame $(x_i)_{i\in\mathcal{I}}$*

(i) the frame operator F satisfies

$$A\langle x, x\rangle \leqslant \langle Fx, x\rangle \leqslant B\langle x, x\rangle \tag{3.5}$$

(ii) F *is an isomorphism and it holds*

$$B^{-1} \leqslant \|F^{-1}\| \leqslant A^{-1} \tag{3.6}$$

(iii) the family $\widetilde{x}_i = F^{-1}x_i$ *constitutes a frame with*

$$B^{-1}\|x\|^2 \leqslant \sum_i |\langle x, \widetilde{x}_i\rangle|^2 \leqslant A^{-1}\|x\|^2$$

(iv) $\widetilde{T}: \mathcal{H} \to \ell^2(\mathcal{I})$, $\widetilde{T}x := (\langle x, \widetilde{x}_i\rangle)_{i\in\mathcal{I}}$ *satisfies*

$$\widetilde{T} = TF^{-1} \qquad \widetilde{T}^*\widetilde{T} = F^{-1} \qquad \widetilde{T}^*T = T^*\widetilde{T} = \mathrm{id}$$

(v) $\widetilde{T}T^*$ *is the orthogonal projection operator from* $\ell^2(\mathcal{I})$ *onto* $\mathrm{ran}(T) = \mathrm{ran}(\widetilde{T})$ *and satisfies* $\widetilde{T}T^* = T\widetilde{T}^*$

Proof. This proof is borrowed from Ingrid Daubechies, [Dau92, pp.59].

ad i) Applying the definition of T one has $\sum_j |\langle x, x_j\rangle|^2 = \|Tx\|^2 = \langle T^*Tx, x\rangle$ and by the frame condition

$$A\|x\|^2 \leqslant \sum_i |\langle x, x_i\rangle|^2 = \langle Fx, x\rangle \leqslant B\|x\|^2.$$

ad ii) By (i) the linear, injective and continuous operator F is in particular bounded from below by $A > 0$. Hence

$\mathrm{ran}(F)$ **is closed in** $\mathcal{H}$ **:** Take a Cauchy sequence $(y_n)_n \subset \mathrm{ran}(F) \Rightarrow \exists\,(x_n)_n \subset \mathcal{H}$ with $Fx_n = y_n$ s.t.

$$\begin{aligned}\|x_n - x_m\|^2 &\leqslant A^{-1}\langle F(x_n - x_m), x_n - x_m\rangle \\ &\leqslant A^{-1}\Big\|F(x_n - x_m)\Big\|\|x_n - x_m\|\end{aligned}$$

$\Rightarrow \exists\xi \in \mathcal{H} : \xi = \lim_n x_n$. Since F is continuous it follows from $\mathrm{ran}(F) \ni F\xi = \lim_n Fx_n = \lim_n y_n$ that $(y_n)_n$ converges in $\mathrm{ran}(F)$.

F **is surjective:** It suffice to show: $\mathrm{ran}(F)^\perp = \{0\}$. Let $y \in \mathrm{ran}(F)^\perp$, i.e. $\forall\, x \in \mathcal{H} : \langle y, Fx\rangle = 0$ which holds in particular for $x = y$. So, $0 = \langle y, Fy\rangle \geqslant A\|y\|^2 \Rightarrow y = 0$.

Summing up, $\mathrm{ran}(F) = \mathcal{H}$, i.e. F is surjective and by Theorem 3.4.4 injective with a continuous inverse, hence F is an isomorphism. Furthermore, from Eq. (3.5) it follows

$$A\|F^{-1}y\|^2 = A\left\langle F^{-1}y, F^{-1}y\right\rangle \leqslant \left\langle FF^{-1}y, F^{-1}\right\rangle = \left\langle y, F^{-1}\right\rangle \leqslant \|y\|\|F^{-1}y\|,$$
$$\text{i.e. } \|F^{-1}y\| \leqslant A^{-1}\|y\| \text{ and in a similar way}$$
$$B^{-1}\|y\| \leqslant \|F^{-1}y\|.$$

ad iii) Since F and F^{-1} are selfadjoint operators it follows by

$$\begin{aligned}
&\langle x, \widetilde{x}_i\rangle = \left\langle x, F^{-1}x_i\right\rangle = \left\langle F^{-1}x, x_i\right\rangle \text{ that}\\
&\|\widetilde{T}x\|^2 = \sum_i |\left\langle x, \widetilde{x}_i\right\rangle|^2 = \sum_i |\left\langle F^{-1}x, x_i\right\rangle|^2 = \|TF^{-1}x\|^2\\
&\qquad = \left\langle TF^{-1}x, TF^{-1}x\right\rangle = \left\langle T(T^*T)^{-1}x, TT^{-1}(T^*)^{-1}x\right\rangle\\
&\qquad = \left\langle F^{-1}x, x\right\rangle . \qquad (3.7)
\end{aligned}$$

Hence, by $B^{-1}\|x\|^2 \leqslant \sum_i |\langle F^{-1}x, x\rangle|^2 \leqslant A^{-1}\|x\|^2$ it is clear that $(\widetilde{x}_i)_i$ constitutes a frame.

ad iv) Additionally, first and last equality of Equation (3.7) implies $\widetilde{T}^*\widetilde{T} = F^{-1}$. Moreover,

$$\begin{aligned}
&(\widetilde{T}x_i)_i = \langle x, \widetilde{x}_i\rangle = \left\langle F^{-1}x, x_i\right\rangle = (TF^{-1}x)_i \iff \widetilde{T} = TF^{-1}\\
&\widetilde{T}^*T = (TF^{-1})^*T = F^{-1}T^*T = \mathrm{id}\\
&\qquad \text{and } T^*\widetilde{T} = T^*TF^{-1} = \mathrm{id}
\end{aligned}$$

ad v) '$\mathrm{ran}(T) = \mathrm{ran}(\widetilde{T})$': $T = TF^{-1}F = \widetilde{T}F \Rightarrow \mathrm{ran}(T) \subset \mathrm{ran}(\widetilde{T})$
$\widetilde{T} = TF^{-1} \Rightarrow \mathrm{ran}(T) \supset \mathrm{ran}(\widetilde{T})$

projection let $y \in \mathrm{ran}(T) \Rightarrow \exists\, x \in \mathcal{H} :\ Tx = y$, $\widetilde{T}T^*y = \widetilde{T}T^*Tx = TF^{-1}Fx = Tx = y$
let $y \in \mathrm{ran}(T)^\perp \Rightarrow 0 = \langle y, Tx\rangle = \langle T^*y, x\rangle\ \forall\, x \in \mathcal{H} \Rightarrow \widetilde{T}T^*y = 0$

□

Corollary 3.4.7. *Each frame $(x_i)_i$ has a dual frame $(\widetilde{x}_i)_i$ s.t. $\forall\, x \in \mathcal{H}$:*

$$\sum_i \langle x, x_i\rangle\, \widetilde{x}_i = x = \sum_i \langle x, \widetilde{x}_i\rangle\, x_i. \qquad (3.8)$$

Moreover, $\forall\, x \in \mathcal{H}\ \exists\, c \in \ell^2(\mathcal{I})$ *with* $x = \sum_i c_i x_i$ *such that*

$$\|c\|_{\ell^2} \geqslant \sum_i |\, \langle x, \widetilde{x}_i \rangle\, |^2$$

with equality attained only for $c_i = \langle x, \widetilde{x}_i \rangle\ \forall\, i \in \mathcal{I}$*. If* $x = \sum_i \langle x, x_i \rangle\, y_i$*, then*

$$\sum_i |\, \langle y_i, y \rangle\, |^2 \geqslant \sum_i |\, \langle \widetilde{x}_i, y \rangle\, |^2 \quad \forall\, y \in \mathcal{H}$$

and ' $=$ ' $\iff$ $y_i = \widetilde{x}_i$*.*

Proof. Equation (3.8) is a straight forward relation of $\widetilde{T}^* T = \mathrm{id} = T^* \widetilde{T}$ where existence of the dual follows indirectly from Riesz representation theorem (c.f. the prelude of Definition 3.4.5).

It remains to show that the reconstruction and superposition of x by means of frames and the appropriate duals is the most economical one:

$$\text{Let } x = \sum c_i x_i = T^* c \text{ for some } c \in \ell^2(\mathbb{Z}) = \mathrm{ran}(T) \oplus \mathrm{ran}(T)^\perp,$$

i.e. $\exists\, a \in \mathrm{ran}(T), \exists\, b \in \mathrm{ran}(T)^\perp \big(\Rightarrow 0 = \langle T\cdot, b\rangle = \langle \cdot, T^* b\rangle \Rightarrow T^* b = 0\big)$ such that $c = a + b$. Since $\mathrm{ran}(T) = \mathrm{ran}(\widetilde{T}) \Rightarrow \exists\, y \in \mathcal{H} : c = \widetilde{T} y + b \Rightarrow x = T^* c = T^* \widetilde{T} y + T^* b = y$.

$$\text{Hence, } c = \widetilde{T} x + b \text{ and } \|c\|^2 = \|\widetilde{T} x\|^2 + \|b\|^2 = \sum_i |\, \langle x, \widetilde{x}_i \rangle\, |^2$$
$$\iff \|b\| = 0 \iff c_j = \langle x, \widetilde{x}_j \rangle\ \forall\, j \in \mathcal{I}.$$

The last inequality is derivable with similar considerations. □

Formula (3.8) is the main reason for considering frames, but it also immediately reveals one of the fundamental problems with frames. In fact, in order for (3.8) to be practically useful, one has to invert the frame operator F, which is difficult when $\mathcal{H}$ is infinite-dimensional. One way to avoid this difficulty is to consider tight frames, i.e., frames $(x_i)_i$ for which

$$\forall\, x \in \mathcal{H} :\ A\|x\|^2 = \sum_{i \in \mathcal{I}} |\, \langle x, x_i \rangle\, |^2 \text{ for some } A > 0.$$

Then, $\langle Fx, x \rangle = A\|x\|^2$, such that $F = \mathrm{id} A$ would imply

$$x = \frac{1}{A} \sum_{i \in \mathcal{I}} \langle x, x_i \rangle\, x_i \quad \text{for each } x \in \mathcal{H}.$$

3.5 Fourier transform

A heuristic approach to a fruitful operator $\mathcal{F}$ will suit as an introduction: Due to Example 3.2.6, $x_k(t) = (2\tau)^{-1/2} e^{i\pi \frac{k}{\tau} t}$ is an onb of $\mathrm{L}^2(I) \subset \mathrm{L}^1(I)$, $I := [-\tau, \tau]$ and therefore by Theorem 3.2.3 each square-integrable function with support in I can be expressed as a superposition of x_k with unique coefficients c_k, i.e.

$$\forall\, f \in \mathrm{L}^2(I) :\ f = \sum_{k\in\mathbb{Z}} c_k x_k, \quad c_k = \langle f, x_k \rangle\,.$$

Hence,

$$\begin{aligned} f(t) =& \sum_k \int_I f(s)\overline{x_k(s)}\ \mathrm{d}s\, x_k(t) \\ =& \frac{1}{2\pi} \sum_k \int_I f(s) e^{-i\omega_k s}\ \mathrm{d}s\, e^{i\omega_k t}\, \Delta\omega_k \end{aligned}$$

with $\omega_k := \frac{\pi k}{\tau}$, $\Delta\omega_k := \omega_k - \omega_{k-1} = \pi/\tau$ which have a striking resemblance to a Riemann's sum such that in the limit, $\tau \to \infty$,

$$f(t) = \frac{1}{2\pi} \int_{\mathbb{R}} \int_{\mathbb{R}} f(s) e^{-i\omega s}\ \mathrm{d}s\, e^{i\omega t}\ \mathrm{d}\omega$$

is expected.

This sketchy point of view clarifies why in the sequel the Fourier transform is defined first for functions living on $\mathrm{L}^1(\mathbb{R})$ and later as an extension to $\mathrm{L}^2(\mathbb{R})$.

Definition 3.5.1. The *Fourier transform* $\mathcal{F}$ is defined as

$$\begin{aligned} \mathcal{F} :\ & \mathrm{L}^1(\mathbb{R}) \to \mathrm{L}^1(\mathbb{R}) \\ & f \mapsto \frac{1}{\sqrt{2\pi}} \int_{\mathbb{R}} f(t) e^{-i\omega t}\ \mathrm{d}t =: \hat{f}(\omega) \end{aligned}$$

It is clear that $\mathcal{F}$ is a linear operator and applying Lebesgue's dominated convergence theorem it is even a bounded operator which maps each $f \in \mathrm{L}^1(\mathbb{R})$ to a continuous function $\hat{f}$ (cf. Eq. (3.9a)). The next theorem will be stated without proof (see [Erd03, pp. 212]) and serves as a motivation for the definition thereafter.

Theorem 3.5.2. *Let $f, g \in \mathrm{L}^1(\mathbb{R})$. Then*

$$\hat{f} \in \mathrm{C}_0(\mathbb{R}) \text{ with } \sup_{\xi\in\mathbb{R}} |\hat{f}(\xi)| \leqslant (2\pi)^{-1/2} \|f\|_{\mathrm{L}^1} \tag{3.9a}$$

$$\text{with } \hat{f} \in \mathrm{L}^1(\mathbb{R}) :\quad f(t) = (2\pi)^{-1/2} \int_{\mathbb{R}} \hat{f}(\omega) e^{i\omega t}\ \mathrm{d}\omega \ \text{ a.e.} \tag{3.9b}$$

$$\hat{f} = \hat{g} \Rightarrow f = g \ \text{ a.e.} \tag{3.9c}$$

Equation (3.9a) implicitly says that $\lim_{|\omega|\to\infty} \hat{f}(\omega) = 0$ which is also known as the *Riemann-Lebesgue-lemma*. The major tool in showing these relations is Lebesgue's dominated convergence theorem.

The two last claims justify Definition 3.5.3, i.e. Eq. (3.9c) guarantees that the mapping $\mathcal{F}^{-1}$ is indeed well defined and the prior equation explains why relation (3.9b) can be understood (at least in L^1-sense) as the inverse of $\mathcal{F}$.

Definition 3.5.3. The *inverse Fourier transform* is defined by

$$\mathcal{F}^{-1} : \mathrm{L}^1(\mathbb{R}) \to \mathrm{L}^1(\mathbb{R}), \quad f \mapsto (2\pi)^{-1/2} \int_{\mathbb{R}} f(\omega) e^{i\omega\cdot} \,\mathrm{d}\omega$$

The next theorem summarises some useful properties of $\mathcal{F}$ which will be expedient in later considerations. Here, the notation $t^k f \in \mathrm{L}^1(\mathbb{R})$ means that the mapping $t \mapsto t^k f(t)$ belongs to $\mathrm{L}^1(\mathbb{R})$.

Theorem 3.5.4 ([Erd03, pp. 218])**.** *Let $n \geqslant 0$ and $f \in \mathrm{L}^1(\mathbb{R})$. Then*

$$t^n f \in \mathrm{L}^1(\mathbb{R}) \Rightarrow \begin{array}{l} \hat{f} \in \mathrm{C}^n(\mathbb{R}) \text{ and} \\ \hat{f}^{(n)} \in \mathrm{C}_0(\mathbb{R}), \end{array} \tag{3.10a}$$

$$\text{with } \left(\tfrac{\mathrm{d}}{\mathrm{d}\omega}\right)^n \mathcal{F}(f)(\omega) = \mathcal{F}\Big((-it)^n f\Big)(\omega); \tag{3.10b}$$

$$f \in \mathrm{C}(\mathbb{R}),\ \omega^n \hat{f} \in \mathrm{L}^1(\mathbb{R}) \Rightarrow \begin{array}{l} f \in \mathrm{C}^n(\mathbb{R}) \text{ and} \\ f^{(n)} \in \mathrm{C}_0(\mathbb{R}); \end{array} \tag{3.10c}$$

$$\exists\, \gamma \in \mathbb{R} :\ |f(t)| \leqslant \gamma |t|^{-n-1-\epsilon} \Rightarrow \hat{f} \in \mathrm{C}^n(\mathbb{R}) \tag{3.10d}$$

$$\left.\begin{array}{r} f \in \mathrm{L}^1(\mathbb{R}) \cap \mathrm{C}^n(\mathbb{R}), \\ \forall\, k = 0, \ldots, n-1 :\ f^{(k)} \in \mathrm{C}_0(\mathbb{R}), \\ f^{(n)} \in \mathrm{L}^1(\mathbb{R}) \end{array}\right\} \Rightarrow \begin{array}{l} \omega^n \hat{f} \in \mathrm{C}_0(\mathbb{R}) \text{ and} \\ |\hat{f}(\omega)| \leqslant \gamma |\omega|^{-n} \end{array} \tag{3.10e}$$

$$\text{with } \mathcal{F}\Big(\big(\tfrac{\mathrm{d}}{\mathrm{d}t}\big)^n f\Big)(\omega) = (i\omega)^n \mathcal{F}(f)(\omega) \tag{3.10f}$$

$$\left.\begin{array}{r} f \in \mathrm{C}(\mathbb{R}),\ \hat{f} \in \mathrm{L}^1(\mathbb{R}) \cap \mathrm{C}^n(\mathbb{R}), \\ \forall\, k = 0, \ldots, n-1 :\ \hat{f}^{(k)} \in \mathrm{C}_0(\mathbb{R}), \\ \hat{f}^{(n)} \in \mathrm{L}^1(\mathbb{R}) \end{array}\right\} \Rightarrow t^n f \in \mathrm{C}_0(\mathbb{R}) \tag{3.10g}$$

Proof. Eqs. (3.10a) and (3.10b) can be shown by induction:

for $n = 1$: assume $tf \in \mathrm{L}^1$. To show $\hat{f} \in \mathrm{C}^1$ and $\widehat{f'} \in \mathrm{C}_0$;

$$\left|\frac{\hat{f}(\omega+h) - \hat{f}(\omega)}{h}\right| = \frac{1}{\sqrt{2\pi}} \left|\int f(t) e^{-i\omega t} \frac{e^{-iht} - 1}{h} \,\mathrm{d}t\right| \leqslant \frac{1}{\sqrt{2\pi}} \int |tf(t)| \,\mathrm{d}t < \infty$$

where inequality is due to

$$\left|\frac{e^{-iht}-1}{h}\right| = \frac{1}{|i|}\left|\int_0^t e^{-ihs}\,\mathrm{d}s\right| \leqslant |t| \max_{h,s}|e^{-ihs}| = |t|.$$

Hence, by Lebesgue dominated convergence theorem it follows

$$\lim_{h\to 0}\frac{\hat{f}(\omega+h)-\hat{f}(\omega)}{h} = \int f(t)e^{-i\omega t}\Big(\underbrace{\lim_{h\to 0}\frac{e^{-iht}-1}{h}}_{=\,(e^{-iht})'\big|_{h=0}=-it}\Big)\,\mathrm{d}t = \mathcal{F}(-itf)(\omega).$$

This implies in particular that $\hat{f}$ is differentiable and by Eq. (3.9a) it proves the assertion for $n = 1$.

For the induction step, $n \mapsto n+1$, suppose that $t^{n+1}f \in \mathrm{L}^1(\mathbb{R})$. Then

$$|t^n f(t)| \leqslant \begin{cases} |f(t)| & |t| \leqslant 1 \\ |t^{n+1}f(t)| & |t| \geqslant 1 \end{cases} \Rightarrow \text{ with } g := t^n f \text{ it follows } g \in \mathrm{C}^1 \wedge \widehat{g'} \in \mathrm{C}_0.$$

Linearity of $\mathcal{F}$ implies in particular

$$\hat{f}(\omega) = \big((-it)^n f\big)\hat{}\,(\omega) = (-i)^n(\underbrace{t^n f}_{=g})\hat{}\,(\omega) \in \mathrm{C}^1 \Rightarrow \hat{f} \in \mathrm{C}^{n+1}$$

and analogously $\hat{f}^{(n+1)} \in \mathrm{C}_0$ with $\hat{f}^{(n+1)} = \big(\hat{f}^n\big)\hat{}\,(\omega) = (-i)^n(-it)\hat{g}(\omega) = (-it)^{n+1}\hat{f}(\omega)$.

Equation (3.10e) is derivable from n-fold integration by parts, s.t. $\forall\,\omega \neq 0$:

$$\int_{-K}^{K} f(t)e^{-i\omega t}\,\mathrm{d}t = -\sum_{k=0}^{n-1}(i\omega)^{-(k+1)}e^{-i\omega t}\underbrace{f^{(k)}(t)\big|_{-K}^{K}}_{\substack{\xrightarrow{|K|\to\infty} 0 \\ f^{(k)}\in \mathrm{C}_0}} + (i\omega)^n\int_{-K}^{K} f^{(n)}e^{-i\omega t}\,\mathrm{d}t.$$

Hence, $\forall\,\omega \neq 0$: $(i\omega)^n\hat{f} = \mathcal{F}\big(f^{(n)}\big)(\omega)$ and due to $\hat{f} \in \mathrm{C}_0$ this holds for all $\omega \in \mathbb{R}$ with $\omega^n\hat{f} \in \mathrm{C}_0$. This automatically implies that $\omega^n\hat{f}$ is bounded such that $|\hat{f}(\omega)| \leqslant \gamma|\omega|^{-n}$, for some γ.

Equations (3.10c) and (3.10g) are true since Eq. (3.9b) implies

$$\hat{\hat{f}}(\nu) = \mathcal{F}(f)(\nu) = \frac{1}{\sqrt{2\pi}}\int \hat{f}(\omega)e^{i(-\nu)\omega}\,\mathrm{d}\omega = f(-\nu) \text{ almost everywhere} \tag{3.11}$$

which by substitution $g := \hat{f}$ completes the proof.

Last but not least, Eq. (3.10d) is equivalent to $|t^n f(t)| \leqslant \gamma |t|^{-1-\epsilon}$ which implies

$$\int |t^n f(t)| \, \mathrm{d}t \leqslant \int_{|t|\leqslant 1} |f(t)| \, \mathrm{d}t + \gamma \int_{|t|\geqslant 1} \frac{1}{|t|^{1+\epsilon}} \, \mathrm{d}t < \infty.$$

□

Since this thesis turns its attention to signals which are living in $\mathrm{L}^2(\mathbb{R})$ the Fourier transform, used as a tool describing their properties, has to be extended to the space of interest properly. Doing so, it will be of much help exploiting the fact that $\overline{\mathrm{L}^1(\mathbb{R}) \cap \mathrm{L}^2(\mathbb{R})}^{\|\cdot\|_{\mathrm{L}^2(\mathbb{R})}} = \mathrm{L}^2(\mathbb{R})$.

Lemma 3.5.5. *(i)* $\forall\, f \in \mathrm{L}^1(\mathbb{R}) \cap \mathrm{L}^2(\mathbb{R}) :\ \hat{f} \in \mathrm{L}^2(\mathbb{R})$ *with* $\|\hat{f}\|_{\mathrm{L}^2} = \|f\|_{\mathrm{L}^2}$

(ii) $\forall\, f \in \mathrm{L}^2(\mathbb{R}) :\ \mathcal{F}\left(f\chi_{[-n,n]}\right)$ *is a Cauchy sequence in* $\mathrm{L}^2(\mathbb{R})$

Proof. The first claim can be easily shown under an additional assumption: $\hat{f} \in \mathrm{L}^1$. Then

$$\begin{aligned} \|f\|^2 = \langle f, f \rangle &= \int f(t) \frac{1}{2\pi} \int \overline{\hat{f}(\omega)} e^{-i\omega t} \, \mathrm{d}\omega \, \mathrm{d}t \\ \text{(by Fubini)} &= \int \overline{\hat{f}(\omega)} \frac{1}{2\pi} \int f(t) e^{-i\omega t} \, \mathrm{d}t \, \mathrm{d}\omega \\ &= \left\langle \hat{f}, \hat{f} \right\rangle = \|\hat{f}\|^2. \end{aligned}$$

A full proof can be checked in Rudin [Rud87, Thm. 9.13(b)].

Point (ii) follows from the first, since for each $f \in \mathrm{L}^2(\mathbb{R}) \Rightarrow f_n := f\chi_{[-n,n]} \in \mathrm{L}^2([-n,n]) \subset \mathrm{L}^1([-n,n])$ and by (i) $\hat{f}_n \in \mathrm{L}^2(\mathbb{R})$ it follows

$$\begin{aligned} \text{w.l.o.g. } \forall\, m \geqslant n :\ \|\mathcal{F}(f_n) - \mathcal{F}(f_m)\|^2 = \|\mathcal{F}(f_n - f_m)\|^2 &\overset{(i)}{=} \|f_n - f_m\|^2 \\ &= \int_{|t|\in[n,m]} |f(t)|^2 \, \mathrm{d}t \xrightarrow{n\to\infty} 0 \end{aligned}$$

□

Since $\mathrm{L}^2(\mathbb{R})$ is a Hilbert space, i.e. in particular complete, point (ii) of the lemma above dictates the nature of this extension to $\mathrm{L}^2(\mathbb{R})$ as in the succeeding definition.

Definition 3.5.6. The *Fourier transform* $\mathcal{F}(f) = \hat{f} \in \mathrm{L}^2(\mathbb{R})$ of $f \in \mathrm{L}^2(\mathbb{R})$ is defined as

$$\hat{f}(\omega) := \lim_{n\to\infty} (2\pi)^{-1/2} \int_{-n}^{n} f(t) e^{-i\omega t} \, \mathrm{d}t.$$

$\mathcal{F}$ is called *the Fourier transform in* $\mathrm{L}^2(\mathbb{R})$

Theorem 3.5.7 (Parseval)**.** $\forall\, f, g \in \mathrm{L}^2(\mathbb{R})$:

$$\begin{aligned} \|\hat{f}\| &= \|f\| \ \textit{and} \\ \left\langle \hat{f}, \hat{g} \right\rangle &= \langle f, g \rangle \,. \end{aligned}$$

Proof. The first assertion is clear due to the lemma above, point (i), continuity of the norm and the fact that $f\chi_{[-n,n]} =: f_n$ is a Cauchy seq. in $\mathrm{L}^2(\mathbb{R})$ with $\|f_n - f\| \to 0$ as like as $\|\hat{f}_n - \hat{f}\| \to 0$ according to Definition 3.5.6. Equality of the last Parseval equation is analogously proven as in the proof of Corollary 3.2.4. □

As a consequence, it holds that the inverse Fourier transform of $\hat{f}\chi_{[-n,n]}$ converges almost everywhere to f as n goes to infinity which gives rise to the definition of an inverse Fourier transform of a $\mathrm{L}^2(\mathbb{R})$ function.

Theorem 3.5.8.

$$\forall\, f \in \mathrm{L}^2(\mathbb{R}) : \ \left\| f - (2\pi)^{-1/2} \int_{-n}^{n} \hat{f}(\omega) e^{i\omega \cdot} \, \mathrm{d}\omega \right\|_{\mathrm{L}^2(\mathbb{R})} \xrightarrow{n\to\infty} 0$$

and the inverse Fourier transform in $\mathrm{L}^2(\mathbb{R})$ *is defined as*

$$\begin{aligned} &\mathcal{F}^{-1} : \mathrm{L}^2(\mathbb{R}) \to \mathrm{L}^2(\mathbb{R}), \\ &\qquad f \mapsto f^{\vee} := \lim_{n\to\infty} (2\pi)^{-1/2} \int_{-n}^{n} f(\omega) e^{i\omega \cdot} \, \mathrm{d}\omega. \end{aligned} \tag{3.12}$$

Moreover, $\forall\, a \in \mathbb{R} \setminus \{0\}$, $b, \mu \in \mathbb{R}$ *the following properties are true*

$$\begin{aligned} \textit{Translation:} \quad & \mathcal{F}(f(\cdot - b)) = e^{-ib\cdot} \mathcal{F}(f) \\ \textit{Dilation:} \quad & \mathcal{F}(f(a\cdot)) = |a|^{-1} \mathcal{F}(f)(a^{-1}\cdot) \\ \textit{Modulation:} \quad & \mathcal{F}(e^{i\mu\cdot} f) = \mathcal{F}(f)(\cdot - \mu) \end{aligned}$$

According to Eq. (3.12) each $f \in \mathrm{L}^2(\mathbb{R})$ satisfies $\hat{f}^{\vee}(t) = \hat{f}(-t)$ (in L^2-sense) which is easily seen by a substitution. This guarantees the surjectivity of the Fourier transform $\mathcal{F} : \mathrm{L}^2(\mathbb{R}) \to \mathrm{L}^2(\mathbb{R})$ and due to Parseval's equations, Theorem 3.5.7, which say that $\mathcal{F}$ is in addition an isometry it is clear that

Theorem 3.5.9 (Plancherel)**.** *The Fourier transform*

$$\mathcal{F} : \ \mathrm{L}^2(\mathbb{R}) \to \mathrm{L}^2(\mathbb{R})$$

is an isometric isomorphism with the inverse given as in Equation (3.12)*.*

3.6 Heisenberg's Uncertainty Principle

Definition 3.6.1. (i) Let $\sqrt{x}f \in \mathrm{L}^2(\mathbb{R})$. The *expectation* (3.13a) and *variance* (3.13b) f are defined as

$$\mathrm{E}(f) := \|f\|^{-2} \int x|f(x)|^2 \, \mathrm{d}x \tag{3.13a}$$

$$\begin{aligned}\mathrm{Var}(f) :=& \|f\|^{-2} \int (x - E(f))^2 |f(x)|^2 \, \mathrm{d}x \\ =& \mathrm{E}(f^2) - \mathrm{E}(f)^2.\end{aligned} \tag{3.13b}$$

(ii) In particular, $t_0 := \mathrm{E}(f)$, $\omega_0 := \mathrm{E}(\mathcal{F}(f))$ are the so-called *locations in time and frequency*, respectively, with the corresponding *standard deviation* of time- and frequency concentration, respectively, at t_0, resp. ω_0 given as $\Delta t := \sqrt{\mathrm{Var}(f)}$, $\Delta\omega := \sqrt{\mathrm{Var}(\hat{f})}$.

(iii) f is called *band-limited* $:\Longleftrightarrow \mathrm{supp}(\hat{f}) \subsetneqq \mathbb{R}$ and

time-limited $:\Longleftrightarrow \mathrm{supp}(f) \subsetneqq \mathbb{R}$

(iv) f is said to be *localised in time domain* $:\Longleftrightarrow \exists\, t_0$, $\Delta t < \infty$ and *localised in frequency domain* $:\Longleftrightarrow \exists\, \omega_o, \Delta\omega < \infty$.

If f is localised in time and frequency domain then f is called *localised*.

Theorem 3.6.2 (Uncertainty principle)**.** *Each localised* $0 \neq f \in \mathrm{L}^2(\mathbb{R})$ *satisfies*

$$\Delta t \Delta\omega \geqslant \frac{1}{2} \tag{3.14}$$

where the bound is attained if and only if $\exists\, a \in \mathbb{C}\backslash\{0\}$, $\nu, b \in \mathbb{R}$, $c \in \mathbb{R}_{>0}$: $f(t) = ae^{i\nu t}e^{-c(t-b)^2}$. *In this case, f is called a* modulated Gaussian.

Proof. W.l.o.g. assume $t_0 = \omega_0 = 0$ (otherwise consider instead of f the mapping $t \mapsto e^{-i\omega_0 t} f(t + t_0)$).

By extra restrictions[2] on f, e.g. $f \in \mathrm{C}^1(\mathbb{R})$, $f^{(1)} \in L^1(\mathbb{R})$ with $\sqrt{t}f \xrightarrow{|t|\to\infty} 0$,

[2] A general proof without extra assumptions on f which can be reduced to this case can be looked up in Dym&McKean, (pp. 119-120) [DM72]

it follows

$$(\Delta t)^2(\Delta\omega)^2 = \left(\mathrm{E}(f^2) - \overbrace{\mathrm{E}(f)^2}^{=0}\right)\left(\mathrm{E}(\hat{f}^2) - \overbrace{\mathrm{E}(\hat{f})^2}^{=0}\right) = \mathrm{E}(f^2)\mathrm{E}(\hat{f}^2)$$

$$\overset{i\omega\hat{f}=\widehat{f'}}{=} \|f\|^{-2}\|\hat{f}\|^{-2}\int |tf(t)|^2\,\mathrm{d}t\ \underbrace{\int |\widehat{f'}(\omega)|^2\,\mathrm{d}\omega}_{=\|\mathcal{F}(f')\|=\|f'\|^2}$$

$$\overset{\substack{\text{Cauchy}\\\text{Schwarz}}}{\geqslant} \|f\|^{-4}|\langle tf, f'\rangle|^2 \geqslant \|f\|^{-4}|\Re\langle tf, f'\rangle|^2$$

$$= \frac{1}{4\|f\|^4}\left|\int \underbrace{tf(t)\overline{f'(t)} + t\overline{f(t)}f'(t)}_{=t(f(t)\overline{f(t)})'}\,\mathrm{d}t\right|^2$$

$$\overset{\substack{\text{integration}\\\text{by parts}}}{=} \frac{1}{4\|f\|^4}\left|(t|f(t)|^2)\big|_{|t|\to\infty} - \|f\|^2\right|^2 = \frac{1}{4}.$$

Now it is still need to show that $\Delta t\Delta\omega = 1/2$ iff f is a modulated Gaussian.

'$\Rightarrow$': By a longer calculation mostly based on substitution it is clear that $\mathcal{F}(ae^{i\nu t}e^{-c(t-b)^2})(\omega) = \frac{ae^{ib\omega}}{\sqrt{2c}}e^{-\frac{(\omega-\nu)^2}{4c}}$ with $t_0 = b$, $\Delta t = \frac{1}{2\sqrt{c}}$ and $\omega_0 = \nu$, $\Delta\omega = \sqrt{c}$ from which directly follows that $\Delta t\Delta\omega = 1/2$.

'$\Leftarrow$':

Let $\Delta t\Delta\omega = 1/2$ then in particular first inequality implies

$$\int |tf(t)|^2\,dt\ \int |f'(t)|^2\,\mathrm{d}t = |\langle tf, f'\rangle|^2,$$

i.e. $\exists\,\gamma \in \mathbb{C}:\ f' = \gamma tf$. Let $\gamma = -2c$ for some $c \in \mathbb{C}$ then $\exists\, a \in \mathbb{C}\backslash\{0\}$: $f(t) = ae^{-ct^2}$, where $a \neq 0$ follows from $f \neq 0$.

Moreover, second inequality implies

$$|\langle tf, f'\rangle| = |\Re\langle tf, f'\rangle| \Rightarrow \langle tf, f'\rangle \in \mathbb{R}$$

and by $\langle tf, f'\rangle = -2\int tae^{-ct^2}\overline{tcae^{-ct^2}}\,\mathrm{d}t = -2\overline{c}\|tf\|^2$ it follows that $c \in \mathbb{R}$.

The supplement claim $f \in \mathrm{L}^2(\mathbb{R})$ is only possible if $c > 0$ ($f \neq 0 \Rightarrow c \neq 0$).

Resubstitution (see comment at the beginning of this proof) yields

$$f(t) = Ae^{i\omega_0 t}e^{-c(t-t_0)^2},\ 0 \neq A \in \mathbb{C},\ t_0, \omega_0 \in \mathbb{R}, c > 0$$

□

In words, Heisenberg's uncertainty principle says that it is impossible to determine the frequency of a signal at an arbitrary fixed time (and vice versa, at which time an arbitrary but fixed frequency was attained by f).

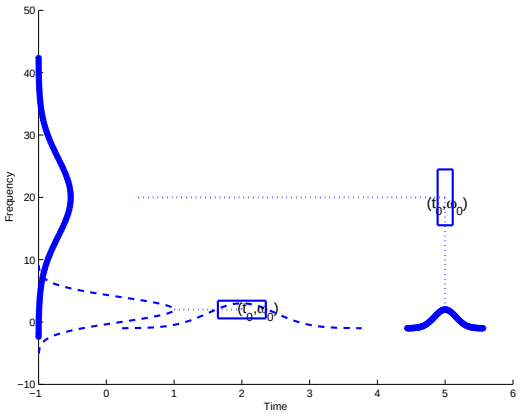

Fig. 3.3: Two Heisenberg boxes in the phase space with their accessory Gaussian $g(t) = ae^{-c(t-b)^2}$ and $\hat{g}$, resp., with parameters $(a, b, c) = (4, 2, 2)$ for the dashed version and plotted in solid with $(a, b, c) = (3, 5, 20)$.

Higher accuracy in one space leads to a 'smear of information', i.e. lower accuracy in the other space. The 'best' achievable compromise, i.e. equal treatment of information coming from frequency and time domain is gained by the only class of functions made up from the so-called modulated Gaussians.

Motivated by this theorem, it is common in signal analysis to 'compare' localised signals with each other in the so-called *phase space* or *time-frequency space* where each signal is represented by a *Heisenberg box* $\mathcal{B} = \{(t, \omega) | t \in [t_0 - \Delta t, t_0 + \Delta t],\ \omega \in [\omega_0 - \Delta\omega, \omega_0 + \Delta\omega]\}$.

From stochastics the Chebyshev inequality is known as $P(|X - \mu| \geqslant \gamma) \leqslant \sigma^2/\gamma^2$ where γ is some threshold, P a probability measure, X a random variable, μ and σ the corresponding expectation and standard deviation, respectively.

Transfered to this case, the Heisenberg box $\mathcal{B}$ of a function f can be interpreted as an area with high energy concentration of f, i.e. a rather high portion of $\|f\|$ is localised around (t_0, ω_0).

On the other hand, it can be proved ([Erd03, p. 235]) that there exists no function such that any box $\mathcal{B}$ in phase space is able to cover it.[3].

[3]A well-known consequence of the *sampling theorem*, see Theorem 4.4.1, is that a signal cannot be both band-limited and time-limited. To see why, assume that such a signal exists, and sample it faster than the *Nyquist frequency*. These finitely many time-domain coefficients should define the entire signal. Equivalently, the entire spectrum of the band-limited signal should be expressible in terms of the finitely many time-domain coefficients obtained from sampling the signal. Mathematically this is equivalent to requiring that a (trigonometric) polynomial can have infinitely many zeros since the band-limited signal

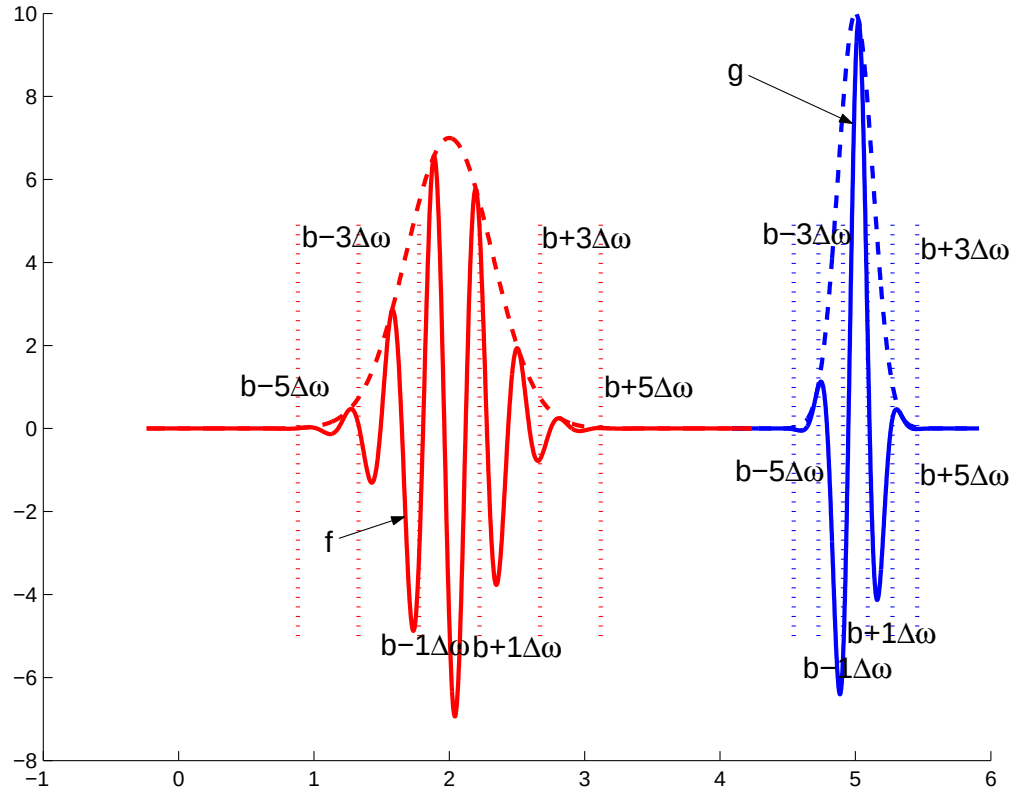

Fig. 3.4: Two modulated Gaussian – on the left side, $f(t) = 7e^{i20t}e^{-5(t-2)^2}$ and on the right side of figure $g(t) = 10e^{i20t}e^{-30(t-5)^2}$ – (solid lines) with three different intervals each $[b - k\Delta\omega, b + k\Delta\omega]$, $k = 1, 3, 5$, intimidated by dotted lines

Theorem 3.6.3. $\nexists\, f \in \mathrm{L}^2(\mathbb{R}),\ f \neq 0 :$ *f is band- and time-limited,*

Concluding, one can say that the properties of f will in general neither show up in detail nor all at once.

must be zero on an interval beyond a critical frequency which has infinitely many points. However, it is well-known that polynomials do not have more zeros than their orders due to the fundamental theorem of algebra. This contradiction shows that our original assumption that a time-limited and band-limited signal exists is incorrect.

Chapter 4

Fixed Time – Frequency Analysis

4.1 Gabor Frames – Windowed Fourier Transform

It is part of our everyday experience that with the sense of hearing it is not only possible to locate sounds or distinguish between high and low frequencies (of it) but also to know when exactly a particular tonality occured - at least this is what our brain makes us believe.

Similar to a language every musician is able to read a musical notation, cf. Figure 4.1, which of course specifies frequency and duration and hence the exact (time) occurrence of each note. Reading and singing, resp. playing the corresponding note in the prescribed way on an instrument can be considered as an encoding process of some decoded information. Conversely, some of these musicians have the ability to write down pieces of music in such kind of notation so that the encoded result and the original sample would effectively posses the same content of information.

The same is true in case of reading and writing words. Truly, some infor-

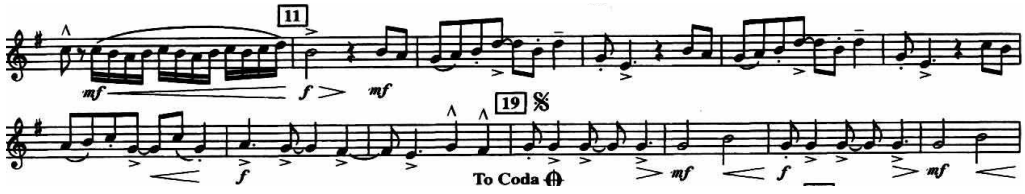

Fig. 4.1: Scores – a notation with both, time and frequency information (and a little more: duration, loudness, stress,...). Excerpt from *Words and Music* by J. Morali, H. Belolo and V. Willis. Arranged by M. Sweeney. Y.M.C.A. The Village People.

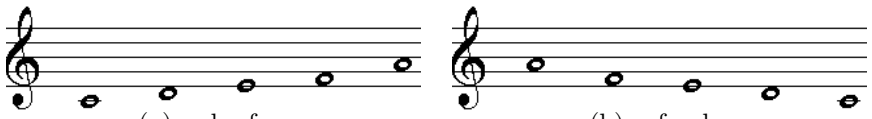

(a) c-d-e-f-a (b) a-f-e-d-c

Fig. 4.2: Two sequences of semi breves. Obviously, in both cases the Fourier transform would consist of 5 frequencies, $261, 293, 329, 349$ and 392 Hz, respectively. Nevertheless, the signal in (a) is different from that in (b)!

mation of a conversation for instance will get lost - e.g. the voice, intonation, dialect, etc. of a speaker. However, the 'main' content of this talk is still accessible via the written letters, words and sentences.

Evidently the sole knowledge about present frequencies in a signal $f \in \mathrm{L}^2(\mathbb{R})$, i.e. without any additional time resolution of the underlying spectrum will not suffice to carry out a kind of classification. Figure 4.2 illustrates this problem.

In mathematics the Fourier transform is a well known tool for studying problems from a different point of view, namely the frequency domain. Sometimes these get simpler and can be solved.

Unfortunately, by means of this transformation it is impossible to draw conclusions on the question when a frequency occurred. It only gives an answer at which amplitude some frequency is part of the signal f.

The absence of any time-dependence of $\hat{f}(\omega)$ can be artificially fixed by introducing a reference function g which windows the signal as $fg(\cdot - t)$ at time t such that a subsequent Fourier transformation with additional parameter t would end up in a localised spectrum if g itself is localised.

Lemma 4.1.1. *Let $g \in \mathrm{L}^2(\mathbb{R})$ with $\|g\| = 1$. Then the modulated by ω and translated by t copy of g, defined as $g_{\omega,t} := (2\pi)^{-1/2} g(\cdot - t) e^{i\omega\cdot} \in \mathrm{L}^2(\mathbb{R})$ and $\langle f, g_{\omega,t} \rangle$ is well defined.*

Proof. The first claim follows by substitution whereas well-definition of $\langle f, g_{\omega,t} \rangle$ is ensured by the Cauchy-Schwarz inequality. □

Definition 4.1.2. Let $g \in \mathrm{L}^2(\mathbb{R})$, $\|g\|_{\mathrm{L}}^2 = 1$. $\mathcal{F}_g f(\omega, t) := \langle f, g_{\omega,t} \rangle$ is called the *windowed Fourier transform* of f where g is the corresponding *window*.

Corollary 4.1.3. *(i)* $\mathcal{F}_g f(\omega, t) = e^{-it\omega} (2\pi)^{-1/2} \int \hat{f}(\nu) \overline{e^{it\nu} \hat{g}(\nu - \omega)}\, d\nu$

(ii) If g is localised with $t_0, \omega_0, \Delta t, \Delta\omega$ then $\overline{g(\cdot - t)} e^{-i\omega\cdot}$ is localised around $t + t_0$ with Δt and $\overline{\hat{g}(\cdot - \omega)} e^{-it\cdot}$ is localised around $\omega + \omega_0$ with $\Delta\omega$.

Proof. The Parseval equation (Theorem 3.5.7) and the properties of $\mathcal{F}$ (Theorem 3.5.8) imply the first assertion. The last statement is proven by simple a substitution. □

Item 1 says that g localises f in time domain and $\hat{g}$ localises $\hat{f}$ in frequency domain. Taking Item 2 into account this lends itself to consider $|\mathcal{F}_g f(\omega, t)|$ as the energy of a local frequency ω at time t of f.

The physicist Gabor was the first who proposed such a decomposition [Gab46]. He also suggested to choose the window g as a Gaussian, such that by Heisenberg's uncertainty principle the spread of uncertainty in frequency and time would be as small as possible (Theorem 3.6.2). Unfortunately, such a decomposition is not as flexible as it seems to be:

An obvious discretisation of $g_{\omega,t}$ can be encompassed by a linear ansatz: $t = nt_0$, $\omega = m\omega_0$, i.e. $g_{m,n} := g(\cdot - nt_0)e^{im\omega_0 \cdot}$ for $n, m \in \mathbb{Z}$ and parameters $t_0, \omega_0 \in \mathbb{R}_{>0}$.

Ingrid Daubechies proved ([Dau92, pp. 81, p.112] that the system $(g_{m,n})_{m,n}$ constitues a frame if and only if $\omega_0 t_0 \leqslant 2\pi$ and in addition, if $\omega_0 t_0 > 2\pi$ then the so-called *Gabor system* even fails to be complete.

Though frames possesses nice properties, uniqueness and numerically stable representation of $f \in \mathrm{L}^2(\mathbb{R})$ require qualities which only can be established by a Riesz basis. Hence, it is advisable to restrict the 'sampling density' (cf. Theorem 4.4.1) to the case $\omega_0 t_0 = 2\pi$.

On the other hand, in most applications it is also of great importance to achieve localisation in time and frequency space. The point is that if $(g_{mn})_{mn}$ constitutes a Riesz basis then such a venture is impossible. Balian and independently Low have found the following result.

Theorem 4.1.4 (Balian - Low)**.** *If $(g_{mn})_{mn}$ constitutes a Riesz basis then*

$$\int x^2 |g(x)|^2 \,\mathrm{d}x \int \omega^2 |\hat{g}(\omega)|^2 \,\mathrm{d}\omega = \infty.$$

A proof can be checked at [Dau92, pp. 109].

This first approach of introducing a window g which can be translated in time in order to correlate f with $e^{i\omega \cdot}$ locally (in contrast to the usual Fourier transform where this is done globally) has yet a disadvantage. It just so happens that the time-spread Δt_g of g is sometimes too large and sometimes too small compared to local properties of f at some point of interest. Figure 4.3 illustrates this problem.

In theearly 80s of the last century J. Morlet was faced with the task of analysing seismic waves. Unhappy with the results provided by the windowed Fourier transformation he proposed to correlate the signal $f \in \mathrm{L}^2(\mathbb{R})$ with

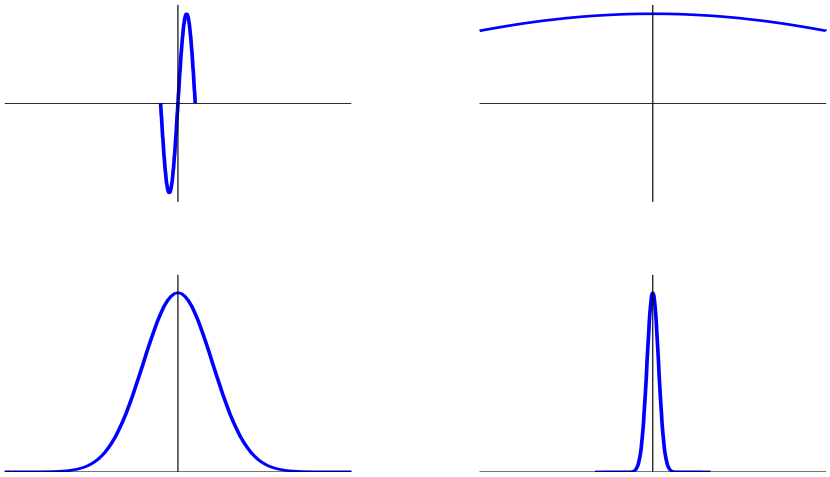

Fig. 4.3: The upper two subfigures represent two signals with corresponding spread Δ_{t_f} whereas the lower subfigures stands for the Gaussians. Case one [left two pictures with $\Delta_{t_f} \ll \Delta_{t_g}$]: No time localisation; the window has no effect on the Fourier transformation. Case two [right two pictures with $\Delta_{t_f} \gg \Delta_{t_g}$]: No frequency localisation; here the windowed Fourier transformation would be 'blind' for such low frequencies. Confer in this context also Figure 4.16

a dilated copy of a 'small wave', i.e. a function $\psi \in \mathrm{L}^2(\mathbb{R})$ which has to be localised in time domain. So, – instead of adjusting manually the width of an auxiliary function g and correlate f with (co-/)sines – by dilating a 'wavelet' ψ, its 'frequency' and time-width changes simultaneously (cf. Figure 4.4).

This also corresponds to the intuitive understanding: the higher the frequency the smaller the cycle! (cf. Figure 4.5).

4.2 Wavelets

Definition 4.2.1. Let $\psi \in \mathrm{L}^2(\mathbb{R})$, with $\|\psi\| = 1$ and define the dilated by a and translated by b version of it as $\psi_{a,b} := a^{-1/2}\psi(\frac{\cdot - b}{a})$.

(i) ψ is called *admissible*:$\Longleftrightarrow$

$$C_\psi := 2\pi \int \frac{|\hat{\psi}(\omega)|^2}{|\omega|}\, \mathrm{d}\omega < \infty \tag{4.1}$$

(ii) If ψ is admissible and $f \in \mathrm{L}^2(\mathbb{R})$ then define $\forall\,(a,b) \in \mathbb{R}\setminus\{0\} \times \mathbb{R}$ $\mathcal{W}f(a,b) := \langle f, \psi_{a,b}\rangle$. $\mathcal{W}f(a,b)$ is called a *continuous wavelet transform* of f.

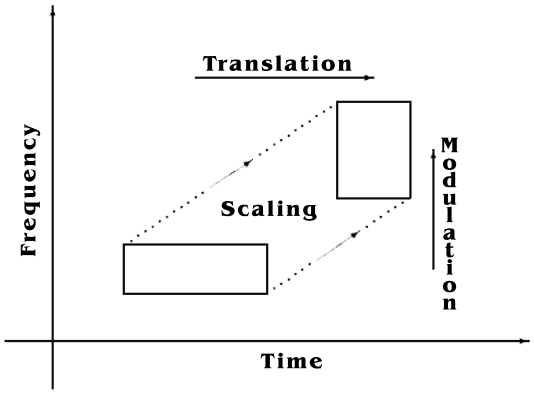

Fig. 4.4: Change of Heisenberg boxes. A scaling process versus modulation and translation.

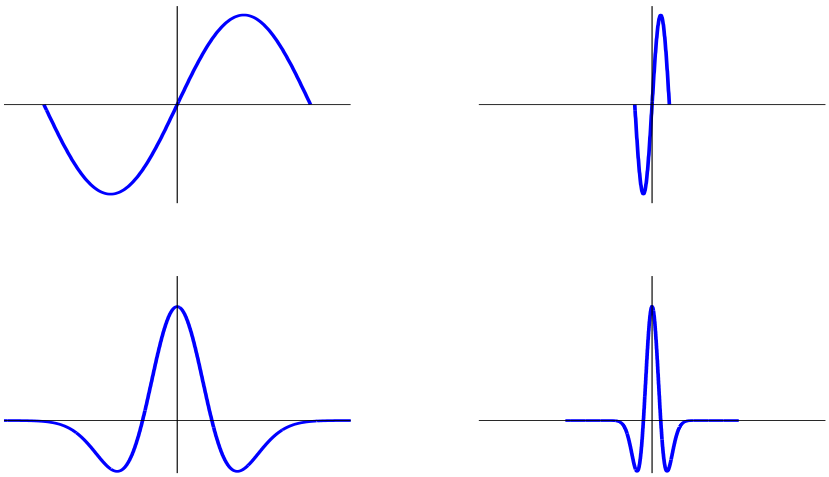

Fig. 4.5: Again, the upper two subfigures stand for two signals with time spreads Δ_{t_f}. Plotted underneath each signal is a dilated 'wavelet' whose time spread automatically adopts to the frequency it can resolve (number of oscillations per time). On the left side $\psi_{a,b}$ is stretched, $a > 1$ and conversely, on the right side compressed $a < 1$.

Remark 4.2.2. Assume that ψ is localised with $t_0, \omega_0, \Delta t, \Delta\omega$, then (by Theorem 3.5.8) $\psi_{a,b}$ is localised with $at_0 + b, \omega_0/a, |a|\Delta t, \Delta\omega/|a|$. This property necessarily transfers to $\mathcal{W}f(a,b)$ s.t. the wavelet coefficients can be understood as a measure of frequency $\omega \in [\frac{\omega_0}{2} - \frac{1}{2}\frac{\Delta\omega}{|a|}, \frac{\omega_0}{2} + \frac{1}{2}\frac{\Delta\omega}{|a|}]$ at the time $t \in [at_0 + b - \frac{|a|\Delta t}{2}, at_0 + b + \frac{|a|\Delta t}{2}]$.

This is basically derived from the Parseval eq. $\langle f, \psi_{a,b}\rangle = \left\langle \hat{f}, \hat{\psi}_{a,b}\right\rangle$ and restricts automatically the size of each Heisenberg box $\mathcal{B}$ of f to the Heisenberg box of $\psi_{a,b}$. A very illustrative picture of this fact is showed in [Dau92, p. 89].

The term 'wavelet' is founded on the fact that a necessary condition for ψ being admissible is $\hat{\psi}(0) = 0$. ψ must oscillate with an appropriate decay in its amplitude. This and an easy to handle sufficient condition on ψ to be admissible will be the essence of the undermentioned lemma.

Lemma 4.2.3. *Let $\psi \in \mathrm{L}^2(\mathbb{R})$, $t\psi \in L^1(\mathbb{R})$. Then*

$$\psi \text{ is admissible } \iff \hat{\psi}(0) = 0$$

Proof. '$\Rightarrow$': $t\psi \in L^1(\mathbb{R}) \Rightarrow \psi \in L^1(\mathbb{R}) \Rightarrow \hat{\psi} \in C^0(\mathbb{R})$. Assume that $\hat{\psi}(0) \neq 0$. Then $\exists\, \delta > 0 \,\text{such that}\, \forall\, \epsilon > 0 :\ |\hat{\psi}(\omega)| \geqslant \delta \quad \forall\, |\omega| \leqslant \epsilon$. This implies that

$$\int \frac{|\hat{\psi}(\omega)|^2}{|\omega|}\, \mathrm{d}\omega \geqslant \int_{-\epsilon}^{\epsilon} \frac{|\hat{\psi}(\omega)|^2}{|\omega|}\, \mathrm{d}\omega \geqslant \delta^2 \int_{-\epsilon}^{\epsilon} \frac{1}{|\omega|}\, \mathrm{d}\omega = 2\delta^2 \int_0^{\epsilon} \omega^{-1}\, \mathrm{d}\omega = \infty$$

which contradicts the admissibility.

'$\Leftarrow$': $t\psi \in L^1(\mathbb{R}) \Rightarrow \hat{\psi} \in C^1(\mathbb{R})$. Hence, using mean value theorem and the fact that $\hat{\psi}'$ takes a maximum on a compact it follows $\forall\, |\omega| \leqslant 1$

$$|\hat{\psi}(\omega)| = |\hat{\psi}(\omega) - \hat{\psi}(0)| \leqslant \max_{\nu \leqslant 1} |\hat{\psi}'(\nu)||\omega|.$$

Therefore,

$$\begin{aligned}\int |\hat{\psi}(\omega)|^2/|\omega|\, \mathrm{d}\omega &= \int_{|\omega|\leqslant 1} |\hat{\psi}(\omega)|^2/|\omega|\, \mathrm{d}\omega + \int_{|\omega|>1} |\hat{\psi}(\omega)|^2/|\omega|\, \mathrm{d}\omega \\ &\leqslant \underbrace{\max_{\nu\leqslant 1} \hat{\psi}(\nu)}_{<\infty} + \underbrace{\int_{|\omega|\geqslant 1} |\hat{\psi}(\omega)|^2/|\omega|\, \mathrm{d}\omega}_{\leqslant \|\hat{\psi}\|_{\mathrm{L}^2} = \|\psi\|_{\mathrm{L}^2} < \infty} < \infty\end{aligned}$$

□

Due to this lemma it is now easy to give some examples for wavelets:

Example 4.2.4. (i) The Haar system $\psi = \begin{cases} 1 & t \in [0, 1/2) \\ -1 & t \in [1/2, 1) \\ 0 & \text{else} \end{cases}$ is a wavelet since $\int \psi(t)\,\mathrm{d}t = \int_0^{1/2} \mathrm{d}t - \int_{1/2}^1 \mathrm{d}t = 0$.

(ii) The Morlet wavelet:

The ansatz $\psi(t) = A(e^{-(\omega-\omega_0)t} - B)e^{-t^2/2}$ yields $\hat{\psi}(\omega) = A(e^{-(\omega-\omega_0)^2/2} - Be^{-\omega^2/2}$ such that ψ is admissible only for $B = e^{-\omega_0^2/2}$ so that $\hat{\psi}(0) = 0$.

The next few assertions of the following theorem will illustrate some similarities and differences of $\mathcal{W}$ compared to $\mathcal{F}$ and $\mathcal{F}_g f$. It will also stress the definition of admissibility, Eq. (4.1).

Theorem 4.2.5. *Let $f \in \mathrm{L}^2(\mathbb{R})$, $(a, b) \in \mathbb{R} \setminus \{0\} \times \mathbb{R}$ and $\psi \in \mathrm{L}^2(\mathbb{R})$ be admissible and let*

$$\mathrm{L}^2(\mathbb{R}^2) := \mathrm{L}^2\left(\mathbb{R}^2, a^{-2}C_\psi^{-1}\,\mathrm{d}a\,\mathrm{d}b\right) := \left\{ h : \mathbb{R}^2 \to \mathbb{R} \,\middle|\, \|h\|^2_{\mathrm{L}^2(\mathbb{R}^2)} := \iint |h(a,b)|^2 a^{-2} C_\psi^{-1}\ \mathrm{d}a\,\mathrm{d}b < \infty \right\}.$$

Then

$$\forall\,(a,b) \in \mathbb{R}\setminus\{0\} \times \mathbb{R} : |\mathcal{W}f(a,b)| \leqslant \|f\| \tag{4.2a}$$

$$\forall\, a \neq 0,\ \mathcal{W}_a :\ b \mapsto \mathcal{W}f(a,b) : \mathcal{W}_a \in C_0(\mathbb{R}) \tag{4.2b}$$

$$\text{for almost all } a \neq 0 : \mathcal{W}_a \in \mathrm{L}^2(\mathbb{R}) \tag{4.2c}$$

$$\mathcal{W} : \mathrm{L}^2(\mathbb{R}) \to \mathrm{L}^2(\mathbb{R}^2) \tag{4.2d}$$

$$\forall\, f, g \in \mathrm{L}^2(\mathbb{R}) : \begin{cases} \|\mathcal{W}f\|_{\mathrm{L}^2(\mathbb{R}^2)} &=& \|f\|_{\mathrm{L}^2(\mathbb{R})} \\ \langle \mathcal{W}f, \mathcal{W}g\rangle_{\mathrm{L}^2(\mathbb{R}^2)} &=& \langle f, g\rangle_{\mathrm{L}^2(\mathbb{R})} \end{cases} \tag{4.2e}$$

$$h \in \mathrm{ran}(\mathcal{W}) \iff \quad h = \iint K(\cdot,\cdot,a,b)h(a,b)\ a^{-2}C_\psi^{-1}\ \mathrm{d}a\,\mathrm{d}b, \tag{4.2f}$$

where $K(a,b;c,d) := \langle \psi_{a,b}, \psi_{c,d}\rangle$ is the corresponding reproducing kernel.

Proof. Assertion (4.2a) follows by the Cauchy-Schwarz inequality where $\|\psi_{a,b}\| = 1$ is used.

Next, $f, \psi \in \mathrm{L}^2(\mathbb{R}) \Rightarrow \hat{f}\,\hat{\psi} \in \mathrm{L}^2(\mathbb{R})$ and again by the Cauchy-Schwarz ineq. it follows that $\hat{f}\overline{\hat{\psi}(a\cdot)} \in \mathrm{L}^1$. Furthermore,

$$\langle f, \psi_{a,b}\rangle = \left\langle \hat{f}, \hat{\psi}_{a,b} \right\rangle = \int \hat{f}(\omega) \frac{1}{\sqrt{a}} \overline{\psi\Big(\frac{\cdot - b}{a}\Big)}\hat{}\,(\omega)\,\mathrm{d}\omega = \sqrt{a}\int \hat{f}(\omega)\hat{\psi}(a\omega)e^{ib\omega}\,\mathrm{d}\omega,$$

such that by

$$\langle f, \psi_{a,b}\rangle = \sqrt{2\pi a}\Big(\hat{f}\overline{\hat{\psi}(a\cdot)}\Big)^{\vee}(b) = \sqrt{2\pi a}\Big(\hat{f}\overline{\hat{\psi}(a\cdot)}\Big)^{\wedge}(-b) \tag{4.3}$$

Equation (4.2b) follows by Riemann-Lebesgue lemma (cf. Theorem 3.5.2).

For Eq. (4.2c) it suffices to show (compare (4.3)) that $\hat{f}\overline{\hat{\psi}(a\cdot)} \in \mathrm{L}^2(\mathbb{R})$ for almost all $a \neq 0$ but this is guaranteed by the admissibility of ψ. It holds:

$$\infty > \|f\|\frac{C_\psi}{2\pi} \overset{\text{Fubini}}{=} \int |\hat{f}(\omega)|^2 \int \frac{|\hat{\psi}(a\omega)|^2}{|a|}\,\mathrm{d}a\,\mathrm{d}\omega \overset{\text{Fubini}}{=} \iint |\hat{f}(\omega)\psi(a\omega)|^2\,\mathrm{d}\omega\frac{\mathrm{d}a}{|a|}$$

which shows Eq. (4.2c).

Such an easy calculation implies also

$$\|\mathcal{W}f\|_{\mathrm{L}^2(\mathbb{R}^2)} \overset{\text{Eq.(4.3)}}{=} \int 2\pi a \int \Big|\Big(\hat{f}\overline{\hat{\psi}(a\cdot)}\Big)^{\vee}(b)\Big|^2\,\mathrm{d}b\frac{\mathrm{d}a}{C_\psi a^2}$$

and since $\mathcal{W}_a \in \mathrm{L}^2(\mathbb{R})$ a.e. Parseval eq. for $\mathcal{F}$ is applicable, i.e.

$$\left\|\Big(\hat{f}\overline{\hat{\psi}(a\cdot)}\Big)^{\vee}\right\| \overset{\text{Eq.(4.3)}}{=} \left\|\Big(\hat{f}\overline{\hat{\psi}(a\cdot)}\Big)^{\wedge}(-\cdot)\right\| \overset{\text{Parseval}}{=} \left\|\hat{f}\overline{\hat{\psi}(a\cdot)}\right\| \text{ such that}$$

$$\begin{aligned}\|\mathcal{W}f\|_{\mathrm{L}^2(\mathbb{R}^2)} &= \int 2\pi a \int |\hat{f}(\omega)\hat{\psi}(a\omega)|^2\,\mathrm{d}\omega\frac{\mathrm{d}a}{C_\psi a^2}\\ &\overset{\text{Fubini}}{=} \int |\hat{f}(\omega)|^2\Big(\frac{2\pi}{C_\psi}\int \frac{|\hat{\psi}(\nu)|^2}{|\nu|}\,\mathrm{d}\nu\Big)\,\mathrm{d}\omega\\ &\overset{\text{Parseval}}{=} \|f\|\,.\end{aligned}$$

$\langle f, g\rangle = \langle \mathcal{W}f, \mathcal{W}g\rangle$ is proven analogously as in the proof of Corollary 3.2.4.

Hence, Eq. (4.2e) holds and implies Eq. (4.2d).

ad Eq. (4.2f);

'$\Rightarrow$':

$$\begin{aligned}h(a,b) = \mathcal{W}f(a,b) = \langle f, \psi_{a,b}\rangle &= \langle \underbrace{\mathcal{W}f}_{=h}, \mathcal{W}\psi_{a,b}\rangle\\ &= \int\int h(c,d)\underbrace{\overline{\mathcal{W}\psi_{a,b}(c,d)}}_{=\langle \psi_{a,b},\psi_{c,d}\rangle}\frac{\mathrm{d}c\,\mathrm{d}d}{C_\psi a^2}.\end{aligned}$$

It remains to show that $h \in \mathrm{L}^2(\mathbb{R}^2)$ fulfilling the consistency relation (4.2f) is in the image of $\mathcal{W}$. For this consider $\mathcal{W}^* : \mathrm{L}^2(\mathbb{R}^2) \to \mathrm{L}^2(\mathbb{R})$. To show: $f := \mathcal{W}^* h$ with $h = \mathcal{W} f$, i.e. $\mathcal{W}\mathcal{W}^* = \mathrm{id}$.

$$h(a,b) = \iint \langle \psi_{a,b}, \psi_{c,d} \rangle \, h(c,d) \, \frac{\mathrm{d}c \, \mathrm{d}d}{C_\psi a^2} = \langle h, \mathcal{W}\psi_{a,b} \rangle = \langle \mathcal{W}^* h, \psi_{a,b} \rangle = \langle f, \psi_{a,b} \rangle$$
$$= \mathcal{W} f(a,b).$$

□

Remark 4.2.6. Due to the theorem above it is clear that $\mathcal{W}$ is a bounded (cf. Eq. (4.2a)) and isometric (cf. Eq. (4.2e)) operator onto $\mathrm{L}^2(\mathbb{R}^2)$ (cf. Eq. (4.2d)) which is not surjective. This is a direct consequence of Eq. (4.2a): e.g. define $h(a,b) := |a|^\gamma g(b)$, $\gamma \in (0, 1/2)$, $g \in \mathrm{L}^2(\mathbb{R})$. Then it follows that $\lim_{a\to\infty} h(a,b) = \infty$ but $h \in \mathrm{L}^2(\mathbb{R}^2)$. Hence $\nexists\, f \in \mathrm{L}^2(\mathbb{R}) : h = \mathcal{W} f$.

On the other hand, $\mathcal{W}$ is invertible on its image $\mathcal{W}^{-1} : \mathrm{ran}(\mathcal{W}) \to \mathrm{L}^2(\mathbb{R})$ and is itself an isometry.

Furthermore, each $f, g \in \mathrm{L}^2(\mathbb{R})$ satisfies

$$\langle f, g \rangle = \langle \mathcal{W} f, \mathcal{W} g \rangle = C_\psi^{-1} \int \int \mathcal{W} f(a,b) \, \langle \psi_{a,b}, g \rangle \; a^{-2} \, \mathrm{d}a \, \mathrm{d}b$$
$$= C_\psi^{-1} \int \int \langle \mathcal{W} f(a,b) \psi_{a,b}, g \rangle \; a^{-2} \, \mathrm{d}a \, \mathrm{d}b,$$

which at least in the weak sense can be interpreted as the inverse of the wavelet transform, i.e.

$$f = \mathcal{W}^{-1} h := C_\psi^{-1} \int \int h(a,b) \psi_{a,b} \, a^{-2} \, \mathrm{d}a \, \mathrm{d}b, \quad \text{for } h = \mathcal{W} f.$$

Calderón found and subsequently Grossmann and Morlet rediscovered the partition of unity (Eq. (4.4)) by means of wavelets:

Theorem 4.2.7. *For each arbitrary $f \in \mathrm{L}^2(\mathbb{R})$ and a wavelet $\psi \in L^1(\mathbb{R})$ the advance relation holds.*

$$\left\| f - C_\psi^{-1} \int_{|a|>\epsilon} \int_{\mathbb{R}} \mathcal{W} f(a,b) \psi_{a,b} \, a^{-2} \, \mathrm{d}b \, \mathrm{d}a \right\|_{\mathrm{L}^2(\mathbb{R})} \xrightarrow{\epsilon \to 0} 0 \tag{4.4}$$

If $f \in \mathrm{L}^1(\mathbb{R}) \cap C^0(\mathbb{R})$ with $\hat{f} \in L^1(\mathbb{R})$, then relation (4.4) holds in the C^0-topology, i.e. in particular pointwise!

Proof. This is beyond the scope of this thesis and can be checked for instance in [Erd03, pp. 305] and the references therein. □

Remark 4.2.8. Imposing on ψ more restrictive conditions than done in Eq. (4.1), e.g.

$$\Big(\frac{C_\psi}{4\pi} =\Big) \int_{-\infty}^{0} \frac{|\hat{\psi}(\omega)|^2}{|\omega|}\,\mathrm{d}\omega \overset{!}{=} \int_{0}^{\infty} \frac{|\hat{\psi}(\omega)|^2}{|\omega|}\,\mathrm{d}\omega < \infty, \tag{4.5}$$

lead to slightly modified Parseval and Caldéron equations, Eqs. (4.2e) and (4.4), respectively, such that the scaling coefficient a can be restricted to positive values – cf. [Erd03, pp.308] for further readings on this topic. Eq. (4.5) is automatically fulfilled if ψ is a real-valued function ($\Rightarrow \hat{\psi}(-\omega) = \overline{\hat{\psi}(\omega)}$) for instance.

4.3 Discretisation

The wavelet transform is until now only of theoretical interest. It allows yet to study functions by means of integrals which in most cases have to be calculated by some quadrature formula. This is rather awkward and ineffective and in practice the longing arise for fast and numerically stable computations of such decomposition. Hence, it is obvious to consider a discrete lattice on which this transform could be calculated by finite summations. The following subsections will show that even frames $\Big(\mathcal{W}f(j,k)\Big)_{j,k\in\mathbb{Z}}$ in $\ell^2(\mathbb{R}^2)$ can be constructed.

4.3.1 Discrete Wavelets

The atoms $\psi_{a,b}$ stands for dilated and translated copies of a 'mother wavelet' ψ. It was already noticed that if ψ is localised then $\psi_{a,b}$ is localised with $|a|$-times the spread of ψ in time domain and $\frac{1}{|a|}$-multiple of the spread of ψ in frequency domain.

Remembering that one property of frames is the ability to cluster the phase space (ω, t) with Heisenberg boxes corresponding to its frame vectors, one intuitive way of discretising the dilation and translation parameters is as follows: let $\nu \neq 0$, $\tau > 0$. Define for $j,k \in \mathbb{Z}:\ a_j := \nu^{-j},\ b_{j,k} := \nu^{-j}k\tau$

$$\psi_{j,k} := \psi_{a_j,b_{j,k}}. \tag{4.6a}$$

where $\nu \neq 0$ can be further restricted to $\nu > 1,\ \tau > 0$ such that

$$\psi_{j,k} = \nu^{j/2}\psi\Big(\frac{\cdot - \nu^{-j}k\tau}{\nu^{-j}}\Big) = \nu^{j/2}\psi(\cdot\nu^j - k\tau) \tag{4.6b}$$

where the restriction of ν to positive values is allowed by Remark 4.2.8 and $\nu > 1$ can be considered as a substitution of the scale index $j \in \mathbb{Z}$.

The definition of $b_{j,k}$ especially the multiplication with ν^{-j} ensures that at each scale j the translation $k\tau$ is refined and stays qualitatively as same as at scale $j-1$.

It is not only a cosmetic reason but also guarantees that $\psi_{j,k}$ have a non-zero overlap (more precisely their Heisenberg boxes) in the phase space, since otherwise $(\psi_{j,k})$ would fail to span $\mathrm{L}^2(\mathbb{R})$.

Ingrid Daubechies (1990) – and subsequently Chui and Shi (1991) with different techniques – were able to prove necessary and sufficient conditions for $(\psi_{j,k})$ constituting a frame in $\mathrm{L}^2(\mathbb{R})$. The next claims, Theorems 4.3.1 and 4.3.3, are borrowed from [Dau92, pp.63 and p.69] where the technical proofs are omitted.

Theorem 4.3.1. *(Daubechies – necessity for frames) Let* $\psi \in \mathrm{L}^2(\mathbb{R})$ *and assume that* $(\psi_{j,k})_{j,k\in\mathbb{Z}}$ *– defined as in Eq.* (4.6a) *– constitutes a frame in* $\mathrm{L}^2(\mathbb{R})$ *with frame bounds* $0 < A \leqslant B < \infty$*. Then*

$$A \leqslant \frac{2\pi}{\tau \ln \nu} \int_{\mathbb{R}} \frac{|\hat{\psi}(\omega)|^2}{|\omega|} \,\mathrm{d}\omega \leqslant B. \tag{4.7}$$

Remark 4.3.2. If ν is restricted to positive values as it is done in Eq. (4.6b) then the estimate Eq. (4.7) splits up into a positive and negative frequency domain, i.e.

$$A \leqslant \frac{2\pi}{\tau \ln \nu} \int_{\mathbb{R}_{\geqslant 0}} \frac{|\hat{\psi}(\omega)|^2}{|\omega|} \,\mathrm{d}\omega \leqslant B \text{ and } A \leqslant \frac{2\pi}{\tau \ln \nu} \int_{\mathbb{R}_{\leqslant 0}} \frac{|\hat{\psi}(\omega)|^2}{|\omega|} \,\mathrm{d}\omega \leqslant B. \tag{4.8}$$

Note also the similarities between the admissibility condition (cf. Definition 4.2.1 and Eq. (4.5)) and these a priori restrictions (Eqs. (4.7), (4.8)) on ψ which imply that these preconditions do not have a severe impact if ψ is already assumed to be a wavelet!

Theorem 4.3.3. *(Daubechies – sufficiency for frames) Let* ψ *be admissible and decay in frequency domain like*

$$|\hat{\psi}(\omega)| \leqslant \begin{cases} C|\omega|^{\epsilon} & |\omega| \leqslant 1 \\ C|\omega|^{-(1+\epsilon)} & |\omega| \geqslant 1 \end{cases} \text{ for some } \epsilon,\, C > 0. \tag{4.9a}$$

If $\exists\, \nu > 1$, $\exists\, \beta \geqslant \alpha > 0$ *such that* $\forall\, |\omega| \in [1, \nu]$:

$$\alpha \leqslant \sum_{j\in\mathbb{Z}} |\hat{\psi}(\nu^j \omega)|^2 \leqslant \beta \tag{4.9b}$$

$\Longrightarrow \exists\, \tau_\nu > 0 :$ $(\psi_{j,k})_{j,k\in\mathbb{Z}}$ *constitutes a frame in* $\mathrm{L}^2(\mathbb{R})$ *,* $\forall\, \tau < \tau_\nu$.

Corollary 4.3.4 ([Erd03, pp. 326])**.** *If ψ is admissible and $\psi \in L^1(\mathbb{R})$ with $\hat{\psi}(\omega) \neq 0 \; \forall \, |\omega| \in (0, h)$, for some $h > 0$ fulfilling the decaying properties as stated by Eq.* (4.9a)*, then $\exists \, \tau_\nu > 0 : \; (\psi_{j,k})_{j,k \in \mathbb{Z}}$ constitutes a frame in* $\mathrm{L}^2(\mathbb{R})$*, $\forall \, \tau < \tau_\nu$.*

Proof. Let $\nu > 1$ and $|\omega| \in (1, \nu)$. Then

$$\begin{aligned} \sum_j |\hat{\psi}(\nu^j \omega)|^2 &\leqslant C^2 |\omega|^2 \sum_{j \in \mathbb{Z}_{\leqslant -1}} \nu^{2j\epsilon} + C^2 |\omega|^{-2(1-\epsilon)} \sum_{j \in \mathbb{Z}_{\geqslant 0}} \nu^{-2j(1+\epsilon)} \\ &\leqslant C^2 \left(\frac{1}{1 - \nu^{-2\epsilon}} + \frac{1}{1 - \nu^{-2(1+\epsilon)}} \right). \end{aligned}$$

Moreover, due to the continuity of $\hat{\psi}$ (since $\psi \in L^1$), it follows that $|\hat{\psi}(\omega)| > 0$ on $(-h, 0) \cup (0, h)$ such that $\exists \, \delta > 0$ and $k < 1$: $|\hat{\psi}(\omega)| > \delta$ on $(-\nu^{k+1}, -\nu^k) \cup (\nu^k, \nu^{k+1}) \subset (-h, 0) \cup (0, h) \Rightarrow$

$$\sum_j |\hat{\psi}(\nu^j \omega)|^2 \geqslant |\hat{\psi}(\nu^k \omega)|^2 \geqslant \delta^2.$$

Hence, Eq. (4.9b) of upper theorem is fulfilled. □

This easy to check properties together with the approach to orthonormal wavelets, presented in the sequel, led in the past to a lot of compelling wavelets, see Section 4.4.1.

4.3.2 Multiresolution Analysis – MRA

Suppose that there exists $\phi \in \mathrm{L}^2(\mathbb{R})$ such that

$$\psi = \sum_k d_k \phi(\cdot - k) \text{ and } \phi = \sum_k c_k \phi(2 \cdot - k) \tag{4.10}$$

hold for c_k, d_k where in each case only finitely many coefficients are non-zeros and ϕ is considered to be normalised. Define $\phi_{k,l} := 2^{k/2} \phi(2^k \cdot - l)$, i.e. $\nu = 2, \; \tau = 1$ and analogously $\psi_{k,l}$. Then

$$\langle f, \psi_{k,l} \rangle = \sum_j d_j \, \langle f, \phi_{k,l+j} \rangle \tag{4.11a}$$

$$\langle f, \phi_{k,l} \rangle = \sqrt{2} \sum_j c_j \, \langle f, \phi_{k-1,2l+j} \rangle \, , \tag{4.11b}$$

such that reconstruction and superposition is carried out in a recursive way by means of finite convolutions (since it was assumed that $c = (c_k)_k$ and $d = (d_k)_k$ have a compact support).

Relation (4.11) furnishes a fast algorithm first described by Mallat which enabled an implementation of this wavelet analysis of same low complexity as for the so-called *Fast Fourier transform*.

The existence of such function ϕ and in particular the relation (4.10) is a necessity of the so-called *multiresolution analysis - MRA* - concept which was introduced in the late 80s by Stephane Mallat and Yves Meyer.

Definition 4.3.5 (MRA)**.** A **multiresolution analysis** of $\mathrm{L}^2(\mathbb{R})$ is a chain of closed subspaces $\{V_j\}_{j\in\mathbb{Z}}$ satisfying following properties

$$\text{Containment:} \qquad V_j \subset V_{j+1} \subset \mathrm{L}^2(\mathbb{R}) \quad \forall j \in \mathbb{Z} \tag{4.12a}$$

$$\text{Increase:} \qquad \overline{\bigcup_{j\in\mathbb{Z}} V_j}^{\|\cdot\|_{\mathrm{L}^2(\mathbb{R})}} = \mathrm{L}^2(\mathbb{R}) \tag{4.12b}$$

$$\text{Decrease:} \qquad \bigcap_{j\in\mathbb{Z}} V_j = \{0\} \tag{4.12c}$$

$$\text{Dilation:} \qquad f(\cdot) \in V_j \iff f(2\cdot) \in V_{j+1} \tag{4.12d}$$

$$\text{Generator:} \qquad \exists\, \phi \in V_0 :\ (\phi(\cdot - k))_{k\in\mathbb{Z}} \text{ is an onb in } V_0 \tag{4.12e}$$

As a direct consequence of requirement (4.12a) it follows that $V_0 \subset V_1$ and, due to Eqs. (4.12e) and (4.12d), $(\phi_{1,n})_{n\mathbb{Z}}$ is an onb in V_1. Therefore there exists $c \in \ell^2 :\ \phi = \sum_k c_k \phi_{1,k} = \sqrt{2}\sum_k \phi(2\cdot - k)$.

Since V_0 is a closed subspace of V_1 there exists a $W_0 \neq \emptyset$, $W_0 \subset V_1$ such that $V_1 = V_0 \oplus W_0$.

Hence, for any $\psi \in W_0$ it can be analogously deduced that $\exists\, d \in \ell^2 :\ \psi = \sum_k d_k \phi_{1,k} = \sqrt{2}\sum_k d_k \phi(2\cdot - k)$.

Theorem 4.3.6 ([Erd03, pp. 384])**.** *(i) There exist coefficients $c := (c_k)_k$ and $d := (d_k)_k$ with $c, d \in \ell^2(\mathbb{R})$ such that*

$$\textit{scaling equation} \quad \phi = \sum_k c_k \phi_{1,k} = \sqrt{2}\sum_k \phi(2\cdot - k) \tag{4.13a}$$

$$\textit{consistency equation} \quad \sum_k c_k \overline{c_{k+2n}} = \delta_{0,n} \quad \forall\, n \in \mathbb{Z} \tag{4.13b}$$

$$\textit{wavelet equation} \quad \psi = \sum_k d_k \phi_{1,k} = \sqrt{2}\sum_k d_k \phi(2\cdot - k) \tag{4.13c}$$

(ii) ψ generates an onb $(\psi_{k,l})_{k,l\in\mathbb{Z}}$ in $\mathrm{L}^2(\mathbb{R})$ $\iff$

$$\psi \in W_0 \Leftarrow \langle \phi(\cdot - n), \psi\rangle = 0 \quad \forall\, n \in \mathbb{Z},\ \textit{i.e. } \psi \perp V_0 \tag{4.14a}$$

$$\langle \psi(\cdot - n), \psi\rangle = \delta_{0,n} \quad \forall\, n \in \mathbb{Z} \tag{4.14b}$$

$$(\psi(\cdot - n))_n \textit{ is complete in } W_0 \tag{4.14c}$$

(iii) Eqs. (4.14) $\Longleftrightarrow \forall\, n$:

$$\sum_k c_k \overline{d_{k+2n}} = 0 \tag{4.15a}$$

$$\sum_k d_k \overline{d_{k+2n}} = \delta_{0,n} \tag{4.15b}$$

$$\sum_k |c_{2k+n}|^2 + \sum_k |d_{2k+n}|^2 = 1 \tag{4.15c}$$

The considerations above hint at further proceedings, e.g. setting $n = 0$ in Eq. (4.15c) and in the consistency Equation (4.13b) it follows

$$\sum_k |c_{2k}|^2 + \sum_k |d_{2k}|^2 = 1 = \sum_k |c_k|^2$$

$$\text{and by subtraction (r.h.s. minus l.h.s.)} \Rightarrow \sum_{k \text{ even}} |d_k|^2 = \sum_{k \text{ odd}} |c_k|^2,$$

which was first proven by Meyer and Mallat.

Corollary 4.3.7 (Mallat & Meyer [Erd03, pp. 390])**.** *The system* $(\psi_{j,k})_{j,k\in\mathbb{Z}}$ *generated by* $\psi := \sqrt{2}\sum_k d_k \phi(2\cdot - k)$ *with* $d_k := (-1)^k \overline{c_{1-k}}$ *is an orthonormal wavelet basis in* $\mathrm{L}^2(\mathbb{R})$ *if* ϕ *is a scaling function with scaling coefficients* $(c_k)_k$*.*

The following theorem shows that under additional assumptions even finite summations of type Eqs. (4.11) can result in exact reconstructions. This is very convenient especially in implementing algorithms on the computer.

Theorem 4.3.8 ([Erd03, pp. 395])**.** *Let* ϕ *be a scaling function with* $\mathrm{supp}(\phi) = [a, b]$*. Then* $a,\, b \in \mathbb{Z}$ *and for each* $k \in \mathbb{Z}$ *it holds*

(i) $\quad 0 = c_k = d_k \quad \forall\, k < a \wedge k > b, \quad c_l \neq 0 \neq d_l,\ l = a, b$

(ii) $\quad \exists\, \psi$ *wavelet with* $\mathrm{supp}(\phi) = \mathrm{supp}(\psi)$.

Obviously there are (at least) three ways to tackle the problem of constructing an MRA which itself was mainly introduced due to difficulties in giving appropriate orthonormal wavelets.

A reasonable starting point could be the design of closed subspaces $V_j \subset \mathrm{L}^2(\mathbb{R})$ which form a ladder as claimed in Eq. (4.12a).

Unfortunately, a proof of the existence of a scaling function $\phi \in V_0$ is not as handy as the easily verified properties (4.12b)-(4.12d). And in general, if the converse - the non-existence of ϕ is shown, it is not evident how to modify V_j in order to obtain an MRA. It turns out that the remaining two approaches are of more profitability:

In the 1988s Ingrid Daubechies managed to construct compactly supported, regular wavelets (see Section 4.4.1) imposing some conditions on the scaling coefficients. This and Mallat's recursive algorithm (as intimated by Eqs. (4.11)) was a breakthrough in the wavelet community since then it was possible to transform and reconstruct signals with the same complexity as payed for the Fast Fourier transform – as the theorem above suggests only finitely many coefficients are different from zero.

In the sequel a third approach will be presented: multiresolution analysis generated by a scaling function.

Theorem 4.3.9. *Let* $\phi \in \mathrm{L}^2(\mathbb{R})$

(i) Relations (4.12d)-(4.12e) *hold* $\iff$ $(\phi(\cdot - k))_k$ *is an onb in* V_0*, where*

$$V_j := \left\{ f \in \mathrm{L}^2(\mathbb{R}) \,\middle|\, \exists\, c \in \ell^2(\mathbb{R}) :\ f = \sum_k c_k \phi_{j,k} \right\} \tag{4.16}$$

(ii) Relations (4.12d)-(4.12e) *imply Eq.* (4.12c)

(iii) Assume that Eqs. (4.12d)-(4.12e) *hold. If* $\forall\, \epsilon > 0\, \exists\, \delta > 0$ *such that for almost all* $\omega \in \mathrm{B}_\epsilon(0) :\ |\hat{f}(\omega)| \geqslant \delta \Rightarrow$ *Equation* (4.12b) *holds*

(iv) Eqs. (4.12d)-(4.12e) *hold and* ϕ *satisfies the scaling equation* (4.13a) *iff* $(V_j)_j$ *complies with Relation* (4.12a)*.*

Proof. These are trivial but lengthy implications of Definition 4.3.5. Check for example [Erd03, pp.401]. □

Corollary 4.3.10. *Let* $\phi \in \mathrm{L}^2(\mathbb{R})$ *meet*

(i) $(\phi(\cdot - k))_{k \in \mathbb{Z}}$ *constitutes an ons in* $\mathrm{L}^2(\mathbb{R})$

(ii) ϕ *satisfies the scaling relation, Eq.* (4.13a)

(iii) $\forall\, \epsilon > 0\, \exists\, \delta > 0$ *such that for a.a.* $\omega \in \mathrm{B}_\epsilon(0) :\ |\hat{f}(\omega)| \geqslant \delta$*.*

Then $(V_j)_j$ *defines an MRA such that* ϕ *is the accompanying scaling function.*

Proof. This follows directly from upper theorem. □

In practice attendant preconditions of upper corollary are still inconvenient such that sufficient or equivalent stipulations which are easier to check have to be acquired.

Above all, by means of Fourier transform it is possible to give exceptional constructive and intuitive conditions on $\hat{\phi}$:

Theorem 4.3.11. *Let $\phi \in \mathrm{L}^2(\mathbb{R})$. Then*

(i) $\phi(\cdot - k)$ is an ons in $\mathrm{L}^2(\mathbb{R}) \iff G(\omega) := \sum_k |\hat{\phi}(\omega + 2k\pi)|^2 = \dfrac{1}{2\pi}$ a.e. and $G \in \mathrm{L}^2_{2\pi}$.

(ii) ϕ satisfies the scaling relation $\iff$

$$\exists\, m_\phi \in \mathrm{L}^2_{2\pi}(\mathbb{R}): \qquad \hat{\phi}(\omega) = m_\phi(\frac{\omega}{2})\hat{\phi}(\frac{\omega}{2}) \text{ a.e. with} \tag{4.17a}$$

$$m_\phi(\omega) = \sqrt{2}\sum_k c_k e^{-ik\omega} \text{ in } \mathrm{L}^2(\mathbb{R}) \text{ -sense} \tag{4.17b}$$

$$\text{respectively,} \qquad c_k = \frac{1}{\sqrt{2}\pi}\int_\pi^\pi m_\phi(\omega)e^{ik\omega}\,\mathrm{d}\omega, \quad k \in \mathbb{Z} \tag{4.17c}$$

c_k scaling coefficients of ϕ.

Proof. First claim follows by sequentially applying Beppo – Levi's and Lebesgue's dominated convergence theorem: Let $(\phi(\cdot - n)_n)$ be an ons. Then $\forall\, n \in \mathbb{Z}$:

$$\begin{aligned}\langle \phi(\cdot - n), \phi\rangle &= \left\langle \hat{\phi}(\cdot - n), \hat{\phi}\right\rangle = \int |\hat{\phi}(\omega)|^2 e^{-in\omega}\,\mathrm{d}\omega \\ &= \sum_{k\in\mathbb{Z}} \int_{k2\pi}^{(k+1)2\pi} |\hat{\phi}(\omega)|^2 e^{-in\omega}\,\mathrm{d}\omega = \sum_{k\in\mathbb{Z}} \int_0^{2\pi} |\hat{\phi}(\omega + 2k\pi)|^2 e^{-in\omega}\,\mathrm{d}\omega.\end{aligned}$$

For $n = 0$ define $g_K(\omega) := \sum_{|k|\leqslant K} |\hat{\phi}(\omega + 2k\pi)|^2$. g_K is non-negative, monotonically increasing and above calculations imply that

$$\sup_{K\in\mathbb{R}} \int_0^{2\pi} g_K(\omega)\,\mathrm{d}\omega \leqslant 1.$$

Now, by Beppo – Levi it follows that

$$\lim_{K\to\infty} \int_0^{2\pi} \sum_{|k|\leqslant K} |\hat{\phi}(\omega + 2k\pi)|^2\,\mathrm{d}\omega = \int_0^{2\pi} \lim_{K\to\infty} \sum_{|k|\leqslant K} |\hat{\phi}(\omega + 2k\pi)|^2\,\mathrm{d}\omega$$

$$\text{i.e. } G \in \mathrm{L}^2_{2\pi} \text{ and } \|g_K - G\|_{\mathrm{L}^2_{2\pi}} \xrightarrow{K\to\infty} 0.$$

Let $n \in \mathbb{Z}$ and define $f_{K,n}(\omega) := g_K(\omega)e^{-in\omega}$, $F_n(\omega) := G(\omega)e^{-in\omega}$. Then

$\forall\, K, n: \ |f_{K,n}| \leqslant G \in \mathrm{L}^1(\mathbb{R})$ a.e. with $f_{K,n} \xrightarrow[\text{a.e.}]{K\to\infty} F_n$ such that by Lebesgue

$$\delta_{0,n} = \langle \phi(\cdot - n), \phi\rangle = \int_0^{2\pi} F_n(\omega)\,\mathrm{d}\omega = 2\pi\hat{G}(n) \iff G(\omega) = \frac{1}{2\pi} \text{ a.e..}$$

ad ii) Let $I \subset \mathbb{R}$.

$$\forall\, n: \ \underbrace{\Big(\sum_{|k|\leqslant n} c_k \phi(\cdot - k)\Big)^{\wedge}(\omega)}_{=:\, f_n} = \sum_{|k|\leqslant n} c_k \Big(\phi(\cdot - k)\Big)^{\wedge}(\omega) = \underbrace{\Big(\sum_{|k|\leqslant n} c_k e^{-ik\omega}\Big)}_{=:\, g_n} \hat{\phi}(\omega).$$

Due to continuity of $\mathcal{F}$ it follows $\Big\| \mathcal{F}(f_n) - \mathcal{F}\Big(\sum_{k\in\mathbb{Z}} c_k \phi(\cdot - k)\Big) \Big\|_{\mathrm{L}^2(I)} \xrightarrow{n\to\infty} 0,$

which also means convergence in $\mathrm{L}^1(I)$-sense, since $\mathrm{L}^2(I) \subset \mathrm{L}^1(I)$. g_n converges in the sense of $\mathrm{L}^2([m, m+2\pi])$, $m \in \mathbb{R}$, and so, by Cauchy-Schwarz, $g_n\hat{\phi} \xrightarrow{n\to\infty} \sum_k c_k e^{-ik\cdot}\hat{\phi}$ converges in $\mathrm{L}^1([m, m+2\pi])$-sense. According to Plancherel's theorem, Theorem 3.5.9, it follows

$$f = \sum_k c_k \phi(\cdot - k) \iff \hat{f} = \Big(\sum_k c_k e^{-ik\cdot}\Big)\hat{\phi} \tag{4.18}$$

and in particular, applying Theorem 3.5.8,

$$\phi(2^{-1}\cdot) = \sqrt{2}\sum_k c_k \phi(\cdot - k) \iff 2\hat{\phi}(2\cdot) = \sqrt{2}\Big(\sum_k c_k e^{-ik\cdot}\Big)\hat{\phi}.$$

□

Corollary 4.3.12. *(Meyer, Mallat) Let $(V_j)_j$ be an MRA with a corresponding scaling function ϕ and m_ϕ. Then ψ defined by*

$$\hat{\psi} = -e^{-i\frac{\cdot}{2}}\overline{m_\phi\Big(\frac{\cdot}{2} + \pi\Big)}\hat{\phi} \tag{4.19}$$

constitutes an orthonormal wavelet corresponding to the MRA $(V_j)_j$.

Proof. This is a direct consequence of Corollary 4.3.7 and Eq. (4.3). □

Remark 4.3.13. (i) The demand of orthonormality of $(\phi(\cdot - n))_n$ can be dropped. More precisely, it can be relaxed by claiming that $(\phi(\cdot - n))_{n\in\mathbb{Z}}$ should constitute a Riesz basis for V_0 which is an equivalent request to $0 < \alpha \leqslant \sum_k |\hat{\phi}(\omega - 2k\pi)|^2 \leqslant \beta < \infty$ a.e. (see [Dau92, pp. 139] for a detailed discussion).

(ii) Imposing additionally $\phi \in \mathrm{L}^1(\mathbb{R})(\cap \mathrm{L}^2(\mathbb{R}))$ Items 1, 2 and 3 of Corollary 4.3.10 gets necessary for ϕ being a scaling function of an MRA ([Erd03, p. 407]).

(iii) Each MRA 'generates' an orthonormal wavelet basis $(\psi_{j,k})_{j,k\in\mathbb{Z}}$ in $\mathrm{L}^2(\mathbb{R})$. The converse is not true. One famous counterexample was given shortly after introducing the concept of an MRA by J. L. Journé ([Mal89, p. 69-87]).

On the other hand, it can be proved that each orthonormal wavelet basis with compact support (cf. [LR92, p. 17-19]) or with some significant decay (cf. [Aus95, p. 181-236]) can be associated with an MRA.

The essence of this subsection is that by imposing very weak requirements it is possible to construct an orthonormal wavelet basis in $\mathrm{L}^2(\mathbb{R})$ such that

- the dual $\widetilde{\psi}_{j,k}$ is naturally given ($\widetilde{\psi}_{j,k} = \psi_{j,k}$) and so reconstruction is ergo less computational expensive, $f = \sum_{j,k\in\mathbb{Z}} \langle f, \psi_{j,k}\rangle \, \psi_{j,k}$,
- and can further be reduced by algorithms which exploits the recursivity mentioned at the outset, Eq. (4.11).

For numerical implementation there remains one aspect to consider, namely the asymptotical behaviour of the wavelet transform $(\langle f, \psi_{j,k}\rangle)_{j,k}$ since only finitely many of the very same coefficients can be computed.

Strictly speaking, the goal is to achieve a good accuracy, i.e.

$$\sup_x \left| \sum_{(j,k)\in\mathbb{Z}^2} \langle f, \psi_{j,k}\rangle \, \psi_{j,k}(x) - \sum_{(j,k)\in F_\epsilon} \langle f, \psi_{j,k}\rangle \, \psi_{j,k}(x) \right| < \epsilon, \tag{4.20}$$

$\epsilon > 0$ small, with as small as possible index set $F_\epsilon \subset \mathbb{Z}^2$ – here $|F_\epsilon|$ denotes the amount of indices contained in F_ϵ.

In other words, the attention lies in finding such wavelets which obey some asymptotics like

$$|\, \langle f, \psi_{a,b}\rangle \,| = \mathcal{O}\,(\ldots)\,. \tag{4.21}$$

Moreover, in many applications the wavelet transform is carried out because the major interest lies in the extraction of the evolutionary process of frequencies. In particular, it is believed by the author that this is the key for solving problems such as speech recognition (see also Chapter 2)

Hence, in addition to the claim (4.21) it is only fair to demand that ψ has to be localised, i.e. ψ and $\hat{\psi}$ have to fulfill some decaying properties.

Fortunately, by Theorem 3.5.4 regularity of ψ is equivalent to a rapid decay of $\hat{\psi}$. This is a lucky link by the simple reason that regularity of an orthonormal wavelet ψ also implies relation (4.21).

In total, orthonormal wavelets ψ have to be regular and decay rapidly in time domain. All the said can be summarised in the following two theorems whose proofs are omitted.

Theorem 4.3.14. *([Dau92, pp. 153]) Let $f, g \in \mathrm{L}^2(\mathbb{R})$ such that they generate an orthonormal set, i.e. $\langle f_{j,k}, g_{l,m}\rangle = \delta_{j,l}\delta_{k,m}\,\forall\, j,k,l,m \in \mathbb{Z}$ for $f_{j,k}$ and $g_{l,m}$ defined as in Eq. (4.10). If f fulfills the decay properties, $|f(x)| = \mathcal{O}\left(1+|x|^{-m-1-\epsilon}\right)$ for some $\epsilon > 0$ and $g \in \mathrm{C}^m(\mathbb{R})$, $g^{(l)}$, $l \leqslant m$ are bounded, then g has m vanishing moments, i.e.*

$$\int x^l g(x)\,\mathrm{d}x = 0, \quad \forall\, l = 0, \ldots, m. \tag{4.22}$$

Theorem 4.3.15. *(Holschneider, Tchamitchian [Dau92, pp. 48]) Let ψ be a wavelet with m vanishing moments (cf. Eq.(4.22)) and $\alpha \in (0,1)$ and $f \in \mathrm{C}^m(\mathbb{R})$, $\forall\, n \leqslant m:\ f^{(n)} \in \mathrm{L}^2(\mathbb{R})$ is bounded. Then*

global

$$f^{(n)} \in \mathrm{C}^{0,\alpha}(\mathbb{R}) \iff |\langle f, \psi_{a,b}\rangle| = \mathcal{O}\left(|a|^{\alpha+\frac{1}{2}+m}\right) \text{ uniformly in } b$$

local

$f^{(n)}$ is Hölder continuous in some $\xi \in \mathbb{R}$ with exponent α, i.e.

$$|f^{(n)}(\xi+h)| = \mathcal{O}\left(|h|^{\alpha}\right) \Rightarrow |\left\langle f^{(n)}, \psi_{a,b+\xi}\right\rangle| = \mathcal{O}\left(\sqrt{|a|}(|a|^{\alpha}+|b|^{\alpha})\right)$$

and conversely

$$\exists\, \gamma > 0:\ |\left\langle f^{(n)}, \psi_{a,b}\right\rangle| = \mathcal{O}\left(|a|^{\gamma+\frac{1}{2}}\right) \text{ uniformly in } b \text{ and}$$

$$|\left\langle f^{(n)}, \psi_{a,b+\xi}\right\rangle| = \mathcal{O}\left(\sqrt{|a|}\left(|a|^{\alpha} + \frac{|b|^{\alpha}}{\left|\log|b|\right|}\right)\right)$$

$$\Rightarrow |f^{(n)}(\xi+h)| = \mathcal{O}\left(|h|^{\alpha}\right)$$

Remark 4.3.16. The renowned property of the wavelet transform behaving like a *mathematical zoom* stems basically from the theorem above. Note also that this is an intrinsic property of the wavelet transform and does not confine oneself to the orthonormal case. By way of illustration the wavelet transform of the function $t \mapsto 1-|t|$ is showed in Figure 4.6.

In general, convergence similar to Eq. (4.20) is also satisfied for wavelet frames, i.e.

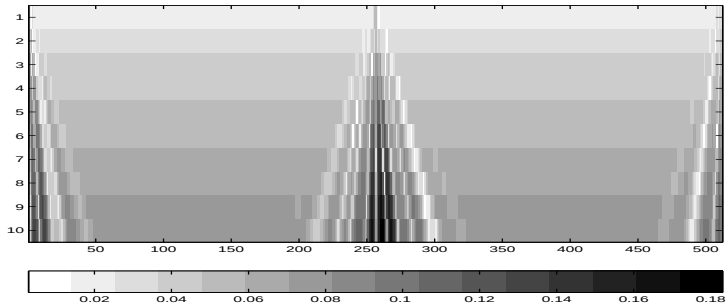

Fig. 4.6: Zooming property of the Wavelet transform. The function $t \mapsto 1 - |t|$, with $t \in [-1, 1]$ is discretised (here it is uniformly sampled, $t_k = -1 + k\Delta$, $k = 0, \ldots, 512$, $\Delta = \frac{2}{512}$, such that the kink (or corner) of the original function is at the sample $t_{256,257}$); the subsequent (continuous) wavelet transformation of that sequence is shown in the plot. The so-called *Meyer* wavelet and Matlab's built-in function *cwt* was used here to compute the coefficients, $c_{l,m} := \langle (t_k)_k, (\psi_{l,m})_m \rangle_{\ell^2}$, with levels: $l = 1, 2, 3, \ldots, 10$, as intimated by the ordinate, check also Remark 4.2.2. The grey tone is proportional to $|c_{l,m}|$, $m = 1, \ldots, 512$. The frequency range decreases as the level increases. Such a plot shows exactly the kink since it narrows at level 1 and samples $t_{256,257}$.

Theorem 4.3.17 ([Dau92, pp. 88])**.** *Let $(\psi_{j,k})_{j,k}$ defined as in Eq.* (4.6b) *constitute a frame with frame bounds A, B with following decay*

$$|\psi(x)| = \mathcal{O}\left((1+x^2)^{-\alpha^2}\right), \qquad |\hat{\psi}(\omega)| = \mathcal{O}\left(|\omega|^{\beta}(1+\omega^2)^{-\frac{\beta+\gamma}{2}}\right)$$

and $\alpha, \gamma > 1$, $\beta > 0$. Then, $\forall\, \epsilon > 0\, \exists\, F_\epsilon(\Omega_0, \Omega_1, T) \subset \mathbb{Z}^2$ s.t. $\forall\, f \in \mathrm{L}^2(\mathbb{R})$:

$$\begin{aligned} &\left\| f - \sum_{(j,k)\in F_\epsilon(\Omega_0,\Omega_1,T)} \langle f, \psi_{j,k}\rangle\, \widetilde{\psi_{j,k}} \right\|_{\mathrm{L}^2(\mathbb{R})} \\ &\quad \leqslant \sqrt{\frac{B}{A}} \Bigg(\Bigg(\underbrace{\int_{\Omega_1<|\omega|<\Omega_0} |\hat{f}(\omega)|^2 \,\mathrm{d}\omega}_{=:\, \|\hat{f}\|^2_{\mathrm{L}^2(\Omega_0,\Omega_1)}} \Bigg)^{1/2} + \Bigg(\underbrace{\int_{|x|>T} |f(x)|^2 \,\mathrm{d}x}_{=:\, \|f\|^2_{\mathrm{L}^2(T)}} \Bigg)^{1/2} + \epsilon\, \|f\| \Bigg) \end{aligned} \tag{4.23}$$

with $F_\epsilon(\Omega_0, \Omega_1, T) := \{(m, n) \big| m_0 < m < m_1,\, |n\tau| \leqslant \nu^{-m} T + t\}$ and m_0, m_1, t as defined in the proof [Dau92, p. 92 and 93, resp.].

As a special case, if $\|f\|_{\mathrm{L}^2(T)} \leqslant \delta \|f\|^2$ and $\|f\|_{\mathrm{L}^2(\Omega_0,\Omega_1)} \leqslant \delta \|f\|^2$, i.e. if f itself is 'essentially' localised in phase space on two rectangles $[-T, T] \times [-\Omega_1, -\Omega_0] \cup [-T, T] \times [\Omega_0, \Omega_1]$ then $\|f - \sum_{(j,k)\in F_\delta} \langle f, \psi_{j,k}\rangle\, \psi_{j,k}\|_{\mathrm{L}^2} = \mathcal{O}(\delta)$.

As already mentioned, the lengthy proof can be checked in [Dau92, pp. 88].

4.4 Speech processing by Common Techniques

Due to the character of this chapter which is intended only as an introduction, respectively summary of a vast area and rapidly developing theory concerning wavelets, only two families of orthonormal wavelets will suit as an example: *Daubechies* and *Meyer (– Lemarié-Rieusset)* wavelets.

The former due to their outstanding properties and the latter because of its similar construction compared to *local trigonometric packets* which will be presented in the next chapter.

In the light of 'real' examples, Section 4.4.2 will summarise some of the drawbacks of $\mathcal{F}_g$ and $\mathcal{W}$.

4.4.1 Daubechies – Meyer

As already seen, the Haar wavelet is an orthonormal wavelet with compact support. In particular,

$$\phi = \chi_{[0,1)} \Rightarrow \phi(2t-k) = \chi_{[\frac{k}{2},\frac{k+1}{2})}(t)$$

such that the scale equation reduces to

$$\phi(t) = \chi_{[\frac{k}{2},\frac{k+1}{2})}(t) + \chi_{[\frac{k}{2},\frac{k+1}{2})}(t) = \sqrt{2}\Big(\frac{1}{\sqrt{2}}\phi(2t) + \frac{1}{\sqrt{2}}\phi(2t-1)\Big)$$

hence, $c_{0,1} = 2^{-1/2}$, $c_{k\neq 0,1} = 0$ and analogously, $d_0 = -d_1 = 2^{-1/2}$, $d_{k\neq 0,1} = 0$.

Unfortunately, this wavelet basis is of no practical importance since it is only piecewise continuous and would automatically introduce artifacts (i.e. supplement information not present in the original signal).

Daubechies made an ansatz based on the function $m_\phi = 2^{-1/2}\sum_k c_k e^{-ik\cdot}$ (cf. Corollary 4.3.12) where$(c_k)_k$ is supposed to have only *finitely many non-zeros* such that m_ϕ is a (continuous complex) trigonometric polynomial.

Furthermore, the scaling function ϕ has to be of compact support. This involves several advantages:

- according to Theorem 4.3.8, ψ is also of compact support
- $\phi, \psi \in \mathrm{L}^1(\mathbb{R})$ and hence $\hat{\phi}, \hat{\psi} \in \mathrm{C}(\mathbb{R})$ which implies that Eq. (4.17a) holds in particular pointwise everywhere
- by iteration of Eq. (4.17a), i.e. $\hat{\phi}(\omega) = m_\phi(\omega/2)\hat{\phi}(\omega/2)$ it goes as $\hat{\phi}(\omega) = \prod_{j=1}^{n} m_\phi(2^{-j}\omega)\hat{\phi}(2^{-n}\omega)$. Due to continuity of ϕ, respectively

$\hat{\phi}(0) = c/(\sqrt{2}\pi)$ for some $c \in \mathbb{C}$ with $|c| = 1$ (cf. Corollary 4.3.10) this product converges for $n \to \infty$ to

$$\hat{\phi}(\omega) = \frac{c}{\sqrt{2}\pi} \prod_{j \geqslant 1} m_\phi(2^{-j}\omega),$$

where the phase of c is irrelevant and will be set to zero, i.e. $c = 1$.

Since the main goal is to construct a (regular) orthonormal wavelet basis (with compact support) corresponding to a multiresolution analysis it is sufficient (and necessary, cf. Corollary 4.3.10 and Remark 4.3.13, second item) to check the following properties

$$M(\omega) := \frac{1}{\sqrt{2\pi}} \prod_{j \geqslant 1} m_\phi(2^{-j}\omega) \text{ converges} \tag{4.24a}$$

$$M \in \mathrm{L}^2(\mathbb{R}) (\text{which would imply } \mathcal{F}^{-1}(M) = \phi \in \mathrm{L}^2(\mathbb{R})) \tag{4.24b}$$

$$(\phi(\cdot - k))_k \text{ constitutes an ons} \tag{4.24c}$$

$$\forall\, \epsilon > 0 : \ |\hat{\phi}(\omega)| > 0 \text{ for almost all } \omega \in B_\epsilon(0). \tag{4.24d}$$

Convergence, even uniform convergence of $M(\omega)$ on every compact set and continuity turns out to be a necessity of

$$m_\phi(0) = 1. \tag{A}$$

$$\text{Imposing } |m_\phi(\omega)|^2 + |m_\phi(\omega + \pi)|^2 = 1, \quad \forall\, \omega \tag{B}$$

it follows that $M \in \mathrm{L}^2(\mathbb{R})$ and on top of it $\mathcal{F}^{-1}(M)$ has compact support and $\hat{\phi}(0) = 1/\sqrt{2\pi}$ which by continuity of $\hat{\phi}$ implies then Eq. (4.24d).

Both conditions (A), (B) are necessary for a multiresolution analysis. This is a consequence of the following:

$$\begin{aligned}
\frac{1}{2\pi} &= \sum_{k \in \mathbb{Z}} |\hat{\phi}(\omega + 2k\pi)|^2 = \Big(\sum_{k \text{ even}} + \sum_{k \text{ odd}} \Big) |\hat{\phi}(\omega + 2k\pi)|^2 \\
&= \sum_{k \in \mathbb{Z}} |\hat{\phi}(\omega + 4k\pi)|^2 + \sum_{k \in \mathbb{Z}} |\hat{\phi}(\omega + 4k\pi + 2\pi)|^2 \\
\text{by Theorem 4.3.11, (ii)} &= \sum_{k \in \mathbb{Z}} \Big| \underbrace{m_\phi\Big(\frac{\omega}{2} + 2k\pi\Big)}_{= m_\phi(\frac{\omega}{2})} \Big|^2 \Big| \hat{\phi}\Big(\frac{\omega}{2} + 2k\pi\Big) \Big|^2 \\
&\quad + \sum_{k \in \mathbb{Z}} \Big| \underbrace{m_\phi\Big(\frac{\omega}{2} + (2k+1)\pi\Big)}_{= m_\phi(\frac{\omega}{2} + \pi)} \Big|^2 \Big| \hat{\phi}\Big(\frac{\omega}{2} + (2k+1)\pi\Big) \Big|^2 \\
\text{Theorem 4.3.11, (i), (ii)} &= \Big| m_\phi\Big(\frac{\omega}{2}\Big) \Big|^2 \frac{1}{2\pi} + \Big| m_\phi\Big(\frac{\omega}{2} + \pi\Big) \Big|^2 \frac{1}{2\pi} \Rightarrow \text{(B)}
\end{aligned}$$

and for $\phi \in \mathrm{L}^1 \cap \mathrm{L}^2$, i.e. in particular $\hat{\phi}(0) \neq 0$ it follows from Eq. (4.17a)

$$m_\phi(0) = \frac{\hat{\phi}(0)}{\hat{\phi}(0)} = 1 \Rightarrow \text{(A)}.$$

The remaining property, $(\phi(\cdot - k))_k$ ons in L^2, is almost guaranteed by (A) and (B) (in fact, orthogonality can be deduced) such that orthonormality can be concluded from

$$m_\phi(\omega) \neq 0 \quad \forall\, \omega \in [-\frac{\pi}{3}, \frac{\pi}{3}], \tag{C}$$

for instance.

All omitted proofs can be checked at [Erd03, pp.488]

In this framework, the Haar wavelet crystallises as the most simple orthonormal wavelet for which the ansatz $m_\phi(\omega) = a + be^{-i\omega}$ is made.

$$\begin{aligned}
m_\phi(0) \overset{!}{=} 0 \Rightarrow m_\phi(\pi) = 0 \Rightarrow a + b = 1 \wedge a - b = 0 \\
\Rightarrow m_\phi(\omega) = \frac{1}{2}(1 + e^{i\omega}) = \cos\Big(\frac{\omega}{2}\Big) e^{-i\frac{\omega}{2}} \\
\Rightarrow m_\phi(\omega) \neq 0 \, \forall\, \omega \in [-\frac{\pi}{3}, \frac{\pi}{3}] \text{ and} \\
|m_\phi(\omega)|^2 + |m_\phi(\omega + \pi)|^2 = \cos^2\Big(\frac{\omega}{2}\Big) + \sin^2\Big(\frac{\omega}{2}\Big) = 1
\end{aligned}$$

such that m_ϕ do generate a scaling function $\phi \in \mathrm{L}^1 \cap \mathrm{L}^2$ corresponding to an MRA,

$$\begin{aligned}
\hat{\phi}(\omega) &= \frac{1}{\sqrt{2\pi}} \prod_{j \geqslant 1} e^{-i\omega 2^{-j-1}} \cos(\omega 2^{-j-1}) \\
\text{uniform conv} &= \frac{1}{\sqrt{2\pi}} \prod_{j \geqslant 1} e^{-i\omega 2^{-j-1}} \prod_{j \geqslant 1} \cos(\omega 2^{-j-1}) \\
&= \frac{1}{\sqrt{2\pi}} e^{-i\omega \sum_{j \geqslant 1} 2^{-j-1}} \prod_{j \geqslant 1} \cos(\omega 2^{-j-1}) \\
\text{L. Euler} &= \frac{1}{\sqrt{2\pi}} e^{-i\omega} \frac{\sin\Big(\frac{\omega}{2}\Big)}{\frac{\omega}{2}} \\
&\Rightarrow \phi = \chi_{[0,1)}
\end{aligned}$$

Imposing regularity (smoothness) on the functions ϕ, ψ at hand it is possible to show that this is an equivalent demand for vanishing moments (cf. Theorem 4.3.14, or [Dau92, pp. 153]) which itself is an equivalent claim for m_ϕ

having a zero at π of sufficiently high order (check [Dau92, pp. 155]) such that the factorisation

$$m_\phi = (1 + e^{-i\cdot})^n \ell_\phi, \quad n \geqslant 1$$

promises to come to fruition. Here ℓ_ϕ stands for a trigonometric polynomial of this kind

$$\ell_\phi = \sum_{k \leqslant m} c_k e^{-ik\cdot}, \quad m \geqslant 1.$$

Ingrid Daubechies was able to give a constructive method how to achieve orthonormal wavelets ${}_n\psi \in \mathrm{C}^{\beta_n}$ of compact support, $\mathrm{supp}({}_n\psi) = [-n+1, n]$ with n vanishing moments, where regularity is understood in an asymptotical way, i.e. ${}_n\phi$, ${}_n\psi \in \mathrm{C}^{\beta_n} :\Longleftrightarrow \frac{\beta_n}{\gamma n} \xrightarrow{n\to\infty} 1$, for $\gamma := 1 - \frac{\ln 3}{\ln 4}$.

In particular,

- $\mathrm{supp}({}_n\phi) = [0, 2n-1]$ with $2n$ non-vanishing scaling coefficients
- $\forall\, n > 1 :\ {}_n\phi_n\psi$ have no anti-/symmetry and no analytical representation by means of elementary function (see also Figure 4.7). Latter curiosity prompted Yves Meyer to grant them the status of new special functions.

All omitted proofs concerning Daubechies wavelets can be checked in [Dau92, Chapter 6].

Meyer wavelets Again, let the Haar scaling function be a starting point to a new family. $\phi_{\mathrm{Haar}} = \chi_{[0,1)}$ is one of the most elementary ansatz for a scaling function in time domain. Consider therefore a translated version of this characteristic function in the frequency domain

$$\mathrm{L}^2 \ni \hat{\phi} := \frac{1}{\sqrt{2\pi}} \chi_{[\nu,\mu)}$$

For $-\nu = \mu = \pi$ this ansatz fulfills the prerequisitions of Corollary 4.3.10 such that

$$\phi(t) = \mathcal{F}^{-1}(\hat{\phi})(t) = \frac{1}{2\pi} \int_{-\pi}^{\pi} e^{it\omega}\, \mathrm{d}\omega = \frac{\sin(\pi t)}{\pi t} \text{ for } t \neq 0$$

and $\phi(0) := 1$. Eq. (4.17a) motivates the definition $(\forall\, |\omega| < \pi :\ \hat{\phi}(\omega/2) \neq 0 \Rightarrow m_\phi(\omega/2) = \hat{\phi}(\omega)/\hat{\phi}(\omega/2))$

$$m_\phi := \chi_{[-\frac{\pi}{2}, \frac{\pi}{2})}, \text{ for } |\omega| < \pi$$

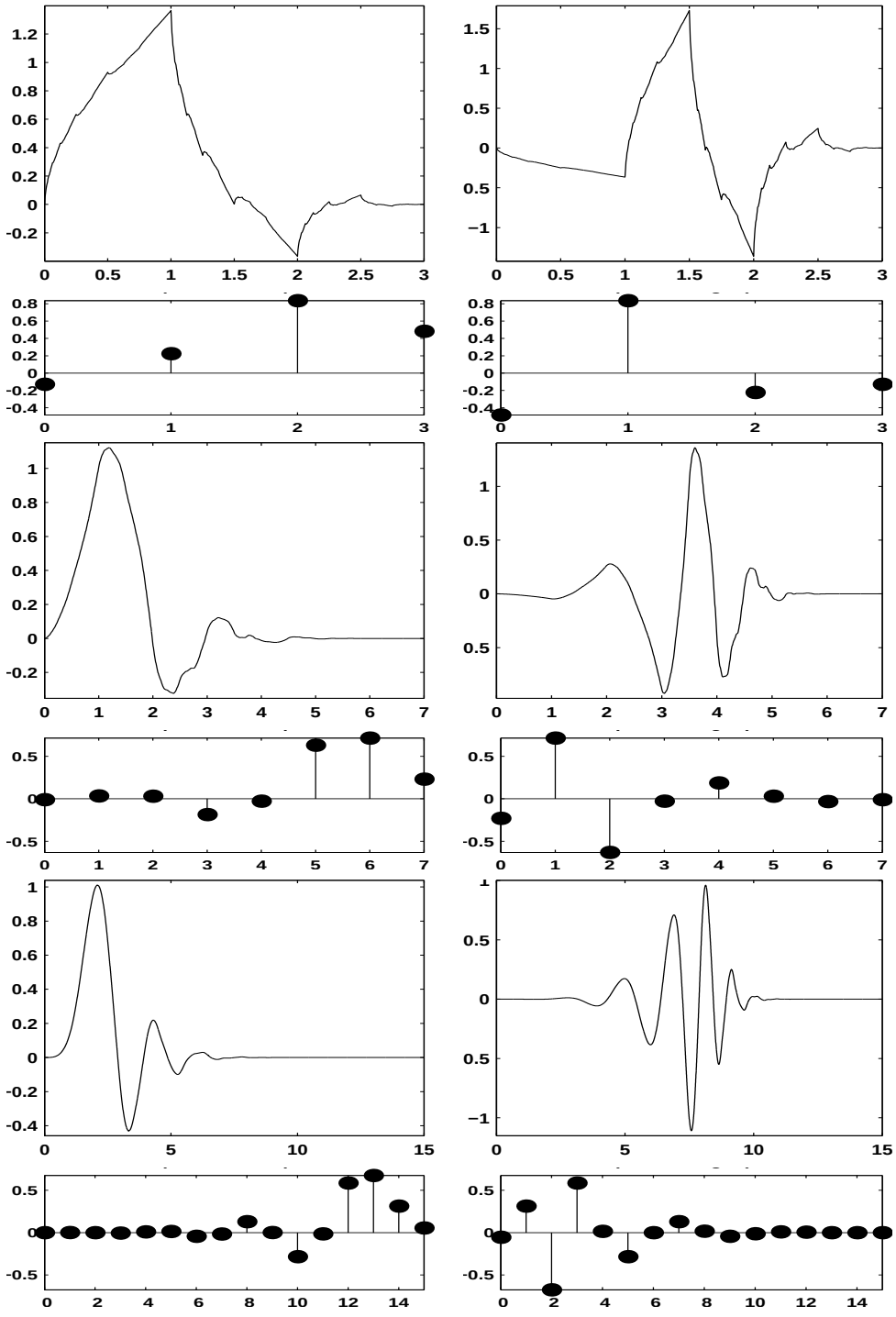

Fig. 4.7: Left column contains alternating scale function and scale coefficients. Same order for right column picturing the corresponding wavelets. In particular, Daubechies's least symmetric wavelets ${}_n\psi$ (and scaling functions ${}_n\phi$) with $n = 2, 4$ and 8 are plotted.

such that $m_\phi \in \mathrm{L}^2_{2\pi}$ and ϕ is indeed a scaling function ($|\hat\phi(\omega)| > 0$ and $\sum_k |\hat\phi(\omega+2k\pi)|^2 = |\hat\phi(\omega)|^2 + |\hat\phi(\omega+2\pi)|^2 = (2\pi)^{-1}$) corresponding to an MRA with scaling coefficients

$$\begin{aligned} c_k &= \frac{1}{\sqrt{2}\pi}\int_{-\pi}^{\pi} m_\phi(\omega)e^{ik\omega}\,\mathrm{d}\omega = \frac{1}{\sqrt{2}\pi}\int_{-\frac{\pi}{2}}^{\frac{\pi}{2}} e^{ik\omega}\,\mathrm{d}\omega \\ &= \frac{1}{\sqrt{2}}\frac{2}{k\pi}\sin\Big(\frac{k\pi}{2}\Big) = \begin{cases} (-1)^{\frac{k-1}{2}} & k \text{ odd} \\ \frac{\sqrt{2}}{k\pi} & 0 \neq k \text{ even} \\ \frac{1}{\sqrt{2}} & k = 0 \end{cases} \end{aligned}$$

and due to Corollary 4.3.12

$$\begin{aligned} \hat\psi(\omega) &:= e^{-i\frac{\omega}{2}}\overline{m_\phi\Big(\frac{\omega}{2}+\pi\Big)}\hat\phi\Big(\frac{\omega}{2}\Big) = \frac{e^{-i\frac{\omega}{2}}}{\sqrt{2\pi}}\chi_{[-2\pi,-\pi)\cap[\pi,2\pi)}(\omega) \\ \Rightarrow \quad \psi &= \frac{\sin(2\pi(t-\frac{1}{2})) - \sin(\pi(t-\frac{1}{2}))}{\pi(t-\frac{1}{2})}. \end{aligned}$$

Sampling Theorem ϕ is called *Shannon scaling* function and ψ *Shannon wavelet* which is named after Claude E. Shannon. He was the first who proved the so called *sampling theorem*. Whittaker was first stating the following

Theorem 4.4.1. *(Sampling Theorem) Let $f \in \mathrm{C}\cap\mathrm{L}^2$, $\mathrm{supp}(\hat f) \subset [-\pi,\pi]$. Then*

$$f(t) = \sum_{k\in\mathbb{Z}} f(k)\frac{\sin(\pi(t-k))}{\pi(t-k)} \quad \textit{almost everywhere.} \tag{4.25}$$

Lemma 4.4.2. *Let $(V_j)_j$ be an MRA with ϕ as the corresponding scaling function. Then*

$$f \in V_0 \iff \exists\, m_f \in \mathrm{L}^2_{2\pi} :\ \hat f(\omega) = m_f(\omega)\hat\phi(\omega).$$

Proof of Lemma 4.4.2. Since ϕ is a scaling function corresponding to an MRA $(V_j)_j$, it follows that $(\phi(\cdot-k))_k$ is in particular an orthonormal basis in V_0. Hence,

$$\begin{aligned} f \in V_0 &\iff \exists\,(c_k)_k \in \ell^2 :\ f = \sum_k c_k\phi(\cdot-k) \\ &\overset{\text{Eq. (4.18)}}{\iff} \hat f = \left(\sum_k c_k e^{-ik\cdot}\right)\hat\phi. \end{aligned}$$

□

Proof of the Sampling theorem. The proof is different from Shannon's and uses the framework of an MRA:

Lemma 4.4.2 holds especially for the Shannon scaling function ϕ where

$$\begin{aligned} V_0 &= \left\{ f \,\middle|\, \exists\, (c_k)_k \in \ell^2 : \sum_k c_k \phi(\cdot - k) \right\} \\ &= \left\{ f \,\middle|\, \hat{f} = \frac{1}{\sqrt{2\pi}} \chi_{[-\frac{\pi}{2},\frac{\pi}{2})} \chi_{[-\pi,\pi)} = \frac{1}{\sqrt{2\pi}} \chi_{[-\pi,\pi)} \right\} \\ &= \left\{ f \,\middle|\, \operatorname{supp}(\hat{f}) \subset [-\pi,\pi] \right\}. \end{aligned}$$

But this complies with the preconditions of the sampling theorem and allows therefore

$$f = \sum_k \langle f, \phi(\cdot - k) \rangle \, \phi(\cdot - k) = \sum_k \langle f, \phi(\cdot - k) \rangle \, \frac{\sin(\pi(\cdot - k))}{\pi(\cdot - k)}$$

and

$$\begin{aligned} \langle f, \phi(\cdot - k) \rangle &= \left\langle \hat{f}, \hat{\phi}(\cdot - k) \right\rangle = \left\langle \hat{f}, e^{-ik\cdot} \hat{\phi} \right\rangle = \frac{1}{\sqrt{2\pi}} \int_{-\pi}^{\pi} \hat{f}(\omega) e^{+ik\omega} \, \mathrm{d}\omega \\ &= \hat{\hat{f}}(-k) = f(k), \text{ if } \hat{\hat{f}} \in \mathrm{C}(\mathbb{R}) \text{ (cf. Eq (3.11))}. \end{aligned}$$

□

Remark 4.4.3. A common generalisation of the Theorem 4.4.1 goes as:

$$\begin{aligned} &\text{Let } f \in \mathrm{C} \cap \mathrm{L}^2 \text{ and } \operatorname{supp} \hat{f} \subset [-\Omega, \Omega],\ a \in \left(0, \tfrac{\pi}{\Omega}\right] \\ &\Longrightarrow f = \sum_k f(ka) \frac{\sin\big(\pi(a^{-1} \cdot - k)\big)}{\pi(a^{-1} \cdot - k).} \end{aligned}$$

One possibility to prove this is

$$\begin{aligned} &g := f(\cdot a) \in \mathrm{C} \cap \mathrm{L}^2 \text{ and } \hat{g}(\omega) = |a|^{-1} \hat{f}(a^{-1}\omega) \Rightarrow \operatorname{supp}(\hat{g}) \in [-\pi, \pi] \\ &\Longrightarrow f(t) = g(a^{-1}t) = \sum_k g(k) \frac{\sin(\pi(a^{-1}t - k))}{\pi(a^{-1}t - k)}. \end{aligned}$$ □

In this context, a^{-1} is called *sampling density*. The higher a^{-1} the more often f is sampled[1]

[1]Sampling is the process of converting a continuous signal into a discrete signal.

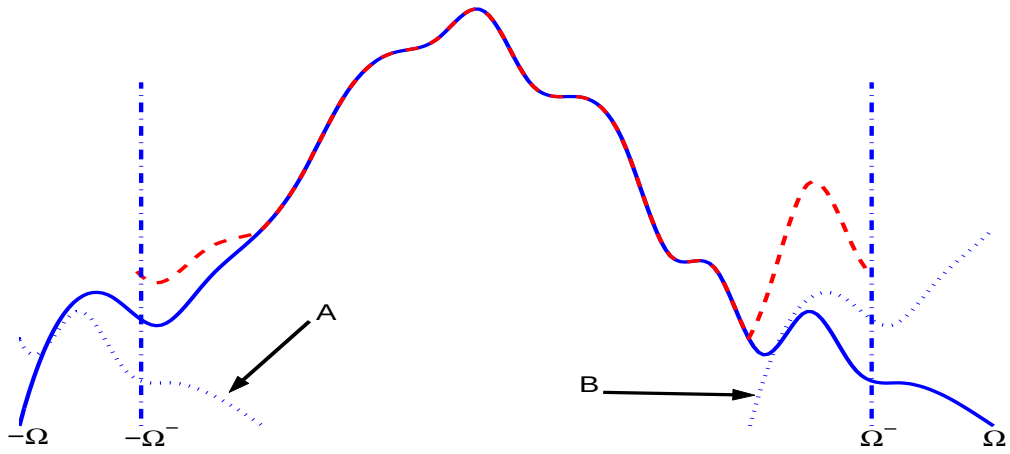

Fig. 4.8: Aliasing. Red dashed line corresponds to the sum $\mathrm{A} + \hat{f} + \mathrm{B} := \hat{f}(\omega + 2\Omega^-) + \hat{f}(\omega) + \hat{f}(\omega - 2\Omega^-)$.

The lowest bound, $a^{-1} \in [\frac{\Omega}{\pi}, \infty)$, is called *Nyquist density*, i.e. $a^{-1} = \frac{|\mathrm{supp}(\hat{f})|}{2\pi}$. The sampling theorem says that above Nyquist's density f can be exactly reconstructed from its samples $f(ka)$.

If f is sampled below its Nyquist density, i.e. $a^{-1} < \frac{\Omega}{\pi}$, then it is not possible to reconstruct the original signal from its samples. For instance, let $a = \frac{\pi}{\Omega^-} > \frac{\pi}{\Omega}$, $\Omega^- := \Omega(1-\epsilon)$ for some $\epsilon > 0$. For convenience, let $\epsilon \in (0, \frac{2}{3})$. Then, cf. [Dau92, pp. 19], exploiting 2-periodicity of $e_n(\omega) := e^{\pi i n \omega}$, i.e. $e_n(\omega + 2) = e_n(\omega)$ it follows

$$\begin{aligned}\sqrt{2\pi} f(ka) &= \int_{-\Omega}^{\Omega} \hat{f}(\omega) e_n\big(\tfrac{\omega}{\Omega^-}\big)\,\mathrm{d}\omega \\ &= \int_{-\Omega^-}^{\Omega^-} \Big(\hat{f}(\omega + 2\Omega^-) + \hat{f}(\omega) + \hat{f}(\omega - 2\Omega^-)\Big) e_n\big(\tfrac{\omega}{\Omega^-}\big)\,\mathrm{d}\omega.\end{aligned}$$

Last equation shows that the undersampled signal $f(ka)$ is an *alias* of a Fourier transform and 'folded over' $\hat{f}$ with narrower band width, cf. Figure 4.8

Very low and high frequency parts are folded back (onto the interval $(-\Omega^-, \Omega^-)$) such that instead of $\hat{f}$ a superposition $\mathrm{A} + \hat{f} + \mathrm{B}$ is obtained.

The Shannon wavelet is so to say diametrically opposed to the Haar wavelet. Excellent localising properties in frequency domain of the former is faced with no localisation at all of the latter and vice versa in time domain.

In both cases the reason of slow decay ($\hat{\psi}_{\mathrm{Haar}}$, ψ_{Shannon}) is due to the discontinuities of the characteristic function. Hence, the first idea is to smooth ϕ_{Shannon} around $\pm\pi$.

Meyer and Lemarié-Rieusset proposed therefore

$$\hat{\phi}_\nu(\omega) := \frac{1}{\sqrt{2\pi}} \begin{cases} 1 & |\omega| \leqslant \frac{2}{3}\pi \\ \cos\Big(\frac{\pi}{2}\nu\big(\frac{3}{2\pi}|\omega| - 1\big)\Big) & \frac{2}{3}\pi < |\omega| < \frac{4}{3}\pi \\ 0 & |\omega| \geqslant \frac{4}{3}\pi \end{cases} \tag{4.26a}$$

$$\text{with } \operatorname{supp}(\nu) \subset [0,1] \text{ and } \nu(x) + \nu(1-x) = 1 \,\forall\, x. \tag{4.26b}$$

Since $\hat{\phi}_\nu$ is of compact support this family of functions is Lebesgue square integrable and for the 2π-periodic function

$$G_\nu(\omega) := \sum_{k\in\mathbb{Z}} |\hat{\phi}_\nu(\omega + 2k\pi)|^2$$

it holds for instance on the interval $\omega \in [-\frac{2}{3}\pi, \frac{4}{3}\pi) : G\nu(\omega) = |\hat{\phi}_\nu(\omega)|^2 + |\hat{\phi}_\nu(\omega - 2\pi)|^2$. For $|\omega| < \frac{2}{3}\pi$ it follows by definition $G_\nu \equiv \frac{1}{2\pi}$ and exploiting the symmetry of ν on the remaining intervall $\omega \in [\frac{2}{3}\pi, \frac{4}{3}\pi)$ it holds

$$\begin{aligned} 2\pi G_\nu(\omega) &= \cos^2\Big(\frac{\pi}{2}\nu\big(\frac{3}{2\pi}\omega - 1\big)\Big) + \cos^2\Big(\frac{\pi}{2}\underbrace{\nu\big(\frac{3}{2\pi}(\omega - 2\pi) - 1\big)}_{\nu\left(2-\frac{3}{2\pi}\omega\right)=1-\nu\left(\frac{3}{2\pi}\omega-1\right)}\Big) \\ &= \cos^2\Big(\frac{\pi}{2}\nu\big(\frac{3}{2\pi}\omega - 1\big)\Big) + \underbrace{\cos^2\Big(\frac{\pi}{2} - \frac{\pi}{2}\nu\big(\frac{3}{2\pi}\omega - 1\big)\Big)}_{=\sin^2\left(\frac{3}{2\pi}\omega-1\right)} = 1 \end{aligned}$$

such that in total $G_\nu \equiv \frac{1}{2\pi}$ on $\mathbb{R}$ almost everywhere. So it only lacks to check an a.e. property: $\hat{\phi}_\nu(\omega) = \sqrt{2\pi}\hat{\phi}(\omega)\hat{\phi}(\frac{\omega}{2})$ from which the existence $m_{\phi_\nu}(\omega) = \sqrt{2\pi}\hat{\phi}_\nu(2\omega)$, $|\omega| < \pi$ could be deduced.

But this follows from $\hat{\phi}_\nu(\frac{\omega}{2}) = \frac{1}{2\pi}$ for $|\omega| \leqslant \frac{4}{3}\pi$ and $\operatorname{supp}(\hat{\phi}_\nu) = [-\frac{4}{3}\pi, \frac{4}{3}\pi]$ such that $\frac{\hat{\phi}_\nu(\omega)}{\sqrt{2\pi}\hat{\phi}_\nu(\omega)} = \hat{\phi}(\frac{\omega}{2})$ is easily veriefied. Hence, $\phi \in \mathrm{L}^2$ is a scaling function and $\hat{\psi}_\nu := e^{-\frac{i}{2}\cdot}\overline{m_{\phi_\nu}(\frac{1}{2}\cdot + \pi)}\hat{\phi}_\nu$ the accompanying wavelet.

For $\nu = \chi_{[\frac{1}{2},\infty)}$, $\hat{\psi}$ reduces to the Shannon wavelet and for $\nu \in \mathrm{C}^n(\mathbb{R})$ (cf. Figure 4.9) it holds

- $\psi \in \mathrm{C}^\infty(\mathbb{R})$,
- $|\psi^{(k)}(t)| = \mathcal{O}\left(|t|^{-k}\right), \quad \forall\, k \geqslant 0,$
- ψ is symmetric around $\frac{1}{2}$ with
- $n-1$ vanishing moments, which are defined as in Eq. (4.22).

A proof can be found at [Erd03, pp.534] and the references therein.

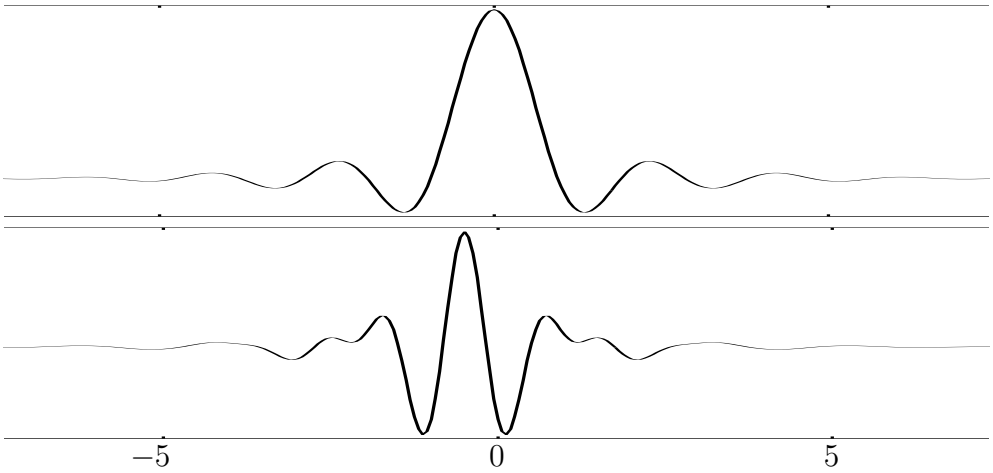

Fig. 4.9: Meyer scaling function (up) and wavelet (down) for the choice $\nu(x) = x^4(35 - 84x + 80x^2 - 20x^3)$ as in [Dau92, p. 119].

4.4.2 Spectrograms

In theory, the wavelet transform has a lot of 'nice' properties whilst the windowed Fourier transform simply lacks.

Nevertheless, it is the application which decide about usefulness of one or the other. In image analysis, for compression or denoising of signals, just to mention only a few areas of application, the wavelet transform might be very handy. But in case of speech processing this highly acclaimed tool fails to do a good job.

DWT for Voiced - Voiceless Distinction

A really simple way to distinguish voiced from unvoiced signals is showed in Figure 4.10. Here, coefficients of the fourth and third level of a discrete wavelet transformed signal (using Matlab's built-in function *wavedec* and Daubechies ${}_3\psi$ wavelet) were used as indicators for frequencies ranging from 1 to 0.5 kHz (third level) and 500 to 250 Hz (forth level) which are known to be characteristic for voiced speech, see Chapter 2.

If the absolute value of a coefficient is above a threshold then it is marked (in Figure 4.10 with a red star). For simplicity, the threshold is set to twice of the mean of all absolute valued coefficients.

The most left and right marked coefficient corresponds to the boundaries of a voiced segment (red dotted line in each waveform).

This method is of low computational complexity since in principle, only a discrete wavelet transform up to level 4 have to be computed.

The same algorithm is used for the word ['fɛnstər] (window) where two

voiced segments should be achieved. Figure 4.11 illustrates such a partition where level four and five were used to compute the boundaries.

The sole reason considering two levels instead of one is that it is more robust. This can be seen in Figure 4.11,(b) for the second vowel [e] where the marked coefficients at level four do not correspond to the right boundary.

Such a proceeding works for all words contained in the catalogue (cf. Section 6.2).

Nevertheless, that partition may be too coarse since frequency intervals smaller than one octave cannot be distinguished one from the other.

$\mathcal{F}_g$ *for Formant Extraction*

Another simplistic example shows the benefits of a windowed Fourier transform. The author has recorded twenty realisations per each vowel [u], [o], [a], [e] and [i] spoken by himself and sampled at 8 kHz (duration approx. 0.63 seconds).

These utterances are windowed Fourier transform with a Matlab's default window called *Hanning*. Those algorithms are built-in functions in Matlab, executable by the command *specgram*.

Similar procedure as above marks the coefficients of each windowed Fourier transform signal which are above a pre-defined threshold.

In each 'windowed power spectrum' the strongest peak should correspond to $F1$. $F2$ must have a higher frequency and if there exists a third peak, corresponding to $F3$, then its frequency should again be higher than that of $F2$.

This yields a sequence of coefficients (actually a $3 \times n$ matrix; each row pertinent to n coefficients of $F1$, $F2$, $F3$, resp.) which is averaged and is assumed to correspond approximately to the curve of each formant (cf. Figure 4.12).

Figure 4.13 shows the so computed $F1$, $F2$ and $F3$. Although the algorithm (averaging the coefficient sequence) is not very sophisticated it leads already to a distinction of vowels which may also derive from the fact that marked coefficients of all vowels are subdued to the averaging process (equal treatment).

This remarkable property is also due to a really good frequency resolution of that particular windowed Fourier transform.

Slight variations of the window size results in a different distinction between the vowels. Which window size to use is a priory not clear, cf. Figure 4.14.

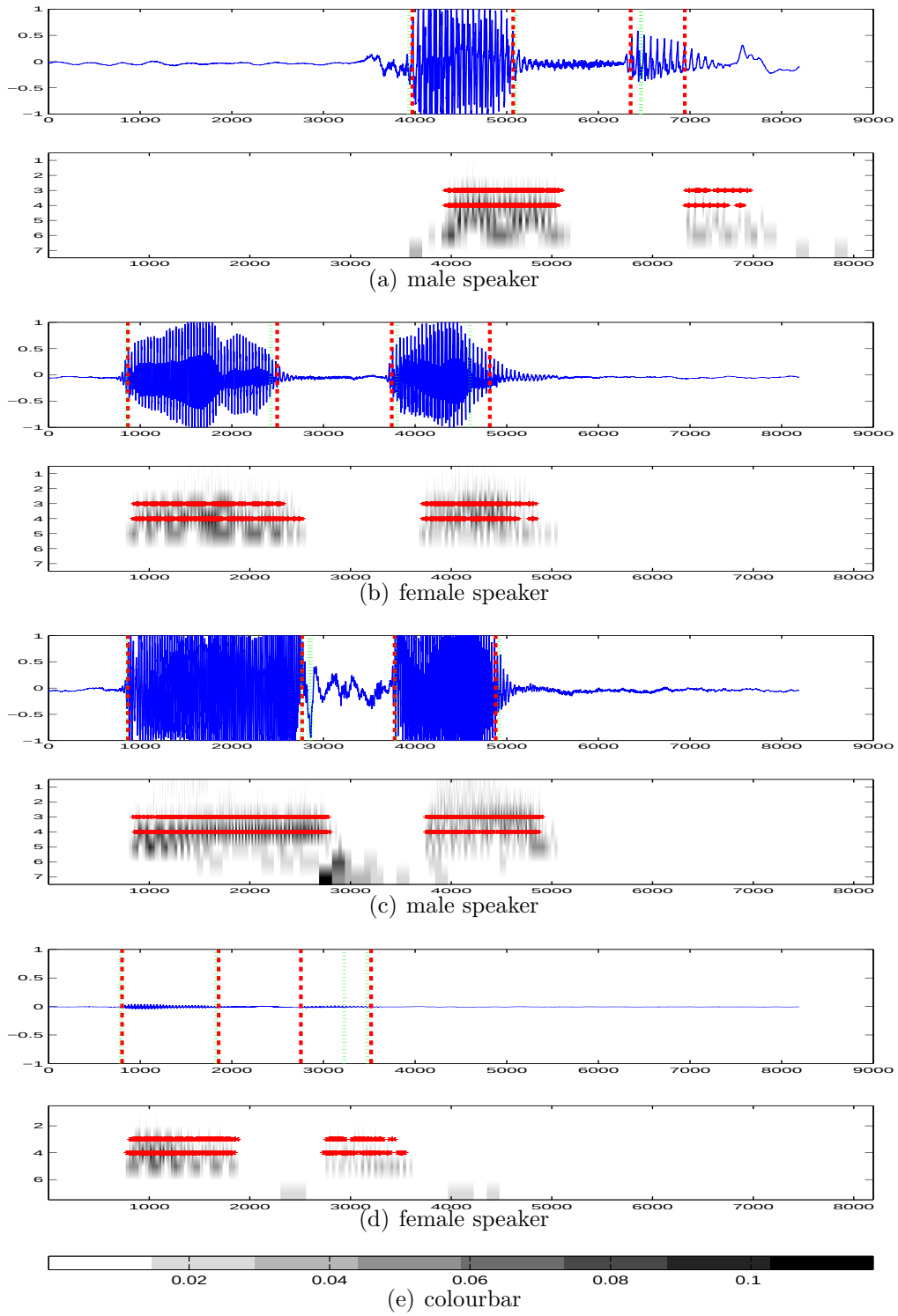

Fig. 4.10: The German word [ˈhilfə] (help) is decomposed in voiced and unvoiced (or *voiceless*) parts using a discrete wavelet transform with Daubechies ${}_3\psi$ wavelet up to level 7 which is shown under each waveform. The colourbar used to plot the *absolute value* of the wavelet coefficients was `colormap(1-gray(8))`

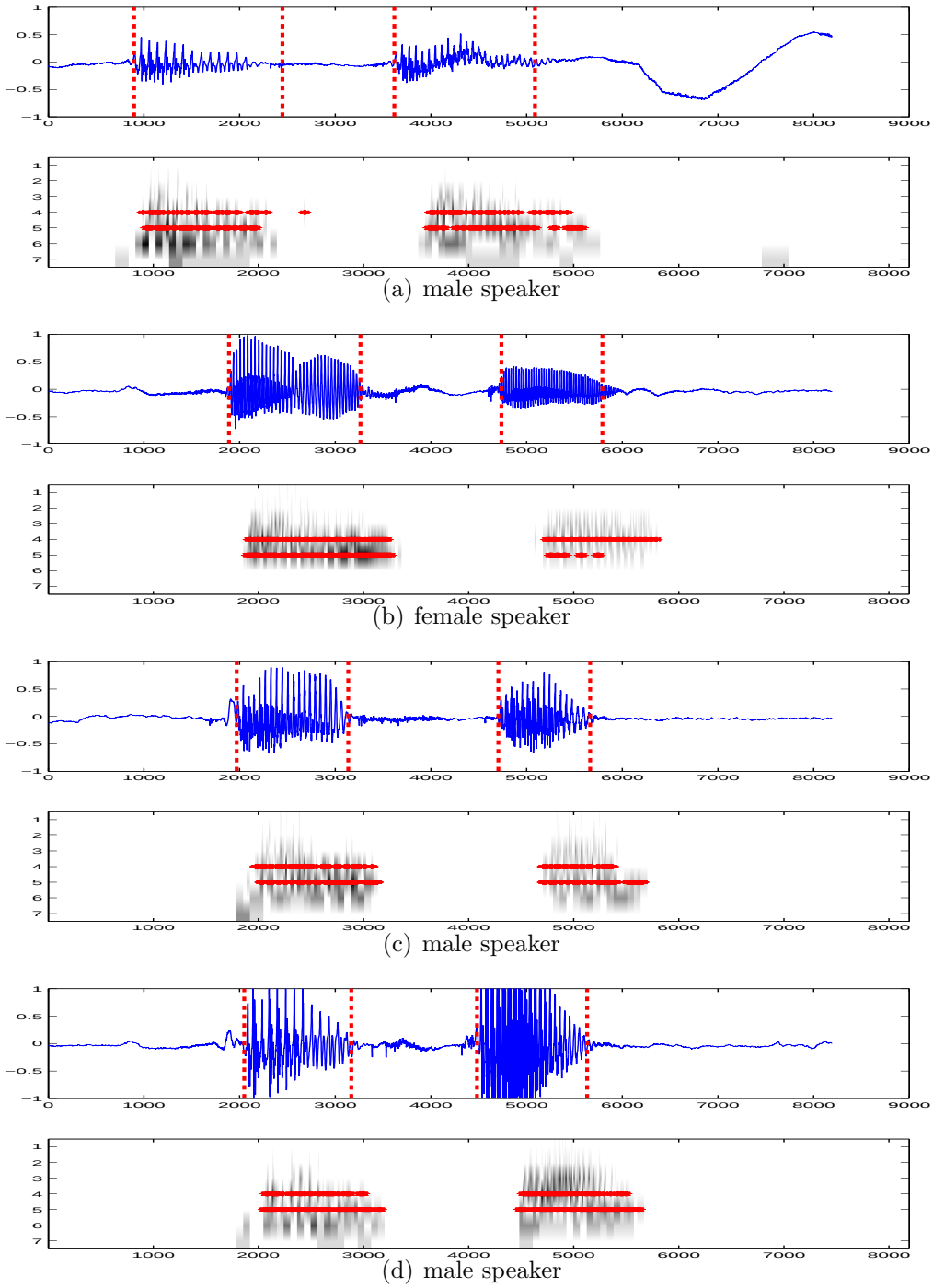

(a) male speaker

(b) female speaker

(c) male speaker

(d) male speaker

Fig. 4.11: Decomposition into voiced/ voiceless parts of the German word ['fɛnstər] using fourth and fifth level.

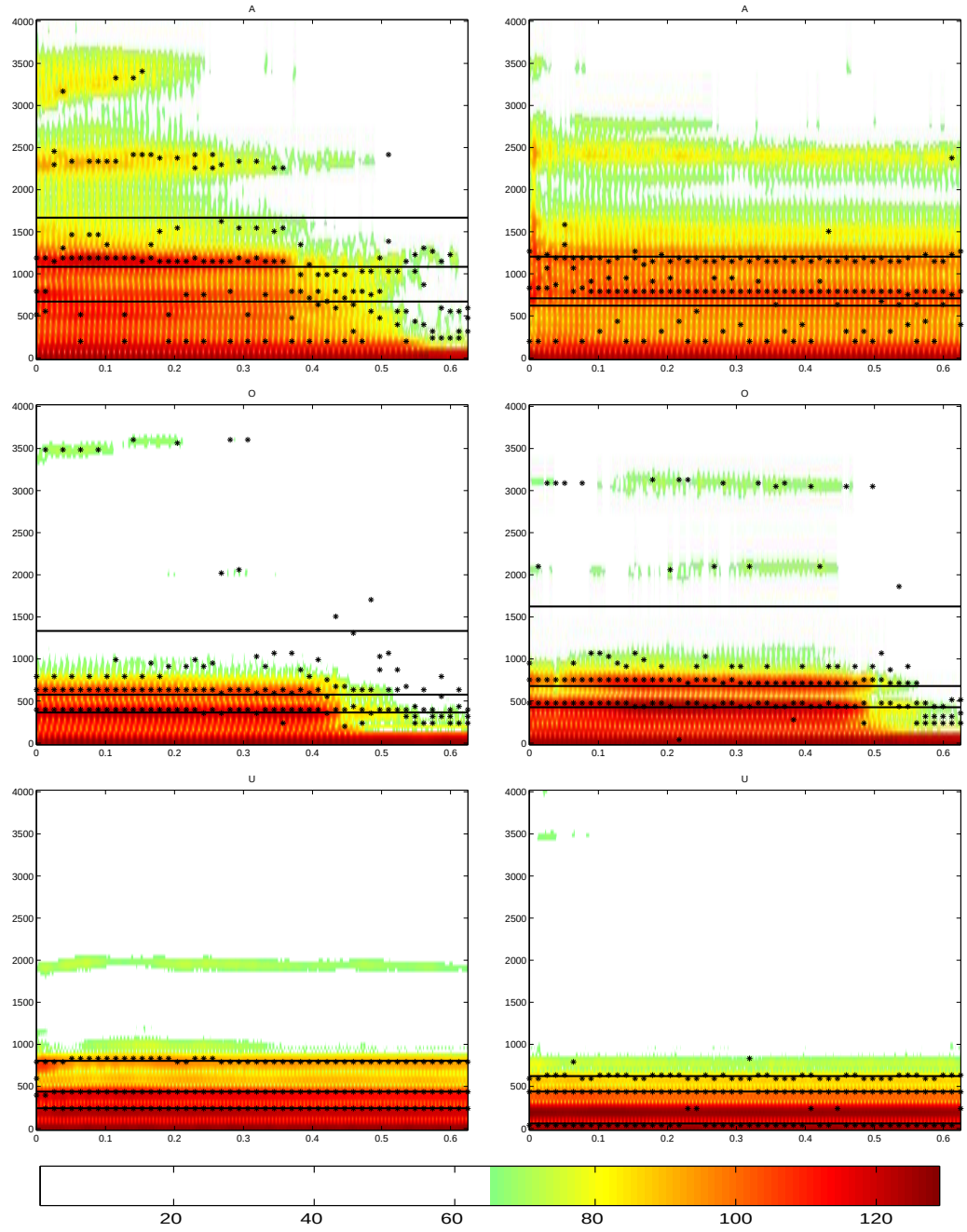

Fig. 4.12: From top to bottom in pairs: [a], [o], [u]; smallest 50% of coefficients were plotted as white, compare the colorbar at the bottom, since they are of no importance (to formant extraction); Note also that the coefficients were submitted to a *gamma* transform, $x \mapsto x^{\gamma}$, with $\gamma = 0.1$ in order to emphasise the different energy levels.

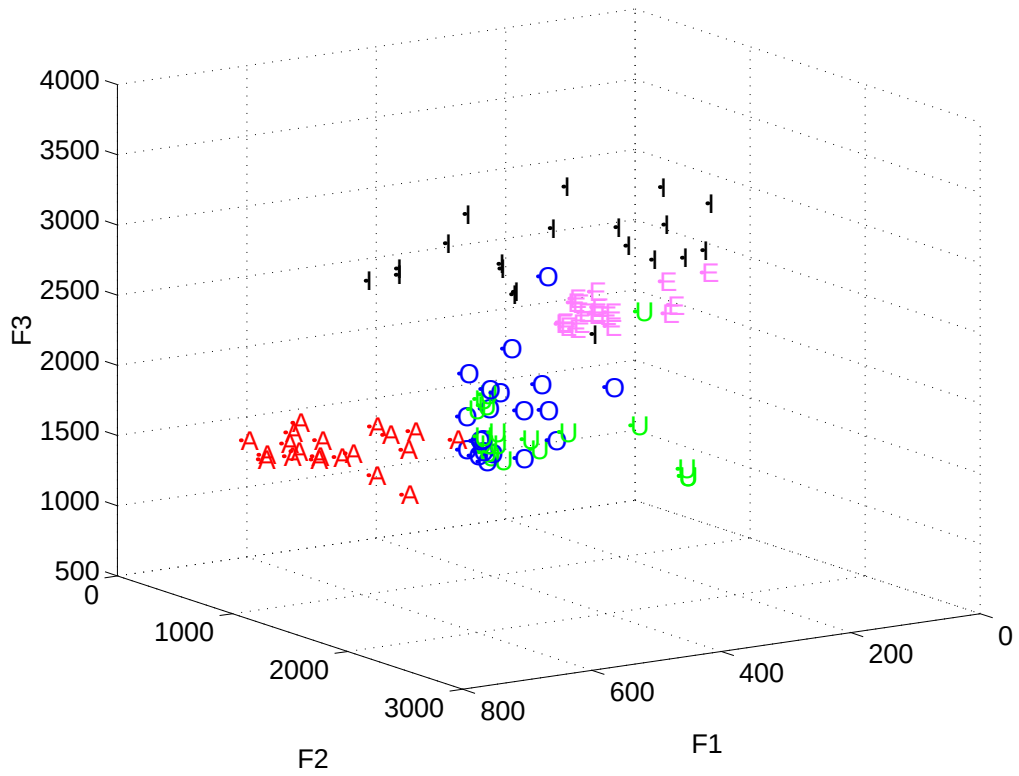

Fig. 4.13: [u], [o], [a], [e], each 20 times repeated by the author; sampling frequency: 8 kHz. The window size for the windowed Fourier transform was 74 samples long – or equivalently, 9.2 ms. In particular, Matlab's built-in function *specgram* was used, `specgram(vowel,200,8e3,74,73)`, in order to compute the spectrogram from which the formants $F1$ - $F3$ were extracted.

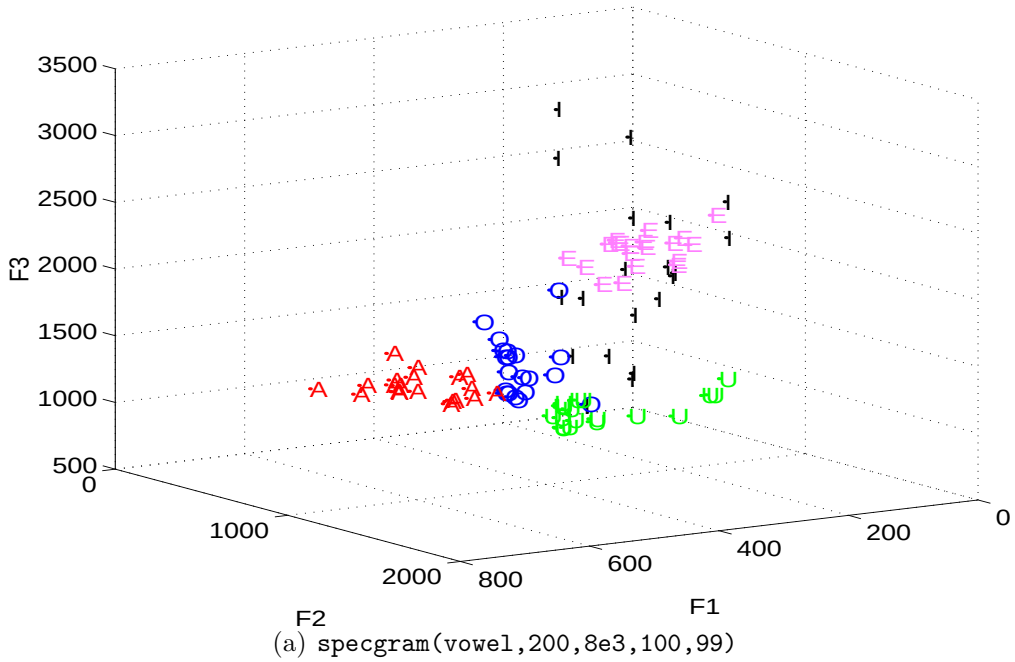

(a) `specgram(vowel,200,8e3,100,99)`

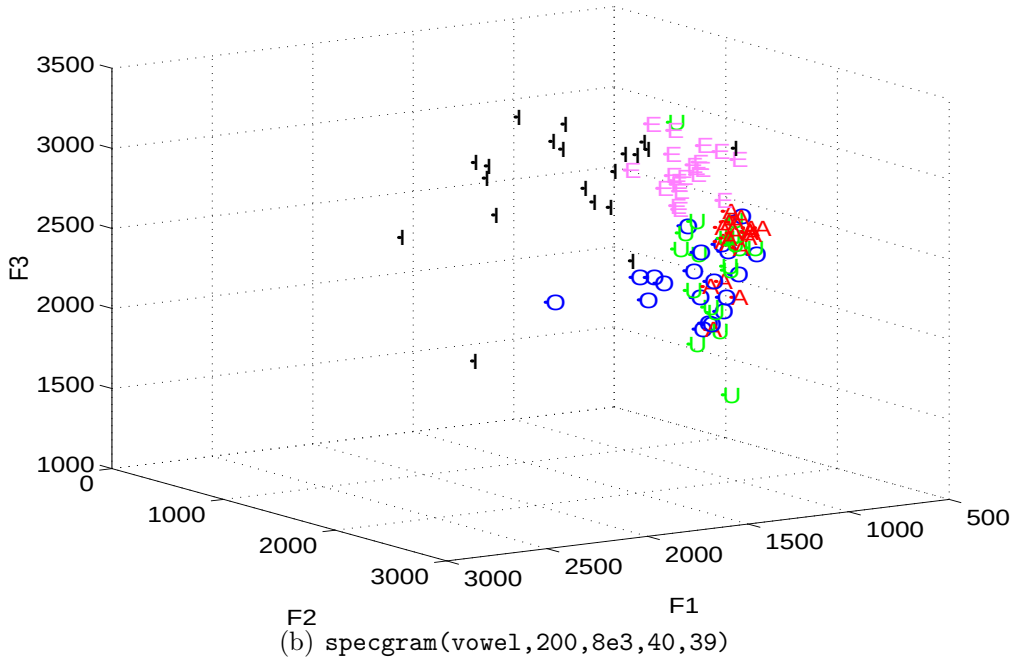

(b) `specgram(vowel,200,8e3,40,39)`

Fig. 4.14: Influence of window size; (a) 100 samples long window (≡ 12.5 ms); (b) 40 samples long window (≡ 5 ms).

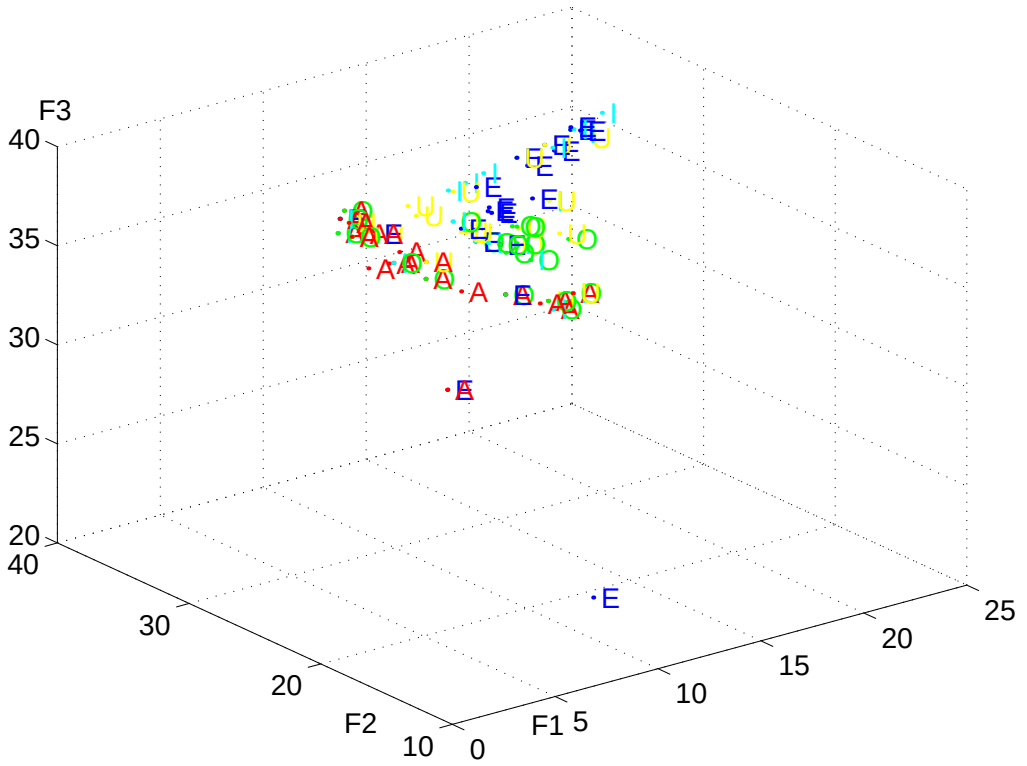

Fig. 4.15: Parameter space similar to Figures 4.13 and 4.14. The three axes show the level of each 'formant' in contrast to those figures where frequency was measured in the unit 'Hertz'. Matlab's built-in function *cwt* was used in connection with Daubechies' ${}_3\psi$ wavelet; scales ranged from 1 to 40 in integer steps.

CWT

As already mentioned, the discrete wavelet transform (dwt) has a rather poor frequency resolution if compared to a (windowed) Fourier transform.

But also the redundant continuous wavelet transform (cwt) does not show a comparable frequency resolution as the (windowed) Fourier transform.

This is visualised in Figure 4.15 where analogously to the two previous described algorithms coefficients of the wavelet transform signal above a threshold are marked and used for 'formant' extraction.

It is evident from that plot that the vocals cluster together but with a much bigger intersection of different classes as in the case of the windowed Fourier transform.

This is mainly because of the worse frequency resolution of the wavelet transform.

Drawbacks of $\mathcal{F}_g$ and $\mathcal{W}$

Finally, consider an artificial signal: a sinusoid signal f sampled at a frequency of 8 kHz and composed of frequencies $500, 550, 2700$ and 3600 Hz, resp. where the two last ones are only of short duration and occur several times, Figure 4.16, (a) and Figure 4.17, (b). That signal is transformed by means of $\mathcal{F}$, $\mathcal{F}_g$ and $\mathcal{W}$ which coefficients are plotted in the phase planes, Figure 4.16, (b-f) and Figure 4.17.

Comparing both transforms with each other it turns out that, if the width of g is optimal adapted to f, $\mathcal{F}_g$ has a better trade-off between localisation in time and frequency domain.

As a matter of course, the wavelet transform has a much better time resolution of these high-frequency bursts and does not need to adapt any window since this is already 'built-in' in the transformation process. But these in some sense convenient properties are not always needed. They are especially of almost no help in trying to achieve both, good frequency resolution and time localisation.

Summarised, the drawbacks of each transform are

windowed Fourier transform

A priori knowledge about signal's frequency is necessary in order to achieve an expressive time-frequency partition.

It is almost impossible to handle different transients with equal care, i.e. $\mathcal{F}_g$ resolves either sharp bursts of high frequency at a cost of localisation in frequency domain or vice versa.

The discretised windowed Fourier transform $(f_{j,k})_{j,k}$ constitutes a frame if and only if $\omega t = 2\pi$ but then Balian-Low theorem says that in this case only a bad time-frequency is possible. Hence, either numerical stability or good time-frequency partition is achievable. Not both!

Wavelet transform

Actually, this kind of transform is desirable if and only if 'discontinuities' are of more importance compared to their frequency resolution. More precise, localisation in time is much preferred to localisation in frequency.

In addition, the discretised wavelet transform is naturally of lower frequency resolution compared to a windowed Fourier transform, for instance. In case of dyadic discretisation, decomposition in frequency results in octave bands which is in some cases not adequate enough.

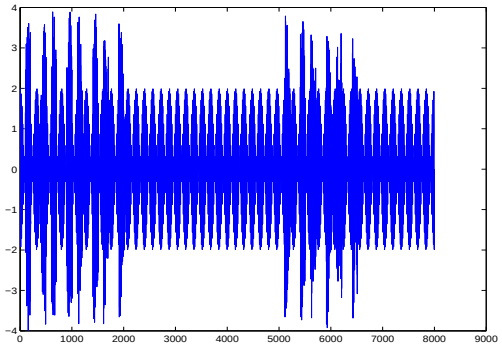

(a) test signal f as a superposition of two others showed in Figure 4.17, (a) and (b)

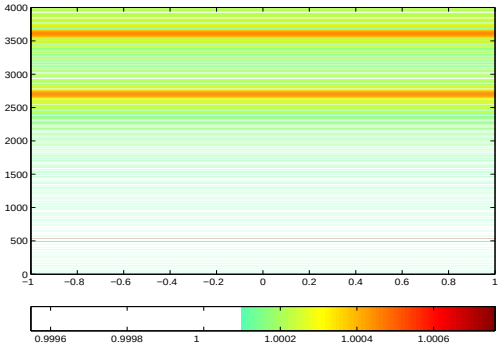

(b) Power spectrum. Frequency axis goes from 0 to 4 kHz.

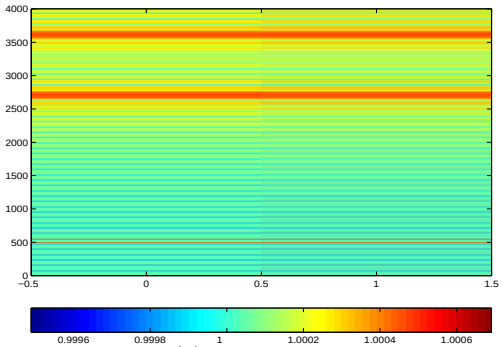

(c) 2 windows

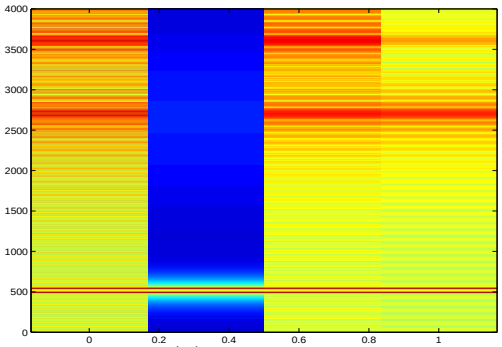

(d) 4 windows

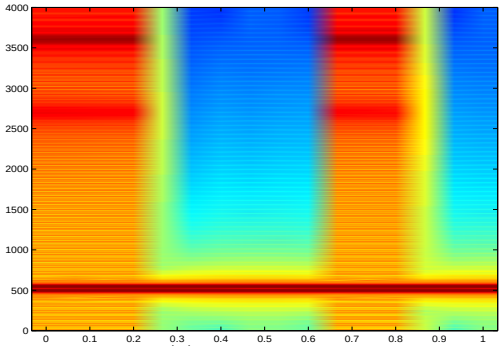

(e) 16 windows

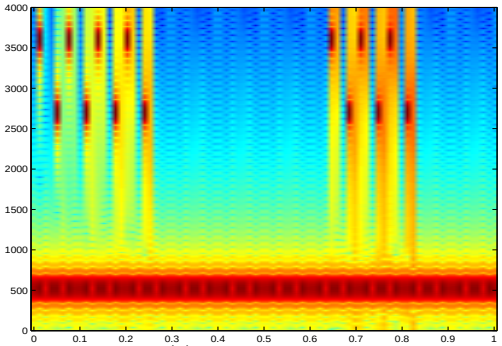

(f) 80 windows

Fig. 4.16: In (a) generated signal f (sampling frequency: 8kHz) is (windowed) Fourier transform (b-f) with different window spreads. Localisation in time of high frequent bursts increases from (b - no localisation at all) to (f) whereas resolution of frequency is getting worse simultaneously (f - low frequent parts, 500 and 550, resp., are undistinguishable). Subplots (b-f) are generated with Matlab's *specgram* built-in function, i.e. in particular with the Hamming window. These are the so-called spectrograms. The phase of each coefficient is not rendered here; the colour is proportional to $\log |\mathcal{F}_g(f)|$ where red corresponds to a maximum and dark blue minimum of all computed coefficients.

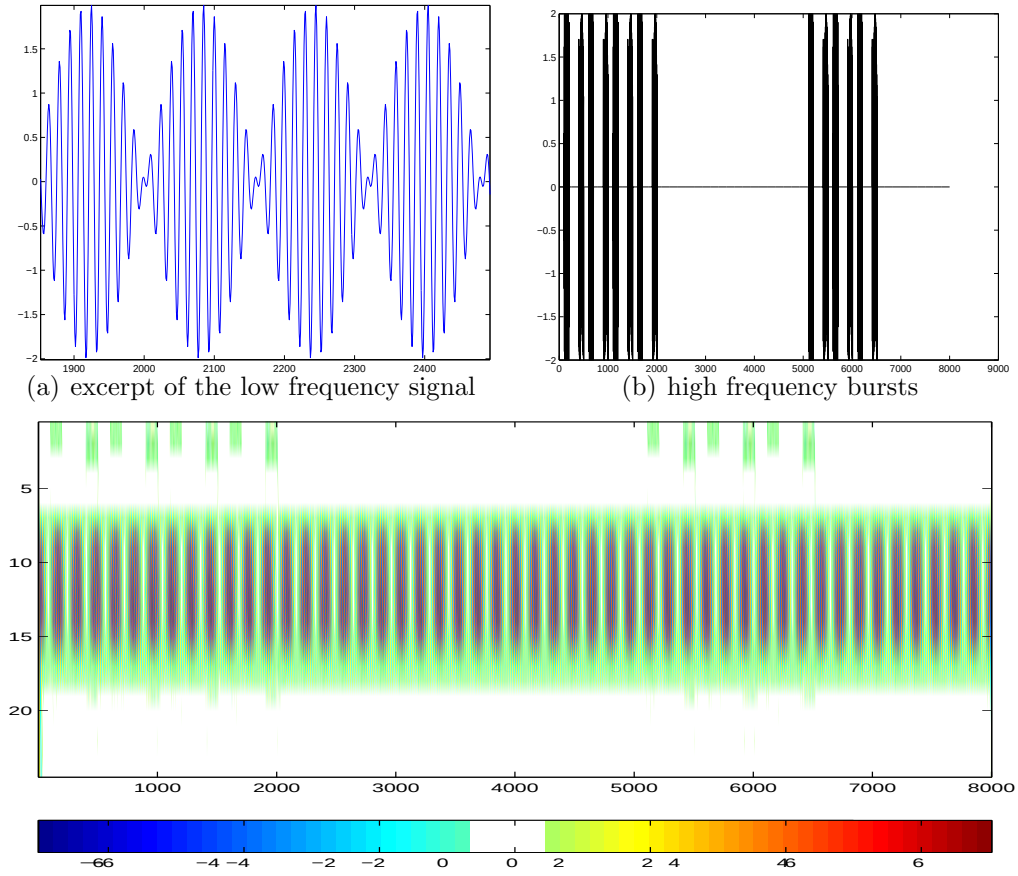

(a) excerpt of the low frequency signal

(b) high frequency bursts

(c) Meyer wavelet transform signal

Fig. 4.17: A continuous wavelet transform of the same signal as in Figure 4.16, (a). Here, Meyer's wavelet is used to compute the wavelet coefficients at scales 1-24. Each discontinuity in f resulting from burst of high frequencies can be seen as small spots of colour at levels 1 to 3. The resolution in frequency is at no level usable – a rather wide colour ribbon at levels 7 - 18 results from the low frequencies 500 and 550 Hz. The width of that ribbon suggest on the other hand a frequency ranging from $\frac{1}{\log(7)} \approx 514$ Hz to $\frac{1}{\log(18)} \approx 360$ Hz, i.e. almost $\frac{170}{2}$ Hz uncertainty and even more for the levels 2 and 3 which would correspond to frequencies from approximately 1443 to 910 Hz. A wavelet transform signal at lower levels, say at 1, 1.1, 1.2, ..., 2, would yield a higher time resolution and a worse frequency certainty.

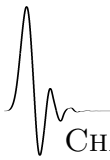

Chapter 5

Adaptive Time – Frequency Analysis

As described in Section 4.4.2, fixed time-frequency tilings of the phase plane resulting from the wavelet or windowed Fourier transforms, for instance, do not provide an adequate analysis of signals with time varying spectral components as for speech recordings.

Almost a decade after the advent of wavelets it was observed by several people (Ronald R. Coifman, Yves Meyer, Mladen V. Wickerhauser et al.) that both transforms could be generalised to *wavelet packets* and *local trigonometric* functions with same mathematical properties, i.e. constituting under mild conditions frames, orthonormal and (bi)orthogonal bases of $\mathrm{L}^2(\mathbb{R})$ and higher dimensions, but with an additional degree of freedom.

In both cases a fast computable basis tree is obtained from which it is then possible to pick the 'most suitable' basis by minimising for instance a cost functional.

5.1 Wavelet Packets

An obvious generalisation of the MRA ansatz is to use more than only two subspaces V_j and W_j, $j \in \mathbb{Z}$, of $\mathrm{L}^2(\mathbb{R})$ yielding a more refined frequency axis tiling.

For a detailed discussion on that specific transform check some of these articles [CW92, Wic91, Wic93a, Wic93b, Wic94, Bar98] and the references therein.

Since this thesis deals with signals which properties change over time, it is preferable to isolate different time intervals with nearly constant frequency parts. This is accomplished by the local trigonometric transform which seg-

ments the time axis in contrast to the wavelet packet transform.

The first part of the following section is mostly based on Kai Bittner's excellent summary (cf. [Bit00]) of biorthogonal properties.

5.2 Local Trigonometric Packets

Consider for the rest of this thesis, if not otherwise stated, the following general

Assumption 5.2.1. Let $(a_j)_{j\in\mathbb{Z}} \subset \mathbb{R}$ be a strict monotonical increasing sequence, i.e. $\forall\, j \in \mathbb{Z} :\ a_j < a_{j+1}$. Choose a sequence $(\epsilon_j)_{j\in\mathbb{Z}} \subset \mathbb{R}_{>0}$ with $\epsilon_j + \epsilon_{j+1} \leqslant a_{j+1} - a_j$ and define $a_j^{\pm} := a_j \pm \epsilon_j$.

By virtue of this settings it follows

$$\mathbb{R} = \bigcup_i [a_j, a_{j+1}) \text{ and } \forall\, j \in \mathbb{Z} :\ [a_j^-, a_j^+) \cap (a_{j+1}^-, a_{j+1}^+] = \emptyset. \tag{5.1}$$

In addition, let $(t_{j,k})_{k\in\mathbb{N}_0} \subset \mathrm{L}^2([a_j, a_{j+1}])$ denote a set of functions, $j \in \mathbb{Z}$ which satisfy for each $j \in \mathbb{Z}$, all $x \in (-\epsilon_j, \epsilon_j)$ and a fixed $\sigma_j \in \{-1, +1\}$ the following three conditions

$$(t_{j,k})_{k\in\mathbb{N}_0} \text{ is an onb in } \mathrm{L}^2([a_j, a_{j+1}]), \text{ and} \tag{5.2a}$$
$$t_{j,k}(a_j + x) = \sigma_j t_{j,k}(a_j - x), \tag{5.2b}$$
$$t_{j-1,k}(a_j + x) = -\sigma_j t_{j-1,k}(a_j - x). \tag{5.2c}$$

Finally, consider a sequence of 'windows' $(w_j)_{j\in\mathbb{Z}}$ fulfilling

$$\text{support :} \quad \operatorname{supp}(w_j) \subset [a_j^-, a_{j+1}^+] \tag{5.3a}$$
$$\text{bounded :} \quad w_j : \mathbb{R} \to [0, 1] \tag{5.3b}$$
$$\text{identity :} \quad w_j|_{[a_j^+, a_{j+1}^-]} \equiv 1 \tag{5.3c}$$
$$\text{symmetry :} \quad w_j(a_j + x) = w_{j-1}(a_j - x), \quad \forall\, |x| \leqslant \epsilon_j \tag{5.3d}$$
$$\text{reconstruction :} \quad w_j^2(a_j + x) + w_{j-1}^2(a_j + x) = 1, \quad \forall\, |x| \leqslant \epsilon_j \tag{5.3e}$$

Equation (5.3a) with (5.1) imply that only the immediate neighbouring windows w_j have a non-empty overlap, see Figure 5.1.

Moreover, parity conditions, Equations 5.2b and 5.2c, imposed on the functions t_{jk} have several consequences: $t_{j,k}$ should have an oscillating nature, since the parity in a_j must be different from a_{j+1}. If $t_{j,k}$ is even (odd) in a_j, i.e. $t_{j,k}(a_j + x) = t_{j,k}(a_j - x)$, $|x| \leqslant \epsilon_j$, then $t_{j,k}$ is odd (even) in a_{j+1}.

Another trivial consequence is that the product of two such functions is always odd in each a_j and that $(t_{j,k})_{j,k}$ is an onb in $\mathrm{L}^2(\mathbb{R})$.

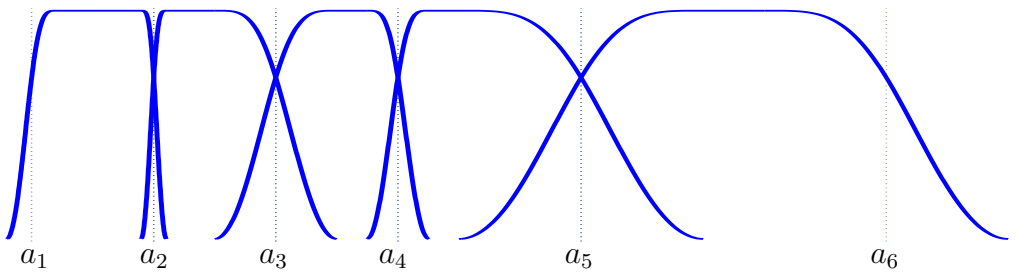

Fig. 5.1: Windows w_j with corresponding parameters a_j and ϵ_j summarised in two vectors: $a = (-4, -2, 0, 2, 5, 10)$, $\epsilon = (0.41, 0.21, 1, 0.51, 2, 2)$

In practice, it is convenient to know $t_{j,k}$ precisely. Next lemma gives for each possible parity condition a set of trigonometric functions at hand which satisfy conditions as described by Eqs. (5.2). Figure 5.2 illustrates both, (anti-)symmetry (in a_j) and the effect of windowing, $w_j t_{j,k}$.

Lemma 5.2.2. *For any admissible choice of σ_j there exists a set of trigonometric functions $(t_{j,k})_{k\in\mathbb{N}_0}$, $j \in \mathbb{Z}$, which satisfies Eqs.* (5.2)*. In particular, these conditions are fulfilled by*

$$t_{j,k}(x) = \begin{cases} \gamma_j \cos\Big((k+\frac{1}{2})\pi\big(\frac{x-a_j}{h_j}\big)\Big), & \sigma_j = \sigma_{j+1} = 1 \\ \gamma_j \sin\Big((k+\frac{1}{2})\pi\big(\frac{x-a_j}{h_j}\big)\Big), & \sigma_j = \sigma_{j+1} = -1 \\ \widetilde{\gamma}_j \cos\Big(k\pi\big(\frac{x-a_j}{h_j}\big)\Big), & \sigma_j = -\sigma_{j+1} = 1 \\ \gamma_j \sin\Big((k+1)\pi\big(\frac{x-a_j}{h_j}\big)\Big), & \sigma_j = -\sigma_{j+1} = -1 \end{cases} \tag{5.4}$$

with

$$\gamma_j := \sqrt{\frac{2}{h_j}}, \quad \widetilde{\gamma}_j = \sqrt{\frac{2-\delta_{0,k}}{h_j}}, \quad h_j := a_{j+1} - a_j$$

Proof. Parity conditions, Eqs. (5.2b) and (5.2c) follow by easy computations such as orthonormality does. Hence, it remains to show that $(t_{j,k})_k$ is complete in every $\mathrm{L}^2([a_j, a_{j+1}])$. For this, consider w.l.o.g. an arbitrary function $f \in \mathrm{L}^2([0,1])$.

The standard trick is to extend f (in a special way) to a function $g \in \mathrm{L}^2([-2,2])$ which itself is then expressed in a Fourier series (cf. Example 3.2.6). Such a special way would be for instance to extend f to the interval $[0,2]$ even ($\sigma_1 = +1$) with respect to $x = 1$, i.e.

$$f_1(x) := \begin{cases} f(x), & x \in [0,1] \\ \sigma_1 f(2-x), & x \in (1,2] \end{cases} \Rightarrow f_1(1+x) = \sigma_1 f(1-x) \,\forall\, x \in (0,1)$$

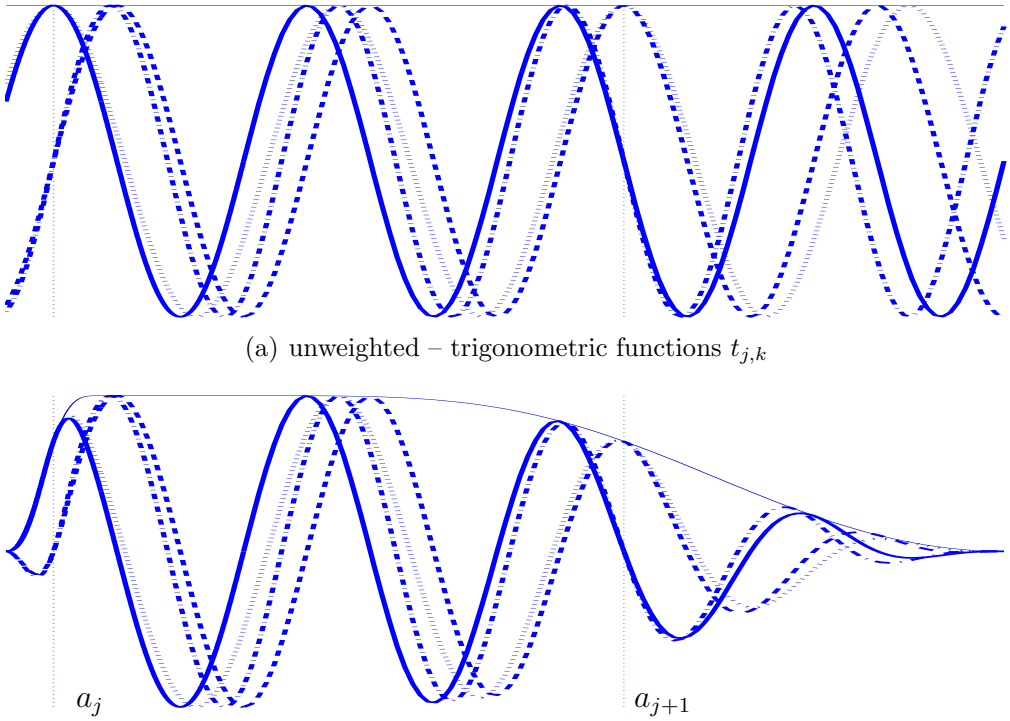

(a) unweighted – trigonometric functions $t_{j,k}$

(b) weighted – *local* trigonometric functions $w_j t_{j,k}$

Fig. 5.2: Trigonometric functions $t_{j,k}$ as proposed in Lemma 5.2.2 wighted by a window w_j, w_j as in Lemma 5.2.4. Parities in points a_j and a_{j+1} are as followed: solid line: *even-odd* ($\sigma_j = \sigma_{j+1} = 1$), dashed line: *even-even* ($\sigma_j = \sigma_{j+1} = -1$), dotted line: *odd-even* ($\sigma_j = -\sigma_{j+1} = 1$), dashed-dotted line: *odd-odd* ($\sigma_j = -\sigma_{j+1} = -1$). 'Frequency'-parameter k was chosen as $k = 4$ (with $a_j = -4$, $a_{j+1} = 8$, $\epsilon_j = 1$, $\epsilon_{j+1} = 6$). Thin solid line corresponds to w_j.

whereas the resulting function, f_1, will be extended to the interval $[-2,0]$ odd ($\sigma_0 = -1$) with respect to $x = 0$, i.e.

$$f_0(x) := \begin{cases} f_1(x), & x \in [0,2] \\ \sigma_0 f_1(-x), & x \in [-2,0) \end{cases} \quad \Rightarrow f_0(x) = \sigma_0 f_0(-x) \,\forall\, x \in (-2,2)$$

To catch all possible cases (as illustrated in Figure 5.3) consider therefore for arbitrary $\sigma_0, \sigma_1 \in \{-1,+1\}$

$$g(x) := f_0(x) = \begin{cases} f(x), & x \in [0,1] \\ \sigma_1 f(2-x), & x \in (1,2] \\ \sigma_0 f(-x), & x \in [-1,0) \\ \sigma_0\sigma_1 f(2+x), & x \in [-2,-1). \end{cases}$$

As already mentioned, g can be expressed in a Fourier series, such that for $y \in [0,1]$ it holds

$$(f(y) =) g(y) = \sum_{k\in\mathbb{Z}} \langle g, e_k\rangle \, e_k(y), \quad \text{for } e_k(x) := \frac{e^{\pi i x k/2}}{2}.$$

Exploiting symmetry in g it follows for an arbitrary scalar product $\langle g, e_k\rangle$

$$\begin{aligned} \langle g, e_k\rangle &= \int_{-2}^{2} g(x) e_k(x)\,\mathrm{d}x \\ &= \int_0^1 f(x) e_k(x)\,\mathrm{d}x + \int_{-1}^{0} \sigma_0 f(-x) e_k(x)\,\mathrm{d}x \\ &\quad + \int_1^2 \sigma_1 f(2-x) e_k(x)\,\mathrm{d}x + \int_{-2}^{-1} \sigma_0\sigma_1 f(2+x) e_k(x)\,\mathrm{d}x \\ &= \int_0^1 f(x) E_k(x)\,\mathrm{d}x, \text{ with} \\ E_k(x) &:= e_k(x) + \sigma_0 e_k(-x) - \sigma_1 e_k(2-x) + \sigma_0\sigma_1 e_k(x-2). \end{aligned} \tag{5.5}$$

Equation (5.5) reduces to the assertion, Eq. (5.4), with $\gamma_j = 1$. □

A really successful approach in theory and practice is made via a folding operator (see Eq. (5.7)) first mentioned by M.V. Wickerhauser ([Wic91, pp. 22], [Wic93a]). It turns out that useful properties of harmonic analysis can be linked (as in Eqs. (5.15)) to a new set of functions ($\psi_{j,k} := w_j t_{j,k}$). Theorem 5.2.7 summerises this fruitful ansatz.

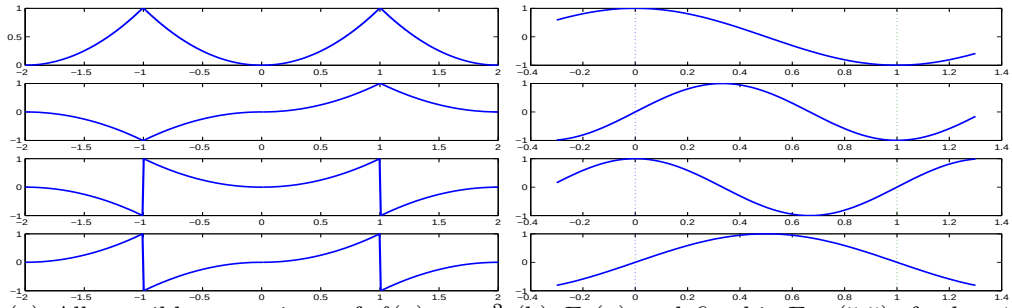

(a) All possible extensions of $f(x) = x^2$ from $[0,1]$ to $[-2,2]$.

(b) $E_k(x)$ as defined in Eq. (5.5). for $k = 1$

Fig. 5.3: Parity conditions, $\sigma := (\sigma_0, \sigma_1)$, at points $x = 0, 1$ from top (left, right) to bottom (left, right) plot as $\sigma = (1,1)$, $\sigma = (-1,1)$, $\sigma = (1,-1)$, $\sigma = (-1,-1)$.

On the other hand, such a folding and unfolding procedure motivates also the structure of fast algorithms. A decomposition like

$$f = \sum_{j,k} \langle f, \psi_{j,k} \rangle \, \widetilde{\psi_{j,k}}$$

where most computational power is devoted to the calculation of scalar products will depreciate in numerical complexity if Relation (5.15b) is used.

$\mathcal{T}_w f$ is then just a preprocess of a $\mathcal{O}(n \log n)$, $f \in \mathbb{R}^n$, fast Fourier-like transform. More precisely, using trigonometric functions as given in Lemma 5.2.2 such integration (of discrete signals, i.e. $(f_i)_i \in \ell^2(\mathbb{R})$) can be accomplished by one of the four discrete cosine transforms, DCT-I,II,III and IV - (see [RY90]).

The DCT of type IV uses for instances functions given as in Lemma 5.2.2 for the even-even case, i.e. $\sigma_j = \sigma_{j+1} = 1$.

Definition 5.2.3. Let $a \in \mathbb{R}$ and $\epsilon > 0$ be arbitrary given. A function $r \in \mathrm{C}^m(\mathbb{R})$, $m \geqslant 0$, is termed a *cut-off function* $:\Longleftrightarrow$

$$\forall\, x \in \mathbb{R} : \; r^2(a+x) + r^2(a-x) = 1 \text{ with } r(x) = \begin{cases} 0, & x \leqslant a - \epsilon \\ 1, & x \geqslant x + \epsilon \end{cases}. \tag{5.6}$$

For such a cut-off function define a *folding operator* U as

$$\begin{gathered} U := U(r,a) : \; \mathrm{L}^2(\mathbb{R}) \to \mathrm{L}^2(\mathbb{R}) \\ Uf(a+x) := \begin{cases} r(a+x)f(a+x) + r(a-x)f(a-x), & x \geqslant 0 \\ r(a+x)f(a+x) - r(a-x)f(a-x), & x \leqslant 0. \end{cases} \end{gathered} \tag{5.7}$$

Lemma 5.2.4. *([AWW91]) For definetness, a particular window sequence* (w_j) *is given by*

$$w_j(x) := s_{\epsilon_j}(x - a_j)c_{\epsilon_{j+1}}(x - a_{j+1}) \quad \textit{with}$$
$$s_\epsilon(x) := \sin \vartheta_\epsilon(x), \quad c_{\epsilon_j}(x) := \vartheta_\epsilon(x), \quad \vartheta_\epsilon(x) := \int_{-\infty}^{x} f_\epsilon(y)\,\mathrm{d}y,$$
$$\operatorname{supp}(f_\epsilon) \subset [-\epsilon, \epsilon],\ f_\epsilon(x) = f_\epsilon(-x)\ \textit{and}\ \int f_\epsilon(x)\,\mathrm{d}x = \frac{\pi}{2}.$$

Proof. The window w_j is of course bounded and satisfy especially Eq. (5.3b). Since f_ϵ is even it follows $\vartheta(x) + \vartheta(-x) = \pi/2$ which implies $c_\epsilon(x) = \cos\big(\frac{\pi}{2} - \vartheta_\epsilon(-x)\big) = \sin \vartheta_\epsilon(-x) = s_\epsilon(-x)$. Hence,

$$1 = c_\epsilon^2(x) + s_\epsilon^2(x) = c_\epsilon^2(x) + c_\epsilon^2(-x) = s_\epsilon^2(x) + s_\epsilon^2(-x) \tag{5.8a}$$

and due to compact support of f_ϵ it is clear (by (5.8b)) that $\operatorname{supp}(c_{\epsilon_{j+1}}) \subset (-\infty, \epsilon_{j+1}]$, $\operatorname{supp}(s_{\epsilon_j}) \subset [-\epsilon_j, \infty)$,

$$\vartheta_\epsilon(x) = \begin{cases} \frac{\pi}{2}, & x > \epsilon \\ 0, & x < -\epsilon \end{cases}$$
$$\Rightarrow c_\epsilon(x) = \begin{cases} 0, & x > \epsilon \\ 1, & x < -\epsilon \end{cases} \text{ and } s_\epsilon(x) = \begin{cases} 1, & x > \epsilon \\ 0, & x < -\epsilon. \end{cases} \tag{5.8b}$$

Note also that Relations (5.8) complies also with the conditions (5.6), i.e. s_ϵ and c_ϵ can especially be used as a cut-off function. Furthermore, Eq. (5.8b) imply that $\operatorname{supp}(w_j) = \operatorname{supp}\Big(s_{\epsilon_j}(\cdot - a_j)c_{\epsilon_{j+1}}(\cdot - a_{j+1})\Big) \subset (-\infty, a_{j+1}^+] \cap [a_j^-, \infty) = [a_j^-, a_{j+1}^+]$. Properties (5.3c), (5.3d) and (5.3e) are an immediate consequence of (5.8b), respectively(5.8a). □

A convenient choice for f_ϵ is for instance

$$f_\epsilon(x) := \frac{\pi}{4} \cos\Big(\frac{\pi x}{2\epsilon}\Big). \tag{5.9}$$

Then, $\vartheta_\epsilon(x) = \frac{\pi}{4}\Big(\sin\big(\frac{\pi x}{2\epsilon}\big) - \sin\big(\frac{-\pi\epsilon}{2\epsilon}\big)\Big) = \frac{\pi}{4}\Big(1 + \sin\big(\frac{\pi x}{2\epsilon}\big)\Big)$. Such a window is also used in Figures 5.1 and 5.2.

Lemma 5.2.5. *The folding operator is a unitary isomorphism, i.e.*

$$U^*Uf(x) = UU^*f(x) = f(x), \quad \forall\, x \neq a \tag{5.10}$$

where the the so-called unfolding operator $U^*:= U^*(r,a)$ *is given by*

$$U^*f(a+x) := \begin{cases} r(a+x)f(a+x) - r(a-x)f(a-x), & x \geqslant 0 \\ r(a+x)f(a+x) + r(a-x)f(a-x), & x \leqslant 0 \end{cases}. \tag{5.11}$$

In particular, both operators, U *and* U^* *act on the interval* $(-\epsilon,\epsilon)$*, i.e.* $Uf(x) = U^*f(x) = f(x)$, $\forall\, x \notin (-\epsilon,\epsilon)$.

Proof. For $x > \epsilon \Rightarrow r(a+x) = 1$ and $r(a-x) = 0$ and vice versa, for $x < \epsilon \Rightarrow r(a+x) = 0$ and $r(a-x) = 1$ holds. Hence, $\forall\, x \notin (-\epsilon,\epsilon)$:

$$Uf(a+x) = \begin{cases} 1f(a+x) + 0f(a-x), & x > \epsilon \\ 1f(a+x) - 0f(a-x), & x < -\epsilon \end{cases} = f(a+x).$$

Now let $x \in (0,\epsilon)$. It follows that

$$\begin{aligned} Uf(a+x) &= r(a+x)f(a+x) + r(a-x)f(a-x) \text{ and for } y := -x < 0 \\ Uf(a-x) &= Uf(a+y) = r(a-y)f(a+y) - r(a+y)f(a-y) \\ &= r(a+x)f(a-x) - r(a-x)f(a+x) \\ \Rightarrow U^*Uf(a+x) &= r(a+x)\Big(r(a+x)f(a+x) + r(a-x)f(a-x)\Big) \\ &\quad - r(a-x)\Big(r(a+x)f(a-x) - r(a-x)f(a+x)\Big) \\ &= \big(r^2(a+x) + r^2(a-x)\big)f(a+x) = f(a+x). \end{aligned}$$

Analogous calculations hold also for $x \in (-\epsilon,0)$ such that in total $U^*Uf(x) = f(x)$ and by similar argumentations $UU^*f(x) = f(x)$, $\forall\, x \neq a$ is satisfied. □

Corollary 5.2.6. *Define a sequence of cut-off functions by*

$$r_j(x) = \begin{cases} 0, & x \leqslant a_j^- \\ w_j(x), & x \in (a_j^-, a_j^+) \\ 1, & x \geqslant a_j^+ \end{cases} \tag{5.12}$$

and let $U_j := U(r_j, a_j)$ *be given as in Eq.* (5.7)*. Then the following holds*

$$w_j t_{j,k} = \begin{cases} U_j^* U_{j+1}^*\big(\chi_{[a_j,a_{j+1}]} t_{j,k}\big), & \sigma_j = \sigma_{j+1} = 1 \\ U_j^* U_{j+1}\big(\chi_{[a_j,a_{j+1}]} t_{j,k}\big), & \sigma_j = -\sigma_{j+1} = 1 \\ U_j U_{j+1}^*\big(\chi_{[a_j,a_{j+1}]} t_{j,k}\big), & \sigma_j = -\sigma_{j+1} = -1 \\ U_j U_{j+1}\big(\chi_{[a_j,a_{j+1}]} t_{j,k}\big), & \sigma_j = \sigma_{j+1} = -1. \end{cases} \tag{5.13}$$

The so called total folding operator $\mathcal{T}_w : \mathrm{L}^2(\mathbb{R}) \to \mathrm{L}^2(\mathbb{R})$ *given by*

$$\mathcal{T}_w := \prod_{\substack{j\in\mathbb{Z}\\ \sigma_j=1}} U_j \prod_{\substack{j\in\mathbb{Z}\\ \sigma_j=-1}} U_j^*, \tag{5.14a}$$

$$\mathcal{T}_w f(x) = \begin{cases} U_j f(x), & \sigma_j = 1,\ x \in (a_j^-, a_j^+),\ j \in \mathbb{Z} \\ U_j^* f(x), & \sigma_j = -1,\ x \in (a_j^-, a_j^+),\ j \in \mathbb{Z} \\ f(x), & x \in [a_j^+, a_{j+1}^-],\ j \in \mathbb{Z} \end{cases}$$

is a unitary isomorphism with the adjoint, called total unfolding operator*,* $\mathcal{T}_w^* =: \mathcal{U}_w$ *which is given as*

$$\mathcal{U}_w = \prod_{\substack{j\in\mathbb{Z}\\ \sigma_j=1}} U_j^* \prod_{\substack{j\in\mathbb{Z}\\ \sigma_j=-1}} U_j. \tag{5.14b}$$

Moreover, this total folding and unfolding operators satisfy

$$w_j t_{j,k} = \mathcal{U}_w\big(\chi_{[a_j,a_{j+1}]} t_{j,k}\big) \tag{5.15a}$$

$$\langle f, w_j t_{j,k}\rangle = \int_{a_j}^{a_{j+1}} \mathcal{T}_w f(x) t_{j,k}(x)\,\mathrm{d}x. \tag{5.15b}$$

Proof. First of all, r_j is indeed a cut-off function, since Eq. (5.3e) implies that $r_j^2(a_j + x) + r_j^2(a_j - x) = 1$ on the interval $x \in (-\epsilon_j, \epsilon_j)$. By virtue of Eq. (5.12) this reconstruction formula holds for all real numbers.

Moreover, due to prior lemma each folding operator U_j is a unitary isomorphism and permits the relation $U_j f(x) = U_j^* f(x) = f(x)\,\forall\, x \notin (a_j^-, a_j^+)$. This implies in particular that $U_k^{(*)}$, $U_l^{(*)}$ commute $\forall\, k, l \in \mathbb{Z}$. For $k = l$ this is again a straightforward implication of Lemma 5.2.5 and for $k \neq l$ it follows from $(a_j^-, a_j^+) \cap (a_{j+1}^-, a_{j+1}^+) = \emptyset$.

Since all folding and unfolding operators commute, Eq. (5.14b) is evident and due to unitary isomorphism of each U_j it follows $\mathcal{T}_w\mathcal{U}_w = \mathcal{U}_w\mathcal{T}_w = \mathrm{id}$.

Obviously, Eq. (5.13) implies Eq. (5.15a). This is mostly because of the fact that $U_k^* f(x) = U_j f(x) = f(x)$ for all $x \notin (a_j^-, a_j^+)$ and $k,\ j \in \mathbb{Z}$.

Furthermore, relation (5.13) can be developed just from symmetry considerations imposed on w_j - Eq. (5.3d) - and on the trigonometric functions $t_{j,k}$ - cf. Eqs. (5.2b) and (5.2c). This is illustrated for the first case, $U_j^* U_{j+1}^*(g_{j,k})$ with $g_{j,k} := \chi_{[a_j,a_{j+1}]} t_{j,k}$ as followed:

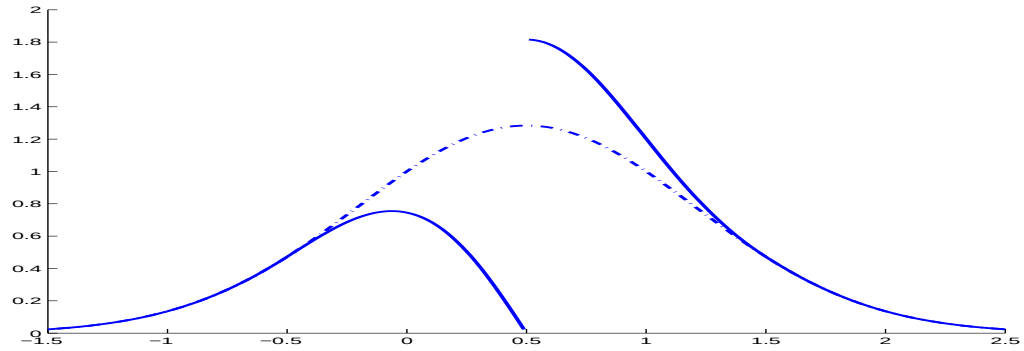

(a) $x_0 = 0.5$, $\epsilon = 1$

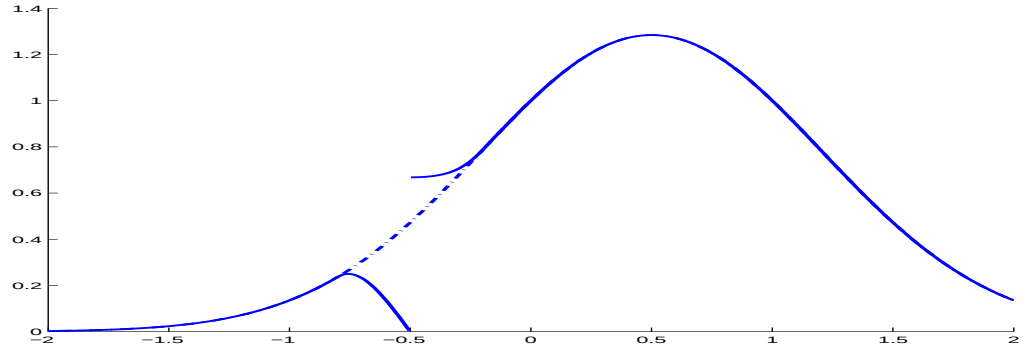

(b) $x_0 = -0.5$, $\epsilon = 0.3$

Fig. 5.4: Solid line: folding operator applied to a function e^{x-x^2} – dotted line – at x_0. Here, the cut-off function was chosen as $\sin(\vartheta(x))$, $\vartheta(x) = \frac{\pi}{4}\big(1 + \sin(\pi\frac{x-x_0}{2\epsilon})\big)$.

$$U_j^* U_{j+1}^*(g_{j,k}(x)) = \begin{cases} U_j^*(g_{j,k}(x)), & x \in (a_j^-, a_j^+) \\ U_{j+1}^*(g_{j,k}(x)), & x \in (a_{j+1}^-, a_{j+1}^+) \\ g_{j,k}(x), & \text{else} \end{cases}$$

$$= \begin{cases} w_j(a_j + x) g_{j,k}(a_j + x) & \\ \quad \mp w_j(a_j - x) g_{j,k}(a_j - x), & \text{'}-\text{'}\colon\ x \in (0, \epsilon_j),\ \text{'}+\text{'}\colon\ x \in (-\epsilon_j, 0) \\ w_{j+1}(a_{j+1} + x) g_{j,k}(a_{j+1} + x) & \\ \quad \mp w_{j+1}(a_{j+1} - x) g_{j,k}(a_{j+1} - x), & \text{'}-\text{'}\colon\ x \in (0, \epsilon_{j+1}),\ \text{'}+\text{'}\colon\ x \in (-\epsilon_{j+1}, 0) \\ t_{j,k}(x), & x \in [a_j, a_{j+1}] \setminus \Big((a_j^-, a_j^+) \cup (a_{j+1}^-, a_{j+1}^+) \Big) \\ 0, & \text{else} \end{cases}$$

$$= \begin{cases} w_j(a_j + x) t_{j,k}(a_j + x) - 0, & x \in (0, \epsilon_j) \\ 0 + w_j(a_j - x) t_{j,k}(a_j - x), & x \in (-\epsilon_j, 0) \\ 0 - w_{j+1}(a_{j+1} - x) t_{j,k}(a_{j+1} - x), & x \in (0, \epsilon_{j+1}) \\ w_{j+1}(a_{j+1} + x) t_{j,k}(a_{j+1} + x) + 0, & x \in (-\epsilon_{j+1}, 0) \\ t_{j,k}(x), & x \in [a_j^+, a_{j+1}^-] \\ 0, & \text{else} \end{cases}$$

$$= \begin{cases} w_j(x) t_{j,k}(x), & x \in (a_j^-, a_j^+) \\ w_j(x) t_{j,k}(x), & x \in (a_{j+1}^-, a_{j+1}^+) \\ t_{j,k}(x), & x \in [a_j^+, a_{j+1}^-] \\ 0, & \text{else} \end{cases} = w_j(x) t_{j,k}(x).$$

First equality uses the fact that these two operators commute, or more precisely, since they 'operate' on disjoint intervals, it is allowed to apply each of them on $g_{j,k}$ separately. Second rewriting follows just by definition of $g_{j,k}$ and U_j^*, U_{j+1}^* resp. Again, third equality exploits the property of the characteristic function.

Now, Eq. (5.2c) can be rewritten in $t_{j,k}(a_{j+1} + x) = -\sigma_{j+1} t_{j,k}(a_{j+1} - x)$ such that

$-w_{j+1}(a_{j+1} - x) t_{j,k}(a_{j+1} - x) = (-1)(-\sigma_{j+1}) w_j(a_{j+1} + x) t_{j,k}(a_{j+1} + x)$. Here, σ_{j+1} must be equal to 1 and

$w_j(a_j - x) t_{j,k}(a_j - x) = w_j(a_j - x) \sigma_j t_{j,k}(a_j + x)$ furnishes $\sigma_j = 1$. The symmetry of w_j allows also $w_{j+1}(a_{j+1} + x) t_{j,k}(a_{j+1} + x) = w_j(a_{j+1} - x) t_{j,k}(a_{j+1} + x)$ which finally clarifies the forth equality.

Analogously, this 'unfolding' can be done for other cases, too.

□

Theorem 5.2.7 (Coifman & Meyer – [CW91], Jawerth & Sweldens – [SJ95])**.** *Let $(w_j)_j$ and $(t_{j,k})_{j,k}$ satisfy conditions* (5.3) *and* (5.2)*. Then $(\psi_{j,k})_{j,k}$, $\psi_{j,k} := w_j t_{j,k}$, is an orthonormal basis in* $\mathrm{L}^2(\mathbb{R})$ *, i.e.* $\langle \psi_{j,k}, \psi_{l,m} \rangle = \delta_{j,l}\delta_{k,m}$.

If condition (5.3e) *is lifted and $(w_j)_j$ satisfies instead a weaker requierment*

$$A \leqslant w_j^2(a_j + x) + w_{j-1}^2(a_j + x) \leqslant B, \quad \forall\, |x| \leqslant \epsilon_j \tag{5.16}$$

then $(\psi_{j,k})_{(j,k)\in\mathbb{Z}\times\mathbb{N}_0}$ constitutes a Riesz basis in $\mathrm{L}^2(\mathbb{R})$ *with Riesz bounds A, B.*

Proof. First assertion is a direct result of upper corrolar.

The system $(\chi_{[}a_j, a_{j+1}]t_{j,k})_{k\in\mathbb{N}_0}$ is an orthonormal basis in $\mathrm{L}^2([a_j, a_{j+1}])$, $\forall\, j \in \mathbb{Z}$ such that $(\chi_{[}a_j, a_{j+1}]t_{j,k})_{j\in\mathbb{Z},k\in\mathbb{N}_0}$ is an onb in $\mathrm{L}^2(\mathbb{R})$. Hence, the theory about Riesz bases, Theorem 3.3.4 , imply that $\mathcal{U}_w(\chi_{[}a_j, a_{j+1}]t_{j,k})$ is also an onb if $\mathcal{U}_w$ is a unitary isomorphism.

A similar argumentation proves the second claim: Define first the total folding and unfolding operator as

$$\mathcal{T}_w f(x) := \begin{cases} r_j(x)f(x) + \sigma_j r_j(2a_j - x)f(2a_j - x), & x \in (a_j, a_j^+) \\ r_j(2a_j - x)f(x) - \sigma_j f(2a_j - x), & x \in (a_j^-, a_j) \\ f(x), & x \in [a_j^+, a_{j+1}^-] \end{cases} \tag{5.17}$$

$$\mathcal{U}_w f(x) := \begin{cases} r_j(x)f(x) - \sigma_j r_j(2a_j - x)f(2a_j - x), & x \in (a_j, a_j^+) \\ r_j(2a_j - x)f(x) + \sigma_j f(2a_j - x), & x \in (a_j^-, a_j) \\ f(x), & x \in [a_j^+, a_{j+1}^-] \end{cases} \tag{5.18}$$

for a cut-off function r_j given as in Eq. (5.12). Same calculations as in the proofs of Lemma 5.2.5 and Corollary 5.2.6 yield

$$\begin{aligned} \mathcal{T}_w^* &= \mathcal{U}_w, \\ \mathcal{T}_w f = \mathcal{U}_w f &= f \text{ on } [a_j^+, a_{j+1}^-] \text{ and} \\ \mathcal{T}_w\mathcal{U}_w f(x) = \mathcal{U}_w\mathcal{T}_w f(x) &= \big(r_j^2(x) + r_j^2(2a_j - x)\big) f(x) \\ &= \big(w_j^2(x) + w_{j-1}^2(2a_j - x)\big) f(x) \quad \forall x \in (a_j^-, a_j^+). \end{aligned}$$

Due to last relation the argumentation concludes in

$$\begin{aligned} &\|\mathcal{U}_w f\|_{\mathrm{L}^2(\mathbb{R})} = \langle \mathcal{T}_w\mathcal{U}_w f, f \rangle \\ &= \sum_{j\in\mathbb{Z}} \int_{a_j}^{a_{j+1}} \big(w_j^2(x) + w_{j-1}^2(2a_j - x)\big) |f(x)|^2 \,\mathrm{d}x + \int_{a_j^+}^{a_{j+1}^-} |f(x)|^2 \,\mathrm{d}x \end{aligned} \tag{5.19}$$

which by condition (5.16) implies $A\|f\|_{\mathrm{L}^2} \leqslant \|\mathcal{U}_w f\|_{\mathrm{L}^2} \leqslant B\|f\|_{\mathrm{L}^2}$. So, $\mathcal{U}_w$ is a (topological) isomorphism with $\|\mathcal{U}_w\| \leqslant B$, and $\|\mathcal{U}_w^{-1}\| \leqslant A^{-1}$ (analogously proven as in Theorem 3.4.6, cf. Eq. (3.5)) satisfying Eq. (5.15a) – the previous proof of this relation condition (5.2a) was not used – such that Theorem 3.3.2 completes the proof. □

Corollary 5.2.8. *Suppose that w_j satisfy Eqs.* (5.3a) – (5.3d)*, and* (5.16)*. Then, $(\psi_{j,k})_{j,k}$ constitutes an orthogonal Riesz basis.*

Proof. Due to Eq. (5.3a), $\operatorname{supp}(\psi_{j,k}) \cap \operatorname{supp}(\psi_{i,h}) = \emptyset$ for $|j-i| > 1$, h, k arbitrary, such that these functions are orthogonal. Ensuing calculation proves orthogonality for neighbouring windows w_j and w_{j-1}.

Since $\operatorname{supp}(w_j) \cap \operatorname{supp}(w_{j-1}) = (a_j^-, a_j^+)$ it follows:

$$\begin{aligned}
\langle \psi_{j,k}, \psi_{j-1,h} \rangle &= \int_{a_j^-}^{a_j^+} w_j(x) w_{j-1}(x) t_{j,k}(x) t_{j-1,h}(x)\,\mathrm{d}x \\
&\overset{\text{Eq.(5.3d)}}{=} \int_{-\epsilon_j}^{\epsilon_j} w_j(a_j+x) w_j(a_j-x) t_{j,k}(a_j+x) t_{j-1,h}(a_j+x)\,\mathrm{d}x \\
&= \int_0^{\epsilon_j} w_j(a_j+x) w_j(a_j-x) t_{j,k}(a_j+x) t_{j-1,h}(a_j+x)\,\mathrm{d}x \\
&\quad - \int_0^{\epsilon_j} w_j(a_j-x) w_j(a_j+x) t_{j,k}(a_j-x) t_{j-1,h}(a_j-x)\,\mathrm{d}x \\
&\overset{\substack{\sigma_j\sigma_j=1 \\ \text{Eq.(5.2b)}}}{=} \int_0^{\epsilon_j} \Big(w_j(a_j+x) w_j(a_j-x) - w_j(a_j-x) w_j(a_j+x) \Big) \\
&\qquad\qquad \times t_{j,k}(a_j+x) t_{j-1,h}(a_j+x)\,\mathrm{d}x \\
&= 0.
\end{aligned}$$

□

Remark 5.2.9. The very stringent condition (5.2a) on the windows w_j can be relaxed by Eq. (5.16) which still generates a Riesz basis. Conversely, normalisation of w_j on the overlapping intervals – satisfying Eq. (5.16), i.e. $\frac{w_j(x)}{W_j(x)}$ on (a_j^-, a_j^+) and $\frac{w_j(x)}{W_{j+1}(x)}$ on (a_{j+1}^-, a_{j+1}^+) for $W_j(x) := \sqrt{w_{j-1}^2(x) + w_j^2(x)}$, gives in return orthonormality (this can be already observed in Eq. (5.19)) such that $(\psi_{j,k})_{j,k}$ is again an onb in $\mathrm{L}^2(\mathbb{R})$. So, switching between biorthogonal and orthonormal bases is very easy.

5.2.1 Discretisation

In this subsection discrete analogues of w_j and $t_{j,k}$ will be presented which generate an orthonormal basis in $\ell^2(\mathbb{Z})$.

Remember, that the trigonometric functions $t_{j,k}(\cdot + \frac{1}{2})$, defined as in Eq. (5.4) are precisely the basis functions for the various discrete cosine/sine transforms (see [RY90]). In particular, DCT-IV transform uses $t_{j,k}(\cdot + \frac{1}{2})$ with $\sigma_j = \sigma_{j+1} = 1$, DCT-II is used for even-even, DST-IV for odd-even and DST-II is used for odd-odd parity, respectively.

As already mentioned, the inner products can then be computed in two conventional stages: First, fold the signal at boundaries $(a_j)_j$ (which can be visualised as folding of the overlapping parts of the bell w_j, i.e. $(a_j^-, a_j) \to (a_j, a_j^+)$) such that in the second stage a non-overlapped, since folded signal is processed by standard fast DCT-IV algorithm (or one of its modifications).

In order to preserve orthogonality properties of $w_j t_{j,k}(\cdot + \frac{1}{2})$ on adjacent (overlapping) intervals it is necessary to translate the window functions w_j in the same manner (cf. [Wic91, p. 23]).

Symmetry properties of the window functions w_j (w.r.t. the boundaries a_j, a_{j+1}) are then sustained (cf. Figure 5.5, (a), where no symmetry is preserved).

Definition 5.2.10. Let $(a_i)_i \subset \mathbb{Z}$ and $(\epsilon_i)_i \subset \mathbb{N}_{\geqslant 0}$ fulfill the general assumptions, Assumption 5.2.1. $t_{j,k}$ shall be given as in Formula (5.4) and w_j satisfy the conditions as in Eqs. (5.3). Define for convenience the notation

$$\llbracket a, b \rrbracket := \llbracket a, b \rrbracket_n := \big\{ a_j \in \mathbb{Z} \big| a_{j+1} = a_j + 1,\, a := a_0,\, b := a_n,\, j = 0, \dots, n \big\} \text{ i.e.}$$
$$\llbracket a, b \rrbracket = \{a, a+1, a+2, \dots, b-1, b\} \subset \mathbb{Z},$$
$$W_j(n) := w_j\big(n + \tfrac{1}{2}\big),$$
$$T_{j,k}(n) := t_{j,k}\big(n + \tfrac{1}{2}\big), \quad \text{for } n \in \mathbb{N}.$$

By straightforward calculations it follows from earlier considerations,

Corollary 5.2.11. *(i)* $\operatorname{supp}(W_j) \subset \llbracket a_j^-, a_j^+ - 1 \rrbracket$, *where* $a_j^-, a_j^+ \in \mathbb{Z}$ *come up to Assumption 5.2.1.*

(ii) Symmetry as in (5.3d) *holds on* $\llbracket a_j^-, a_j^+ - 1 \rrbracket_{h_j}$ *if this interval is of even size, i.e.* $h_j = 2z$ *for some* $z \in \mathbb{Z}$. *More precisely*

$$\forall\, n \in \llbracket a_j^-, a_j^+ - 1 \rrbracket :\ W_j(n) = W_{j-1}(2a_j - n - 1)$$

(iii) Since all windows are translated by the same amount, reconstruction formula (5.3e) *is not altered, i.e.*

$$\forall\, n \in \llbracket a_j^-, a_j^+ - 1 \rrbracket :\ W_j^2(n) + W_{j-1}^2(n) = 1.$$

Furthermore, if $(x_{j,k})_{k \in \llbracket 0, h_j - 1 \rrbracket}$ *is a onb in* $\ell^2(\llbracket a_j, a_{j+1} - 1 \rrbracket)$, *where* $h_j = a_j^+ - a_j^- \in \mathbb{N}_{>0}$, *then* $(\Psi_{j,k})_{j \in \mathbb{Z}, k \in \llbracket 0, h_j - 1 \rrbracket}$ *is a onb in* $\ell^2(\mathbb{Z})$.

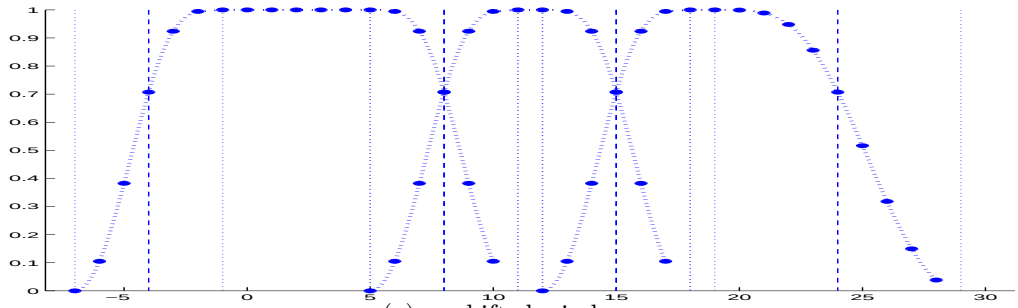

(a) unshifted windows

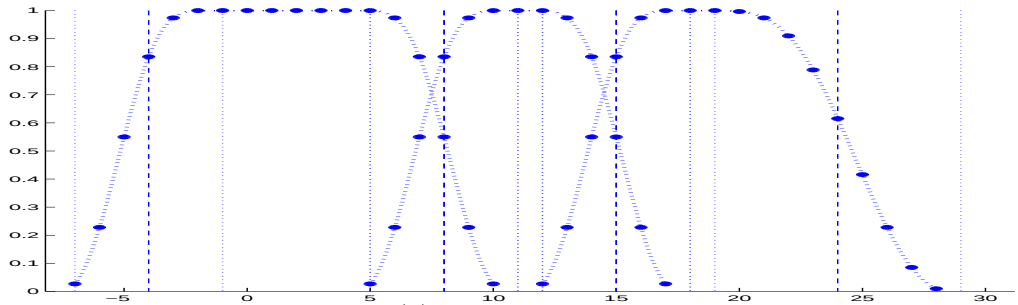

(b) shifted windows

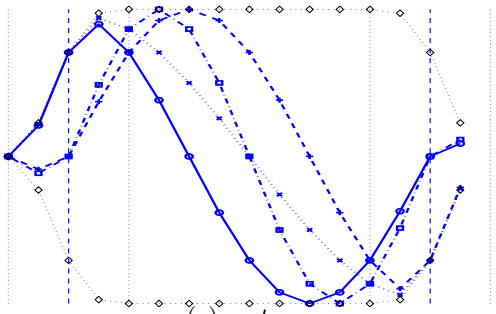

(c) $w_j t_{j,k}$

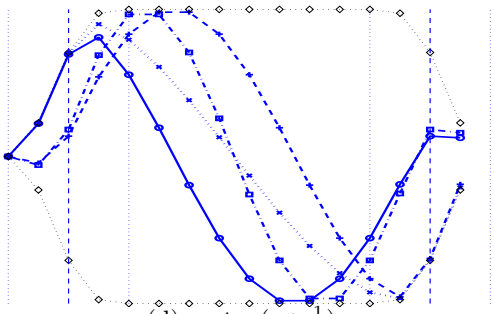

(d) $w_j t_{j,k}(\cdot + \frac{1}{2})$

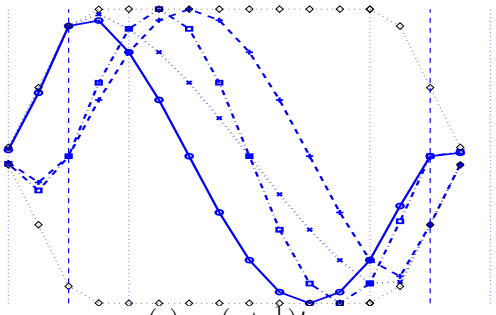

(e) $w_j(\cdot + \frac{1}{2})t_{j,k}$

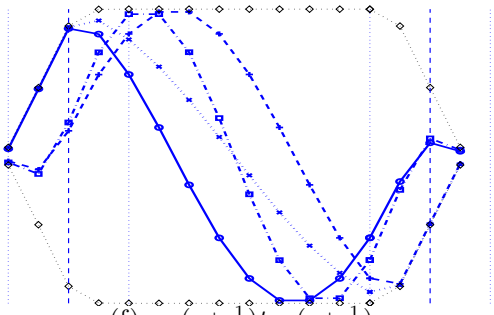

(f) $w_j(\cdot + \frac{1}{2})t_{j,k}(\cdot + \frac{1}{2})$

Fig. 5.5: (a-b): window function with $a = (-4, 8, 15, 24)$, (dashed, vertical lines), and $\epsilon = (3, 3, 3, 5)$ indicated by vertical dotted lines. In (b) it holds $w_2(5) = w_1(10)$, $w_2(8) = w_1(7)$, for instance. (c-f): Windowed $t_{j,k}$ as in Eq. (5.4) with $k = 1$ and parities as in Figure 5.2.

Here, $\Psi_{j,k} := W_j X_{j,k}$ and $X_{j,k}$ is a periodisation of $x_{j,k}$ analogously as in the proof of Lemma 5.2.2, i.e. for $\sigma_j, \sigma_{j+1} \in \{-1, +1\}$

$$X_{j,k}(n) := \begin{cases} x_{j,k}(n), & n \in [\![a_j, a_j^+ - 1]\!] \\ \sigma_j x_{j,k}(2a_j - n - 1), & n \in [\![a_j - h_j, a_j - 1]\!] \\ \sigma_{j+1} x_{j,k}(2a_{j+1} - n - 1), & n \in [\![a_{j+1}, a_{j+1} + h_j - 1]\!] \end{cases}$$

Proof. Let $k \in [\![0, 2\epsilon_j]\!]$. Then by definition of W_j and Relation (5.3d) it holds

$$\begin{aligned} W_j(a_j^- + k) &= w_j(a_j - \epsilon_j + \tfrac{1}{2} + k) = w_{j-1}(2a_j - a_j + \epsilon_j - \tfrac{1}{2} - k) \\ &= w_{j-1}(a_j + \epsilon_j - 1 + \tfrac{1}{2} - k) = W_{j-1}(a_j^+ - 1 + k) \\ &\iff \\ n \in [\![a_j^-, a_j^+ - 1]\!] &: W_j(n) = W_{j-1}(2a_i - n - 1). \end{aligned}$$

First and third points are trivial.

It remains to prove last claim which follows from easy but lengthy calculations (cf. [Kur97, pp. 35]). More precise, $\Psi_{j,k}$ and $\Psi_{i,l}$ are obviously orthogonal to each other if $|j - i| > 1$ since then their support is empty. Hence, it suffice to show:

'interior orthonormality':

$$\forall\, k, l \in [\![0, h_j - 1]\!] : \sum_{z \in \mathbb{Z}} \Psi_{j,k}(z) \Psi_{j,l}(z) = \delta_{k,l}$$

'exterior orthogonality (for neighbours)':

$$\forall\, k, l \in [\![0, h_j - 1]\!] : \sum_{z \in \mathbb{Z}} \Psi_{j,k}(z) \Psi_{j-1,l}(z) = 0.$$

□

5.2.2 Adaptivity and Localisation

Each local trigonometric function $(\psi_{j,k})_{j,k}$ (as defined in Theorem 5.2.7) is well localised in both time and frequency domain. Obviously, $\psi_{j,k}$ has compact support, $\operatorname{supp}(\psi_{j,k}) \subset [a_j^-, a_j^+]$ and thus $\psi_{j,k}$ has 'position uncertainty' at most equal to $h_j + (\epsilon_{j+1} - \epsilon_j) = a_j^+ - a_j^-$.

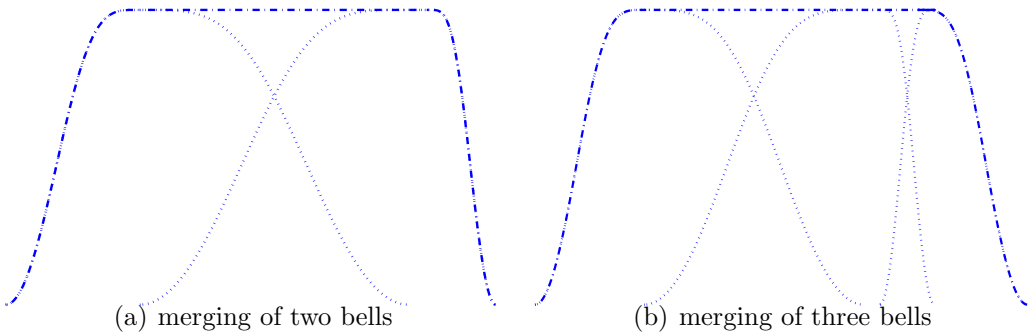

(a) merging of two bells (b) merging of three bells

Fig. 5.6: Two or more children (dotted) summed up to one parent window (dashed-dotted)

Exploiting the relations $\sin(x) = \frac{e^{ix}-e^{-ix}}{2i}$ and $\cos(x) = \frac{e^{ix}+e^{-ix}}{2}$ Formula (5.4) can be rewritten as

$$t_{j,k}(x) = \frac{e^{i\frac{\pi}{2h_j}(x-a_j)\nu_k} + (-1)^{\rho_0} e^{-i\frac{\pi}{2h_j}(x-a_j)\nu_k}}{2i^{\rho_0}},$$

where ρ_0, $\rho_1 \in \{0,1\}$ are related to $\sigma_j, \sigma_{j+1} \in \{-1,+1\}$ in the following way

$$\sigma_j = (-1)^{\rho_0}, \quad \sigma_{j+1} = (-1)^{\rho_1} \text{ and } \quad \nu_k := 2k + 1 + \rho_0 - \rho_1.$$

Using this connection it follows for the Fourier transform $\hat{\psi}_{j,k}(\omega)$:

$$\begin{aligned}\mathcal{F}\big(w_j t_{j,k}\big) &= \frac{1}{2i^{\rho_0}}\Big(\mathcal{F}\big(w_j e^{i\frac{\pi}{2h_j}(\cdot-a_j)\nu_k}\big)(\omega) + (-1)^{\rho_0}\mathcal{F}\big(w_j e^{-i\frac{\pi}{2h_j}(\cdot-a_j)\nu_k}\big)(\omega)\Big) \\ &= \frac{1}{2i^{\rho_0}}\Big(\hat{w}_j\big(\omega - \frac{\pi}{2h_j}(\cdot - a_j)\nu_k\big) + (-1)^{\rho_0}\hat{w}_j\big(\omega + \frac{\pi}{2h_j}(\cdot - a_j)\nu_k\big)\Big)\end{aligned}$$

which can be interpreted as two 'bumps' around $\pm\frac{\pi}{2h_j}\nu_k(\cdot - a_j)$. The uncertainty in the frequency space equals that of $\hat{w}_j$ and hence depends on the smoothness and steepness of w_j – cf. [Wic91, p. 24]. In fact, Rieman-Lebesgue lemma, Theorem 3.5.2, ensures already a 'weak' localisation since $\lim_{|\omega|\to\infty} \hat{w}_j(\omega) = 0$.

Imposing additional conditions on the window function results in more accurate predictions on the localisation.

The matter of convergence of the coefficients $(\langle\psi_{j,k}, f\rangle)_k$ is naturally linked to this topic. Theorem 3.5.4 hints to that if f and w_j are smooth enough, i.e. $f, w_j \in \mathrm{C}^n(\mathbb{R})$ then $\langle f, \psi_{j,k}\rangle = \mathcal{O}\left(k^{-n}\right)$ (see for instance [SJ95, Zyg59]).

Adaptivity The fact that $w_j^2(a_j + x) + w_{j-1}^2(a_j + x) = 1 \,\forall\, |x| \leqslant \epsilon_j$ which is equivalent to $w_j^2(x) + w_{j-1}^2(x) = 1 \,\forall\, x \in (a_j^-, a_j^+)$ implies that $\tilde{w}_{j-1} :=$

$\sqrt{w_{j-1}^2 + w_j^2}$ is a window function with $\mathrm{supp}(\tilde{w}_{j-1}) \subset [a_{j-1}^-, a_{j+1}^+]$. Such a process of 'fusion' is illustrated in Figure 5.6.

This yields a local trigonometric function $\tilde{\psi}_{j-1,k} = \tilde{w}_{j-1}\tilde{t}_{j-1,k}$, where $\tilde{t}_{j-1,k}$ is re-normalised and re-dilated appropriately by $\tilde{h} := h_j + h_{j-1}$ (cf. Eq (5.4) and Figure 5.7). Due to Theorem 5.2.7 and Corollary 5.2.8, $\mathrm{L}^2(\mathbb{R})$ can be decomposed into orthonormal subspaces spanned by the orthonormal set $(w_j t_{j,k})_{k\in\mathbb{Z}}$, i.e. for every admissible partition $a := (a_j)_j \subset \mathbb{R}$ (with $\mathbb{R} = \dot{\cup}_{j\in\mathbb{Z}}(a_j, a_{j+1})$), provided that Assumption 5.2.1 is assured it holds

$$\begin{aligned} \mathrm{L}^2\big((a_j, a_{j+1})\big) &= \mathrm{span}\Big\{ w_j t_{j,k} \Big| k \in \mathbb{Z} \Big\} \qquad (5.20)\\ \mathrm{L}^2\big((a_{j-1}, a_{j+1})\big) &= \mathrm{span}\Big\{ w_{j-1} t_{j-1,k} \Big| k \in \mathbb{Z} \Big\} \oplus \mathrm{span}\Big\{ w_j t_{j,k} \Big| k \in \mathbb{Z} \Big\} \\ \mathrm{L}^2(\mathbb{R}) &= \bigoplus_{j\in\mathbb{Z}} \mathrm{span}\Big\{ \psi_{j,k} = w_j t_{j,k} \Big| k \in \mathbb{Z} \Big\}. \end{aligned}$$

This means in particular, that the set

$$\mathcal{D} := \left\{ \bigoplus_{j\in\mathbb{Z}} \mathrm{span}\{\psi_{j,k} | k \in \mathbb{Z}\} \,\middle|\, a \text{ admissible} \right\} \qquad (5.21)$$

furnishes an over-complete 'dictionary' – or *library* – of orthonormal bases with the potential of switching between different bases by refinement or mergence of contiguous intervals $(a_{j-1}, a_j) \cup (a_j, a_{j+1}) \leftrightsquigarrow (a_{j-1}, a_{j+1})$ which are associated to a basis, cf. Eq. (5.20).

There is a partial ordering[1] of such partitions which can be made into a tree, visualised in Figure 5.8, and searched for a 'best basis' w.r.t a cost function. In that context the *depth* of the tree is the total number of *levels* whilst a level is the number associated to a basis in that tree counting from the root which has level zero. The tree in Figure 5.8 has then depth 3 for instance.

The idea behind such a procedure may be explained by an analogy: Interpretation of a multilingual speech may be accomplished best by an appropriate mix of many dictionaries. Obviously, a German-English dictionary alone is incapable to translate a talk between a Chinese and an Englishman. On the other hand, a Chinese-English dictionary is insufficient for giving an impression of this conversation to a German. Correlating the speech with

[1] A basis B_1 is greater than a basis B_2 if the cover associated to B_1 is a refinement of the cover associated to B_2. Such partial order has a minimal element, the basis B_0 associated to the coarsest cover, and a maximal element corresponding to the most refined cover.

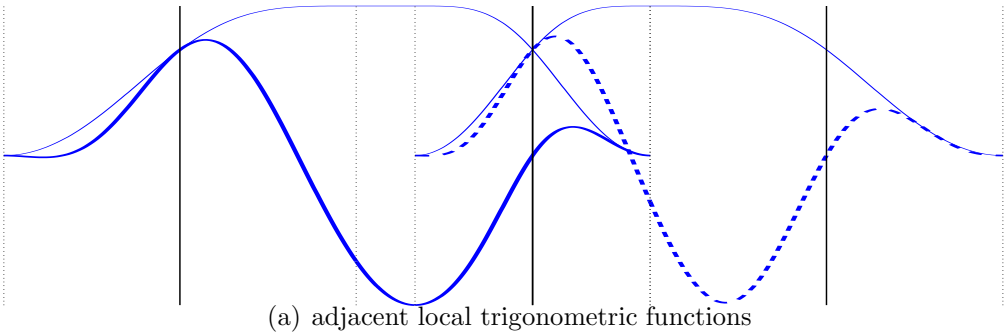

(a) adjacent local trigonometric functions

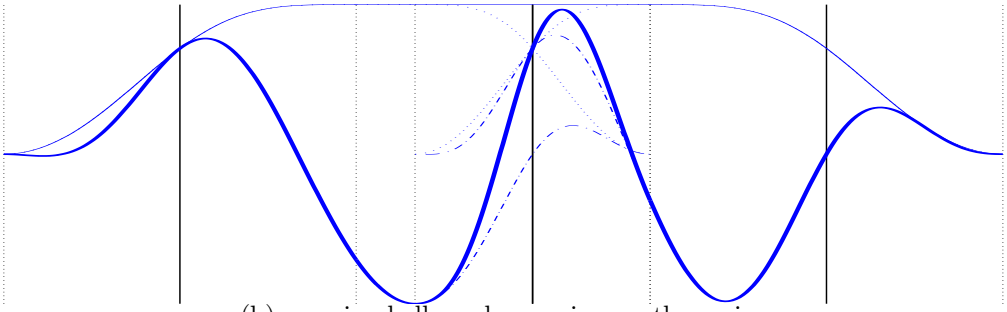

(b) merging bells and summing up the cosines

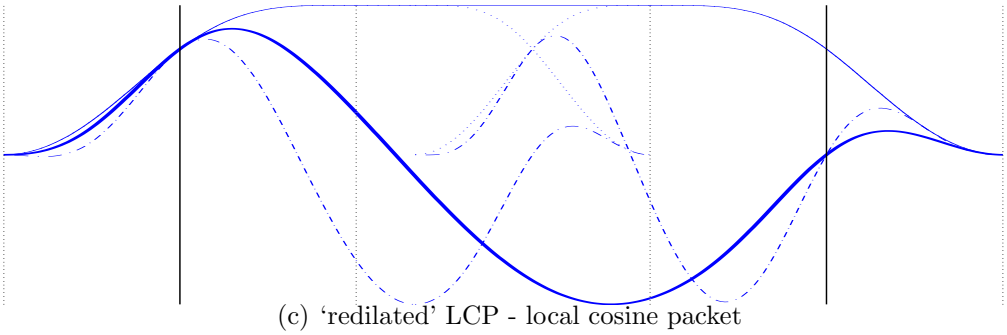

(c) 'redilated' LCP - local cosine packet

Fig. 5.7: Plots (a-c) describe the 'fusion' process. First, Figure (a), merge adjacent bells $\sqrt{w_{j-1}^2 + w_j^2} =: \tilde{w}_{j-1}$, (solid thin line in Fig. (b)), then, Figure (c), translate (to a_{j-1}) and dilate a trigonometric function $\tilde{t}_{j,k}$ (by $\tilde{h} = h_j + h_{j-1} = a_{j+1} - a_{j-1}$) such that $\tilde{t}_{j,k}$ have the same oscillation index k as $t_{j-1,k}$ windowed by $\tilde{w}_{j-1}$.

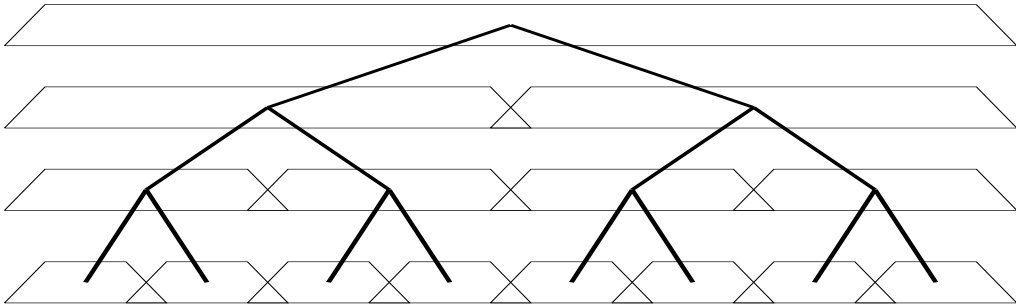

Fig. 5.8: Iterative de-/composition from children to parent and grand-parent windows. Here a dyadic splitting of windows is presented.

both dictionaries, i.e. picking just the information needed, will result in a more comprehensible talk between all three participants, Chinese, German and Englishman.

Such profit of many similar (since concerning same objects (as language for instance)) but different dictionaries can also be elucidated as an attempt of orchestrating a signal, e.g. assigning (musical) instruments to a piece of music.

Here, the dictionary would be an orchestra synthesising the signal, trying to mimic it.

Analogously, the instruments of the local trigonometric transform

$$\begin{aligned} &\mathrm{L}^2((a_j, a_{j+1})) \ni f_j \mapsto (\langle f_j, \psi_{j,k}\rangle)_k \in \ell^2(\mathbb{R}), \quad j \in \mathbb{Z} \\ &f_j := \mathcal{T}_w f \chi_{[a_j, a_{j+1}]} = U_j f \quad \text{cf. Eqs. (5.14a), (5.15b)} \end{aligned}$$

are time-localised sines or cosines, respectively, of different frequencies.

A crucial degree of freedom in this transform is the sequence $(a_j)_j$.

Analogously to the windowed Fourier transform it may happen that the window size does not match the frequency behaviour of a particular signal, e.g. when the signal has short bursts (fast change of frequencies) but the size of w_j captures to many of them, or vice versa. All the same, the result would yield a poor time-frequency resolution. Compare in this context the examples elucidated in Figures 4.16 and 4.17 in contrast to Figure 6.3.

Fortunately, the local trigonometric transform permits a kind of nesting, Eq. (5.21), such that the size of arbitrary many windows may be adapted locally (refinement or coalescence) without changing the rest of them. So, switching between one basis, associated to a sequence $a \subset \mathbb{R}$ satisfying weak assumptions, Assumption 5.2.1, to another basis, associated to $a' \subset \mathbb{R}$ allow the transform to adapt 'on the fly', or more precisely without any prior knowledge about the properties of the considered signal.

A measure of how well such a partition is suited may be established by a cost functional leading to a basis with optimal properties (with respect to that functional).

This is accomplished by comparing the cost of the expansions associated to the two small intervals to that expansion associated to the union of these adjacent windows. Picking that intervals for which the cost is smaller results in an expansion of minimal cost.

In practise, a dyadic partition is preferred, i.e. $a_{l,j} := 2^{-l}j$ with $l \in [\![0, L]\!]$, $j \in [\![0, 2^l]\!]$ which leads to a partition of the interval $[0, 1]$ at different levels l. With each $a_l := (a_{l,j})_j$ a local trigonometric basis can be associated with the properties as called for the next definition.

Definition 5.2.12. Let I be the unit interval, $I := [0, 1)$ and $I_{l,j}$ a dyadic subinterval of I, i.e. $I_{l,j} := [2^{-l}j, 2^{-l}(j+1))$ for $l \in [\![0, L]\!]$, $j \in [\![0, 2^l - 1]\!]$, $L \in \mathbb{N}$.

A dictionary $\mathcal{D}$ of orthonormal bases is a *binary tree* if it satisfies

(i) Subsets of basis vectors cn be identified with subintervals $I_{l,j}$ of I.

(ii) Each basis in the dictionary $\mathcal{D}$ corresponds to a disjoint cover of I by intervals $I_{l,j}$.

(iii) If $D_{l,j} \subset B \in \mathcal{D}$ can be identified with $I_{l,j}$, then $D_{l,j} = D_{l+1,2j} \oplus D_{l+1,2j+1}$.

Any binary tree is termed an *admissible* tree iff each node has either zero or exactly two children.

Hence, any admissible tree is associated to an orthonormal basis of local trigonometric functions (which is mostly based on the first part of Theorem 5.2.7).

5.3 Best Basis - Divide et Impera

As mentioned in the foregoing section the best-basis algorithm, developed by Coifman and Wickerhauser, cf. [CW92], enables an automatic switching between different bases assigned to a suitable partition in time domain (for local trigonometric packets) or in frequency domain (for wavelet packets)[2].

In order to diminish the complexity both authors suggested to use functionals which are additive.

[2]For more details, especially on the *graph basis theorem* which ensures that the leaves of any *admissible binary tree*, cf. Definition 5.2.12, of a wavelet packet or a local trigonometric tree form a basis, check [Wic94, p. 244].

Definition 5.3.1. A functional $\mathcal{M} : \ell^2 \to \mathbb{R}_{\geqslant 0}$ is said to be *additive*$:\Longleftrightarrow$

$$\mathcal{M}\big((x_i)_i\big) = \sum_i m(|x_i|) \quad \text{for some concave function } m : \mathbb{R} \to \mathbb{R},$$
$$\mathcal{M}((0)_i) = 0$$

Consider a discretised signal $(f_i)_{i\in[\![1,n]\!]}$ with $n \in \mathbb{N}$ samples at positions $(a_i)_{i\in[\![1,n]\!]}$ and let Eq. (5.21) be rewritten in the form

$$\mathcal{D} = \bigcup_{\lambda\in\Lambda} \mathcal{B}_\lambda, \quad \mathcal{B}_\lambda := (b_{\lambda,i})_{i\in[\![1,n]\!]=:I_{\lambda,n}},$$

where $\mathcal{B}_\lambda$ denotes the λ-th orthonormal basis of $\ell^2([\![a_1, a_n]\!])$ with $\Lambda \in \mathbb{N}$ finite.

The approximation error, ϵ_λ with $M \in [\![1, n]\!]$,

$$\epsilon_\lambda(M) := \sum_{m\notin I_{\lambda,M}} |\,\langle (f_i)_i, b_{\lambda,m}\rangle\,|^2 = \|(f_i)_i\|^2_{\ell^2} - \sum_{m\in I_{\lambda,M}} |\,\langle (f_i)_i, b_{\lambda,m}\rangle\,|^2 \quad (5.22)$$

can then be used as a comparison measure between different bases, i.e. $\mathcal{B}_\alpha$ is a better basis for $(f_i)_i$ than $\mathcal{B}_\beta$ if each truncated series in the former basis is of lower approximation error than the later, i.e. $\forall M \geqslant 1 : \epsilon_\alpha(M) \leqslant \epsilon_\beta(M)$, which reduces by Eq. (5.22) to

$$\forall M \geqslant 1 : \sum_{m\in I_{\alpha,M}} |\,\langle (f_i)_i, b_{\alpha,m}\rangle\,|^2 \geqslant \sum_{m\in I_{\beta,M}} |\,\langle (f_i)_i, b_{\beta,m}\rangle\,|^2.$$

The Hardy-Littlewood-Polya theorem[3] which is a classical result in the theory of majorisation, consult [MO79], gives then a convenient description of an improved basis representation. A basis $\mathcal{B}_\alpha$ is a better basis than $\mathcal{B}_\beta$ approximating $(f_i)_i$ iff any concave function $\phi : \mathbb{R} \to \mathbb{R}$ admits the relation

$$\sum_{i\leqslant n} \phi\big(x_{\alpha,i}\big) \leqslant \sum_{i\leqslant n} \phi\big(x_{\beta,i}\big), \quad x_{\kappa,i} := \frac{|\,\langle (f_j)_j, b_{\kappa,i}\rangle\,|^2}{\|(f_j)_j\|^2_{\ell^2}} \text{ and } b_\kappa \in \mathcal{B}_\kappa. \quad (5.23)$$

Above consideration, especially Eq. (5.23) do not exploit the special tree structure of the dictionary $\mathcal{D}$. Therefore, minimality of a particular concave function ϕ w.r.t. to a basis $\mathcal{B}_\alpha$ is not sufficient to guarantee that $\mathcal{B}_\alpha$ is indeed a better basis than any other.

Fortunately, when dealing with binary trees, as defined in Definition 5.2.12, it suffices completely to minimise only one cost function in order to obtain a 'best basis'. Note that $\mathcal{M}(Bx)$ as defined in the following definition basically reduces to the sum Eq. (5.23), see also [Mal98, pp. 397].

[3] Any two positive sequences $(x_i)_{i\leqslant n}$, $(y_i)_{i\leqslant n}$ sorted in decreasing order, $x_i \geqslant x_{i+1}$, with equal ℓ^1 norm admits $\forall m \leqslant n \sum_{i\leqslant m} x_i \geqslant \sum_{i\leqslant m} y_i$ iff for any concave function $\phi : \mathbb{R} \to \mathbb{R}$ it holds $\sum_{i\leqslant n} \phi(x_i) \leqslant \sum_{i\leqslant n} \phi(y_i)$. A proof can be checked at [Mal98, pp. 398]

Definition 5.3.2 (Best Basis, [CW92])**.** Let $\mathcal{D}$ be a finite dictionary of ℓ^2, i.e. a set of finitely many orthonormal bases in ℓ^2.

A vector $x \in \ell^2$ has an *information cost restricted to a basis $B \in \mathcal{D}$ w.r.t.* $\mathcal{M}$, denoted by $\mathcal{M}(Bx)$ and defined as

$$\mathcal{M}(Bx) := \mathcal{M}\Big(\big(\langle x, b_k\rangle\big)_k\Big) \text{ for } b_k \in B.$$

$A \in \mathcal{D}$ is termed *best basis* for $x :\Longleftrightarrow \mathcal{M}(Ax) \leqslant \mathcal{M}(Bx) \quad \forall\, B \in \mathcal{D}$

The information cost of $\mathcal{M}(x \oplus y)$ can then be reduced locally, i.e. by reducing $\mathcal{M}(x)$ and $\mathcal{M}(y)$ individually.

Suppose for instance that the bases A, $B \in \mathcal{D}$ partially coincide, i.e. have at least one common basis element. A vector $x \in \ell^2$ is then representable in A as $Ax = (A \cap B)x \times A'x$ and analogously, $Bx = (A \cap B)x \times B'x$ with $A' = A \setminus B$, $B' = B \setminus A$. Then $\mathcal{M}(Ax) < \mathcal{M}(Bx) \iff \mathcal{M}(A'x) < \mathcal{M}(B'x)$, i.e. it suffice to reduce the information cost on a smaller subset.

Example 5.3.3. Thresholding Let $(x_i)_i$ be any finite sequence. Then a simple additive function is given by $\mathcal{M}((x_i)_i) := \sum_i \delta_\epsilon(x_i)$ where $\delta_\epsilon(x_i) := 0$ if $x_i \leqslant \epsilon$ and one otherwise. Additivity follows from $\mathcal{M}\big((\delta_{k,i}\eta_1)_k + (\delta_{k,j}\eta_2)_k\big) = \delta_\epsilon(\eta_1) + \delta_\epsilon(\eta_2) = \sum_k \delta_\epsilon(\delta_{k,i}\eta_1) + \sum_k \delta_\epsilon(\delta_{k,j}\eta_2) = \mathcal{M}\big((\delta_{k,i}\eta_1)_k\big) + \mathcal{M}\big((\delta_{k,j}\eta_2)_k\big)$ for any i, j and $\eta_{1,2}$. Here $\delta_{j,k}$ is the Kronecker delta.

Concentration in $\|\cdot\|_{\ell^p}$, $p \in (0,2)$ $\mathcal{M}(x) := \|x\|_{\ell^p}^p$ is clearly additive: $\sum_i |x_i|^p = \sum_{i \neq j} |x_i|^p + |x_j|^p$, for all j. Concavity, $\phi(x) = x^{p/2}$, is ensued from the necessary restriction of p.

Choice, Uncertainty, Information For any sequence $x \in \ell^2$ the value $p_i := \frac{|x_i|^2}{\|x\|_{\ell^2}^2}$ can be understood as a probability measure. How uncertain the outcome of a state i is or how much information is hidden in the vector x can then be described by the so-called *Shannon-Weaver entropy* $H(x) := -\sum_i p_i \log p_i$ with the agreement $p \log p := 0$ in case of $p = 0$. Some classical properties of H are:

minimal $H(x) = 0 \iff x_i = 0\, \forall\, i \neq i_0 \wedge x_0 = 1$. This means that iff all probabilities (but one) are zero then the outcome i_0 is for sure and H must vanish.

maximal H is maximal if all p_i have same probability, $p_i = \frac{1}{n}$, and equals $\log(n)$ if $p \in \mathbb{R}^n$. This makes sense since then a certain outcome is most uncertain.

monotonicity Any change towards equalisation of p_i increases H, i.e. $p' := Ap$, $p \in \mathbb{R}^n$ with a positive (averaging) weight matrix $A = (a_{i,j})_{i,j\leqslant n}$, $a_{i,j} \geqslant 0$ and $\sum_i a_{i,j} = \sum_j a_{i,j} = 1 \Rightarrow H(p) \leqslant H(p')$. A more detailed discussion about H can be find in [Sha48].

Another classical fact is the relation $H(x) = \|x\|^{-2} h(x) + \log(\|x\|^2)$ where $h(x) := -\sum_i |x_i|^2 \log |x_i|^2$ is an additive function and therefore is the choice for the best basis algorithm. Minimising h leads indirect to a minimisation of H.

Logarithm of energy $\mathcal{M}(x) := \sum_i \log |x_i|^2$ is obviously an additive function with same convention, $\log 0 := 0$, as for the Shannon-Weaver entropy which is motivated by ignoring any unchanging components in the process.

The number of all possible bases ($|\mathcal{D}_L|$) associated to a binary tree (of depth L) is equal to the number of different admissible binary trees and can be estimated by induction (on the depth) as $|\mathcal{D}_L| > 2^{2^L}$.

For $L = 0$ there exists only one basis which is associated to the root, i.e. $|\mathcal{D}_0| = 1$.

Two binary trees of depth at most L with $|\mathcal{D}_L|$ different admissible trees can be combined to a binary tree of depth $L+1$ plus a new root, i.e. $|\mathcal{D}_{L+1}| = |\mathcal{D}_L|^2 + 1$ which implies $|\mathcal{D}_L| > 2^{2^L}$.

A discrete signal of size n can be associated to a binary tree of depth at most $L = \log_2 n$ and thus has at least $2^{n/2}$ different bases representations.

A minimum information cost basis is then computed from the most refined partitions upwards (depth-first). Due to finite resolution level the following algorithm terminates. And if the information cost functional is additive comparisons only between two adjacent generations of the binary tree are necessary to obtain a basis representation with smaller cost which is why the complexity of such a procedure is proportional to the number of nodes in this tree. In contrast, finding a minimum cost by a brute force comparison of all possible packets would require more than $\mathcal{O}\left(n2^{n/2}\right)$ operations, a 'non-polynomial hard' problem which is computationally prohibitive.

Algorithm 5.3.4 (Best Basis, [CW92])**.** Let $x \in \mathbb{R}^n$, $n = 2^m$ for some $m \in \mathbb{N}$, be a vector. Given a binary tree $\mathcal{D}$, an additive cost functional $\mathcal{M}$ and an expansion of x in each possible basis $B \in \mathcal{D}$ with coefficients $\left(B_{l,j}x\right)_{l\in[\![0,L]\!],j\in[\![0,2^l-1]\!]}$, $Bx := (\langle x, B(k)\rangle_{\ell^2})_k$, the best basis Algorithm (5.24) terminates after $\mathcal{O}(n)$ operations. The output, a basis $A \in \mathcal{D}$, is the best basis of x - cf. Definition 5.3.2.

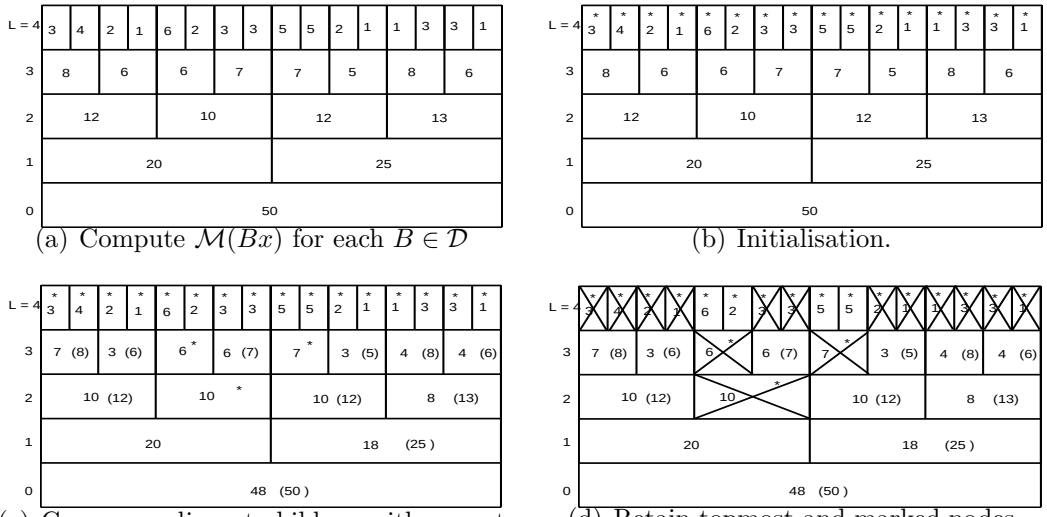

(a) Compute $\mathcal{M}(Bx)$ for each $B \in \mathcal{D}$

(b) Initialisation.

(c) Compare adjacent children with parent nodes

(d) Retain topmost and marked nodes

Fig. 5.9: Best basis search. Numbers in rectangles elucidate the information cost inside each node. (b): Depth-first algorithm means that all nodes at the deepest node (here $L = 4$) are initially marked, i.e. assigned with an asterisk which stands for $A_{L,j} = B_{L,j}$, $j = 0, \ldots, 15$. Their total information cost will be tried to reduce. (c): If the children have lower cost than parent node, then assign the total information cost of the children to the parent node – displayed now in brackets. Otherwise mark the parent node with an asterisk (– join of children nodes). This prevents the computer from examining any node more than twice, once as a child and once as a parent. (d): After all nodes have been examined, take that marked nodes which are at the topmost level (crossed rectangles). These constitute a basis with minimal information cost.

Initialisation Start at the most refined subsets (depth-first) and set $A_{L,j} := B_{L,j}$, $j \in [\![0, 2^L - 1]\!]$.

Iteration: $l = l - 1$**.** For $j \in [\![0, 2^l - 1]\!]$ set

$$A_{l,j} := \begin{cases} B_{l,j}, & \mathcal{M}\big(B_{l,j}\big) \leqslant \mathcal{M}\Big(A_{l+1,2j}x \cup A_{l+1,2j+1}x\Big) \\ A_{l+1,2j} \oplus A_{l+1,2j+1}, & \text{otherwise} \end{cases} \tag{5.24}$$

An example is shown in Figures 5.9 and 5.10.

Proof. A proof can be checked in [Wic91, CW92, Wic93b]. □

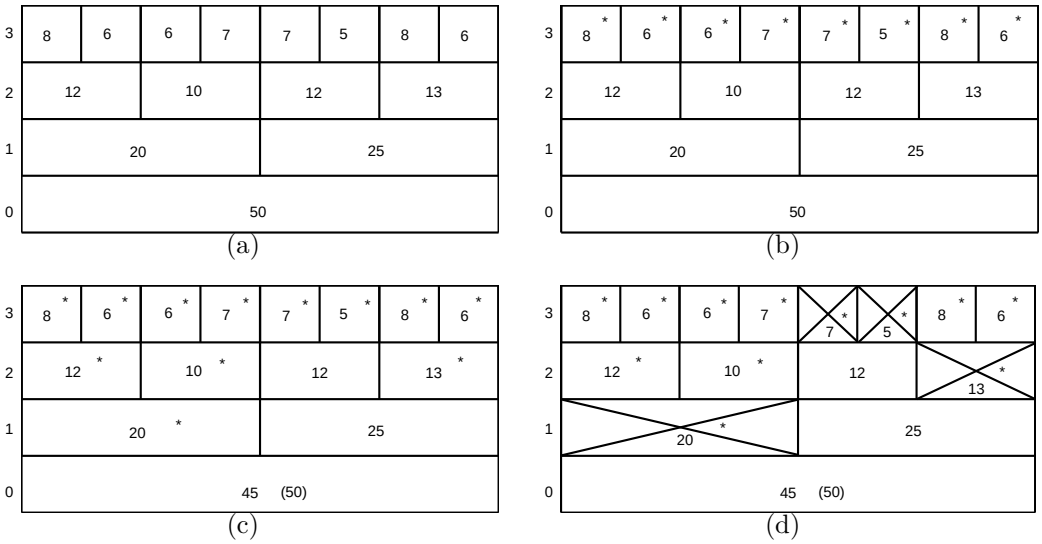

Fig. 5.10: Same dictionary $\mathcal{D}$ and same expanded signal but $L = 3$. From this example it is obvious that best basis obtained here is different from previous, for $L = 4$.

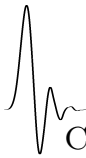

Chapter 6

Implementation – Results

Given a data set or a catalogue of words (or commands) spoken by different people, the task is to extract speaker independent but characteristic features of these words which allow an algorithm to map (injectively) user's audible expressions to pre-defined actions.

For instance, if a statement like '*Open the fridge*' is known by the system, i.e. there exists a collection of features accessible by that algorithm, then, any recorded speech containing that phrase should be recognised as '*Open the fridge*' and nothing else. Of course, if the system fails to recognise a pattern then the output should also be an a priory prescribed error report or act.

In order to guarantee a fast respondent system, the number of operations needed by any algorithm used by that system should be kept as small as possible.

This implies in particular that the number of features have to be kept small. Any performance enhancement depends highly on the selection of these features.

The still vague process of classifying signals into known categories, termed as *classification*, will be put in a concrete mathematical model.

6.1 Mathematical Description Of The Problem

Consider a data set of sampled signals, i.e. a set of vectors, $(x_i)_{i\leqslant n} \subset \mathbb{X}$, where $\mathbb{X}$ represents a so-called *signal space*.

Due to discrete data x_i which will be processed by special algorithms optimised for inputs of dyadic length the signal space $\mathbb{X}$ is set to

$$\mathbb{X} := \mathbb{R}^{2^\nu} \text{ for some } \nu \in \mathbb{N}. \tag{6.1a}$$

Let $c \in \mathbb{N}$ be the number of different classes and denote by $\mathbb{Y}$ the *response space*. Then, each elements of $\mathbb{Y}$ can be identified with an integer such that $\mathbb{Y}$ can be defined as

$$\mathbb{Y} := \Big\{ y \,\Big|\, y \in \{1, \ldots, c\} \Big\}. \tag{6.1b}$$

The goal is then to find a *feature extractor*

$$f : \mathbb{X} \to \mathbb{F} \subset \mathbb{R}^{\mu},\ \mu \ll 2^{\nu} \tag{6.1c}$$

such that relevant information is extracted (mapped to the *feature space* $\mathbb{F}$).

The accuracy of the classification process, a mapping

$$g : \mathbb{F} \to \mathbb{Y} \tag{6.1d}$$

can be measured by a classical performance measure

$$p_f(\mathcal{T}) := \frac{\sum_{(x_i,y_i)\in\mathcal{T}} \delta\big(y_i - g \circ f(x_i)\big)}{|\mathcal{T}|}, \tag{6.1e}$$

with the symbol $\delta(0) := 0$ and equal to 1 everywhere else and $|\mathcal{T}|$ standing for the amount of elements contained in $\mathcal{T}$.

The feature extractor f should be adapted to the *learning* set $\mathcal{L}$, i.e. $p_f(\mathcal{L}) = 0$ where

$$\mathcal{L} := \{(x_i, y_i) \,|\, i = 1, \ldots, n\} \subset \mathbb{X} \times \mathbb{Y} \tag{6.1f}$$

with pairs of measured signals x_i and predetermined targets $y_i \in \mathbb{Y}$, prior f is tested on a *training set* $\mathcal{T} \subset \mathbb{X} \times \mathbb{Y}$ with $\mathcal{T} \cap \mathcal{L} = \emptyset$.

Then, h is a better feature extractor than f iff $p_h(\mathcal{T}) < p_f(\mathcal{T})$ for any training set $\mathcal{T}$.

6.2 General Setting

As it was presented in Chapter 2 and especially in Section 4.4.2, it suffices to (uniformly) sample speech with a sampling frequency of 8 kHz since then the maximum detectable frequency is still at approximately 4 kHz.

The data set recorded in a rather quiet computer room (several computer fans and sometimes distant very quiet talk between students were recorded too) contains ten different classes of words, $c = 10$ in Eq. (6.1b): [an], [ˈauf], [ˈaus], [ˈfɛnstər], [heːrt], [ˈhilfə], [liçt], [ˈnoːtruːf], [tyːr], [ˈtsuː]; (translated as: *on, open, off, window, (kitchen) cooker, help, light, emergency, door, close*) spoken by four females and nine males; each word was repeated once.

That makes in total $n = 260$ words; each class consisting of 26 words of approximately one second duration, or exactly 2^{ν}, $\nu = 13$, samples.

The whole recordering was accomplished by a 'Realtek AC97 Audio' sound card and Matlab's *Data Acquisition Toolbox*.

The basic idea for feature extraction was first tackled by means of wavelets. The author believed that a subdivision of a signal into voiced and unvoiced parts would at least further simplify the proceedings. Such a partition is presented in Section 4.4.2 and due to Mallat's fast tree algorithm (cf. Chapter 4, Eqs. (4.11) and the discussion thereafter) is also of cheap computational complexity.

Voiced parts should then be analysed with a windowed Fourier transform in order to achieve a formant representation (cf. Chapter 2) whereas voiceless parts could be characterised by higher level wavelet coefficients. This seemed to be an adequate starting point since formants necessitate a higher frequency resolution – not achievable by wavelets – and are not as time varying entities as bursts resulting from consonants (again, cf. Chapter 2) which seemed to be suitable described by wavelet coefficients (zooming property - cf. Theorem 4.3.15).

The so computed sequence (in time) of formants, timestamps of voiced/ voiceless parts and bursts could then lead to features of sufficiently robustness since the catalogue consists of rather distinct words.

Several problems were encountered as soon as the author was faced with a satisfactory parametrisation of formant's scattering from a windowed Fourier transform signal of voiced speech (cf. Section 4.4.2).

Of course, a suitable metric have had to be defined on the phase space prior to parametrisation (it is necessary to know which high energy parts belong to the one formant and which constitute another).

Additional inconvenience was resulting from the fact that subdivision into voiced/ voiceless parts was not as accurate as it should be. This is mostly due to the octave-band tiling of the wavelet transform since then only first few levels 'encode' the relevant frequency information for formants.

For instance, a discrete wavelet decomposition (of a 8 kHz sampled signal) up to level $L = 4$ would yield a frequency tiling $(c4, d4, d3, d2, d1)$ with pertinent frequency ranges as follows: $0-250$ Hz, $250-500$ Hz, $0.5-1$ kHz, $1-2$ kHz, $2-4$ kHz; each voiced piece of a signal has frequencies in the range $250-500$ Hz. In that case, any further decomposition would not gain more accuracy. Therefore, uncertainty in time for voiced/ voiceless boundaries is rather high.

At that stage a paper dealing with wavelet and local trigonometric *packets* (cf. [CW92]) supervened further investigations into the problems described above.

This new ansatz, a generalisation of wavelets, seems to be very promising.

In contrast to the case of wavelet packets, where the frequency axis is subject to a dyadic division, local trigonometric packet transform establishes

a library such that each subspace contains frequencies at *fixed locations*, as illustrated in Figures 6.1 and 6.2.

Once again, in order to emphasise the superiority of the adaptive phase tiling over the fixed time-frequency partition (as typified by the transforms $\mathcal{F}_g$ and $\mathcal{W}$) the sinusoidal signal from Section 4.4.2, showed in Figure 4.16, (a), is analysed again by means of the 'new' transforms WPT and CPT, which result is visualised in Figure 6.3.

For the time being, the local trigonometric transform (from now on abbreviated as LCT, local cosine transform) is preferred over the WPT (wavelet packet transform) since the goal is to obtain an 'optimal' time partition of the signal with associated frequencies.

The author considers such a phase tiling (like in Figure 6.2, (b)) as more readable compared to the other way around achieved by a WPT.

It has a striking resemblance to a spectrogram. The only difference is that the windows applied to the signal in order to localise information may not be fixed!

Colouration is similar to that of spectrograms, i.e. the higher the value of a coefficient the darker the grey tone.

The majority of the algorithms which plot such phase tilings and compute cosine (wavelet) packets as well as the 'best basis' are implemented in Matlab's toolbox *WaveLab*, vers. 802, a freeware obtainable via World-Wide-Web: `http://www-stat.stanford.edu/~wavelab`, see also [BD]. Moreover, a grey scale transform was applied to the coefficients in order to achieve more shaded areas in the phase planes. In particular, the *gamma* transform, $x \mapsto x^\gamma$, with the exponent $\gamma = 0.3$ was used to plot all the following phase plane plots and especially Figure 6.2, (a) and (c).

6.3 Influence of Cost Functional

Despite the fact that the best basis is unique (for a precise cost functional) it is by no means independent of the choice of a particular concave function ϕ – see Section 5.3. This allows to compare cost functionals between each other.

On the basis of the previously described data set of words several cost functionals such as those introduced in Example 5.3.3 plus a few more were tested. Results are summarised below and in Figures 6.4, 6.5, 6.6 and 6.7, where phase plane tiling is only plotted for one word,['fɛnstər], Figure 6.4 (a), spoken by a female. For comparison, the same procedure was applied to the same word,['fɛnstər], but now spoken by a male; check Figure 6.8–Figure 6.11.

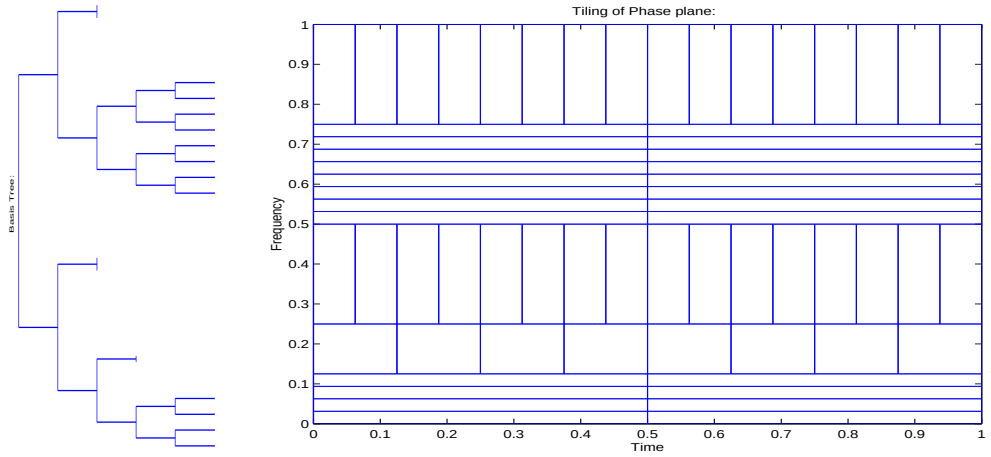

(a) wavelet packet basis

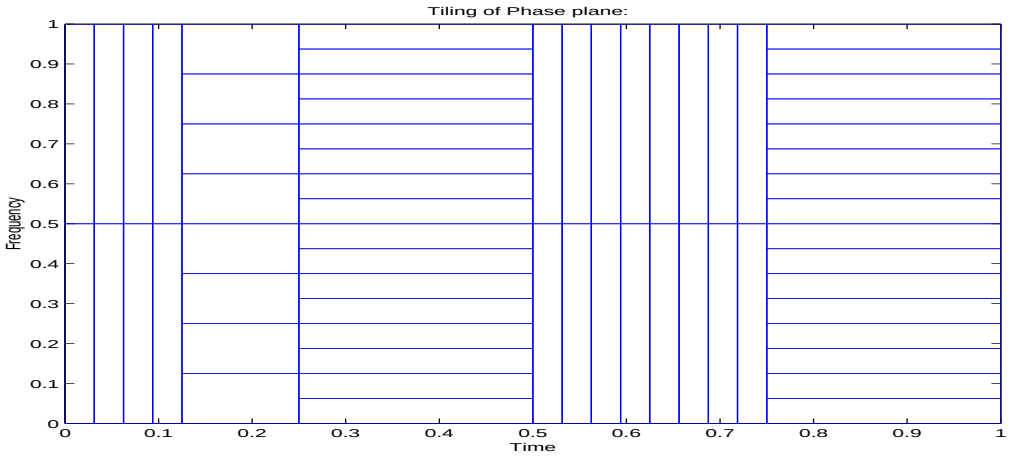

(b) local trigonometric packet basis

Fig. 6.1: Heisenberg boxes; In Subplot (a), left side, a possible basis tree is plotted (up to level 5); Right Subplot (a), subdivision of frequency axis, and Subplot (b), subdivision of time axis, shows the pertinent tilings. Note that the tiling of the phase plane corresponding to a WPT is a rotated copy of a tiling corresponding to a LCT, iff same basis tree is chosen.

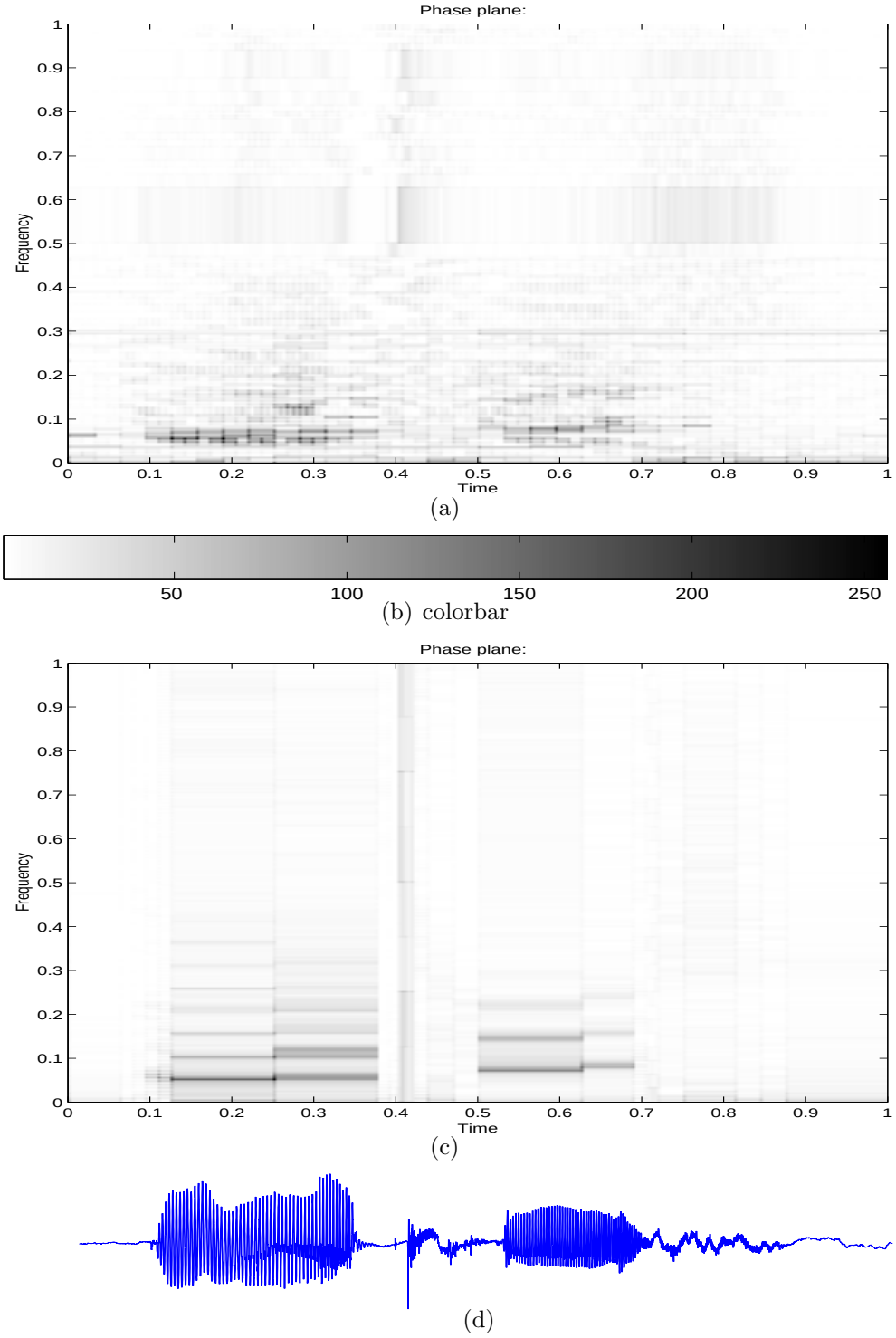

Fig. 6.2: Wavelet Packets (WP), (a), vs. Cosine Packets (CP), (c), for the phrase [notruːf] pronounced by a female speaker. Waveform is shown in Subfigure (d). The Level goes up to $D = 12$ and the cost function was chosen as $\|\cdot\|_{\ell^p}$, $p = 0.01$. Both, time and frequency axes are normalised such that they range from zero to one.

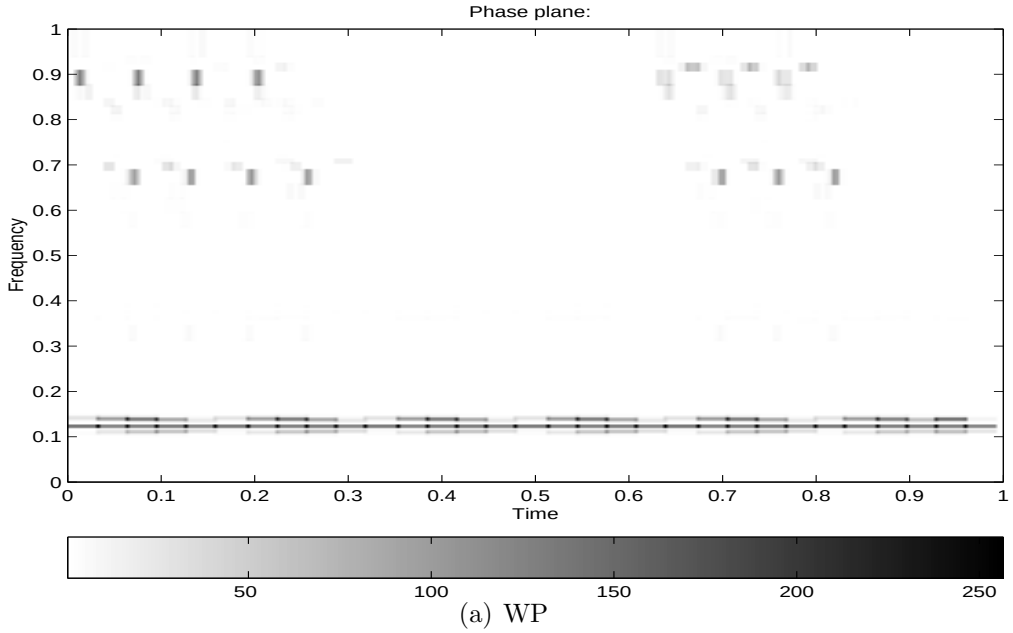

(a) WP

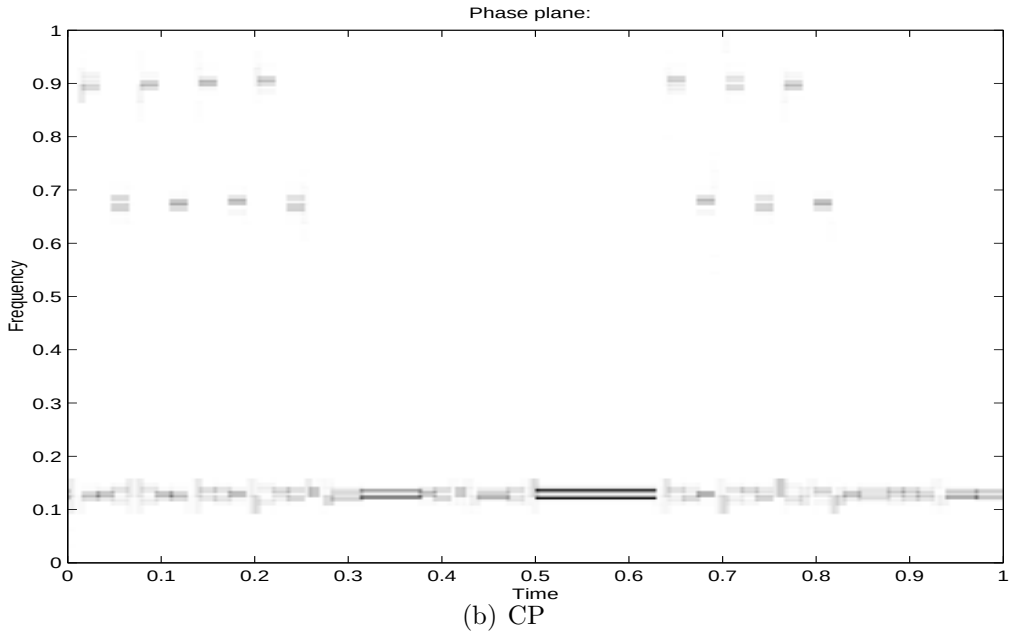

(b) CP

Fig. 6.3: Wavelet and cosine packet transform of the same signal as presented in Figures 4.16 and 4.17. Decomposition level is $D = 8$ whereas cost function in (a) is *entropy* and in (b) the ℓ^p norm with $p = 0.1$.

'Entropy': That particular cost functional measures the 'flatness' of the signal's energy distribution and minimisation of former leads to a coordinate system in which the presentation is optimal in the sense of compression. This cost functional achieve a concentration in the phase plane to only few coefficients of considerable high value. Setting the remaining coefficients to zero yields then a smoothing of the data and compress the signal on the side.

Such an ansatz may not necessarily lead to high classification rates. Although only a small fraction of signal's energy is 'lost' by a thresholding process– which is important for dimension reduction, cf. Eq. (6.1c) – the extracted features may be useless.

In speech, see Chapter 2, it is known that formants and especially their path in the phase plane may reveal the nature of a special phone. In particular, it is possible to distinguish between (voiced) phones only by looking at their formants.

In order to obtain a kind of parametrisation of a particular path it is crucial to find a well balanced trade-off between the resolutions in the two spaces (time & frequency, respectively).

In general, the entropy cost functional achieves a too good frequency resolution at the expense of accuracy in time such that any attempt of classification (by considering the formant's path) fails due to a worse parametrisation. Compare for instance the phase plots in Figure 6.5 (a), with Figure 6.6, (a) or (b), from which is obvious that the latter has a superior partition ability (for parametrisation purpose) over the former.

'ℓ^p': $\sum_i |x_i|^p$, $0 < p < 2$; Several experiments with different words and exponents show that only high energetic with high frequency parts are decomposed into finer time intervals. Noise-like parts with high frequencies and less energy are merged as much as possible. Voiced segments with almost constant spectra are not further subdivided.

The higher $p < 2$ was chosen the more the partition in time resembled that one obtained via the entropy cost, cf. Figures 6.6 and 6.10. For small $0 < p \leqslant \frac{1}{10}$ it behaved similar to the log-cost, $\sum_i \log(|x_i|)$.

In Figures 6.12, 6.13, 6.14, 6.15 and 6.16 the similarity and difference between the two cost functionals 'entropy' and ℓ^p, $p = 0.1$, $p = 1.6$, is showed for ten different words spoken by a male. These plots emphasise once again that the 'entropy' cost is not always a 'good' criterion

in order to obtain a phase plane tiling from which one could extract features – such as a kind of path of formants.

'Risk': $\sum_i \min(x_i^2, p^2)$; For p near 0.1 there is a kind of zoom-in for low-energetic and high-frequent intervals. Voiced like parts are rather kept large, see Figure 6.7 and Figure 6.11 For p being near the coefficients' maximum the best basis algorithm tiles the time frequency plane similar as with the $\sum$-cost, $\sum_i x_i$. In that case the tiling has too much emphasis on the time partition which is also not necessarily effective, cf. Figures 6.5 and 6.9, (c).

'$N(p)$': $\left|\{x \,\middle|\, |x| \geqslant p\}\right|$, $0 < p \leqslant 2$; As p increases the tiling-nature change abruptly from very fine time partition to very coarse time resolution and back, see Figure 6.4 and Figure 6.8. It is clear that this is only based on the threshold p but still it is not obvious to the author how to predict that kind of behaviour.

These 'findings' are typical for all the other words in the data set, i.e. very analogous conclusions are drawn from studies on words and speakers not presented here.

Motivated by these results, the ℓ^p cost functional with parameter $0.1 \leqslant p \leqslant 0.2$ is considered to be more or less suitable to partition the phase plane such that short bursts (interval of relatively high variance in frequency of short duration with non-negligible energy) are well localised in time whereas voiced parts have a good frequency resolution.

6.4 Extraction of Features

The so obtained 'best basis' representation is used to extract n, $n \in \mathbb{N}$, centre of frequencies and the pertinent energies of each time interval such that each utterance of 2^{13} samples is mapped to a sequence of approximately sixty $n \times 2$ matrices.

The number of matrices depends on the maximal tree depth and on the particular cost functional. Since the signal is represented in the local cosine packet basis the extraction of these $2n$ features, centre of frequencies plus energies, is easily obtained.

6.4.1 Formants & Cosine Packets

Remember the notation of Section 5.2 and the results obtained there, Theorem 5.2.7 and Corollary 5.2.11. Without loss of generality the author restricts

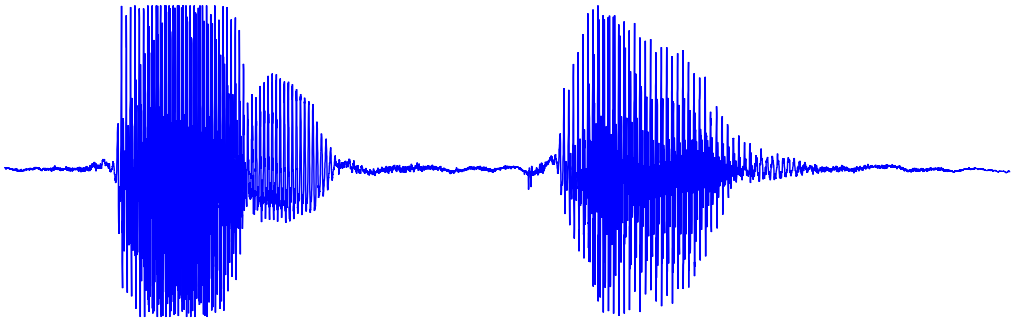

(a) speech signal: ['fɛnstər], female speaker

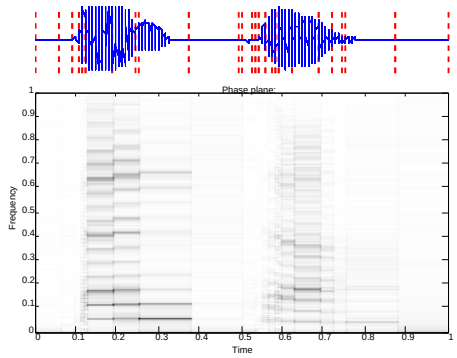

(b) $p = 0.1$

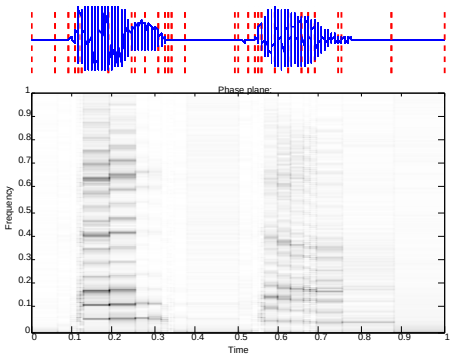

(c) $p = 0.2$

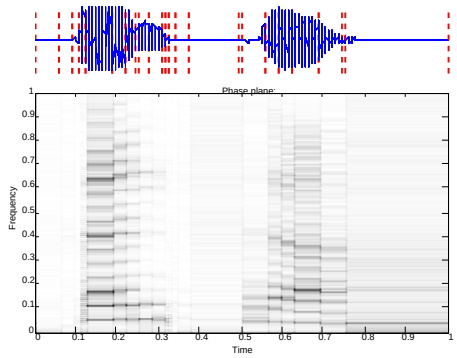

(d) $p = 0.4$

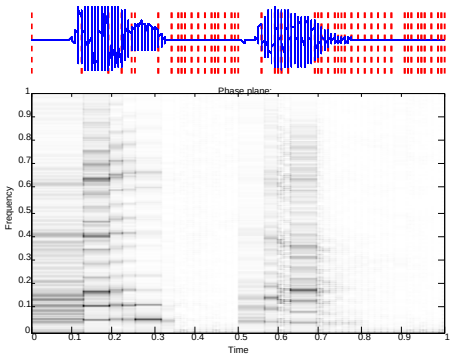

(e) $p = 0.6$

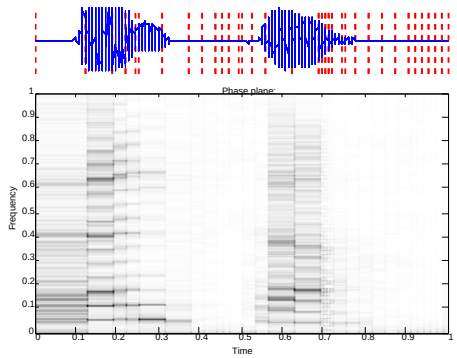

(f) $p = 0.8$

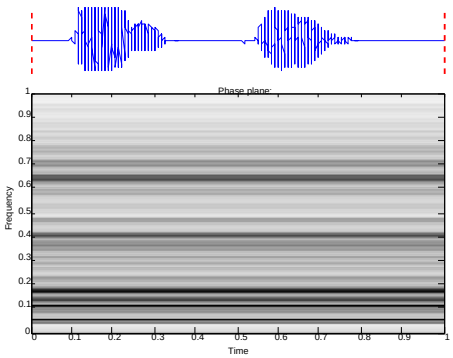

(g) $p = 1.4$

Fig. 6.4: '$N(p)$' cost functional; ['fɛnstər], female speaker

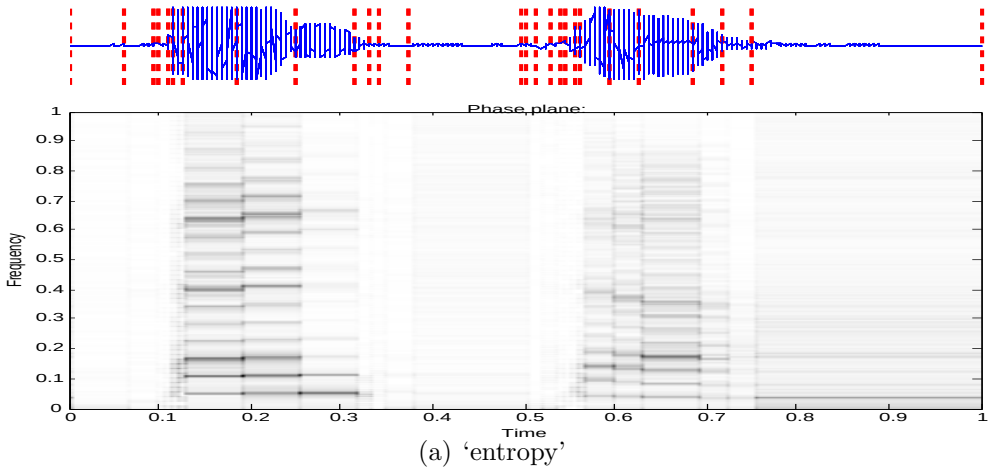

(a) 'entropy'

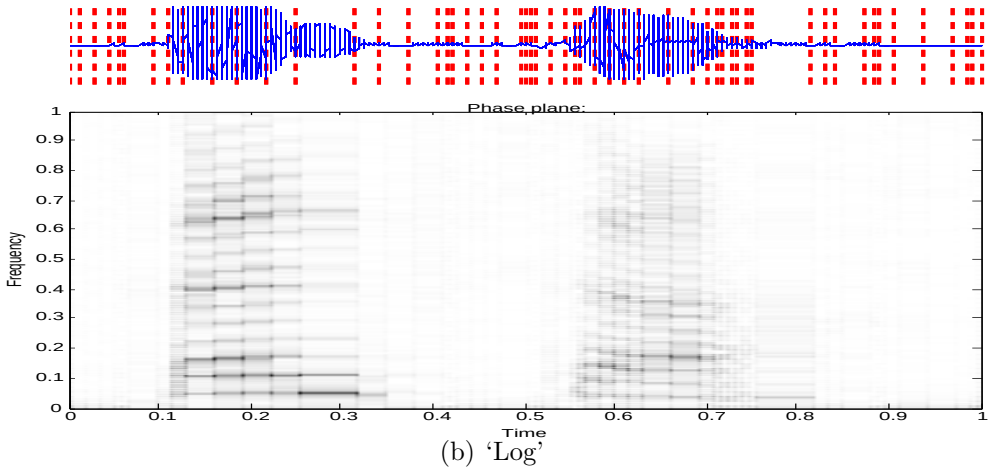

(b) 'Log'

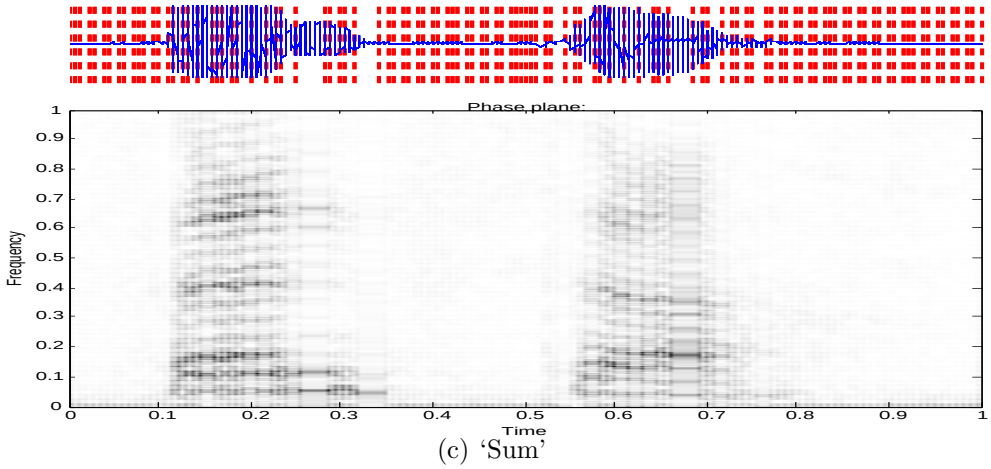

(c) 'Sum'

Fig. 6.5: cost functionals without extra parameter; ['fɛnstər], female speaker

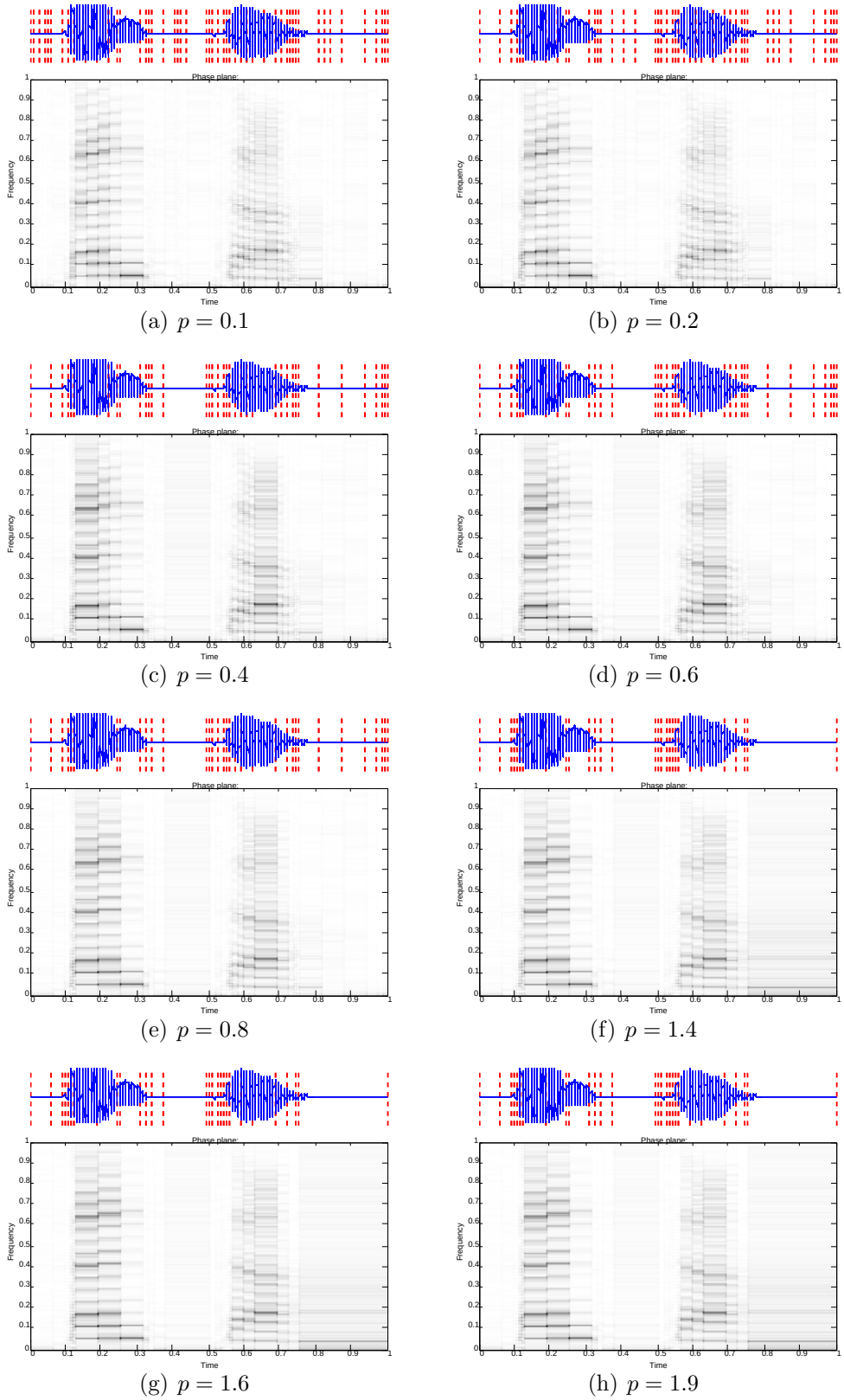

(a) $p = 0.1$ (b) $p = 0.2$

(c) $p = 0.4$ (d) $p = 0.6$

(e) $p = 0.8$ (f) $p = 1.4$

(g) $p = 1.6$ (h) $p = 1.9$

Fig. 6.6: 'ℓ^p' cost functional; ['fɛnstər], female speaker

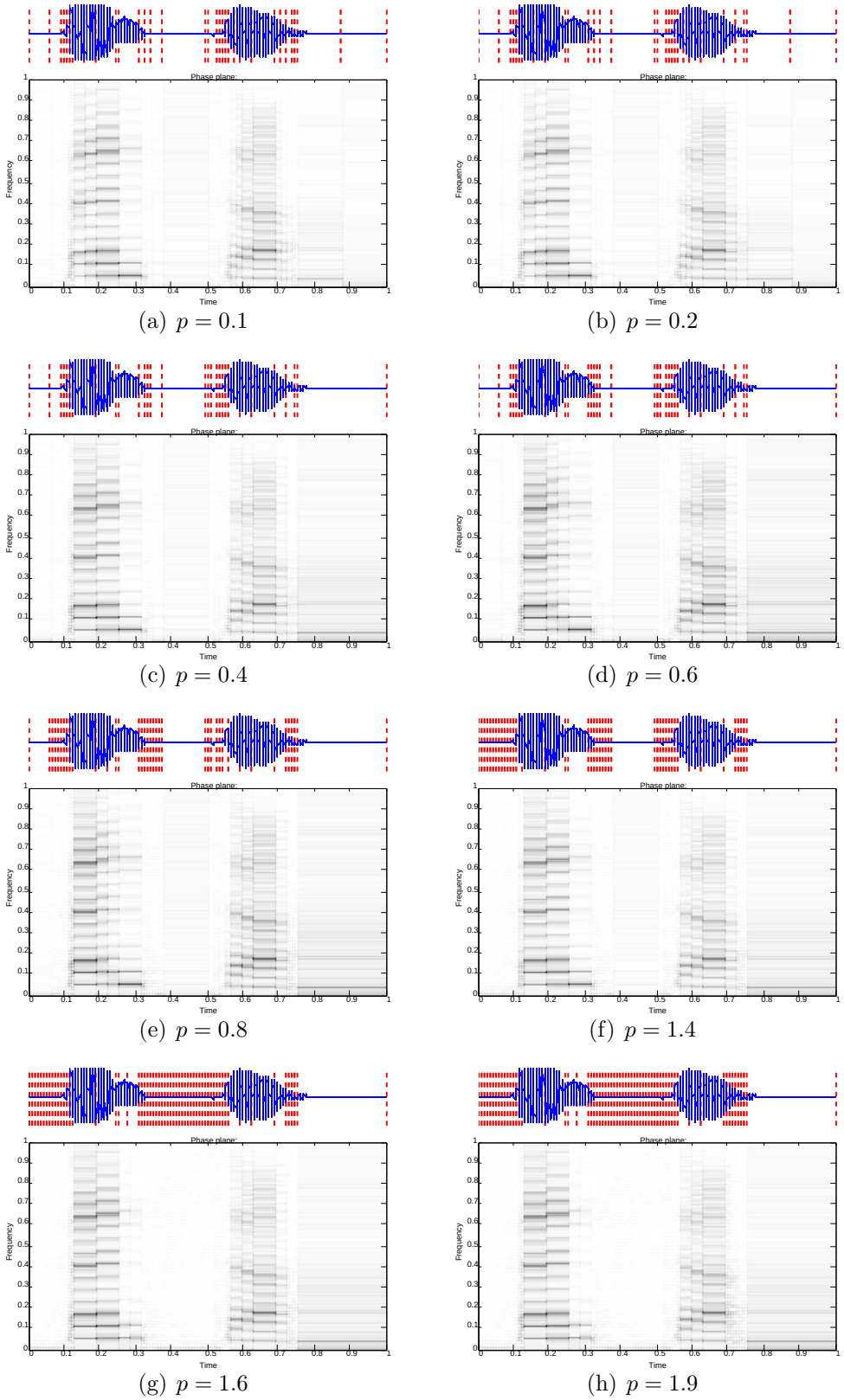

(a) $p = 0.1$ (b) $p = 0.2$

(c) $p = 0.4$ (d) $p = 0.6$

(e) $p = 0.8$ (f) $p = 1.4$

(g) $p = 1.6$ (h) $p = 1.9$

Fig. 6.7: 'Risk' cost functional; ['fɛnstər], female speaker

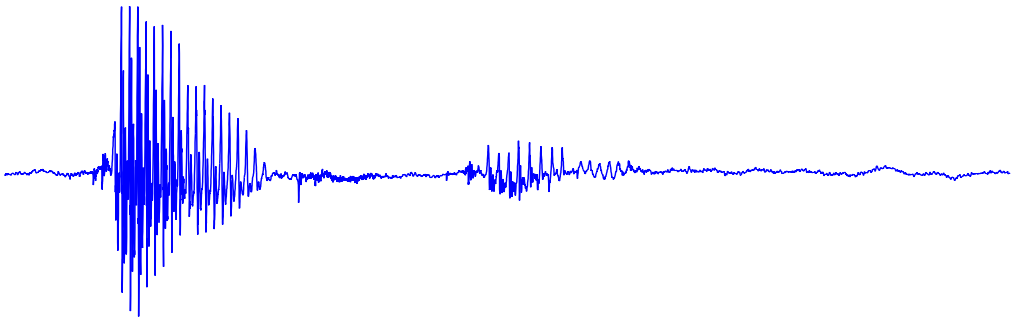

(a) speech signal: ['fɛnstər], male speaker

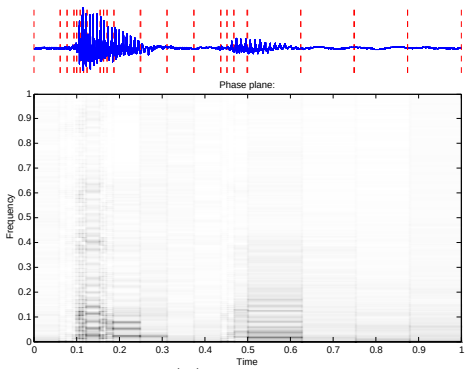

(b) $p = 0.1$

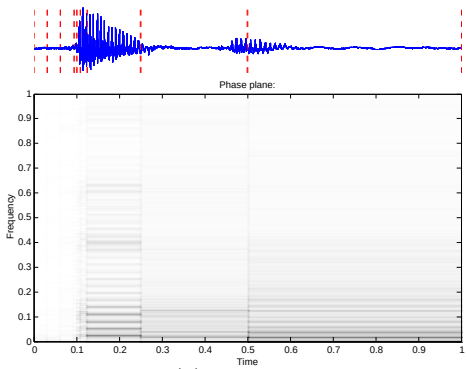

(c) $p = 0.2$

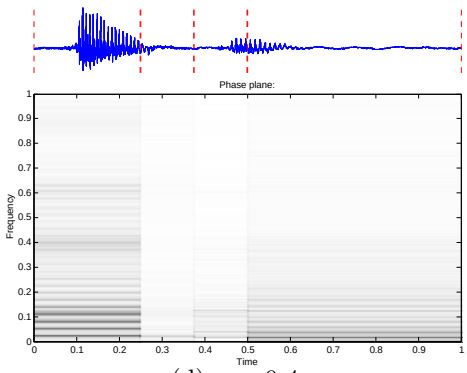

(d) $p = 0.4$

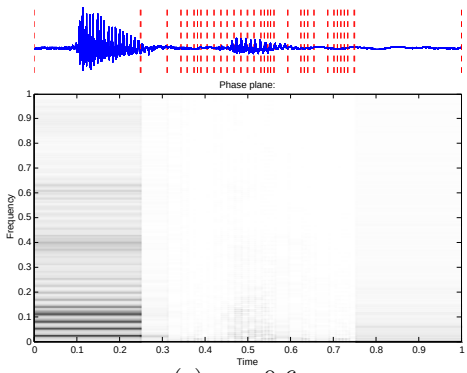

(e) $p = 0.6$

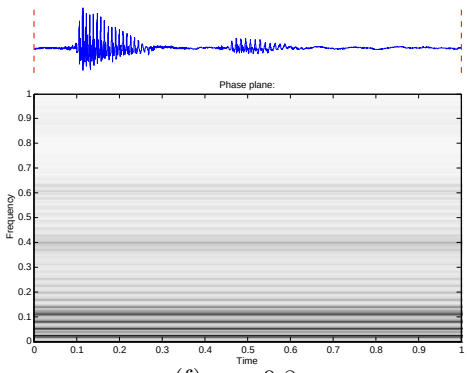

(f) $p = 0.8$

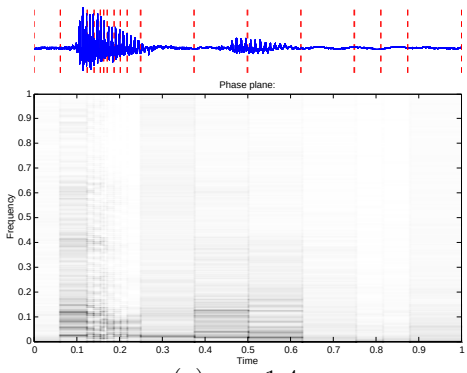

(g) $p = 1.4$

Fig. 6.8: '$N(p)$' cost functional; ['fɛnstər], male speaker

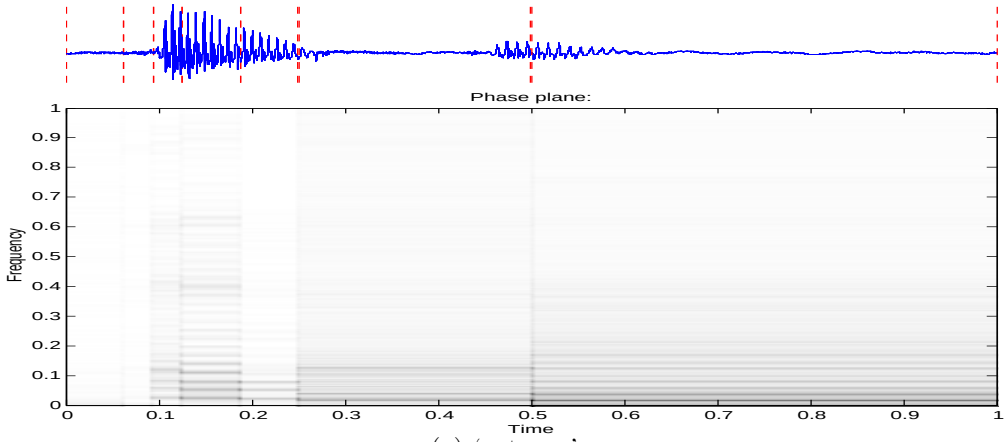

(a) ‘entropy’

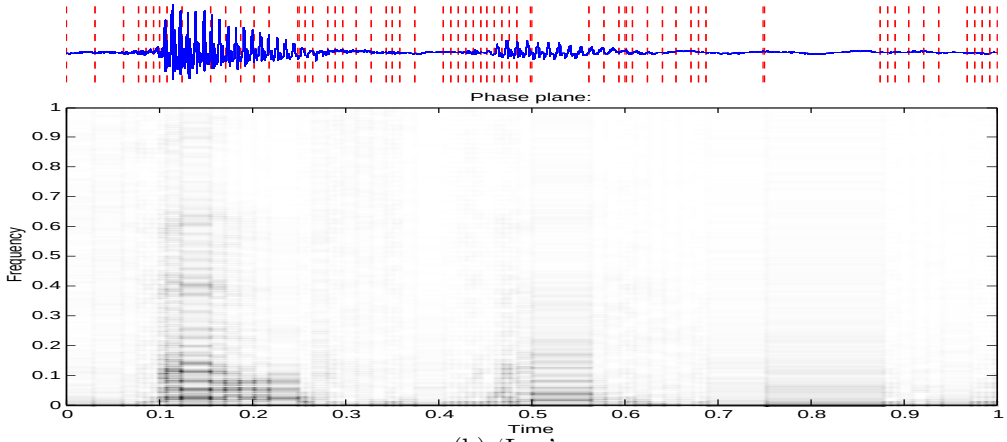

(b) ‘Log’

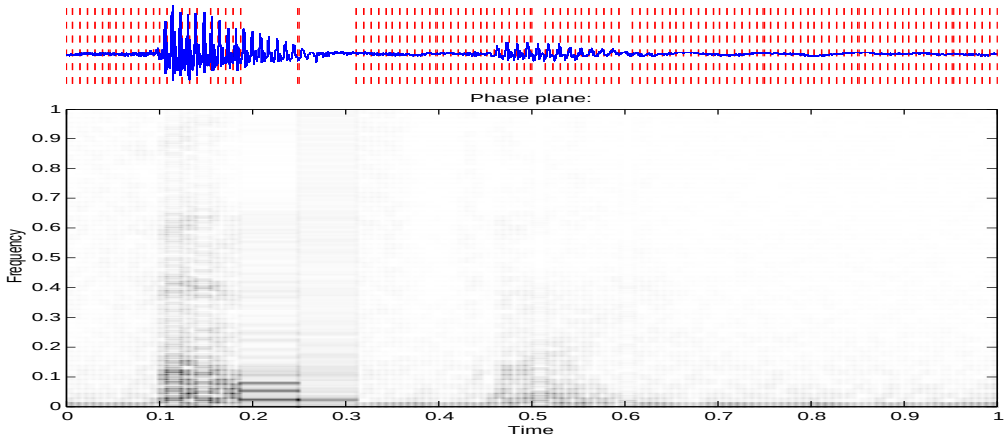

(c) ‘Sum’

Fig. 6.9: cost functionals without extra parameter; [ˈfɛnstər], male speaker

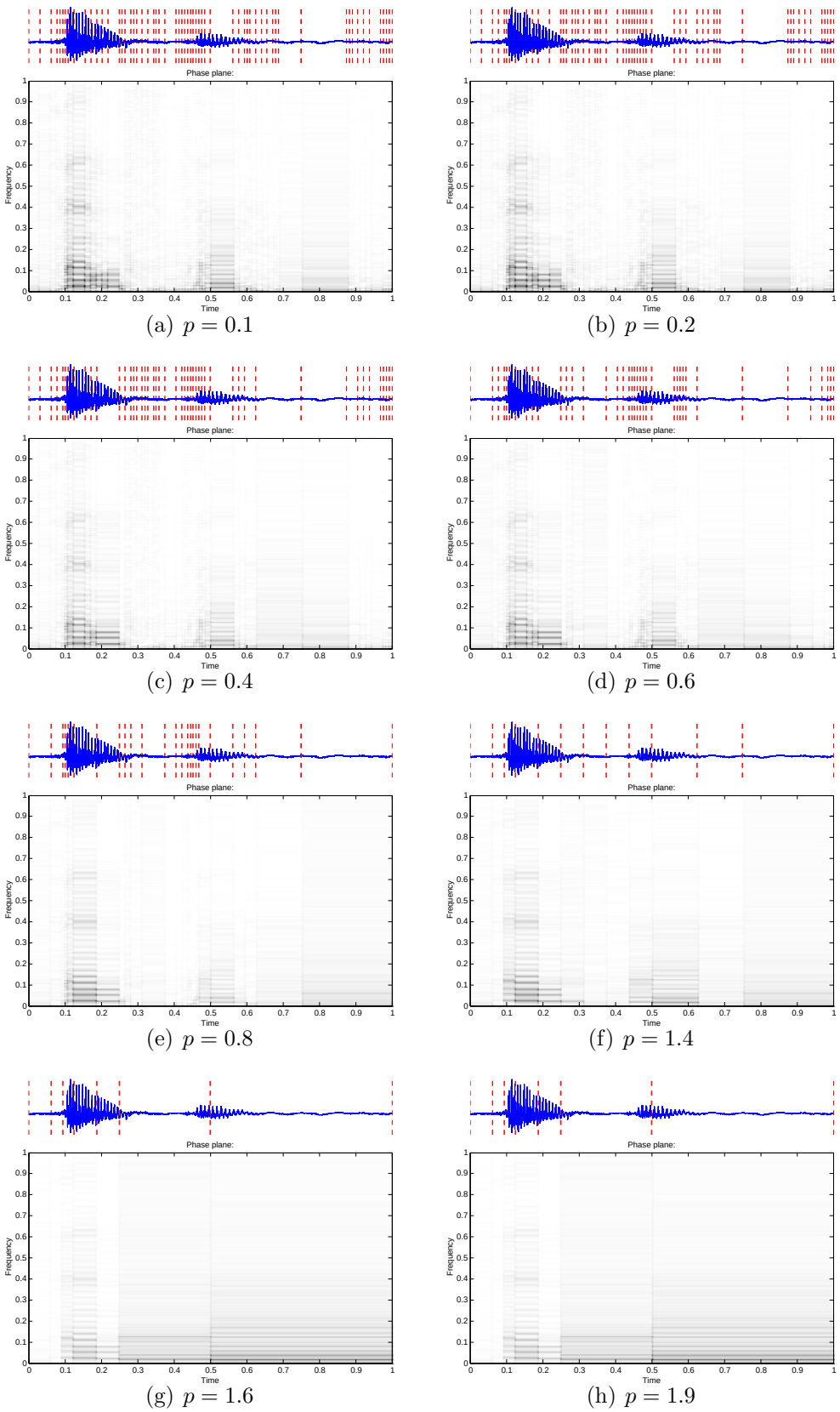

(a) $p = 0.1$ (b) $p = 0.2$

(c) $p = 0.4$ (d) $p = 0.6$

(e) $p = 0.8$ (f) $p = 1.4$

(g) $p = 1.6$ (h) $p = 1.9$

Fig. 6.10: 'ℓ^p' cost functional; ['fɛnstər], male speaker

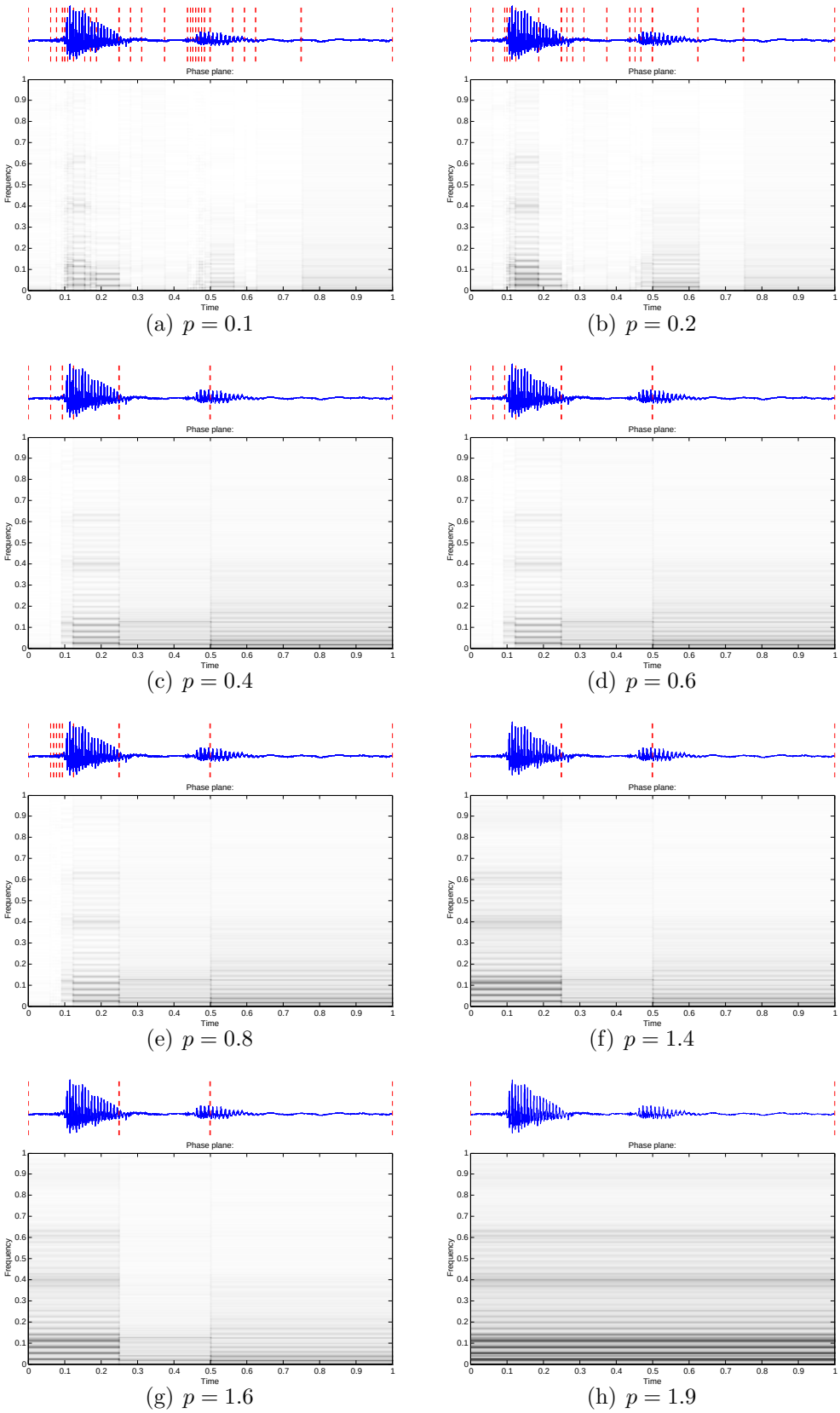

(a) $p = 0.1$ (b) $p = 0.2$

(c) $p = 0.4$ (d) $p = 0.6$

(e) $p = 0.8$ (f) $p = 1.4$

(g) $p = 1.6$ (h) $p = 1.9$

Fig. 6.11: 'Risk' cost functional; ['fɛnstər], male speaker

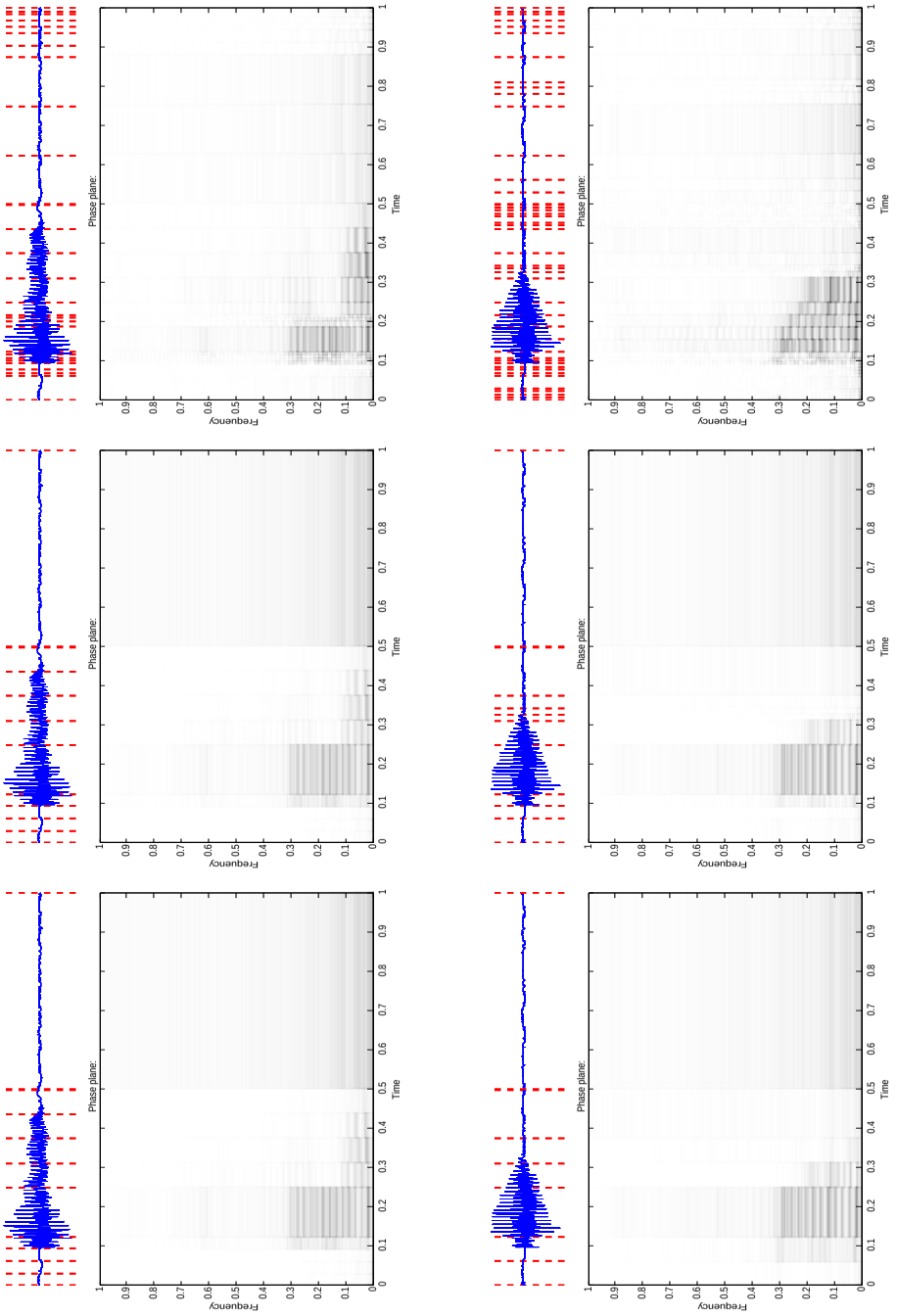

(a) [an] (b) [ˈauf]

Fig. 6.12: from top to bottom: ℓ^p, $p = 0.1$, $p = 1.6$, 'entropy'

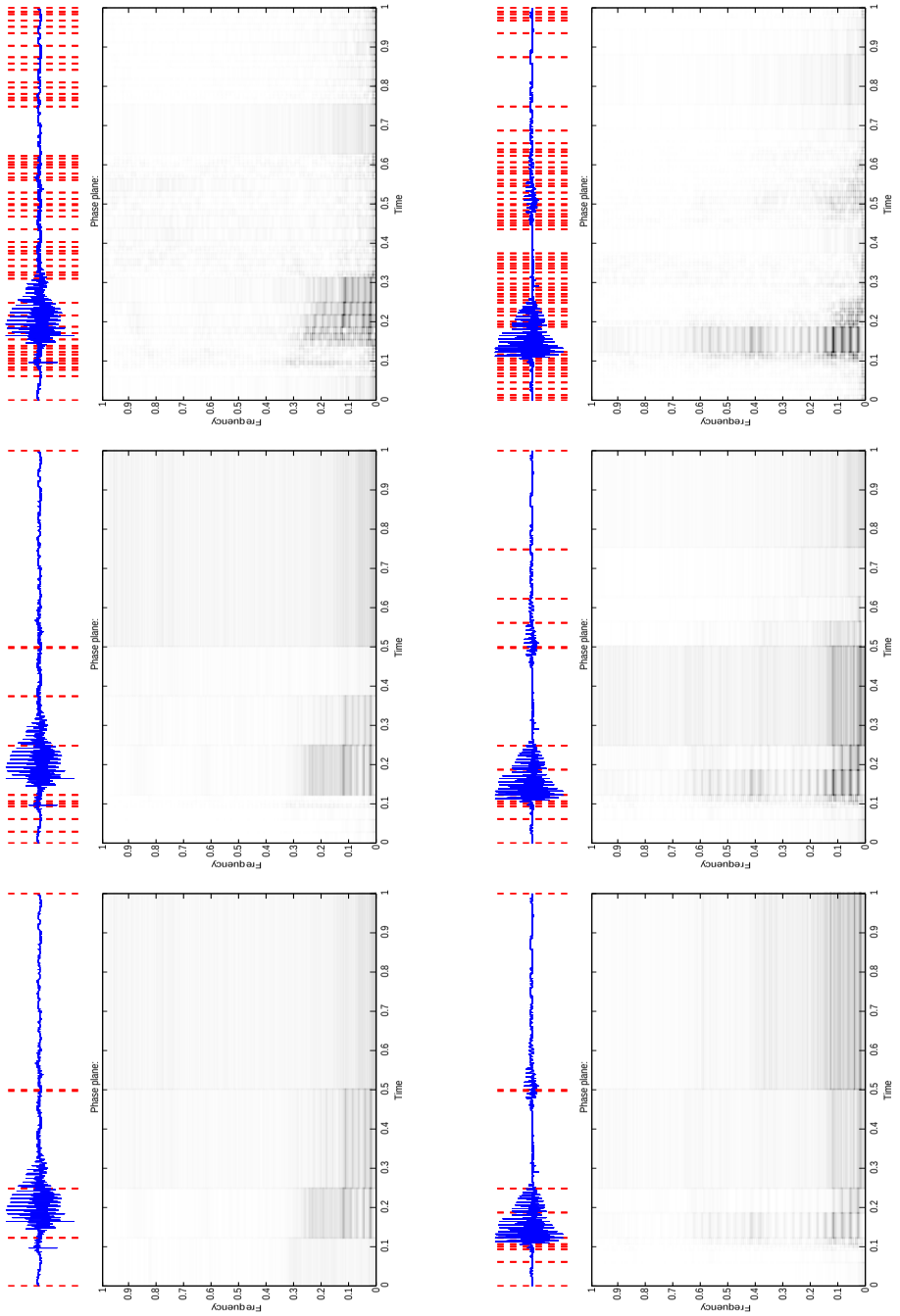

(a) ['aus] (b) ['fɛnstər]

Fig. 6.13: from top to bottom : ℓ^p, $p = 0.1$, $p = 1.6$, 'entropy'

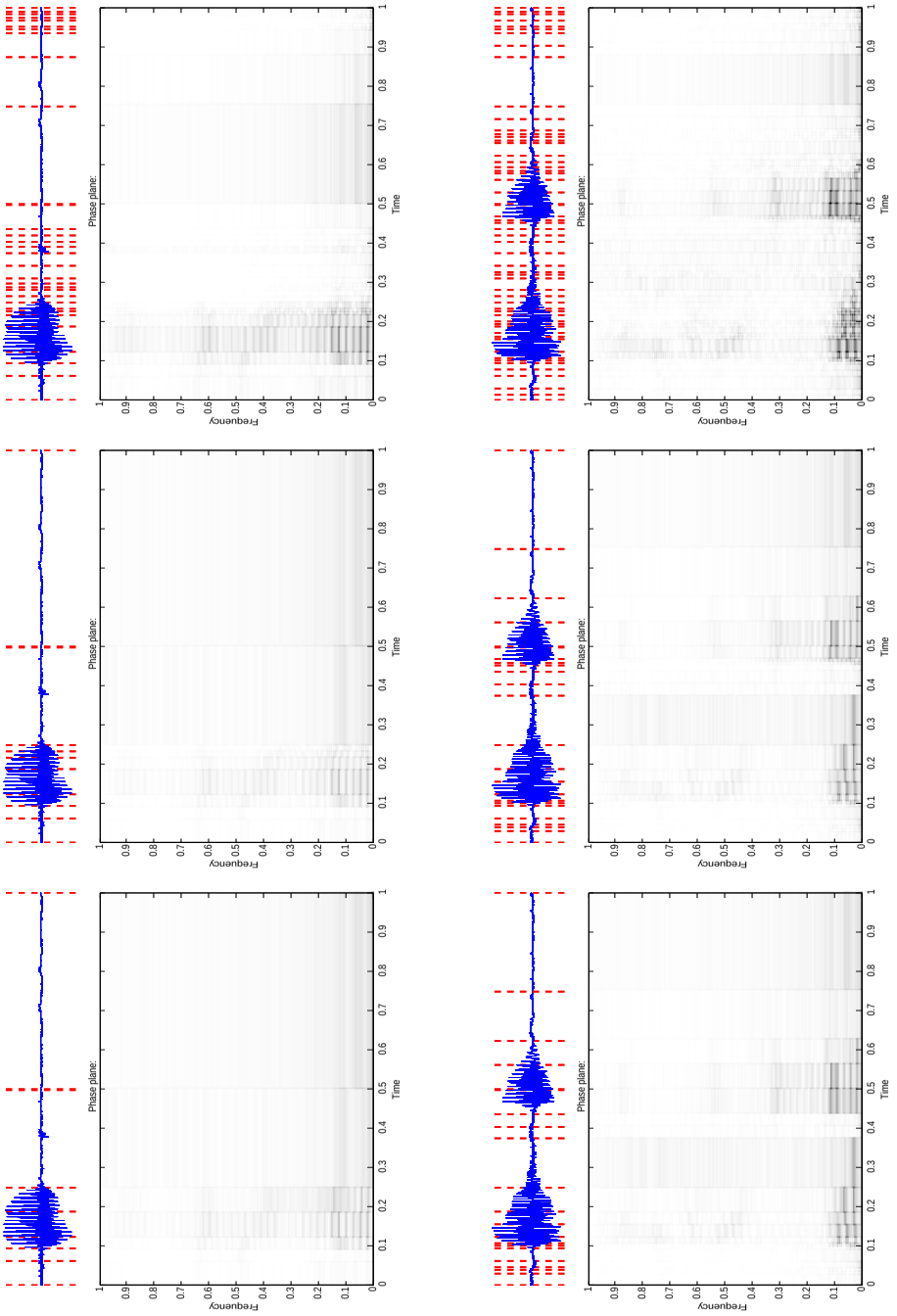

(a) [heːrt] (b) [ˈhilfə]

Fig. 6.14: from top to bottom : ℓ^p, $p = 0.1$, $p = 1.6$, 'entropy'

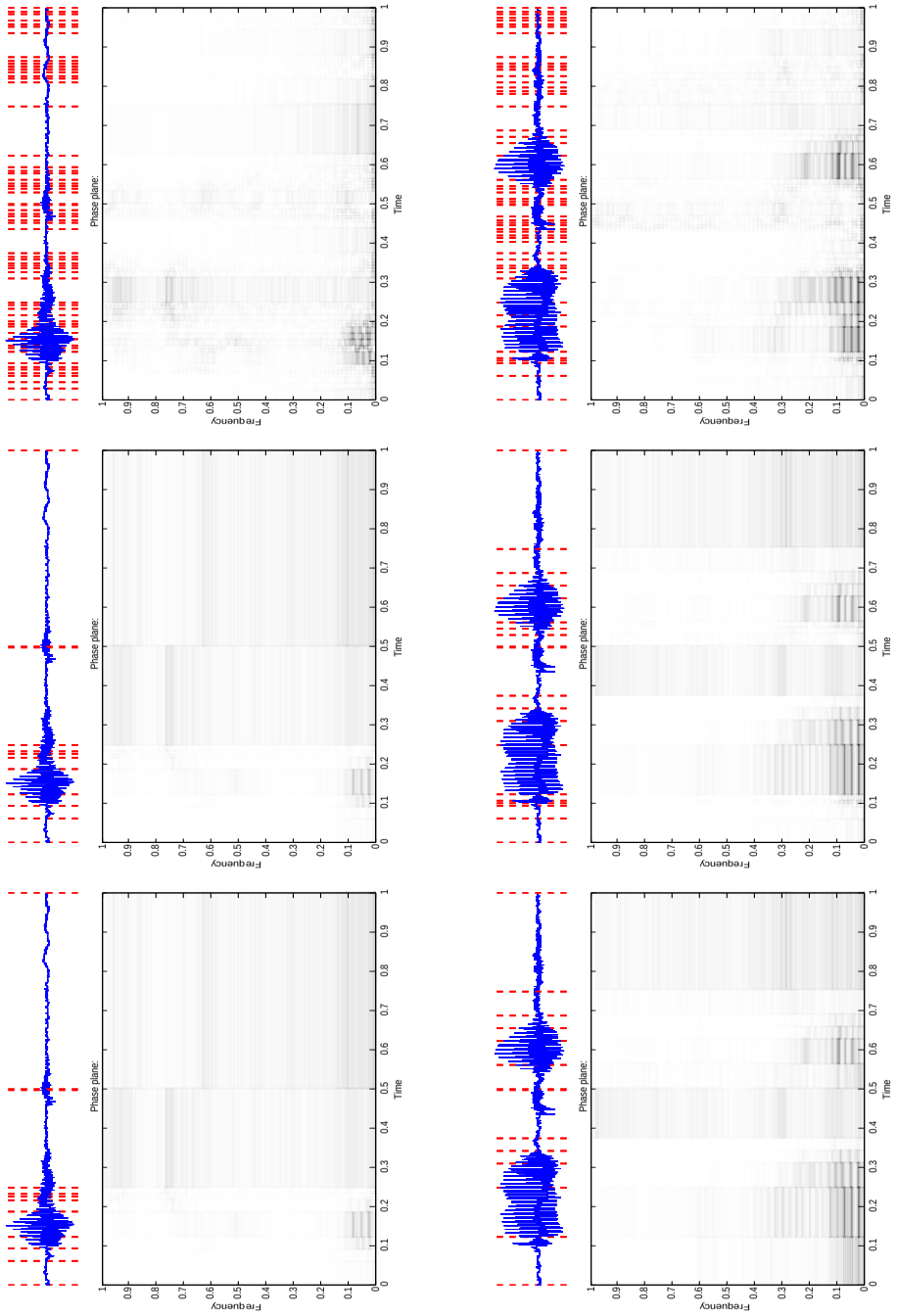

(a) [liçt] (b) [ˈnoːtruːf]

Fig. 6.15: from top to bottom : ℓ^p, $p = 0.1$, $p = 1.6$, 'entropy'

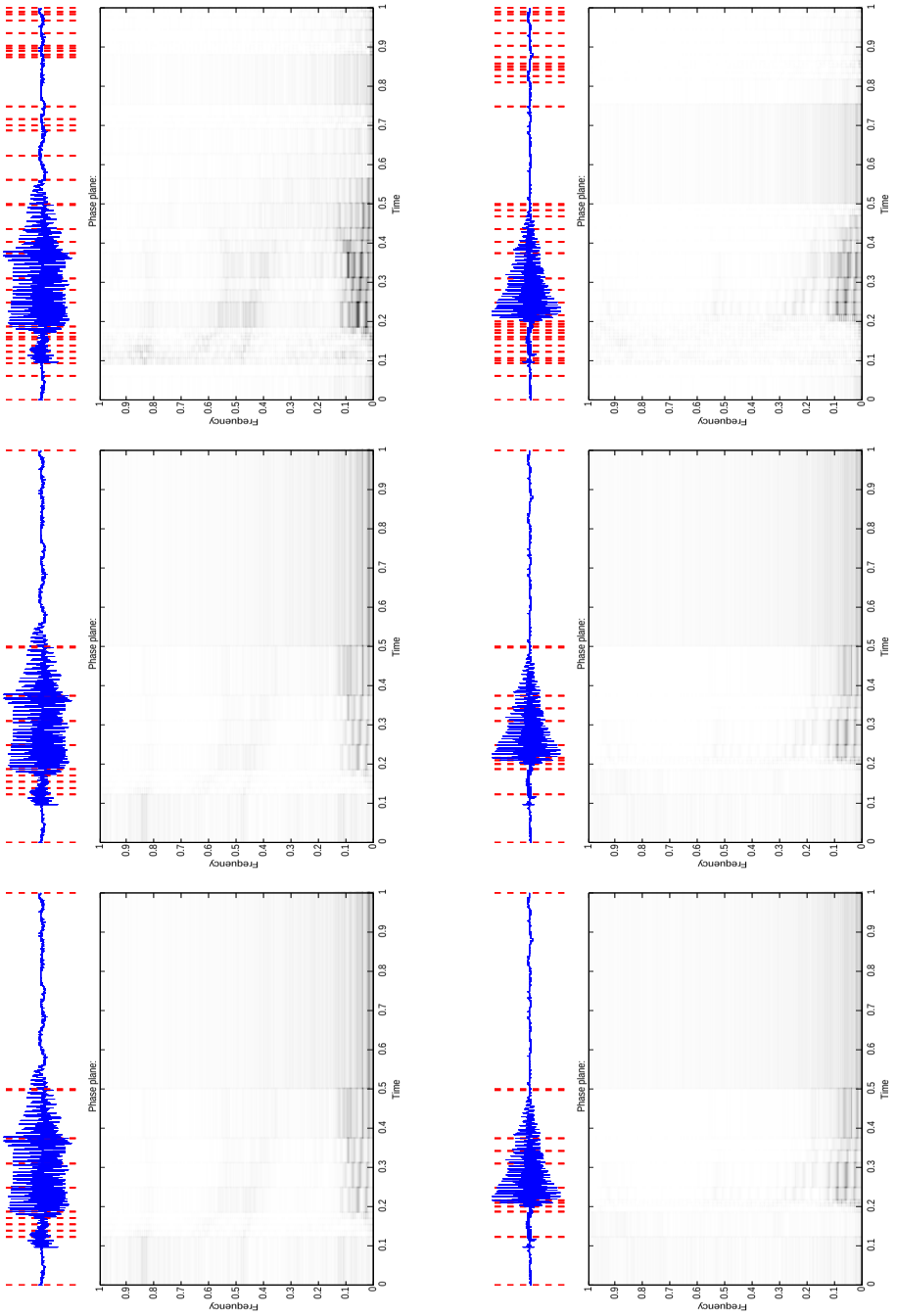

(a) [tyːr] (b) [ˈtsuːr]

Fig. 6.16: from top to bottom : ℓ^p, $p = 0.1$, $p = 1.6$, 'entropy'

$T_{j,k}$ to the so-called DCT-IV basis, i.e.

$$T_{j,k}(n) := t_{j,k}(n+\tfrac{1}{2}) := \sqrt{\frac{2}{h_j}}\cos\Big(\big(k+\frac{1}{2}\big)\pi\big(\frac{n-a_j}{h_j}\big)\Big) \text{ where } h_j = a_{j+1}-a_j$$

and $(a_j)_{j\leqslant J}$ is an admissible dyadic partition of the time interval $[0,T]$ at a fixed level l, i.e. $a_j := a_{j,l} := jT2^{-l}$, such that $[0,T) = \cup_{0\leqslant j<J}[a_{j,l}, a_{j+1,l})$. Here, $n \in [\![1, 2^{13}]\!]$ and J is proportional to the level l of the tree, $J = 2^l \leqslant 2^d$ if d, $0 < l \leqslant d < 13$, denotes the maximal tree depth.

Moreover, let the window fuction be given as in Lemma 5.2.4 with f_ϵ as in Eq. (5.9) with $\epsilon = 1$, and $\nu_S = 8$ kHz, denoting the sampling frequeny, i.e.

$$W_j(n) := w_j(n+\tfrac{1}{2}) = \begin{cases} \sin\vartheta\Big(\frac{n+\frac{1}{2}-A_j}{r}\Big), & n \in [\![A_j-\delta, A_j+\delta]\!] \\ 1, & n \in [\![A_j+\delta+1, A_{j+1}-\delta-1]\!] \\ \sin\vartheta\Big(A_{j+1}-\frac{n+\frac{1}{2}}{r}\Big), & n \in [\![A_{j+1}-\delta, A_{j+1}+\delta]\!] \\ 0, & \text{else} \end{cases}$$

$$\text{where } \vartheta(x) := \frac{\pi}{4}\Big(1+\sin\big(\frac{\pi}{2}x\big)\Big),\ A_j := \frac{a_j}{\nu_S} = \frac{jT2^{-l}}{\nu_S},\ \delta := \frac{A_{j+1}-A_j}{2}.$$

Due to Eqs. (5.15) (a) and (b), decomposition of a signal $f \in \ell^2([\![1, 2^{13}]\!])$ is then obtained by first folding the signal at the points A_j, $0 \leqslant j < J$, with cut-off function given by ϑ, $f \mapsto f_j := U_j f$, for U_j as in Corollary 5.2.6, and then compute for each folded part, f_j, the discrete cosine transform (DCT-IV), as e.g. in [Mal98, pp. 347], $cos_{j,k} := \langle f_j, T_{j,k}\rangle$ for $k \in [\![0, s_j - 1]\!]$ if s_j denotes the number of integers (samples) in the interval $[\![A_j, A_{j+1}-1]\!]$.

A best basis algorithm prunes the so obtained tree (of spectral coefficients $cos_{j,k}$) and achieves an adapted basis (or analogously in the case of local trigonometric packets: adapted time partition) w.r.t. a cost functional with $\tilde{J} \leqslant 2^d$ terminal nodes. For convenience, let the adapted time partition be symbolised by the sequence $(a_j)_{j\leqslant\tilde{J}}$, cf. Figure 6.17, (a).

Actually, since all the DCT-IV coefficients are computed beforehand, the best basis procedure shows which of them contain the most suitable spectral information (of course w.r.t. a cost functional).

Each of the scalar product coefficients, $cos_{j,k}$, can be associated to a frequency, $\nu_k = \frac{\omega_k}{2\pi} = \frac{k+\frac{1}{2}}{2h_j}$ where ω_k is the angular frequency of $T_{j,k}$, $\omega_k := \frac{\pi}{h_j}(k+\frac{1}{2})$.

Due to the sampling theorem, the top frequency, i.e. the maximal distinguishable frequency is half of the sampling rate in each interval and since the sampling is uniform, each interval has approximately the same number of

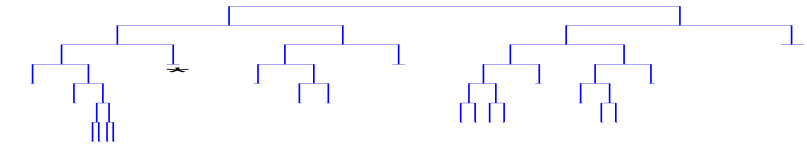

(a) 'basis tree' of the utterance [no:tru:f]

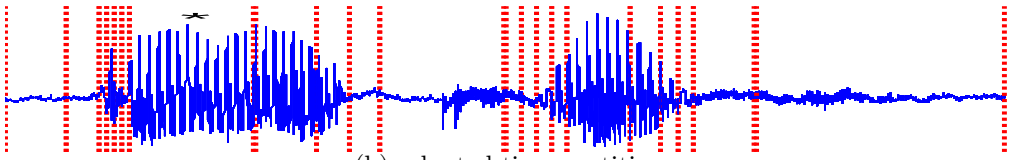

(b) adapted time partition

Fig. 6.17: The Best basis (w.r.t. '$N(p)$', $p = 0.1$) is obtained from the lowest nodes, so-called *terminal* nodes of the tree in Subfigure (a). Here $\tilde{J} = 21$ – in contrast to the number of maximal nodes at level $d = 7$, $J = 2^7 = 128$. Lower subplot shows the waveform of the utterance [no:tru:f] and the adapted time partition, $(a_j)_{j \leqslant 21}$, visualised by red dashed vertical lines. The feature matrix M_7 is illustrated by a star in both, (a) and (b).

samples which imply an almost constant sampling frequency of 8kHz; hence $\nu_k \leqslant 4\text{kHz}$.

The maximal tree depth was set to $d = 7$ which yielded a time subinterval of minimal $2^{13-d} = 64$ samples or $\frac{64}{8000} = 8$ ms.

Intuitive features are the i-th strongest spectral components, c_{k_i}, in each cosine packet $(cos_{j,k})_{k \in [\![0, s_j - 1]\!]}$,

$$c_{k_i} := \left\{ \max_{0 \leqslant k < s_j} |cos_{j,k}| \;\middle|\; |k_i - k_{i-1}| \geqslant \tau > 0 \right\}, \quad i \geqslant 2,$$
$$\text{with } c_{k_1} := \max_{0 \leqslant k < s_j} |cos_{j,k}|.$$

So, the proceeding is as follows: compute the strongest spectral component, c_{k_1} and suppress in a neighbourhood of k_1 all the other peaks in the spectrum, for instance by setting $cos_{j,k} = 0$ for $|k - k_1| < \tau$. Look then at the strongest survivor, c_{k_1}, of such a thresholding and set again in a neighbourhood of that one, $|k - k_1| < \tau$, the spectral coefficients to zero. Iterate as long as there are non-zero coefficients, $cos_{j,k} \neq 0$, for $k < s_j$, or until $i = I$ for some $I \in \mathbb{N}$.

A more sophisticated approach is to use the extra information contained in the coefficients $cos_{j,k}$ for $|k - k_i| < \tau$ which, for instance, can be exploited to compute the energy E_i in each neighbourhood and the corresponding centred

frequency μ_i,

$$E_i := \sum_{|k-k_i|<\tau} cos^2_{j,k} \qquad \mu_i := E_i^{-1} \sum_{|k-k_i|<\tau} k \cdot cos^2_{j,k}. \tag{6.2}$$

The author restricted the number of extracted frequencies and energies to $I = 10$. The neighbourhood, $[\![k-\tau, k+\tau]\!]$, is set adaptively such that for a fixed $j \in \mathbb{N}, \alpha \in \mathbb{R}$ and for each $\kappa \in [\![k, k+\tau_0]\!]$, $\tau = \alpha\tau_0$, it holds $|cos_{j,\kappa}| > \frac{|c_{k_i} - \text{mean}(cos_{j,k})|}{100}$.

It was observed that artificial enlargement of the neighbourhood, accomplished by $\tau = \alpha\tau_0$, yields a better matching of μ_i with the actual peaks of the spectrum. Compare Figure 6.18 where the proceedings of such an algorithm are visualised. Here the enlargement constant, α, is set to $\alpha = 20$. The plotted DCT-IV transform of a signal, here [no:tru:f], is typical for all voiced utterances. The three biggest peaks correspond to frequencies $108, 215$ and 318 Hz. The first two peaks may be just a consequence of the glotteral excitation. For instance, the fundamental frequency approximately ranges for a male speaker from 100 to 150 Hz and for a female from $140-250$ Hz. Therefore, it is possible to separate voiced from voiceless excitation using relatively easy criteria; any voiceless excitation cannot have high energetic frequencies below a particular frequency threshold ν_V. Setting $\nu_V = 250$ Hz it follows then that c_{k_1} must be below ν_V if the corresponding speech segment is voiced and unvoiced if $c_{k_1} \geqslant \nu_V$. Using the *rule of three* the former considerations (since 4 kHz $\approx \frac{s_j+\frac{1}{2}}{2h_j} \Rightarrow 250$ Hz $\approx \frac{s_j}{16}$) simplify to an easy to check condition: $k_1 < \frac{s_j}{16}$ iff the speech segment is voiced.

Since the local trigonometric packets constitute an orthonormal basis, which implies in particular the conservation of energy, i.e. for any admissible sequence $(b_j)_j \leqslant J$ and especially for $(a_j)_{j \leqslant \tilde{J}}$ it holds

$$\|f\|^2 = \sum_{j \leqslant J, k < s_j} |cos_{j,k}|^2.$$

In that context, it may be of some interest to note that with only these ten extracted energies pertinent to the ten centred frequencies almost three quarter of the norm $\|f\|$ is captured, cf. Figure 6.19 and the continued argumentations.

A representative result of the formant extraction algorithm applied to the DCT-IV transform visualised in Figure 6.18, is the matrix M_7,

$$M_7 := \begin{pmatrix} 1251.3 & 451.6 & 362.3 & 52.8 & 525.6 & 417.8 & 11.0 & 318.0 & 214.6 & 107.8 \\ 0.0150 & 0.0727 & 0.0825 & 0.0878 & 0.2651 & 0.3325 & 2.7202 & 3.4167 & 4.4534 & 9.7558 \end{pmatrix}^{\mathrm{T}},$$

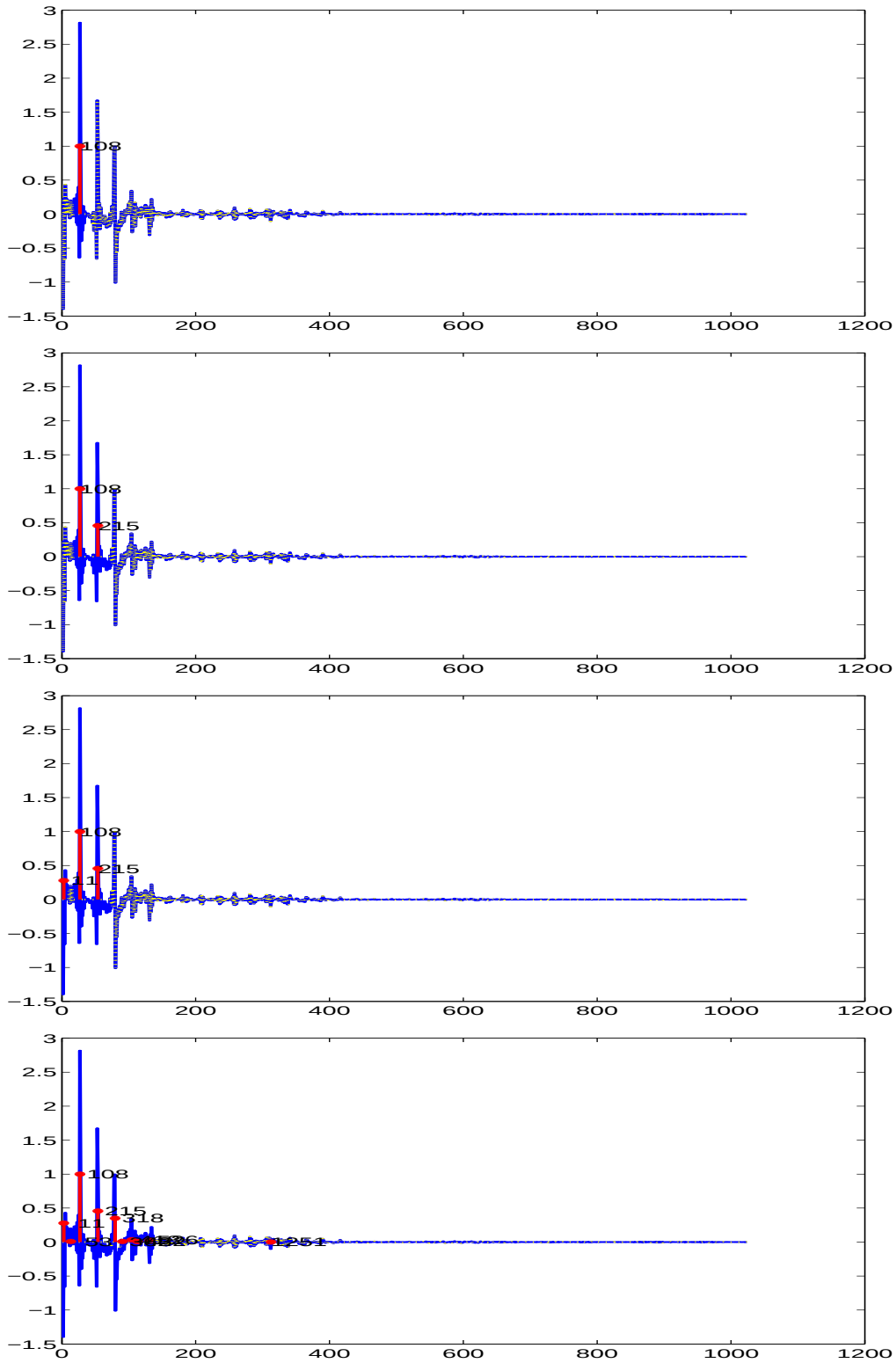

Fig. 6.18: Extraction of features from a DCT-IV transform of a signal: centre of frequency and pertinent squared energy; from top to bottom: first, second, third and tenth strongest 'survivor', $c_{k_{i=1,2,3,10}}$; In particular, visualised are the coefficients, $cos_{j,k}$, of the di-phone [no] extracted from the male-spoken [no:tru:f], where k goes from zero to 1024 as outlined by the x-axis (abscissa) and j is set to $j = 3$.

which is associated to the time interval $[a_{12}, a_{13}) = [128, 256)$ ms corresponding to the discrete analogous set $[\![1025, 2048]\!]$ samples, cf. Figure 6.17.

The first column stores the ten most energetic frequencies (in Hertz) whereas the second column contains the associated energies in an increasing order. Henceforth, the elements of a feature matrix M_j, $j \in \mathbb{N}$, are called *feature coefficients* and each frequency of M_j is termed a *formant*.

Summing up these energies it holds then that $\frac{\sum_{i\leqslant 10} E_{12,i}}{\sum_{k\leqslant 1024} |cos_{j,k}|^2} \approx \frac{21.20}{21.42} \approx 98.9\%$.

For that precise utterance it can be calculated, by using matrices $(M_j)_j$ of all adapted intervals $[a_j, a_j + 1)$, say $j \leqslant \tilde{J}$, that $\frac{\sqrt{\sum_{j\leqslant \tilde{J}, k<10} E_{j,k}}}{\|f\|} \approx \frac{5.54}{7.35} \approx 75.3\%$.

It is also clear that this fraction depends on the special neighbourhood parameter, τ, the number of formants, I, corresponding to the number of rows of M_j, and possibly other constants in the algorithm. However, it is independent of $\tilde{J}$ (due to conservation of energy)!

Such a compression of information seems not only to be effective in the sense that 2^{13} samples are mapped to only a few, say $N \in \mathbb{N}$, feature coefficients but it also promises to be important for further classification tasks.

The number of adapted subintervals $[a_j, a_{j+1})$ ranges in general from $\tilde{J} = 50$ to $\tilde{J} = 70$ (for ℓ^p cost with $p \approx 0.1$) which yields $N \in [\![2I \cdot 50, 2I \cdot 70]\!]$; hence a high compression which is of factor, $(\frac{8192}{N})$, ranging from eight to five, can be easily achieved!

This ansatz, which is very similar to that described in [WW93], allows in particular to linearly interpolate the spectrogram of a signal by (locally constant) frequencies μ_i over the interval $[a_i, a_{i+1})$, cf. next section and Figures 6.21 and 6.22.

6.4.2 Formant Representation

In contrast to reckon all the matrices $(M_j)_{j\leqslant\tilde{J}}$ it may be useful to consider the most energy contributing features $(M_j)_{j\leqslant K\ll\tilde{J}}$ which would gain efficiency in the representation of speech, i.e. yield much higher compression rates by only a slight loss of the energy fraction $\frac{\sum_{j\leqslant K\ll\tilde{J}, k\leqslant 10} E_{j,k}}{\|f\|^2}$, cf. Figure 6.19. Here, approximately the top ten energy contributing features suffices to represent an utterance with almost the same energy fraction.

In summary, it is possible to extract ≈ 200 $(= 2KI)$features which still may contribute to a suitable classification of rather distinct words, similar to the case of the data set used by the author.

That this small number of features is sufficient for classification tasks is yet only motivated by the fact that voiced segments can be fully characterised

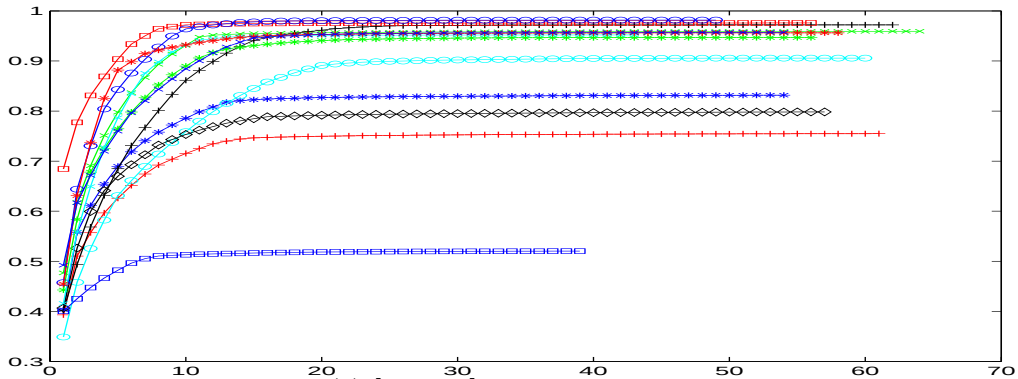

(a) [noːtruːf]; thirteen speakers

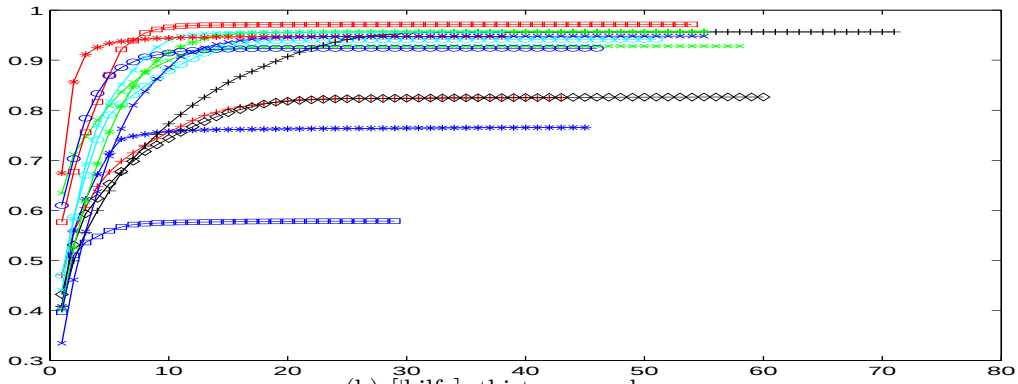

(b) [ˈhilfə]; thirteen speakers

Fig. 6.19: Fraction of energy, $\frac{\sqrt{\sum_{j\leqslant K\leqslant \tilde{J},k\leqslant 10} E_{j,k}}}{\|f\|}$, is plotted against K for the utterances [noːtruːf] and [ˈhilfə] spoken by thirteen different people. Note that a lot of feature matrices M_j do not have a high energy assistance; in most cases it suffices to restrict K to $K = 10$.

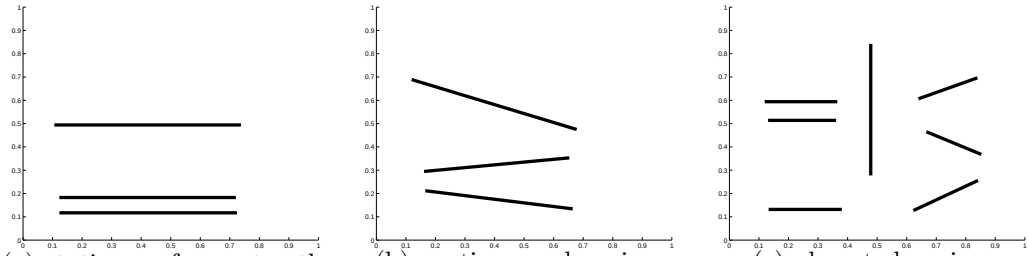

(a) stationary formant path (b) continuous changing (c) abrupt changing

Fig. 6.20: Schematic paths of formants in the phase plane (with normalised frequency and time axes) typical for monophthongs, (a), for diphthongs, (b), and for consonants, (c); the vertical bar results from a relatively short burst where no special frequency band is favoured.

by the first few (three and more) formants which in fact are the most energetic parts of an utterance, cf. Section 4.4.2 and especially Figure 4.13.

A major problem extracting formants by means of the windowed Fourier transform is the disadvantage of a fixed window support and the a priory unknown properties of the analysed signal, e.g. for speech utterances produced by females it is more suitable to use smaller window sizes compared to those which should be applied to speech utterances spoken by males due to different pitch. Such problems are completely removed by an adaptive phase plane tiling!

Another supporting argument relies on the study of the path (evolution in time) of each formant. Early observations by phonologists shows that several consonants and diphthongs[1] have distinctive patterns in the phase plane which may contribute to a recognition of those. Figure 6.20 shows schematically possible paths in the phase plane typically for vowels, (a), diphthongs, (b) and consonants, (c), which may be characterised by the anterior and posterior path and position of each formant. Such diagrams are obtainable via local trigonometric packets and a subsequent basis search algorithm[2].

The features, described by Eq. (6.2), reflects the most important infor-

[1]Diphthongs are vowels which manifest a clear change in quality from start to end as in the words [baɪt] (bite), [bɔɪ] (boy), [steɪk] (steak) or [baʊns] (bounce).

[2]The 'best basis' algorithm which minimises a cost functional is by no means the only one and for speech classification tasks of yet questionable success. Another search algorithms are presented in [Mal98, pp. 409, 465] which *may* be more suitable for noise corrupted signals and for data sets (of words) with only a small number of classes. There, the basic idea is to extract the most coherent segments of a signal w.r.t a dictionary.

Moreover, *local discriminant bases*, which maximise the class separability, cf. [SC94], may also be a candidate for speech recognition.

mation in the sense that the extracted energy associated to those formants, cf. Figure 6.19, is 'almost' unaltered compared to the energy of the signal itself.

Figure 6.21 elucidates the low-dimensionality of the extracted features which also permits the usage of artificial neural nets (ANN) as classifiers. It also shows that most energy comes from voiced segments and Figure 6.22 stresses the speaker independence of the features which is clearly seen in the subplots (a,c,e) for the utterance [liçt] spoken by three different people.

Note also the typical transitions of the formants for the phone [i] in the word [liçt].

More sophisticated statistical (or other) entities, similar to those defined in Eq. (6.2) may have an important contribution to classifying voiced segments.

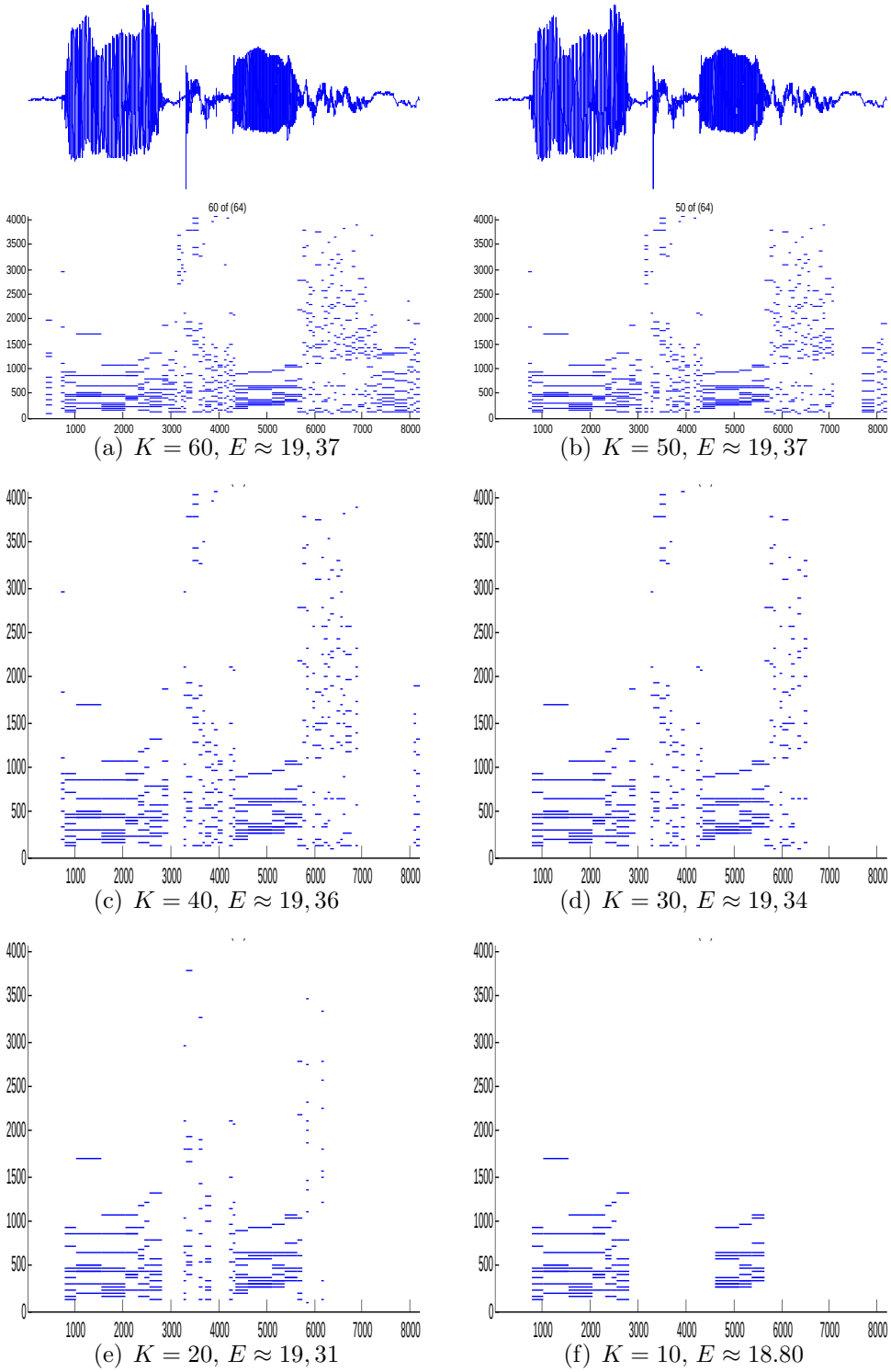

(a) $K = 60$, $E \approx 19,37$ (b) $K = 50$, $E \approx 19,37$

(c) $K = 40$, $E \approx 19,36$ (d) $K = 30$, $E \approx 19,34$

(e) $K = 20$, $E \approx 19,31$ (f) $K = 10$, $E \approx 18.80$

Fig. 6.21: K feature matrices M_j of the female spoken word [no:tru:f] with most energy allocating intervals are used here to plot the formants, matrix elements of the first column, as linear approximations of the actual formant paths; a best basis search with ℓ^p, $p = 0.1$ cost functional chose prior $\tilde{J} = 61$ basis elements. Energy of the word is $\|f\| \approx 20.19$ and $E := \sqrt{\sum_{j \leqslant K, k \leqslant 10} E_{j,k}}$ denotes the extracted energy pertinent to the KI formants showed in each subbplot, (a-f).

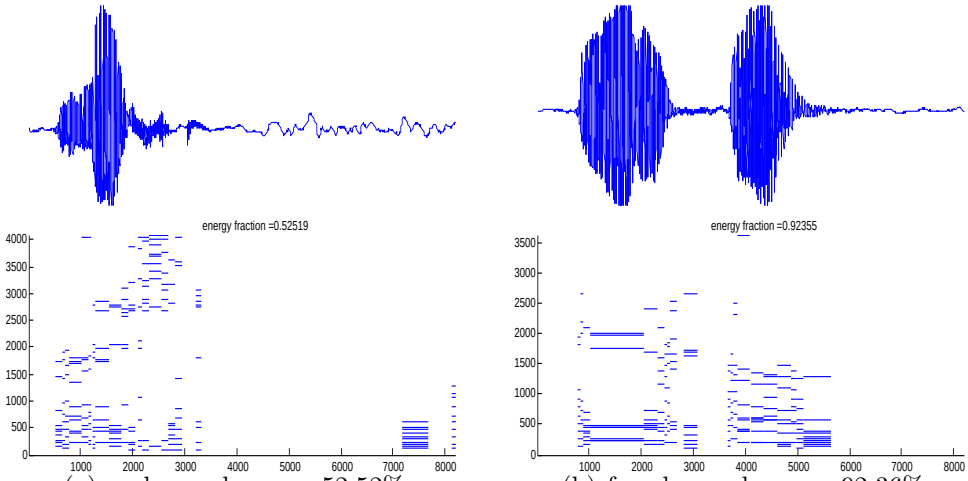

(a) male speaker; $e \approx 52.52\%$ (b) female speaker; $e \approx 92.36\%$

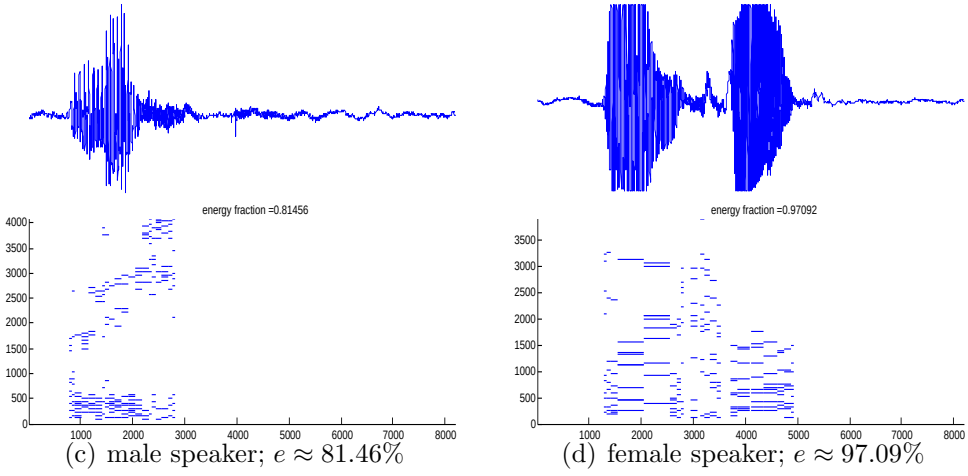

(c) male speaker; $e \approx 81.46\%$ (d) female speaker; $e \approx 97.09\%$

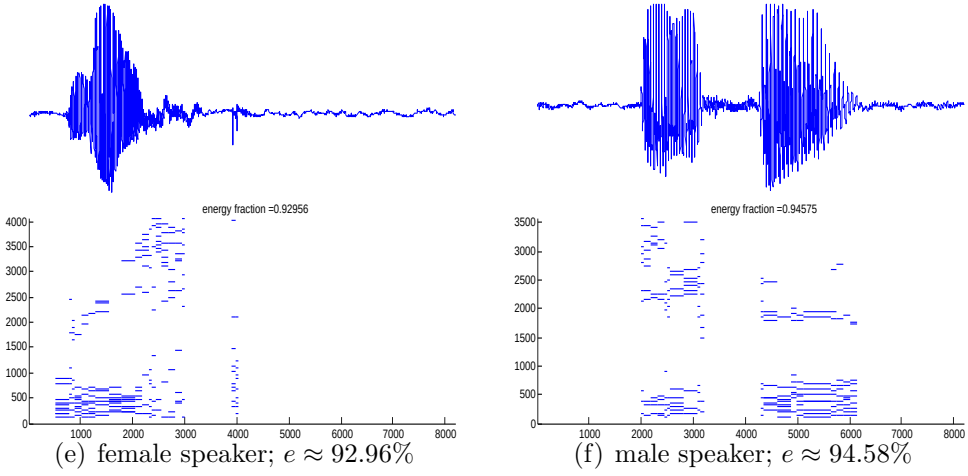

(e) female speaker; $e \approx 92.96\%$ (f) male speaker; $e \approx 94.58\%$

Fig. 6.22: Same procedure as in Figure 6.21; $K = 20$, $I = 10$; left column shows the utterance [liçt] whereas right column visualise ['hilfə] and the corresponding locally constant formants plotted in the phase plane. The associated energy fraction $e := \frac{\sqrt{\sum_{j \leqslant K, k \leqslant 10} E_{j,k}}}{\|f\|}$ is given below each subplot (a-f).

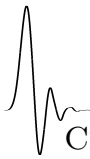

Chapter 7

Conclusions & Outlook

The presented work emphasises the limits of the windowed Fourier transform as also the wavelet ansatz. Section 4.4.2 shows that each has major disadvantages if the aim is a measurement of the time varying spectrum. The former has a good frequency resolution which is necessary for speech recognition tasks but does not permit an adapted care of transients, i.e. the phase plane tiling is fixed, since the window support is arbitrary but fixed.

Moreover, from the Balian-Low theorem it is clear that numerical stability excludes a good time – frequency resolution and vice versa. The windowed Fourier transform is not optimal without a priory knowledge about the expected frequency path in the sense that different window sizes may lead to a better formant resolution.

A more sophisticated mathematical tool provides the wavelet transform constituting a frame, bi(orthogonal) or even orthonormal basis.

Via a scaling approach it is possible to achieve a multiresolution with even a lower computational complexity compared to the windowed Fourier transform.

Unfortunately, this ansatz sacrifices frequency resolution for time resolution. The wavelet transform is a good tool for regularity analysis of signals, for compression and for a lot of other tasks.

However, it fails to resolve frequency intervals which are of interest in speech processing. This is summarised in the aforementioned section: The author gives a simplistic algorithm which detect voiced segments. It exploits the octave band tiling of the wavelet transform and the fact that voiced speech has distinct frequencies not presented in voiceless speech. A subsequent windowed Fourier transform of each voiced part *may* yield a good formant representation which depends on the window size.

In contrast, the spectral components are separated by the local trigono-

metric transform that has sufficient frequency resolution *and* which also has enough time resolution to provide time varying measurements.

A so-called *best basis* algorithm adapts the phase plane tiling which is then optimal (w.r.t. a metric resulting here from a cost functional) for each utterance. It achieves a good frequency resolution for voiced segments and zooms in like the wavelet transform where the frequency is of high variation typical for consonants. This transform also constitutes frames, bi(orthogonal) or orthonormal bases. The so obtained adapted decomposition is used for feature extraction.

Section 6.4 discusses why the centred frequencies with pertinent energies may yield a good foundation for speech recognition.

A straightforward development of the ansatz described in the last chapter could be the usage of a neural net which would considerably profit by the enormous data shrinkage; a sampled utterance of 2^{13} coefficients is reduced to approximately 64 $n \times 2$ matrices, e.g. for $n = 10$ a 'squeeze' of more than 600%!

Alternative constructions of bases from out a binary tree may also be of interest. For instance, a basis which maximises a class separability instead of correlating the signal, a so-called *local discriminant basis*, cf. [SC94], may achieve better classification results.

Shift-invariance of the wavelet packet and local trigonometric transform may impair the so extracted features. There exist different solutions confined to that problem, [Coh98]. Since they are, without exception, of a higher computational complexity they were not considered yet.

As a matter of course, other features may be extracted which are more robust to noise and more speaker independent. Analogously to that problem, a more suitable cost functional in the best basis algorithm could also contribute to a higher classification rate.

In that context another partition ansatz is presented by Eva Wesfreid and Mladen Victor Wickerhauser in [WW99]. They compute the time points where an associated *instantaneous frequency change function* has its local maxima. Those points are then used to segment the signal into intervals of nearly piecewise constant spectra, as presented in [Fan94]. The so achieved partition is not dyadic and may split the signal in a more accurate sequence of phones than obtained via a best basis search algorithm. At the moment it is not known to the author if the higher computational complexity of $\mathcal{O}(N^2)$, N number of samples, reduce any misclassification rates.

Nevertheless, the local trigonometric transform seems to be a very promising tool with at least two crucial degrees of freedom: partition $(a_i)_i$ of the real line and the special geometry of the window sequence $(w_j)_j$ can be kept very lax and allow therefore to be adapted to a particular problem at hand.

Bibliography

[Aus95] P. Auscher. Solution of two problems on wavelets. *J. Geom. Anal.*, 5:181–236, 1995.

[AWW91] P. Auscher, G. Weiss, and M. V. Wickerhauser. Local Sine and Cosine Bases of Coifman and Meyer and the Construction of Smooth Wavelets. pages 237–256. url: `citeseer.ist.psu.edu/--auscher91local.html`. 1991.

[Bar98] T. Bartosch. Abschlußbericht: August 1994 – August 1997. Friedrich-Alexander Universität Erlangen-Nürnberg, May 1998.

[BD] J. B. Buckheit and D. L. Donoho. Wavelab and Reproducible Research. Stanford University.

[Bit00] K. Bittner. Biorthogonal local trigonometric bases. In G. Anastassiou, editor, *Handbook on Analytic-Computational Methods*. CRC Press, 2000.

[Chr06] O. Christensen. Recent Developments in Frame Theory. In O. Christensen et al., editor, *Modern Mathematical Models, Methods and Algorithms for Real World Systems*. Anamaya, New Delhi, India, Feb. 2006.

[Coh98] I. Cohen. *Shift-Invariant Adaptive Wavelet Decompositions and Applications*. PhD thesis, Israel Institute of Technology. Haifa, Israel. url: `citeseer.ist.psu.edu/article/-cohen98shiftinvariant.html`, May 1998.

[CW91] R. R. Coifman and M. V. Wickerhauser. Remarques sur l'analyse de Fourier á fenetre. *C.R. Acad. Sci. Paris*, 38(312):259–261, 1991.

[CW92] R. R. Coifman and M. V. Wickerhauser. Entropy-based algorithms for best basis selection. *IEEE Transactions on Information Theory*, 38(2):713–718. url: `citeseer.ist.psu.edu/--coifman92entropybased.html`, 1992.

[Dau92] I. Daubechies. *Ten Lectures on Wavelets*. Society for Industrial and Applied Mathematics, 1992.

[DM72] Dym and McKean. *Fourier series and integrals*. Academic press, 1972.

[Erd03] K.-G. Große – Erdmann. *Wavelets*, volume 1-7. FernUniversität in Hagen, Fachbereich Mathematik, 2003.

[Fan94] X. Fang. Automatic Phoneme Segmentation of Continuous Speech Signals. *IEEE Transactions on Speech and Audio Processing*, 1994.

[Gab46] D. Gabor. *Theory of communication*. J. IEE, 93:429-457, 1946.

[Hes05] W. Hess. Fundamentals of Phonetics. Rheinische Friedrich-Wilhelms-Universität Bonn, Oct., 2005.

[Heu86] H. Heuser. *Funktionalanalysis*. B.G. Teubner, Stuttgart, 2 edition, 1986.

[Heu02] H. Heuser. *Lehrbuch der Analysis*. B.G. Teubner, Stuttgart, 2 edition, 2002.

[IPA63] The Principles of the International Phonetic Association. Departement of Phonetics, University College, 1963.

[Kur97] F. Kurth. Adaptive Waveletpackets und Anwendungen in der Audiosignalverarbeitung, 1997. Rheinische Friedrich-Wilhelms-Universität Bonn, Diploma Thesis.

[LR92] P.G. Lemarié-Rieusset. Existence de fonction-père pour les ondelettes à support compact. *C.R. Acad. Sci. Paris. Sér. I, 314*, 1992.

[Mal89] S. Mallat. Multiresolution approximations and wavelet orthonormal bases of $\ell^2(\mathbb{R})$. *Trans. Amer. Math. Soc. 315*, 1989.

[Mal98] S. Mallat. *A Wavelet Tour of Signal Processing*. Academic Press, London, 1998. ISBN 0-12-466605-1.

[MO79] A.W. Marschall and I. Olkin. *Inequalities: Theory of Majorization and its Applications*. Academic Press, 1979.

[Rud87] W. Rudin. *Real and complex analysis*. McGraw-Hill, 1987.

[RY90] K.R. Rao and P. Yip. *Discrete Cosine Transform*. Acad. Press, NY, 1990.

[SC94] N. Saito and R. R. Coifman. Local Discriminant Bases. In A.F. Laine and M.A. Unser, editors, *Mathematical Imaging: Wavelet Applications in Signal and Image Processing II*, volume 2303. 1994.

[Sha48] C. E. Shannon. A Mathematical Theory of Communication. *The Bell System Tech. journ.*, 27:379–423,623–656, Jul.,Oct. 1948.

[SJ95] W. Sweldens and B. Jawerth. Biorthogonal Smooth Local Trigonometric Bases. *J. Fourier Anal Appl.*, 38(2):109–133, 1995.

[ST95] E. G. Schukat-Talamazzini. *Automatische Spracherkennung - Statistische Verfahren der Musteranalyse*. Vieweg Verlag, 1995.

[vdB58] J.-W. van den Berg. Myoelastic-aerodynamic theory of voice production. *J. Speech Hear. Res.*, 1:227–244, 1958.

[Wer95] D. Werner. *Funktionalanalysis*. Springer Verlag, Berlin, 1995.

[Wic91] M. V. Wickerhauser. Lectures on wavelet packet algorithms. unpublished, Nov. 18, 1991.

[Wic93a] M. V. Wickerhauser. *Smooth localized orthonormal bases*. C.R. Acad. Sci., Paris, 1993.

[Wic93b] M. V. Wickerhauser. Best-adapted wavelet packet bases. March, 1993.

[Wic94] M. V. Wickerhauser. *Adapted Wavelet Analysis from Theory to Software*. AK Peters, Ltd., Wellesley, Massachusetts, May 1994. with optional diskette.

[WW93] E. Wesfreid and M. V. Wickerhauser. Adapted Local Trigonometric Transform and Speech Processing. *IEEE Transactions on Signal Processing*, 41(12):3596–3600. url: `citeseer.ist.psu.edu/--wesfreid93adapted.html`, Dec. 1993.

[WW99] E. Wesfreid and M. V. Wickerhauser. Vocal Command Signal Segmentation and Phonemes Classification. url: `citeseer.ist.psu.edu/wesfreid99vocal.html`, 1999.

[Zyg59] A. Zygmund. *Trigonometric Series*. Cambridge University Press, 2nd edition edition, 1959.

Index

Eidesstattliche Erklärung

Hiermit erkläre ich, dass die vorliegende Arbeit von mir selbständig angefertigt und keine anderen als die angegebenen Quellen und Hilfsmittel benutzt wurden.

..... Kaiserslautern, 24. Juli 2006

(Andreas Simon)